Establishing a scalable manufacturing process for the clinical scale production of CAR-T cell therapies in stirred-tank bioreactors

by

Elena Costariol

Department of Biochemical Engineering

University College London

A thesis submitted for the degree of

Doctor in Engineering (EngD)

2020

Declaration

I, Elena Costariol confirm that the work in this thesis is my own, except when indicated. The work presented in this thesis was carried out under the supervision of Dr. Qasim Rafiq and Professor Martina Micheletti at the Department of Biochemical Engineering, University College London between September of 2017 and January of 2020. This thesis has not been submitted, either in whole or in part, for another degree or another qualification at any other university.

Elena Costariol

London, September 2020

Abstract

CAR-T immunotherapies present a novel therapeutic modality for the treatment of various blood tumours. However, the development of such immunotherapies requires the manufacture of large numbers of CAR-T cells (2-6 x 10^8 total viable CAR-T cells per dose), which remains a major translational and commercial bottleneck due to the manual, small-scale, and often static culture systems used for their production. Such systems are easy to use in a pre-clinical research settings, but are not efficient when a higher number of doses need to be produced. Furthermore, there is a general concern that primary T-cells are shear sensitive and do not grow in agitated systems, such as stirred-tank bioreactors.

This doctoral thesis aims to demonstrate that primary human T-cells and CAR-T cells can be cultivated in stirred-tank bioreactors at different scales (15 ml, 250 ml, and 1 L), which can be used for both autologous and allogeneic products. Furthermore, data in this thesis shows that the growth of T-cells and transduced CAR-T cells was significantly better in stirred-tank bioreactors than in T-flask static culture. At agitation speeds of 200 rpm and greater (up to 500 rpm) in the ambr® 250 stirred-tank bioreactor, the CAR-T cells were able to proliferate effectively, reaching viable cell densities of $> 5 \times 10^6$ cells ml^{-1} over 7 days. This is comparable with current expansion systems and significantly better than static expansion platforms (T-flasks and gas-permeable culture bags). Importantly, the cell quality and potency was assessed at the end of the expansion

and was equivalent to the one presented by the cells grown under static conditions as control. It was demonstrated that higher agitation rates, corresponding to higher power inputs lead to a better proliferation. This improvement is likely due to the inability at the lower agitation rates to effectively suspend the Dynabeads® used to activate T-cells. Importantly, from the data obtained, there is no indication that T-cells prefer being grown under static conditions or are sensitive to fluid dynamic stresses within a stirred-tank bioreactor system at the agitation speeds investigated.

Impact statement

In recent years multiple CAR-T therapies have been approved and reached the market. Although they have proven great curing potential for blood tumours, the manufacturing process for CAR-T therapies has not reached its optimal in terms of efficiency, which is reflected in the high cost ($\sim$ £300,000) per single dose. Many of the expansion platforms used to manufacture CAR-T products have the potential to be scaled-out, but do not offer the possibility to scale-up the process. This doctoral thesis aims to demonstrate that expanding CAR-T cells in stirred-tank bioreactors is feasible and advantageous compared to static vessels processes. The focus of the thesis is to develop a robust and scalable expansion process for CAR-T therapies in stirred-tank bioreactors. In order to do so, an ambr® 250 stirred-tank bioreactor was used, together with an ambr® 15 high-throughput stirred-tank bioreactor and a 1 L UniVessel® stirred-tank bioreactor.

Stirred-tank bioreactors provide a better mass-transfer and allow for online monitoring of culture parameters, such as pH and dO_2, compared to static platforms (T-flasks, gas-permeable bags, and G-Rex vessels). When compared with rocking-motion bioreactors or the CliniMACS Prodigy® systems, stirred-tank bioreactors are easier to scale-up and there is a great choice of suppliers, making it possible to choose from different geometries and scales, but also lowering the risk of chain of supply disruption.

Proving that results obtained at small scale can be replicated at 1 L volumes, makes

the ambr® 15 a powerful tool for process development and shortening the time for CAR-T therapies to reach the clinical trials and commercialisation. The ambr® 15 system allows up to 48 bioreactors to be operated in parallel, and is an excellent high-throughput model for the initial screening of critical culture conditions and parameters.

The expansion process was successfully scaled-up from 15 ml to 250 ml and 1 L stirred-tank bioreactors based on the power per unit volume comparison. This shows that stirred-tank bioreactors can be used to produce allogeneic CAR-T therapies, where starting from healthy donor materials, multiple doses can be produced at once in a larger volume. This will revolutionise the manufacturing of CAR-T cell products allowing to use a single system rather than multiple systems in parallel (scale-out approach), reducing the space needed in expensive clean rooms and making the process more cost efficient.

Unfortunately the ambr® systems are not GMP compliant, however they are still a powerful tool to be used to fast-forward the process development stage of cell and gene therapies.

This study is the first demonstration of primary T-cell and CAR-T cell *ex vivo* manufacture activated by Dynabeads® in stirred-tank bioreactors, and the findings have the potential to be applied to multiple other cell candidates for advanced therapy applications.

List of Publications

Publications

Costariol, E., Rotondi, M. C., Amini, A., Hewitt, C. J., Nienow, A. W., Heathman, T. R., Rafiq, Q. A. (2020). Demonstrating the Manufacture of Human CAR-T Cells in an Automated Stirred-tank Bioreactor. *Biotechnology Journal, 2000177.*

Costariol, E., Rotondi, M., Amini, A., Hewitt, C. J., Nienow, A. W., Heathman, T. R., Micheletti, M., Rafiq, Q. A. (2019). Establishing the scalable manufacture of primary human T-cells in an automated stirred-tank bioreactor. *Biotechnology and bioengineering, 116(10), 2488-2502.*

Costariol, E., Rotondi, M., Hewitt, C. J., Nienow, A. W., Rafiq, Q. A. Scaling-up the manufacture of CAR-T cell therapies in stirred-tank bioreactors. *In preparation*

Conference Presentations

World Advanced Therapies & Regenerative Medicine Congress, London, UK (Online); held 8th - 11th September 2020: **Oral Presentation** - *Process Development and Manufacture of Primary Human T-cells in Scalable, Automated Stirred-Tank Bioreactors*

Vein-to-vein Congress, London, UK; held 28th - 30th January 2020; **Oral Presentation** - *Establishing the Scalable Manufacture of Primary Human T-Cells in an Automated Stirred-Tank Bioreactor*

Festival of Biologics, Basel, Switzerland; held 15th - 17th October 2019; **Oral presentation** - *Process Development and Manufacturing Strategies for ATMPs*

BioProcess International Conference and Exhibition, Boston, Massachusetts, USA; held 9th - 12th September 2019; **Oral Presentation** - *Establishing the Scalable Manufacture of Primary Human T-Cells in an Automated Stirred-Tank Bioreactor*

International Society Cell and Gene Therapy (ISCT), Melbourne, Australia; held 29th May - 1st June 2019; **Poster Presentation** - *Bioprocessing of CAR-T cell Therapies in an Automated Single-Use Stirred-Tank Bioreactor*

World Advanced Therapies & Regenerative Medicine Congress, London, UK; held 15th - 17th May 2019: **Oral Presentation** - *Process Development and Manufacture of Primary Human T-cells in Scalable, Automated Stirred-Tank Bioreactors*

ECI Advancing Manufacture of Cell and Gene Therapies, San Diego, California, USA; held 27th - 31st January 2019: **Oral Presentation** - *Process Development and Manufacture of Primary Human T-cells in Scalable, Automated Stirred-Tank Bioreactors*

Phacilitate World Leaders, Miami, Florida, USA; held 22nd - 25th January 2019: **Oral Presentation** - *Process Development and Manufacture of Primary Human T-cells in Scalable, Automated Stirred-Tank Bioreactors*

ESACT UK Conference, Tamworth, UK; held 9th - 10th January 2019: **Poster Presentation and Oral presentation** - *Process Development and Manufacture of Primary Human T-cells in Scalable, Automated Stirred-Tank Bioreactors*

BioProcess UK Conference, Edinburgh, UK; held 20th - 22nd November 2018: **Poster Presentation** - *Bioprocessing of T-cell Therapy Manufacture in a Single-Use High-Throughput Stirred-Tank Bioreactor*

Parenteral Drug Association (PDA) Cell and Gene Therapy Conference, Bethesda, Maryland, USA; held 23rd - 24th October 2018: **Oral Presentation** - *Automated Approaches for the Process Development and Manufacture of Cell and Gene Therapies*

Acknowledgments

I would like to thank my supervisor Dr. Qasim Rafiq for his guidance and mentorship throughout this project. I would also like to thank my secondary supervisor Prof. Martina Micheletti for her support.

I would like to further acknowledge the advice and mentorship of Prof. Christopher Hewitt and Prof. Alvin Nienow throughout this EngD project.

I would like to thank Marco, Arman, Gerry, Ana, Pedro, Theano, and all the others from the cell and gene therapy group for being there when needed, either for experimental or life advice.

Last but not least, I would like to thank my parents, Mario and Luisa, and my sister Irene for their ongoing support.

Contents

List of Figures

List of Tables

List of Abbreviations

ALL	Acute lymphocytic leukemia
AML	Acute myeloid leukemia
APC	Antigen presenting cell
BCMA	B-cell maturation antigen
BSA	Bovine serum albumine
BSC	Biological safety cabinet
CAR	Chimeric antigen receptor
CBA	Cytometric Bead Array
CEA	Carcinoembryonic antigen
CGT	Cell and Gene Therapy
CHO	Chinese hamster ovary
CLL	Chronic lymphocytic leukemia
CML	Chronic myeloid leukemia
CMV	Cytomegalovirus
CRISPR	Clustered Regularly Interspaced Short Palindromic Repeats
CRS	Cytokine release syndrome
dO_2	Dissolved oxygen
DoE	Design of experiments
DLBCL	Diffuse large B-cell lymphoma

DMEM	Dulbecco's modified Eagle medium
DMSO	Dimethylsulphoxide
ECACC	European Collection of Authenticated Cell Cultures
EDTA	Ethylenediaminetetraacetic acid
EGFR	Epidermal growth factor receptor
EMA	European Medicines Agency
ESGCT	European Society of Gene and Cell Therapy
FBS	Foetal bovine serum
FDA	Food and Drug Administration
GMP	Good manufacturing practice
GSK	GalaxoSmithKline
GVHD	Graft-versus-host-disease
HEK	Human embryonic kidney
HEPES	N-2-hydroxyethylpiperazine-N-ethanesulfonic acid
HER2	Human epidermal growth factor receptor 2
HLA	Human leukocyte antigen
hMSC	Human mesenchymal stem cells
HPC	Hematopoietical progenitor cells
HSCT	Hematopoietic stem cell transplantation
IL-2	Interleukin-2

IL-2	Interleukin-2
IL-6	Interleukin-6
IL-7	Interleukin-7
IL-10	Interleukin-10
IL-15	Interleukin-15
IL-17	Interleukin-17
INF-γ	Interferon-gamma
ITR	Inverted terminal repeat
LAG3	Lymphocyte activation gene 3
mAb	Monoclonal Antibody
MHC	Major histocompatibility complex
NHL	Non-Hodgkin lymphoma
NHS	National Health Service
NK	Natural killer
OTB	Ornithine transcarbamylase
OXPHOS	Oxidative phosphorylation
PBMC	Peripheral blood mononuclear cell
PBS	Phosphate-buffered saline
PHA	Phytohemagglutinin
PFA	Paraformaldehyde

PSMA	Prostate specific membrane antigen
PD-1	Programmed death protein 1
RPMI	Roswell Park Memorial Institute
SB	Sleeping beauty
scFv	Single-chain variable fragment
sgRNA	Single guide RNA
SMA	Spinal Muscular Atrophy
SME	Small to medium enterprise
TALEN	Transcription activator like effector nuclease
TCR	T-cell receptor
Th1	T helper 1
Th2	T helper 2
Th17	T helper 17
TIL	Tumour infiltrating lymphocyte
TIM3	T-cell immunoglobulin and mucin-domain containing-3
TME	Tumour micro environment
TNF-α	Tumour necrosis factor alpha
TRAC	T-cell receptor-α chain
UK	United Kingdom
USA	United States of America

VVM Volume of liquid per minute

ZFN Zing-finger nucleases

Nomenclature

D	Impeller diameter	m
ε	Maximum specific energy dissipation rate	W kg^{-1}
FE	Fold expansion	Dimensionless
λ_K	Kolmogorov scale of turbolence	m
N	Impeller speed	rev s^{-1}
μ	Specific growth rate	h^{-1}
P	Power input	W
P_0	Power input	Dimensionless
P/M	Specific power input	W kg^{-1}
q_{met}	Specific consumption rate	pmol $cell^{-1}$ day^{-1}
ρ	Density of the medium	kg m^{-3}
t_d	Doubling time	h
υ	Kinematic viscosity	m^2 s^{-1}
Y_{lac}/Glc	Lactate yield from glucose	mol mol^{-1}

Chapter 1

Introduction

1.1 Cell and gene therapies

Novel cell and gene therapies (CGTs) have generated significant commercial interest due to their demonstrated long-term clinical efficacy. These new therapies bring new hope to patients with previously incurable diseases and will likely revolutionise the conventional pharmaceutical industry (Panagopoulou et al., 2019). Despite their huge potential and proven therapeutic success, CGTs are overly expensive due to their inefficient manufacturing process and lack of suitable manufacturing tools (Costariol et al., 2020; Xiuyan Wang et al., 2016).

The growing interest in CGTs is reflected by the multiple products gaining Food and Drug Administration (FDA) and European Medicines Agency (EMA) approval, in the

United States of America (USA) and Europe respectively, in the past few years (Table 1.1). CGTs cover a wide range of different therapies; for the purposes of this thesis the following definitions, adapted from the European Society of Gene and Cell Therapy (ESGCT), will be used:

- **Gene therapy** -"Introduction of exogenous genes into cells with the goal of curing or improving a disease condition." (ESCGT, 2016). This involves the use of engineered biological vectors that can be viral or non-viral, to deliver genetic material. (ESCGT, 2016; Verma et al., 2000; Mulligan, 1993)

- **Cell therapy** - "The use of cells in regenerative medicine to replace defective, damaged, or missing tissue" (ESCGT, 2016). The cells are not genetically altered. (Golchin et al., 2019)

- **Gene modified cell therapy** - "The use of genetically altered cells that are taken either from the patient themselves or a donor to treat diseases" (ESCGT, 2016).

Furthermore, CGTs can take place inside or outside the body. If the modifications occur inside the patient's body they are referred to as *in vivo* therapies, while the ones that take place outside the body are referred to as *ex vivo* therapies.

Table 1.1: FDA approved cell and gene therapies in chronological order. Data retrieved from Food and Drug Administration, 2019. HPC = Hematopoietical Progenitor Cells; ALL = acute lymphoblastic leukemia; SMA = spinal muscular atrophy.

Trade Name & Manufacturer	**Proper Name**	**Indication**	**Year of Approval**	**CGT Type**
PROVENGE® *Dendreon Corporation*	Sipuleucel-T	Metastatic prostate cancer	2010 FDA 2013 EMA	Cell therapy
HEMACORD® *New York Blood Center*	HPC, Cord Blood	Disorders affecting the hematopoietic system	2011 FDA	Cell therapy
LAVIV® *Fibrocell Technologies*	Azificel-T	Nasolabial fold wrinkles in adults	2011 FDA	Cell therapy
DUCORD® *Duke University School of Medicine*	HPC, Cord blood	Disorders affecting the hematopoietic system	2012 FDA	Cell therapy
GINTUIT® *Organogenesis Incorporated*	Allogeneic cultured keratinocytes and fibroblasts in bovine collagen	Topical application to a surgically created vascular wound bed in the treatment of mucogingival conditions in adults	2012 FDA	Cell therapy
None *Clinimmune Labs, University of Colorado Blood Bank*	HPC, Cord blood	Disorders affecting the hematopoietic system	2012 FDA	Cell therapy
ALLOCORD® *SSM Cardinal Glennon Children's Medical Center*	HPC, Cord blood	Disorders affecting the hematopoietic system	2013 FDA	Cell therapy
None *LifeSouth Community Blood Centers, Inc.*	HPC, Cord blood	Disorders affecting the hematopoietic system	2013 FDA	Cell therapy

Trade Name & Manufacturer	Proper Name	Indication	Year of Approval	CGT Type
IMLYGIC® *Amgen Inc.*	Talimogene laherparepvec	Local treatment of cutaneous, subcutaneous and nodal lesions in patients with melanoma	2015 FDA 2015 EMA	*In vivo* gene therapy
CLEVECORD® *Cleveland Cord Blood*	HPC, Cord blood	Disorders affecting the hematopoietic system	2016 FDA	Cell therapy
None *Bloodworks*	HPC, Cord blood	Disorders affecting the hematopoietic system	2016 FDA	Cell therapy
KYMRIAH® *Novartis Pharmaceutical Corporation*	Tisagenlecleucel	Patients up to 25 years of age with ALL and adults with relapsed or refractory B-cell lymphoma	2017 FDA 2018 EMA	Gene modified cell therapy
LUXTURNA® *Spark Therapeutics*	Voretigene neparvovec-rzyl	Biallelic *RPE65* mutation-associated retinal distrophy	2017 FDA 2018 EMA	*In vivo* gene therapy
YESCARTA® *Kite Pharma Incorporated*	Axicabtagene Ciloleucel	Adults with relapsed refractory B-cell lymphoma	2017 FDA 2018 EMA	Gene modified cell therapy
None *MD Anderson Cord Blood Bank*	HPC, Cord blood	Disorders affecting the hematopoietic system	2018 FDA	Cell therapy
MACI® *Vernicel Corporation*	Autologous cultured chondrocytes on a porcine collagen membrane	Repair of cartilage defects of the knee in adults	2019 FDA 2013 EMA	Cell therapy
ZOLGENSMA® *AveXis, Inc.*	Onasemnogene abeparvovec-xioi	Treatment of SMA in pediatric patients less than 2 years of age	2019 FDA 2020 EMA	*In vivo* gene therapy

The data from the first clinical trial on humans were reported by Rosenberg et al. (1990), using gene modified autologous tumor-infilitrating lymphocites (TILs) transduced with a retroviral vector on 5 patients with advanced melanoma.

Despite numerous successes, these therapies did not come without adverse events and safety concerns. Jesse Gelsinger was the first patient who died in a Phase I gene therapy clinical trial in 1999. His death was directly attributed to the inflammatory reaction to the adenoviral vector used in the studies to treat ornithine transcarbamylase (OTB) deficiency (Somia et al., 2000). Shortly thereafter, in 2002, a leukemia-like illness was developed in a subject enrolled in a clinical trial due to retroviral insertional mutagenesis and the patient required chemotherapy treatment (Hacein-Bey-Abina et al., 2003).

Despite these setbacks the field of CGTs has significantly improved and evolved. A better understanding of the safety implications, and more advanced technologies have helped to make these therapies safer and more effective. CGTs are being used to treat different monogenic disorders, vascular diseases, infectious diseases, and cancers (Edelstein et al., 2004). Significant investments have been made between 2010 and 2016 in CGTs by large biopharmaceutical companies (D. M. Smith et al., 2018). This is reflected in the growing number of FDA approved CGTs in the last 10 years (Table 1.1).

Amongst the CGTs approved by the FDA (Table 1.1) IMLYGIC® is the first approved *in vivo* gene therapy. It uses a weakened form of Herpes Simplex Virus Type

1 for the treatment of unresectable melanoma in adults. It is a viral therapy that is directly injected into melanoma tumours, in which the virus targets cancerous cells and healthy cells, but it is unable to replicate in the latter ones, limiting the side effects. PROVENGE®, the first FDA approved cell therapy, involves peripheral blood mononuclear cells (PBMCs) activated with a recombinant protein *ex vivo* and re-infused in the patient. MACI® is another example of cell therapy, where the cells are taken from the patient, expanded *ex vivo* and returned to the patient to repair or restore damaged cartilage in the knee. The cell therapy definition comprehends also all the therapies that utilise hematopoietical progenitor cells. Chimeric antigen receptor (CAR)-T cell therapies fall into the gene modified cell therapies, where the cells are genetically modified *ex vivo* and re-infused into the patient. Two examples of such therapies are KYMRIAH® and YESCARTA® used to treat refractory or relapsed haematological malignancies. It can be noted that these two CAR-T therapies have been approved within 6 months one from another. This indicates the need for new therapies to treat haematological malignancies and the willingness of the regulatory bodies to accelerate the development and commercial production of such treatments, still guaranteeing the safety of the product.

Although two CAR-T cells therapies have been approved by the FDA and EMA in 2017 and 2018 respectively, they are prohibitively expensive to manufacture (Vormittag et al., 2018). This is mainly due to the fact that these products are manufactured in universities or small laboratories during the early stages of development, while to have a

reduced cost the manufacturing process needs to be efficiently translated to commercial scale (Xiuyan Wang et al., 2016; Tyagarajan et al., 2019). Scalable manufacturing technologies are needed to engineer and expand the cells in order to have a reduction in the cost of these therapies. Although the field is still far away from an automated, fully closed manufacturing process, CAR-T therapies have shown promising results for a variety of cancers with long term clinical success in the haematological malignancies sector (Tyagarajan et al., 2019; Brudno et al., 2019).

1.2 Haematological malignancies and current therapies

There are four main types of haematological malignancies all originating from cells in the bone marrow or in the lymphatic system: leukemia, myeloma, Hodgkin's and non-Hodgkin's lymphomas. Some of these malignancies were first described in the 19^{th} century, but no cure was available (Lichtman, 2008). Data about the incidence of different haematological malignancies are shown in Table 1.2.

Table 1.2: Haematological malignancies incidence, male to female ratio, median age at diagnosis and 5-year relative survival. Leukemia was further divided into acute lymphocytic leukemia (ALL), chronic lymphocytic leukemia (CLL), acute myeloid leukemia (AML), and chronic myeloid leukemia (CML). Non-Hodgkin lymphoma sub-category includes Marginal zone lymphoma, follicular lymphoma, Burkitt lymphoma, Mantle cell lymphoma, diffuse large B-cell lymphoma (DLBCL), and T-cell lymphoma. Data retrieved from Epidemiology and Cancer Statistics Group, 2019.

Haematological Malignancy	**% of total haematological malignancies**	**Male to Female rate ratio**	**Median age at diagnosis**	**5-year relative survival (%)**
Myeloma	10.2	1.4	72.7	47.6
ALL	1.7	1.6	15.8	66.1
CLL	10.6	1.8	71.8	85.9
AML	6.5	1.2	62	43.6
CML	1.6	1.4	59.2	89.2
Marginal zone lymphoma	6.2	1.2	72.5	80
Follicular lymphoma	5	0.9	65.2	88.6
Burkitt lymphoma	0.6	3.4	55.5	57.6
Mantle cell lymphoma	1.3	2.6	72.9	41.9
DLBCL	12.5	1.2	70	61.1
T-cell lymphoma	1.6	1.5	65.8	49.7
Hodgkin lymphoma	4	3.4	43.2	90.8

The first palliative treatment for haematological malignancies was introduced in the early 20^{th} century with the radiation treatment for Hodgkin lymphoma evolving then in radiotherapy. The development of anticancer drugs started in the second half of the century with the introduction of alkylating agents, adrenocorticotropic hormone or cortisone acetate, and folic acid. In the last 30-40 years additional agents against haemato-

logical malignancies have been developed and used (Lichtman, 2008). In current times most blood cancers are treated with chemotherapy. Chemotherapy can then be followed by allogeneic hematopoietic stem cell transplantation (HSCT) (Evers et al., 2017). Most of the therapies combine multiple conventional treatments such as chemotherapy and HSCT with more innovative molecular targeting drugs. This combination of treatments has improved the survival rate of patients affected by blood tumours (Shimada, 2019). However, a definitive treatment has not been yet found.

In the last decades the advent of CGTs, and in particular CAR-T therapy, has given new hope for patients who failed to react to conventional cancer cures or relapsed (Nirali N Shah et al., 2019). CAR-T therapies have shown clinical efficacy for haematological malignancies, with proven long-term patient outcomes and starting to show promising results in solid tumours treatments (Newick et al., 2017). In order to understand the enormous potential of CAR-T therapies it is important to have knowledge of the adaptive immune system and how it works.

1.3 T-cells

T lymphocytes, commonly referred to as T-cells, are white blood cells actively involved in the immune system. These cells are known to express the T-cell receptor (TCR) on their surface (Boehmer, 1990). The human immune system can be divided in innate and adaptive. The innate immune system is the first one to react to infection, it is

non-specific and it lacks memory. On the other hand, the adoptive immune system has a slower response, but it is characterised by specific antigen recognition and long-lasting immunity (Lanier, 2013). The innate immune system includes soluble factors and different cellular effectors, such as granulocytes, mast cells, macrophages, dendritic cells and natural killer (NK) cells. B and T-cells, together with antibodies, are part of the adaptive immune system (Luster, 2002). NK-T cells and $\gamma\delta$ T-cells, which have a cytolytic activity and rapid secretion of cytokines, function at the intersection of the two immune systems (Gandhi et al., 2010).

T-cells are a functionally heterogeneous population of cells that express unique heterodimeric ($\alpha\beta$ or $\gamma\delta$) TCRs (Kisielow et al., 1995). Different lineages of T-cells, i.e. helper T-cells and killer T-cells, are programmed to respond to different types of antigens. Killer T-cells are the ones that recognise the specific antigens on infected cells and stimulate them to release molecules lysing the infected target cells. On the other hand, helper T-cells stimulate T-cells to release growth factors and stimulate the activity of other cells in the immune system, as antibody production in B-cells. In order to proliferate in the human body, B and T-cells need an activation signal which is normally triggered by the interaction with various antigens present on the surface of other cells. T-cells can be divided into two subsets: $CD4^+$ and $CD8^+$ T-cells. Effector $CD4^+$ cells enhance $CD8^+$ effector development via secretion of various cytokines (Gattinoni et al., 2006).

After antigen exposure, $CD4^+$ and $CD8^+$ Naïve T-cells undergo clonal expansion and differentiation into self-renewing stem cell memory T-cells. Stem cell memory T-cells have shown to be able to differentiate into T central memory, T effector memory and terminally effector T-cells. (Figure 1.1) (L. Xu et al., 2015).

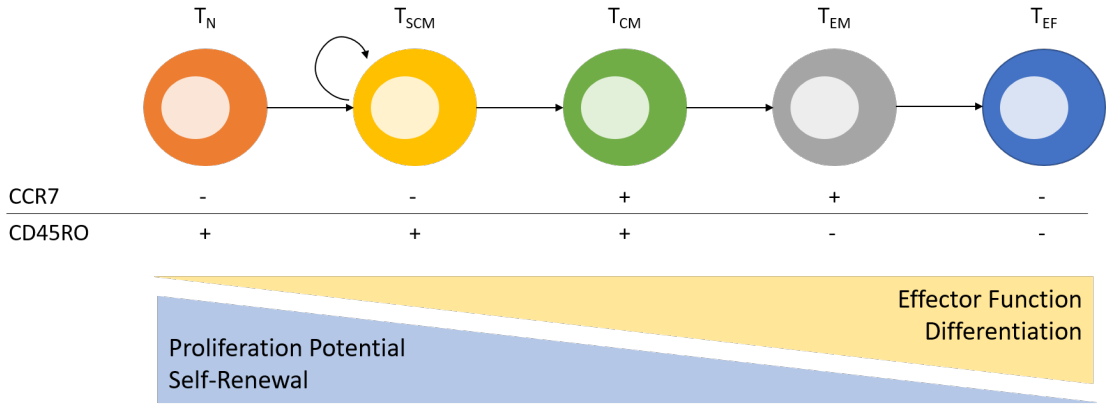

Figure 1.1: Schematic model of T-cell differentiation from Naïve (T_N), to Stem cell memory (T_{SCM}), to Central memory (T_{CM}), to Effector memory (T_{EM}) to Terminal effector (T_{TE}) T-cells. The proliferation and self-renewal potential of T-cells decreases in the more differentiate phenotype, while the effector function increases. CCR7 and CD45RO are two of the markers used to identify the differentiation stages of T-cells.

Effector T-cells are known to promote the secretion of cytokines and exhibits cytolytic activities and are undergo fast apoptosis once the antigen has been eradicated from the body. On the other hand, memory like T-cells are long-lasting cells that remain in the human body even when the antigen is not present and can undergo a rapid proliferation upon secondary challenge (Appay et al., 2008).

1.4 CAR-T cell therapies

CAR-T cell therapies combine the gene therapy and monoclonal antibodies (mAbs) specificity with the transfer of living cells in a single treatment. T-cells are genetically modified *ex-vivo* to express a CAR (e.g. anti-CD19 CAR) before being infused into the patient. Once equipped with the CAR, T-cells are able to recognise and kill the malignant cells against which the CAR was designed in the patient body (Braendstrup et al., 2020). A milestone was reached in 2017 with the FDA and EMA approval of the first two CAR-T therapies (KYMRIAH® (tisagenlecleucel) and YESCARTA® (axicabtagene ciloleucel)) for the treatment of ALL and B-cell lymphoma. These treatments are currently used for relapsed and refractory malignancies when more conventional treatments (i.e. radiotherapy and chemotherapy) fail (Khalil et al., 2015).

1.4.1 Chimeric antigen receptor

CARs are recombinant receptors that have the ability to target specific antigens (Sadelain et al., 2013). At the time of writing there are four generations of CARs (Figure 1.2).

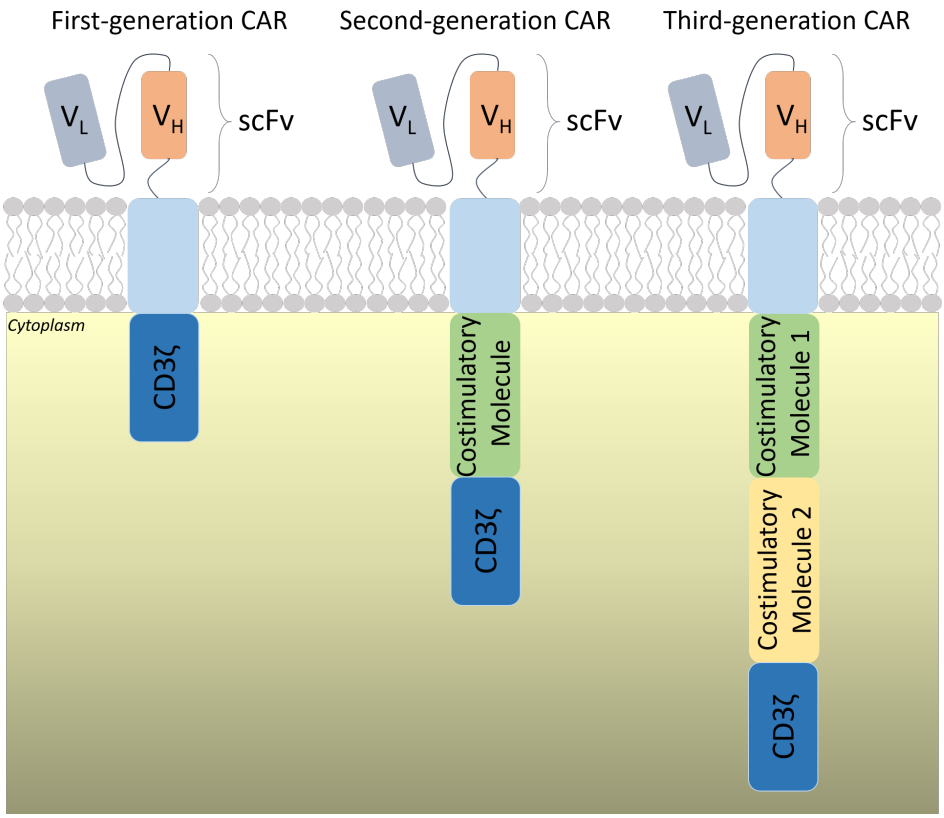

Figure 1.2: Structure of chimeric antigen receptors (CARs). First generation CARs only contain the CD3-ζ endodomain; second generation CARs contain one constimulatory domain (i.e. CD28 or 4-1BB); third generation CARs contain two costimulatory domains (e.g. CD28 and 4-1BB).

The first generation of CARs was the simplest, consisting of an extracellular antigen-binding domain (usually a single-chain variable fragment (scFv) of an antibody), which gives specificty to the CAR-T cells, and a CD3-ζ (T-cell activating domain) transmembrane domain (Sadelain et al., 2009). The T-cells equipped with the first generation CARs were not able to produce enough interleukin-2 (IL-2), which was administered separately and showed limited persistence *in vivo* (M. A. Pule et al., 2008; C. Zhang et al., 2017).

The costimulatory endodomain (e.g. CD28 or 4-1BB) was introduced in second generation CAR constructs, which have a positive effect on the proliferation, cytotoxicity and persistence of CAR-T cells *in-vivo* (Majzner et al., 2019). Second generation CARs are used in the KYMRIAH® and YESCARTA® products, using CD28 and 4-1BB as an endodomain respectively (Salmikangas et al., 2018).

Third generation CARs have been developed and they present two costimulatory domains (i.e. CD28-OX40 or CD28-4-1BB) linked to the CD3-ζ (C. Zhang et al., 2017). These CARs are believed to improve the cytokine production and therefore the potency and killing ability of CAR-T cells and they are currently being used in clinical trials (Marin et al., 2010; Enblad et al., 2018; ClinicalTrials.gov, 2020).

A fourth generation CAR, also called TRUCK, has been recently developed. In this last generation CAR, there is an additional cytokine expression cassette. The production of cytokines starts upon ligation of the CAR and can enhance the anti-tumour response of the CAR-T therapy (Cheadle et al., 2014).

1.4.2 The commercial side of CAR-T therapies

CAR-T therapy has revolutionised the field of cancer therapies, however its application is mostly limited to blood tumours in patient with relapsed or refractory malignancies. The approval of KYMRIAH® and YESCARTA® has been a significant landmark in the CGT field, but these therapies can be used on less than 5% of all cancer patients

(Sarah Nam, 2019). McKinsey & Company have estimated the global market revenues in CAR-T to reach $\sim$ \$10.4 billion by 2024.

The first non-clinical data for KYMRIAH® were published in 2008 followed by YESCARTA® non-clinical data a year later. Both therapies gained FDA approval after 8-9 years from the first published data (Elsallab et al., 2020). This highlights the long procedure from pre-clinical development to clinical trials and later commercial approval. Since then many CAR-T companies have emerged bringing the number of existing companies developing CAR-T therapies above 100 worldwide with North America being the leader on the CAR-T market.

Juno Therapeutics was in the contention for the CAR-T therapeutic market together with Novartis and Gilead, however the death of 3 patients during its ROCKET clinical trial, led to a hold imposed by the FDA. Their CAR-T product JCAR015 for refractory and relapsed ALL caused severe cerebral edema and consequent death in 3 patients in 2016 (DeFrancesco, 2016). Juno Therapeutics suggested the combination of fludara (preconditioning drug) with the CD28 co-stimulatory domain present on the CAR construct and convinced the FDA to resume the trial after only 5 days with a modified protocol. They also leveraged their argument with the data on JCAR014 product where no adverse event was seen on the 10 patients in phase I clinical trial. However, JCAR014 had a different co-stimulatory domain (4-1BB). Once the trial was resumed without the use of fludara, 2 additional patients out of the 12 treated died, due to cerebral edema.

The ROCKET trial was put on hold again and in March 2017 Juno Therapeutics announced that the development of JCAR015 would be completely discontinued (Gilbert, 2017). Novartis and Gilead are therefore the only two companies with approved CAR-T products on the market.

Although the cause of death in the ROCKET trials remains unclear, Juno Therapeutics have analysed the situation carefully trying to learn from previous mistakes. It was underlined how in the deceased patients the CAR-T proliferation reached a peak after 6-8 days, while in other therapies this peak would occur after 11-14 days. Due to the variability of the initial material, the CD4:CD8 ratio was not the same amongst the administered therapies. It was noticed that patients who received the treatment with a higher CD4:CD8 ratio were more prone to severe neurotoxicities. Furthermore, elevated level of interleukin-15 (IL-15) have been noticed in the cases of death prior to the CAR-T infusions. All the patients who passed were less than 30 years of age and they underwent 2, or less than 2 previous treatments. Juno hypothesised that their immune system was more hostile to the therapy and the neurotoxicity become fatal due to the rapid expansion of the CAR-T cells (Pharmaceutical Technologies, 2017; Gilbert, 2017).

Juno Therapeutics is currently recruiting patients for a phase I clinical trial with a new CAR-T product (JCAR017) to target Non-Hodgkin lymphoma (Table 1.3). This product is manufactured with a fixed ratio of CD4:CD8 cells and the co-stimulatory

domain used is 4-1BB rather than the CD28 used for JCAR015. This should lead to a slower expansion of the cells after infusion and limit the adverse events (Abramson et al., 2018; Gilbert, 2017). Juno Therapeutics was acquired by Celgene in January 2018 for $9 billions.

There are many relatively new companies emerging on the CAR-T market with different products undergoing clinical trials as summarised in Table 1.3. Amongst them Autolus Therapeutics was founded in 2014 in UK as a spin-off from University College London. It has been since growing and developing different CAR-T products, some of which are undergoing phase I/II clinical trials at the moment for acute lymphoblastic leukemia, Non-Hodgkin lymphoma, and diffuse large B-cell leukemia (Table 1.3). In 2017 the company secured $80 million in Series C funding.

Recently, different companies have started to look into allogeneic therapies. Some of them are Allogene Therapeutics, Atara Biotherapeutics, Cell Medica, Cellectis, Timmune Botech Inc. Other companies have introduced products for solid tumours in their pipeline (i.e. Takeda, Cellectis, Allogene Therapeutics, and Tmunity).

The biggest challenges faced by CAR-T therapies are the overly expensive (listed price for KYMRIAH® is £282,000) and complicated manufacturing and supply chain, high-touch commercial model, and reimbursement challenges. Most of the CAR-T therapies on the market and undergoing final stage clinical trials are autologous (Depil et al., 2020). The manufacturing of these therapies is centralised, uses clean rooms and it

is far from the environment in manufacturing plants for large scale production. These challenges have set the high cost of CAR-T therapies and need to be tackled in order to make them broadly available and less expensive. Furthermore, the level of training needed at the centres where these therapies are administered is also significant, with standard operating procedures that may vary from one center to the other (Xiuyan Wang et al., 2016; L. Taylor et al., 2019). The reimbursement of these therapies is also uncertain. Medicare & Medicaid Services are yet uncertain and their reimbursement polices are not clear (C. Jacobson et al., 2019). After reaching a deal with Novartis and Kite-Gilead in September and October 2108 respectively, the National Health Service (NHS) has authorised 9 hospitals for the administration of CAR-T therapies for ALL and 7 hospitals for the administration of DLBCL in the UK.

CAR-T therapies need large investments to fill existing gaps and overcome current barriers. Solid tumors are the next frontier for CAR-T therapies (Xiuyan Wang et al., 2016). The need for strong academic-clinical partnership is needed to progress in this field. We have already seen the partnership between University of Pennsylvania and Novartis in 2012, which led to the FDA approved therapy KYMRIAH® in 2017. In 2013 Celgene and Bluebird Bio announced a collaboration on gene therapy in oncology, with the main focus being CAR-T therapies. This was followed, in 2014, by the collaboration between Pfizer and Cellectis to develop novel CAR-T technologies. Pfizer gained the access to the allogeneic approach from Cellectis, who received an upfront payment of

$80 million. In January 2015, Amgen and Kite stipulated a collaboration agreement that combines Amgen's oncology targets and Kite's CAR-T platform to advance in the field (Walker et al., 2016).

Table 1.3: Products undergoing clinical trials from different CAR-T companies. NHL = Non Hodgkin Lymphoma; ALL = Acute Lymphocytic Leukemia; AML = Acute Myeloid Leukemia; NSCLC = Non Small-Cell Lung Carcinoma; DLBCL = Diffuse Large B-cell Leukemia; MM = Multiple Myeloma; PSMA = Prostate-Specific Membrane Antigen; GPC2 = Glypican 2; DLL3 = Delta-like Protein 3.

Company	**Product Name**	**Disease**	**Clinical Trial Phase**	**Target**
Juno Therapeutics	JCAR017	NHL	Phase I	CD19
Juno Therapeutics	JCAR014	NHL	Phase I	CD19
Juno Therapeutics	JCAR018	NHL	Phase I	CD22
Juno Therapeutics	JCAR018	Pediatric ALL	Phase I	CD22
Juno Therapeutics	JCAR016	AML	Phase I/II	WT1
Juno Therapeutics	JCAR016	NSCLC, Neuroblastoma	Phase I	WT1
Juno Therapeutics	JCAR023	Pediatric Neuroblastoma	Phase I	CD171
Juno Therapeutics	JCAR020	Ovarian Cancer	Phase I	MUC16ecto
Juno Therapeutics	JCAR024	NSCLC, Triple Negative Breast Cancer	Phase I	ROR1
Autolus Therapeutics	AUTO1	ALL	Phase I	CD19
Autolus Therapeutics	AUTO3	R/R Pediatric ALL	Phase I/II	CD19 & CD22
Autolus Therapeutics	AUTO3	DLBCL	Phase I/II	CD19 & CD22
Autolus Therapeutics	AUTO4	NHL	Phase I/II	TRBC1

Company	Product Name	Disease	Clinical Trial Phase	Target
Allogene Therapeutics	UCART19	ALL	Phase I	CD19
Allogene Therapeutics	ALLO-501	NHL	Phase I	CD19
Allogene Therapeutics	ALLO-715	MM	Phase I	BCMA
Cell Medica	CMD-501	Neuroblastoma	Phase I	GD2
Cell Medica	CMD-502	Haematological Malignancies	Phase I	CD19
Timmune Biotech	TI-1007 CAR-T	Haematological Malignancies	Entering Phase I	CD19
Tmunity	PSMA CAR-T	Metastatic Castrate-Resistant Prostate Cancer	Phase I	PSMA
Tmunity	TnMUC1	Advanced TnMUC1 Positive Solid Tumours	Phase I	TnMUC1
Tmunity	GPC2 CAR-T	Neuroblastoma, neuroendocrine	Phase I	GPC2
Novartis	Kymriah	Lymphoma (new indication)	Phase I	CD19
Celgene	ide-cel	R/R Multiple Myeloma	Phase II/III	BCMA
Celgene	orva-cel	R/R Multiple Myeloma	Phase I	BCMA
Celgene	bb21217	R/R Multiple Myeloma	Phase I	BCMA
Celgene	liso-cel	R/R DLBCL	Phase II	CD19
Amgen	AMG 119	Small-Cell Lung Cancer	Phase I	DLL3

Despite the significant progress in the CAR-T field, there is no real standardisation in the process used to manufacture CAR-T therapies. The initial number of cells varies due to the leukapheresis collection and intrinsic variability of the starting material. There are no established guidelines on the number of the target cells required. Furthermore, different therapies are manufactured using different raw materials and different systems, which are not directly comparable. Often the manufacturing process is not disclosed by the producer, making it impossible to have a standardised process that would allow for a less variable final product (Vormittag et al., 2018).

The manufacturing process needs to be modified, automated, and cell production should be either scaled-up or out. A decentralised manufacturing model (scale-out) could also reduce the manufacturing cost, cutting on the logistics, and reducing the vein-to-vein time of the product. However, this would require the use of GMP-in-a-box solutions that are currently not available for such therapies (Xiuyan Wang et al., 2016; Vormittag et al., 2018). The onset of allogeneic therapies could also provide significant advantages. The manufacturing process could be scaled-up reducing the cost of goods, allogeneic therapies would imply a reduced product variability, and shorten the waiting time for drug administration, being an off-the-shelf therapy (Sarah Nam, 2019). Even after the manufacturing has been improved, the cost for autologous CAR-T cells will likely be in the \$25-35,000 range per treatment, which will be significantly increased ($\sim$ \$300,000) if pre-treatments are considered (Walker et al., 2016).

1.4.3 Therapeutic potential and limitations of CAR-T therapies

The manufacturing process of CAR-T cells therapies starts with T-cell collection from the patient or donor via leukapheresis. The cells are then genetically modified to express a CAR receptor, which recognises a specific antigen expressed on the surface of the malignant cells the therapy wants to target. The first step for an efficacious treatment requires to identify an appropriate target for the CAR, which would ideally be expressed only on the malignant cells and not by healthy tissues. Furthermore, the chosen target must be essential for the tumour survival in order for the therapy to be efficacious (Filley et al., 2018).

YESCARTA® and KYMRIAH® both target CD19 malignancies with a second-generation CAR. CD19 is a marker expressed also by healthy B-cells, however no other healthy tissue expresses it. The depletion of healthy B-cells during the therapy does not lead to a therapy-limiting toxicity (Porter et al., 2011). CD19 CAR-T therapies showed a response rate of 80% in patients with ALL and a durable clinical benefit in patients with CLL and Non-Hodgkin lymphoma (Davila et al., 2014; Kochenderfer et al., 2012; Geyer et al., 2016; Gardner et al., 2017). Furthermore, positive outcomes have been shown in phase I clinical trials for multiple myeloma targeting B-cell maturation antigen (BCMA) (Raje et al., 2019).

For a successful treatment, CAR-T cells must expand and persist in the patient. Prior to CAR-T cell infusion, patients need to undergo lympho-depleting chemotherapy,

which has proven to enhance efficacy of the therapy (Brentjens et al., 2011; Cruz et al., 2013). The majority of clinical studies up to date have administered a pre-determined number of CAR-T cells per dose, however no limitations were imposed on the immunophenotype of T-cells (Brentjens et al., 2013; D. W. Lee et al., 2015; Brentjens et al., 2011). $CD4^+$ and $CD8^+$ T-cell subsets are known to have different roles. $CD8^+$ CAR-T cells have direct lytic activity, thier memory sub-populations have been shown to have a greater anti-tumour potency compared to more differentiated phenotypic profiles (i.e. effector T-cells). On the other hand, $CD4^+$ CAR-T cells are capable of producing greater amount of interferon (INF)-γ, tumour necrosis factor (TNF)-α, and interleukin (IL)-2, which help the cytotoxic activity of $CD8^+$ CAR-T cells (Geyer et al., 2016). Studies in patients with B-ALL (Phase I/II clinical trial) and B-NHL have shown benefit when infused with 1:1 $CD4^+$:$CD8^+$ CAR-T cell ratio, suggesting a better defined product could decrease the number of cells per dose needed and lead to improved results (Sommermeyer et al., 2016; Turtle et al., 2016; Turtle et al., 2015).

Although the recent FDA approval of two CAR-T therapies and numerous ongoing clinical trials, there are still limitations and side effects to be solved. Poor CAR-T cell expansion *in vivo* has been partially addressed with second and third generation CARs adding different costimulatory domains. One of the main causes for relapse in B-cell malignancies is due to the so called antigen escape, where there is a loss of CD19 receptor on previously CD19 positive B-cells (Geyer et al., 2016). Cytokine release

syndrome (CRS) and neurotoxicity also occur in a high number of treated patients and could be life-threatening (Turtle et al., 2016; Jae Hong Park et al., 2016; Turtle et al., 2017; Neelapu et al., 2017; Schuster et al., 2017). CRS is caused by the release of inflammatory cytokines after the infusion of CAR-T cells associated with cell proliferation and activation, while the causes for neurotoxicity are less clear (Brudno et al., 2019; Maude et al., 2014). CRS is the most common severe toxicity and results in high fevers, sinus tachycardia, hypotension, vascular leak, hypoxia, cardiac and renal insufficiency (Maude et al., 2014; D. W. Lee et al., 2015). A greater incidence of CRS has been observed in patients with higher CAR-T cell dose and in patients with higher disease burden (Jae Hong Park et al., 2016; N. V. Frey et al., 2016; Neelapu et al., 2018). Not all of the tumour defense mechanisms have been fully understood and, although CRS and neurotoxicity have been related to the administered dose of CAR-T cells, more studies need to be carried out in order to fully understand and overcome these limits.

1.4.3.1 CAR-T therapies for solid tumours

CAR-T cell products have been used in a number of clinical trials against glioblastoma, gastrointestinal cancers, genitourinary cancers, breast cancer, and lung cancer (Q. Zhang et al., 2016; Newick et al., 2017). The identification of an appropriate target is not easy due to the lack of uniformly expressed antigens in solid tumours or the presence of the same antigen on healthy tissues. Some target antigens (i.e. carcinoembryonic antigen (CEA), human epidermal growth factor receptor 2 (HER2), epidermal growth factor

receptor (EGFR), mesethelin, and prostate specific membrane antigen (PSMA)) used in clinical trials are still present in low levels on healthy tissues (Bagley et al., 2020). On-target off-tumour toxicity has been one of the main challenges in solid tumours and it can be life threatening for the patient (Morgan et al., 2010; Richman et al., 2018; Bagley et al., 2020). Multiple solutions have been tried to overcome this limit, (1) two CARs expressed on the same T-cells in order to activate the T-cells only in presence of two antigens, (2) using CARs which can be activated only by an exogenously administered stimuli, and (3) CARs which keep the T-cells in an 'off-state' until the cells reach the tumour site (Kakarla et al., 2014; Bagley et al., 2020). A further challenge is posed by the fact that CARs can only target surface antigens while only 1% of all the proteins is expressed on the cell surface. This significantly reduces the available target antigens (Walseng et al., 2017).

The success of solid tumour therapies depends on CAR-T cells migrating to the tumour site, which is usually not found on routine T-cell migration routes (peripheral blood, lymph nodes, and bone marrow) (Filley et al., 2018). Direct injections of CAR-T cells to the tumour site could overcome this issue and are currently being assessed for ovarian cancer in a clinical trial (Bagley et al., 2020).

Finally, after successful trafficking to the tumour site, CAR-T cells must undergo rapid expansion and persist in patients despite the hostile solid tumours micro-environment (TME) (Martinez et al., 2019; Hanahan et al., 2012; Oliver et al., 2018). Tumours are

known to express checkpoint ligands (i.e. programmed death protein 1 (PD-1), PD-L1, T-cell immunoglobulin and mucin-domain containing-3 (TIM3), and lymphocyte activation gene 3 (LAG3)) which suppress the function of immune cells. CARs to enhance the survival of CAR-T cells in hypoxic TME have been designed (Ligtenberg et al., 2016; Juillerat et al., 2017).

Progress has been made in the past years for solid tumours, and more and more products are entering clinical trials (Hou et al., 2019). However, CAR-T therapies for solid tumours have not shown the same efficacy as the one developed for liquid tumours mainly due to the limits listed above (i.e. finding an appropriate target, trafficking to the tumour site, expansion, and persistence). Further studies and better understanding of the mechanism of action need to be undertaken in order to reach a turning point in this field.

1.4.4 Autologous vs. allogeneic CAR-T

KYMRIAH® and YESCARTA® both use patient-derived autologous second generation CAR-T cells. These therapies require a tailored process for each patient's starting material, which can substantially differ form one another having a negative impact on the cost of manufacturing. Furthermore, due to the length of the current production of each therapy (approximately 3 weeks), the delay in the availability of the process might become a life-threatening issue for patients with acute malignancies (Depil et al.,

2020). Autologous derived CAR-T cells efficacy *in vivo* can also be impaired due to tumour suppression mechanisms making the treatment unsuccessful (Thommen et al., 2018). Furthermore, in some cases, the activation, transduction, and expansion of autologous CAR-T cells might be sub-optimal and the cell number for a single dose can not be reached. In this cases the final product can not be administered to the patient (Salmikangas et al., 2018).

These are the main reasons behind the increasing number of allogeneic off-the-shelf CAR-T products in companies pipelines. An increased number of allogeneic CAR-T treatments are entering clinical trials and generating early results (Table 1.4).

The advantages of having off-the-shelf products are multiple. CAR-T cell products starting from healthy donor material could potentially bring down the cost for these therapies as the current manufacturing process can be scaled-up. Several doses can be produced from a single donor and a careful donor selection would also allow for a standardisation of the manufacturing process and of the final product, limiting the heterogeneity brought in by patient material. Furthermore, allogeneic therapies would make CAR-T immediately available for patients, and because of the larger production, re-dosing would become possible for patients that need it. An allogeneic approach would also allow for the administration of CAR-T cells engineered against different antigens (Depil et al., 2020).

Table 1.4: Ongoing clinical trials for allogeneic CAR-T therapies. KO = knock out; MHC = major histocompatibility complex; PD-1 = programmed death protein 1; TALEN = transcription activator like effector nuclease; TRAC = T-cell receptor-α chain. Table adapted from Depil et al., 2020.

Developer & *Name of the Product*	**Target Antigen**	**Allogeneic Technology**	**Tools for Genetic Modification**
Allogene Therapeutics & Servier *UCART19*	CD19	TRAC KO with or without CD25 KO	TALEN mRNA (KO)
Cellectis *UCART-123*	CD123	TRAC KO	TALEN mRNA (KO)
Celyad *CYAD-101*	NKG2D	TRAC-inhibitory molecule peptide	Retroviral vector
Chinese People's Liberation Army General Hospital UCART019	CD19	TRAC and B2M KO	CRISPR/Cas9 (KO)
Chinese People's Liberation Army General Hospital *Mesothelin CAR T cells*	Mesothelin	TRAC and PD1 KO	CRISPR/Cas9 (KO)
Chinese People's Liberation Army General Hospital *Universal dual-specificity CD19 and CD20 or CD19 and CD22 CAR T cells*	CD19 and CD22 or CD19 and CD20	TRAC KO	CRISPR/Cas9 (KO)
Precision Biosciences & Servier *PBCAR-0191*	CD19	TRAC KO; CAR at the TRAC locus	Meganuclease mRNA (KO); AAV6
Shanghai Bioray Laboratory *CD19 UCART*	CD19	TRAC and MHC class I KO	CRISPR/Cas9

However, allogeneic CAR-T therapies also face two major issues. First, allogeneic CAR-T cells can cause graft-versus-host disease (GVHD), putting the patient's life at danger (Y. Yang et al., 2015). The second issue that needs to be addressed is the persistence of allogeneic CAR-T cells in the patient body after infusion. It has been shown

that the host immune system can eliminate the injected cells in a short amount of time, limiting their anti-tumour activity (Anwer et al., 2017).

1.4.4.1 Graft-versus-host disease (GVHD)

GVHD occurs when there is a mismatch between donor and patient major histocompatibility complex (MHC) molecules, also called human leukocyte antigen (HLA) in humans. The foreign MHC is recognised by the TCR expressed on patient's $\alpha\beta$ T-cells and is the main cause for GVHD and transplant rejection (Ren et al., 2017). In order to prevent the GVHD post allogeneic CAR-T cell infusion different approaches have been implemented: deletion of the TCR using gene editing methods, use of T-cells that do not express the TCR (i.e. $\gamma\delta$ T-cells), and the use of virus-specific T-cells (Depil et al., 2020). Furthermore, different cell types such as NK cells therapies have been developed for cancer therapy. Allogeneic CAR-NK cells do not cause GVHD (Lim et al., 2015).

The predominant solution adopted in most clinical trials (Table 1.4) is the gene editing to prevent the expression of the TCR on $\alpha\beta$ T-cells. Due to the conformation of the α and β chains, the first one is easier to target and disrupting the gene encoding for the TCRα chain (TRAC) is a widely used method to disrupt the TCR and prevent GVHD (Torikai et al., 2012; Ren et al., 2017). Transcription activator like effector nuclease (TALEN) technology has been used to cut specific DNA sequences and create off-the-shelf CAR-T products (Qasim et al., 2017). A multiplex gene editing approach has been adopted by various groups simultaneously electroporating TALENs that tar-

get different genes (i.e. TRAC and CD52) (Poirot et al., 2015). Current studies using TALEN-mediated gene editing of the TRAC show approximately 80% of the cells lack the expression of the TCR after genetic modification. The 20% of the T-cells still expressing the TCR need to be magnetically removed in order to minimise the incidence of GVHD.

Another approach widely used for the production of gene modified off-the-shelf CAR-T therapies is the CRISPR/Cas9 system (Eyquem et al., 2017; Salas-Mckee et al., 2019; Stadtmauer et al., 2020). It relies on RNA-DNA base pairing, where a single guide RNA (sgRNA) is appositely designed to pair to the target DNA and cleave it (Mali et al., 2013).

1.4.4.2 Allogeneic CAR-T persistence *in vivo*

It has been shown that for autologous therapies the remission of the tumour is correlated with the persistence of CAR-T cells in the patients (Kochenderfer et al., 2012). However, it is not yet clear what is the optimal persistence and it may differ from disease to disease, tumour burden, and the potency of the administered cells (Guedan et al., 2018). Autologous CAR-T therapies have already proven efficacious, while one of the main limits of allogeneic CAR-T therapies remains the poor persistence shown in the first clinical trials. However, due to the nature of the therapy, the allogeneic products can be re-administered to the patients if needed, aiming at maintaining a sufficient number of CAR-T cells in the patient body (Depil et al., 2020).

Although it is not yet clear what is the optimal population mix of CAR-T cells, different studies have shown that T-cells with a less differentiated phenotype (i.e. T-naïve cells and stem cell-like memory T-cells) are fundamental for *in vivo* expansion and long-term persistence in the patient (Berger et al., 2008; Gattinoni et al., 2011; Gattinoni et al., 2005). The cells derived from the patients often have a higher incidence of more differentiated T-effector memory cells, due to the chemotherapy administered (Busch et al., 2016). Therefore, using healthy donors might be a significant advantage considering the fact that donors with a high frequency of less differentiated T-cells types can be selected. It would then be necessary to control the manufacturing of these allogeneic CAR-T therapies in order to retain a less differentiated phenotype in the final product. The maximum length of the expansion process in order not to compromise the potency of the therapy due to a too differentiated profile of the CAR-T cells is yet to be determined (Kaartinen et al., 2017). This will further influence the scale at which these therapies could be manufactured and the number of batches that can be produced from the starting material of a single healthy donor.

1.4.4.3 Future perspectives

To sum up, allogeneic therapies could significantly bring down the cost of manufacturing for CAR-T cell therapies. The GVHD and persistence of such products need to be further addressed and definitive solutions to mitigate risk for the patients need to be found. The fact that an increasing number of companies are looking into the off-the-

shelf CAR-T products (Table 1.4) indicates the potential of allogeneic therapies, which could revolutionise the current manufacturing process.

Manufacturing failures due to poor patient starting material would be ruled out as the starting material coming from healthy individuals can be carefully selected. The product would be immediately available, avoiding severe consequences for patients with acute diseases that can lead to death while the autologous therapies are being manufactured. The manufacturing process for allogeneic therapies would need to be scaled-up rather than scaled-out and re-dosing would become possible in case of need.

Furthermore, careful picking of the healthy donors will allow to have more control over the final product composition in terms of T-cell immunophenotype, resulting in a more standardised treatment.

1.5 Manufacturing of CAR-T therapies

The manufacturing of CAR-T products requires different steps and may take several weeks, 22 days in the case of Novartis KYMRIAH® (Tyagarajan et al., 2019). The first step is to collect the patient's (in case of autologous CAR-T therapy) or donor's (for allogeneic therapies) peripheral blood via leukapheresis. This is then followed by an *ex-vivo* enrichment and expansion of T lymphocytes. The T-cells are activated and genetically modified, using viral (i.e. γ-retroviral or lentiviral vectors) or non-viral (i.e. mRNA electroporation, DNA or RNA trasposons systems) methods for the expression of the CAR or for gene silencing (M. H. Wilson et al., 2007; Kebriaei et al., 2016; Eyquem et al., 2017; Ren et al., 2017; Stadtmauer et al., 2020). The CAR-T cells are then expanded *ex-vivo* until the required number of cells for the administration is reached. The product gets then prepared for the infusion into the patient and cryopreserved for the shipment. The CAR-T cells need then to be transported to the site where the infusion is happening, thawed and infused in the patient (Figure 1.3). Once in the patient body CAR-T cells are able to target and eradicate malignant cells that express the antigen targeted by the CAR construct (Xiuyan Wang et al., 2016).

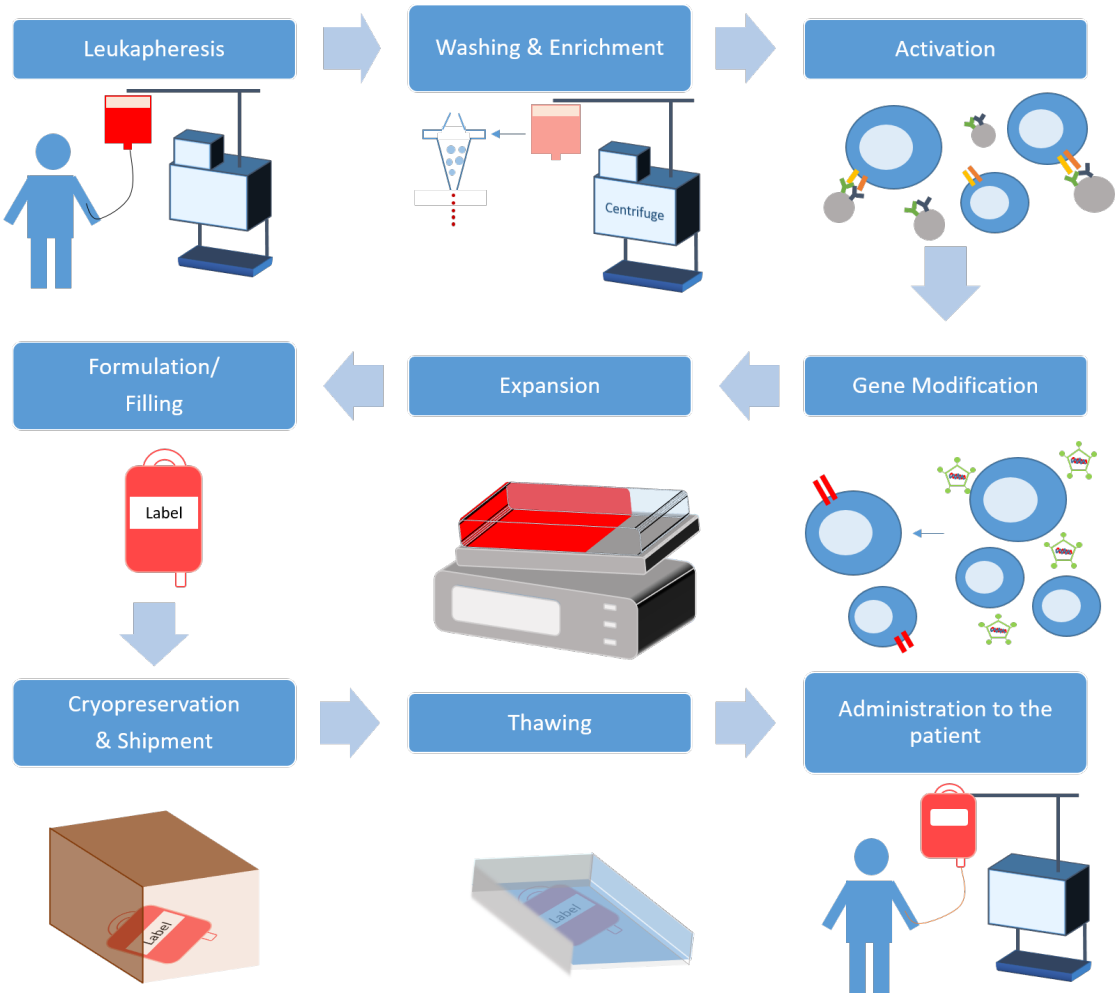

Figure 1.3: Flow diagram of the CAR-T cells manufacturing process. Starting from the leukapheresis product, the T-cells are washed and enriched, activated, genetically modified, and expanded. This is followed by the formulation/filling step, CAR-T cells are cryopreserved, shipped to the final site, thawed and administered to the patient.

1.5.1 Leukapheresis, washing, and enrichment

The leukapheresis collection takes place at specialised sites and its duration varies depending on different factors, such as: machine used and its efficiency, number of target cells in the blood, patient weight and number of cells wanted. Apheresis machines al-

low to separate and collect leukocytes form the patient or donor blood and return the rest of the blood into circulation. The collection and processing of the leukapheresis further contributes to the high starting material variability, which is one of the main issues in the CAR-T cell manufacturing (B. Levine, 2015). The apheresis product is then processed in different ways, depending on the desired starting material for the manufacturing process, which can require PBMCs or purified T-cells (Xiuyan Wang et al., 2016). The product it is also washed in order to remove anticoagulant, red blood cells and platelets (B. Levine, 2015).

There are different machines available on the market for the enrichment and washing steps. The LOVO Cell Processing System (Fresenius Kabi), COBE 2991 cell processor (Terumo BCT), and Cell Saver® 5+ (Haemonetics) have the ability to remove the red blood cells and platelets and to concentrate, dilute or wash the product. The Terumo Elutra® counter-flow centrifugal elutriation system and the Biosafe Sepax allow for the isolation of leukocytes based on size separation (Fesnak et al., 2017). Furthermore, the CliniMACS Prodigy® enables the enrichment of specific T-cell subsets via magnetic separation following the washing steps (Xiuyan Wang et al., 2016).

1.5.2 Activation methods

After the enrichment and washing steps T-cells need to be activated in order to start the expansion phase *ex vivo*. Until activated, T-cells are in a quiescent state and require low

amount of metabolic activity (L. Almeida et al., 2016). In order to be activated T-cells require a CD3 proliferative signal together with a costimulatory signal (i.e. CD28 costimulatory signal). T-cells can be activated via soluble anti-CD3 mAbs in combination with IL-2 (Vormittag et al., 2018). Co-culture with antigen presenting cells (APCs) cells such as dendritic cells has also been used for T-cell activation. However, these methods are not practical, the process is hard to scale-up and inconvenient for clinical settings, which leads to a very high cost and to a time consuming process (Xiuyan Wang et al., 2016; B. Levine, 2015). The industry has therefore moved towards antibody coated paramagnetic beads (i.e. Dynabeads®). These beads have a diameter of ~ 4.5 μm and are coated with anti-CD3 and anti-CD28 mAbs which stimulate the proliferation of primary T-cells in culture (B. Levine, 2015). Dynabeads® need to be removed at the end of the culture using a magnet. Furthermore, in order to achieve an effective activation and proliferation of the T-cells, Dynabeads® need to be well suspended and interact with the cells in non-static environments, as for example WAVE bags and stirred-tank bioreactors (Costariol et al., 2019).

Other activation methods are present on the market, as for example the Miltenyi TransAct™ CD3/CD28 polymeric nanomatrix coated particles. They have the advantage of being degradable and therefore do not require for a removal step at the end of the culture. Studies have shown that the proliferation of T-cells results comparable when using TransAct™ or Dynabeads® (Wang et al., 2015). On the other hand, a

study by Mock et al. (2016) showed a significantly higher expansion rate when using Dynabeads® compared to the TransAct™ technology.

Thermo Fisher Scientific, the Dynabeads® producer, has signed a seven-year CAR-T teach nonexclusive licensing deal with Juno Therapeutics and Novartis in 2018 (Flora Southey, 2018). This made Dynabeads® an appealing activation method for many CAR-T product developer; despite the need to remove the beads at the end of the culture they are still the most used activation method in clinical trials and currently used in the manufacturing of both KYMRIAH® and YESCARTA® (Vormittag et al., 2018; Mock et al., 2016).

However, the difficulty with removing the Dynabeads® at the end of the manufacturing process has resulted in other companies and research groups to develop innovative activation methods that are easily removable without the need of additional steps. One example is the Cloudz™ T-cell activation Kit developed by Quad Technologies and acquired by Bio-Techne in 2018 (Hippel, 2018). Cloudz™ are dissoluble micro spheres fictionalised with human anti-CD3 and CD28 antibodies. At the end of the T-cell expansion, the Cloudz 6X Release Buffer can be added directly to the culture media and will rapidly dissolve the Cloudz™ without the need of additional steps.

Although Dynabeads® are still widely used in the CAR-T industry, there is a need for more advanced technologies that allow an easier removal at the end of the expansion phase. Some of these technologies include the Miltenyi TransAct™ and the recently

developed Cloudz™ by Bio-Techne, both made of dissoluble matrices.

1.5.3 Gene delivery and gene-editing tools for CAR expression

Different gene-editing tools have been used for the CAR expression and/or for gene knockout or silencing. Gene editing tools can be divided in viral and non-viral. The two FDA approved CAR-T therapies, KYMRIAH® and YESCARTA®, both use viral vectors for the expression of the CAR. Viral vectors are the most common gene-editing tool for CAR expression in commercialised product and for products in clinical trials (Food and Drug Administration, 2019; M. C. Milone et al., 2018; Tipanee et al., 2017).

γ-retrovirus was the first type of viral vector used to transduce T-cells (Xiuyan Wang et al., 2016), however lentiviral vectors have many advantages over γ-retroviruses. They can integrate in the genome of non-dividing cells and present a lower risk of insertional mutagenesis due to their tendency to integrate away from host promoters compared to the γ-retroviruses (Vannucci et al., 2013). Despite their high and stable transduction efficiency, both viral vectors are expensive to produce and require intensive biosafety testing (B. Levine, 2015). Viral vectors need to be produced under good manufacturing practice (GMP) conditions in separate clean rooms adding to the final cost of CAR-T therapies (Vormittag et al., 2018). Different lots of lentiviral vectors are likely to have a different performance, increasing the variability in the final product (Gee, 2018). These are some of the reasons behind the interest and initial transition towards non-viral gene-

editing tools for CAR expression and gene silencing (P. V. R. Manuri et al., 2010; H. Singh et al., 2013).

Non-viral gene-editing tools are considered to be safer, easier to manufacture and scale-up compared to viral-vectors (S. Li et al., 2006). Up to date non-viral methods have been mostly used as gene-editing tools in allogeneic CAR-T therapies for gene knockout and silencing (Depil et al., 2020; Stadtmauer et al., 2020). However, non-viral gene-editing for CAR integration has been explored (Monjezi et al., 2017; P. V. R. Manuri et al., 2010; Huang et al., 2008; S. Gonzalez et al., 2004). Electroporation of naked DNA or plasmid-based trasposone/transposase systems are commonly used for non-viral gene delivery (Vormittag et al., 2018). Electroporation causes transient disruption of the cell membrane due to cell exposure to an electric field. Charged molecules, such as DNA and RNA are therefore able to enter into the cell cytoplasm. The membrane is then restored within a few hours and the DNA or RNA integrates in the cell genome (Chicaybam et al., 2013).

The more commonly used technologies for gene-editing are Zinc-finger nucleases (ZFNs), TALENs, CRISPR/Cas9 system, Sleeping Beauty (SB) and PiggyBac (Depil et al., 2020; Themeli et al., 2015; Vormittag et al., 2018; Gee, 2018). The ZFN can be designed using three to six zinc-finger units to cleave a specific domain on double-stranded DNA in order to remove an unwanted gene. TALENs are composed of a catalytic domain (*Fok-I*) and a transcription activator-like effector (TALE) DNA binding-domain.

ZFN and TALENs are mainly used for gene knockout (Depil et al., 2020). The CRISPR system is derived form a microbial adaptive immune system. This system works in combination with a nuclease (Cas9 is the most commonly used) and a short RNA. The specificity of the CRISPR system relies on RNA-DNA base paring. The Cas9 nuclease generates blunt ends in contrast with all the above mentioned nucleases (Depil et al., 2020). The SB transposon/transposase system can be used to integrate the gene of interest in the genome (i.e. CAR). The PiggyBac system recognises transposon-specific inverted terminal repeats (ITRs) and integrates DNA into the genome at TTAA sites. Furthermore, using transposon/transposase system, such as the PiggyBac system, larger constructs can be integrated in the genome compared to the ones allowed by viral-vectors ($\sim$ 10kB base pairs) (Ptáčková et al., 2018).

SB has shown lower risk for instertional oncogenesis compared to the PiggyBac system. SB systems have also shown promising results in CAR-T cells therapies and has been used for gene-editing of CAR-T cells in clinical trials (Kebriaei et al., 2014; H. Singh et al., 2015).

1.5.3.1 Future perspective

Viral vectors have been widely used and they integration has been studied in depth. Their mechanism of action is well understood and viral vectors are approved by FDA and EMA for current therapies. Viral vectors are also known to have a high transduction efficiency (from 30% to 80%), however they are significantly more expensive than

non viral vectors (Vormittag et al., 2018; Z. Zhang et al., 2018). Moving away from viral vectors will therefore bring down the manufacturing costs for the manufacturing of CAR-T therapies. Current non-viral methods have lower efficiencies compared to viral transduction and have been mainly used for gene silencing and knockout rather than for CAR expression (Ramamoorth et al., 2015). However the increasing interest in non-viral gene-editing tools and constant development in the field suggest that the next generation of CAR-T therapies could move away from viral vectors and prefer non-viral gene-editing tools for CAR expression and gene silencing, when needed.

1.5.4 Expansion methods

Once T-cells have been enriched, activated, and genetically modified they need to be expanded *in vitro* in order to reach the wanted target dose numbers (Table 1.5). CAR-T cell therapies currently fall under the category of 'personalised medicines'. This implies that only one batch is released from each expansion process and there is no need to scale it up. However, once the therapies reached the market, it was soon realised that the cost of manufacturing is not sustainable. Strategies to scale-up or scale-out the process need to be put in place in order to reduce the manufacturing cost and make these therapies accessible to a wider public.

Table 1.5: The target dose and the maximum total number of CAR positive viable T-cells injectable in patients treated with the two FDA approved CAR-T products - YESCARTA® and KYMRIAH®. Data retrieved from Food and Drug Administration, 2019.

CAR-T Product	Target dose (CAR positive viable T-cells)	Maximum Total Number of CAR positive viable T-cells per dose
YESCARTA®	2 x 10^6 per kg of body-weight	2 x 10^8
KYMRIAH® for paediatric & young adult B-cell ALL (up to 50 kg of weight)	0.2 - 5 x 10^6 per kg of body-weight	2.5 x 10^8
KYMRIAH® for paediatric & young adult B-cell ALL (above 50 kg of weight)	0.1 - 2.5 x 10^8 (irrespective of body-weight)	2.5 x 10^8
KYMRIAH® for adult relapsed or refractory diffuse large B-cell lymphoma	0.6 - 6 x 10^8 (irrespective of body-weight)	6 x 10^8

Until now, most of the expansion platforms used have been adapted from other cell types rather than being specifically designed for T-cells. Therefore, different steps need to be carried out in different vessels. This requires the transfer of material from one system to another in expensive clean room facilities. The operators need to be highly skilled and experienced and the open nature of the process implies there is a risk for contamination (Vormittag et al., 2018). Small-scale production of CAR-T cells is currently performed or at least started in static cell expansion platforms, e.g. T-flasks, gas-permeable gas, and G-Rex vessels. These systems require frequent manipulation (except for the G-Rex) and are difficult to scale (Xiuyan Wang et al., 2016).

The only fully closed system available on the market is the CliniMACS Prodigy®, which makes isolation, activation, transduction, and expansion possible in a single plat-

form. Closed all-in-one systems such as Octane Cocoon™ (Lonza) and the Quantum® Cell Expansion System (Terumo BCT) have been recently launched in the market. The implementation of manufacturing in completely closed systems would allow to move from a class 100 (ISO 5) environment to a class 10 000 one (ISO 7), reducing the clean room cost (Dai et al., 2019). However, the majority of CAR-T products manufactured for clinical trials and commercialisation use a rocking motion bioreactor (Xiuyan Wang et al., 2016; Vormittag et al., 2018).

As identified in Table 1.5, the target dose for CAR-T therapies is in the range of 2-6 x 10^8 viable CAR-T cells for each infusion. This highlights the need for effective expansion methods, moving away from platform with a limited potential for scale-up. Scalable expansion systems will enable multiple doses being manufactured in a shorter time making the therapies promptly available for critical patients. The shorter expansion time will also limit the differentiation of CAR-T cells and will result in a potentially more efficacious *in vivo* treatment (Gattinoni et al., 2005).

1.5.4.1 T-flasks, gas permeable bags and G-Rex

T-flasks, gas permeable bags and G-Rex vessels are commonly used platforms for the expansion and production of small-scale CAR-T therapies, with 22% of the products still manufactured in T-flasks and 35% in gas permeable bags (Vormittag et al., 2018).

T-flask are the most traditionally used culture platforms for a variety of cell types,

and therefore it is not surprising that they have been used for the expansion in many CAR-T clinical trials. They are completely static platforms where the mass-transfer occurs only on the gas-liquid interface, which results to be highly inefficient and limits the achievable cell number and fold expansion. T-flask also require frequent manipulation by trained operators and expensive clean room space, as multiple flasks are required for a single dose production (Mizukami et al., 2020). All this affects the cost of the manufacturing process, where T-flasks have been shown to be significantly more expensive compared to gas permeable bags and rocking motion bioreactors (Jenkins et al., 2018).

Gas permeable bags, made of flexible polymers, can be operated in a semi-closed manner with a needle access for cell sampling and media addition or exchange (Mizukami et al., 2020). The mass-transfer is improved compared to the T-flasks, since the whole surface area of the bag allows for the transfer of oxygen, carbon dioxide, and nitrogen (Fekete et al., 2018). Gas permeable bags can be used for T-cell trasduction as well, avoiding the trasfer of the material from one vessel to another. Tumaini et al. (2013) reported a fold expansion of CAR-T cells in permeable bags in the range of 8-14 using a 13-days expansion protocol. The same manufacturing process has then been used in multiple CD19 CAR-T clinical trials (D. W. Lee et al., 2015; Stroncek et al., 2016). Although Vormittag et al. (2018) reported 35% CAR-T cells for clinical trials being manufactured in permeable bags, details about the fold expansion are not always made available (Till et al., 2008).

In the G-Rex system (Wilson Wolf) T-cells are cultured on a gas-permeable membrane, which provides a highly oxygenated environment and has shown comparable or improved fold expansion compared to the rocking motion bioreactors (Somerville et al., 2012; B. Levine, 2015). A 100-fold cell expansion in 10 days without any medium exchange has been reported in the G-Rex M series vessel using K562 cell line (Bajgain et al., 2014). Others report 2-3 x 10^9 total CAR-T cells in the G-Rex 100M vessel, with a surface of 100 cm^2 (Ludwig et al., 2020). The G-Rex platform has also shown linear scalability in terms of surface area. G-Rex 5 (surface area of 5 cm^2), G-Rex 100M (surface area of 100 cm^2), and G-Rex 500M (surface area 500 cm^2) showed comparable fold expansion and similar cells cm^{-2} and can support very low seeding densities, such as 1.25 x 10^5 cell cm^{-2} (Bajgain et al., 2014). Wilson Wolf claims that the G-Rex have the most efficient use of medium and reagents and a single device can be used for each patient, reducing the need for expensive GMP space. A study has reported the activation, transduction and expansion of T-cells in the G-Rex 6-well plates obtaining up to 42-fold expansion in 11-14 days (Gagliardi et al., 2019), while other protocols transduce T-cells in different platforms (Pampusch et al., 2020). Wilson Wolf has also implemented a semi-automated method for the final cell harvest, reducing the risk for contamination (Bajgain et al., 2014).

These static systems are operated in batch or fed batch, with no perfusion option available. In order to produce a large number of cells in these systems, a scale-out

approach is needed, which can end up with multiple vessels at once. This becomes troublesome in terms of space needed, manipulation required and laborious in terms of harvesting procedure (B. Levine, 2015). These systems might be sufficient for small scale clinical trials with a limited number of patients. However, although they are GMP-compliant (Bajgain et al., 2012), they are not suitable for larger scale manufacturing due to their open-handling steps and scalability issues. An additional drawback is posed by the fact that none of these systems allows for the control or monitoring of culture parameter such as temperature, pH, and dissolved oxygen.

1.5.4.2 Rocking motion bioreactors

Rocking motion bioreactors are currently the most used bioreactors for the manufacturing of CAR-T cell therapies (Vormittag et al., 2018). This is a semi-closed system that provides a better uniformity in terms of oxygenation, nutrients, and pH compared to the static culture platforms, due to the mixing occurring through the rocking of the bags (Somerville et al., 2012). Rocking motion bioreactors can be operated in perfusion mode, enabling a cell density of 10^7 cells ml^{-1} (Xiuyan Wang et al., 2016), resulting in much higher final numbers compared to T-flasks and gas permeable bags. The rocking motion platform also enables to control and monitor the pH, dissolved oxygen, rocking speed, rocking angle, and the pressure inside the bag.

The two main manufacturers of the rocking motion bioreactors are Sartorius Stedim Biotech with the BIOSTAT® RM and GE Healthcare Life Sciences with the Xuri™ Cell

Expansion System. All the systems operate with single-use bags that range from 1 to 25 liters. One of the limits for this system is the relatively large volume $\sim$ 300-500 ml needed for inoculation, which requires to pre-expand the cells in a smaller platform (i.e. T-flask, gas permeable bag or G-Rex) prior to inoculation (Mizukami et al., 2020; Hollyman et al., 2009). Hollyman et al. (2009) have reported a 668 fold expansion of anti-CD19 CAR-T cells after 18 days of expansion under constant perfusion regime in the Xuri™ bioreactor. Although rocking motion bioreactors are widely used for CAR-T cell products undergoing clinical trials, it is hard to find studies detailing the manufacturing process and the fold expansion achieved using this platform (Vormittag et al., 2018). Another drawback is the lack of scale-down models for rocking motion bioreactors, which would allow for high throughput screening. Although rocking motion bioreactors have been extensively characterised form a fluid dynamic point of view (Marsh et al., 2017a) the suspension of the Dynabeads® and their interaction with the T-cells has not been studied. A poor suspension of the beads and a low interaction with the T-cells can lead to a sub-optimal T-cell expansion (Costariol et al., 2019).

1.5.4.3 CliniMACS Prodigy

The CliniMACS Prodigy® is the only fully closed system available on the market (Marin Morales et al., 2019). It allows to perform cell selection, activation, transduction, cell washing and expansion all in a single fully closed platform (Zhu et al., 2018). This platform reduces the risk of contamination compared to an open-process and reduces

the need for highly skilled personnel for its operation. However, a single CliniMACS Prodigy® can manufacture the dose for one patient at the time, making the machine unavailable for any other task in that time frame. This implies that, if doses for multiple patients need to be manufactured in parallel, different CliniMACS Prodigy® need to be used, making the manufacturing process really expensive (fixed cost of the CliniMACS prodigy $\sim$ \$180,000 (Zhu et al., 2018)).

GlaxoSmithKline (GSK) plc partnered with Miltenyi Biotec in March 2016 to develop CGTs, outlining how important it is to have a closed-fully automated product that can be used for different types of manufacturing (GSK, 2016). In early 2018, Autolus Therapeutics announced an extensive partnership with Milteny Biotec to use the CliniMACS Prodigy®. The company have since been using the automated CAR-T platform to manufacture CAR-T therapies (Autolus Therapeutics plc, 2018). The CliniMACS Prodigy® also received the EMA approval for the GMP manufacture of Zalmoxis® (a patient-specific cell therapy involving haplo-HSCT) manufactured by MolMed SpA (Miltenyi Biotec GmbH, 2018).

Although there appear to be various commercial partnerships using this system, there is little data in the peer-reviewed literature and no approved CAR-T products using the CliniMACS Prodigy® for product manufacture. Data from different studies are shown in Table 1.6.

Table 1.6: Fold expansions in the CliniMACS Prodigy® platform. The duration of the expansion phase and starting material are also listed.

Author	Fold Expansion	Days of expansion	Starting material
Mock et al., 2016	16.2 ± 7.9	8-10	Healthy donors
Lock et al., 2017	43 ± 14	12	Healthy donors
W. Zhang et al., 2018	16-20	8	Healthy donors
Zhu et al., 2018	24.5-41.0	13	Not stated
Aleksandrova et al., 2019	41-81	12	Healthy donors

Others report the use of the CliniMACS Prodigy® in their manufacturing process, but no data about cell growth have been found (Zhu et al., 2016; Nirav N Shah et al., 2018; Blaeschke et al., 2018). Furthermore, two clinical trials in early phase I that use the CliniMACS Prodigy® for the manufacturing of CAR-T cells have been reported on ClinicalTrials.gov, 2020.

Although the CliniMACS Prodigy® is the only fully closed system currently available on the market, manufacturers relying on this platform are limited to a single supplier. This poses a great risk in case of discontinuity of some of the products due to manufacturing or other issues, since no alternatives are available. Furthermore, if there is no competition on the market, the price for the platform and the consumables can be set by Miltenyi with almost no constrictions.

A single CliniMACS Prodigy® can only be used to manufacture on average 2 to 3 patient doses per month (A. Kaiser et al., 2015). This implies the need for scaling-out for commercial production, which increases the costs of the manufacture significantly. Moreover, the price of the single use equipment for each run is estimated to be ap-

proximately $26,000, excluding the personnel cost (GEN, 2016). Therefore, the cost to manufacture an average of 24 doses per year is $\sim$ $624,000, which adds up to the cost of the CliniMACS Prodigy® ($\sim$ $180,000).

The expansion chamber of the CliniMACS Prodigy® has a working volume that goes from 100 to 250 ml. However, there are no scale-down nor scale-up models that are commercially available, making this platform unsuitable for high throughput screening and allogeneic therapies. Furthermore, there are concerns about the CliniMACS Prodigy® being a fully closed system that can be operated in a grade D clean room. Some of the processes might still require preparation steps to be undertaken in biosafety cabinets and therefore the need for a grade B clean room, which is more expensive to build and run compared to a grade D (Dai et al., 2019).

1.5.4.4 Emerging expansion platforms

Due to the lack of purpose-built bioreactors for the expansion of CAR-T cells, there is a number of new closed automated systems being developed or that have just reached the market.

The recently launched Lonza Cocoon™ is an automated GMP-in-a-box device that allows end-to-end manufacturing from cell isolation to harvest. The system is based on single use highly customised cassettes, adding flexibility to the manufacturing process. Up to 10 Cocoon systems can be fitted on the Cocoon tree which has a footprint of just 1 m^2. This makes the scaling-out particularly appealing, limiting the expensive clean

room space needed. Lonza has stipulated a clinical collaboration with one of the larger hospitals in the Middle East (Sheba Medical center), where the device is being used to manufacture products for autologous CAR-T clinical trials (Barba, 2019). No data on CAR-T cell growth have been published using this system up to date.

Aglaris Ltd, a company based in the United Kingdom, has developed a closed system called Facer 1.0. It is an automated and fully closed system, which is based on an iteratively-expanding culture chamber, allowing to have a reduced amount of cells at seeding. The Facer 1.0 bioreactor also allows to grow cells from three different sources at once avoiding cross-contamination. This would allow for multiple patients batches to be manufactured in parallel. This system, however, does not seem to include the isolation step, which would have to be performed prior to inoculation.

Adva Biotechnology, an Israeli company, has launched its closed system ADVA X3 in January 2020. ADVA X3 is described as a robust and modular cell manufacturing cGMP system, that allows autologous therapies to be manufactured at bed side. Since the technology has only recently been launched, there is no information about the expansion system used, nor data showing CAR-T cell expansion.

London based start-up Ori Biotech has recently secured $8.6 million in their seed round to innovate the manufacture of CGTs. Although their product has not been released yet, they promise to bring down the cost of CGTs addressing the main manufacturing bottlenecks.

All these systems are trying to automate the manufacturing process or parts of it, reducing the human interactions needed. The ADVA X3 system is described as a bed side device, which means it does not need to be placed in a clean room environment. This system is therefore limited for autologous therapies and can only be used to manufacture one product at the time. Similarly, the Cocoon™ system is suitable for scaling-out the manufacturing process, however it does not consider the need to scale-up for allogeneic therapies.

1.5.4.5 Stirred tank bioreactors

Commercially available stirred-tank bioreactors have been extensively used the expansion of Chinese hamster ovary (CHO) for mAb production and for other biopharmaceutical products (Alvin W Nienow, 2015; Schirmer et al., 2018). Stirred-tank bioreactors have been used also to grow adherent cells on microcarrieres (Q. A. Rafiq et al., 2016a; Alvin W Nienow et al., 2016; A. K.-L. Chen et al., 2015; Heathman et al., 2015; Carmelo et al., 2014).

Stirred-tank bioreactors have significant advantages over other platforms used for cell expansion. They are easy to scale and are available in a wide range of volumes, making them suitable for both autologous and allogeneic therapies (Q. A. Rafiq et al., 2015). Stirred vessels enable more uniform culture conditions, ease of sampling, and the ability to control process parameters as pH and dissolved oxygen (Carswell et al., 2000; van den Bos et al., 2014). They can be operated in perfusion mode and the oxy-

gen mass transfer can be increased via agitation and sparging. All these characteristics make them ideal for high density cell culture (van den Bos et al., 2014). Furthermore, due to their large usage in the industry, stirred-tank bioreactors have been extensively characterised both from an engineering and biological point of view. Stirred-tank bioreactors are available as single-use systems or as reusable systems made of steel and glass (Schirmer et al., 2018). There are different manufacturers for stirred-tank bioreactors (i.e. Sartorius Stedim Biotech, Eppendrof, Pall Life Sciences, Merck, Thermo Fisher Scientific, Applicon, GE Healthcare), which makes the market competitive and not monopolised as in the case of the CliniMACS Prodigy®, where the only producer for the system and consumables is Miltenyi Biotec. Furthermore, having multiple suppliers mitigates the supply risk and provides flexibility on the design of the vessel and impeller, as well as on the wanted scale for the manufacturing of the product.

Despite the numerous advantages listed above, limited studies using stirred-tank bioreactors have been carried out in the T-cell space, primarily due to the general belief that T-cells are shear sensitive (van den Bos et al., 2014). Two studies were conducted in the early 2000 (Carswell et al., 2000; Bohnenkamp et al., 2002), after which no work has been performed until recently, showing a renewed interest in stirred-tank bioreactors for the production of CAR-T therapies (Klarer et al., 2018; Ou et al., 2019). Different concerns have prevented these bioreactors to out-compete more 'gentle' expansion platforms (rocking motion bioreactors, permeable bags, G-Rex, T-flasks). Hydrodynamic

forces have risen different concerns in regards with mammalian cells and they are believed to limit their growth, viability, altering their metabolite profiles, and expression of surface receptors (Carswell et al., 2000; Bohnenkamp et al., 2002; van den Bos et al., 2014).

Carswell et al. (2000) have investigated the impact of stirring in a 2 liter Setric Genie stirred-tank bioreactor (60-300 rpm range tested). The T-cells were obtained via leukapheresis from non hematological cancer patients or as whole blood samples from healthy donors. Healthy donor samples were processed using a histopaque density gradient in order to isolate the PBMCs. The PBMCs were not further processed and they were cultured in Roswell Park Memorial Institute (RPMI) medium supplemented with 100IU IL-2, 10% foetal bovine serum (FBS), 2mM glutamine, 1mM sodium pyruvate, 0.1mM non-essential ammino acids, 25mM N-2-hydroxyethylpiperazine-N-ethanesulfonic acid (HEPES), 100 U ml^{-1}, 100 μg ml^{-1} streptomycin, and 5 μg ml^{-1} phytohemagglutinin (PHA) used only for activation. Further medium addition did non contain PHA. The main finding was the down-regulation of the CD25 (IL-2R) receptor in stirred culture conditions under headspace and sparging aeration conditions. The down-regulation increased linearly with the increase in the stirring speed. However, the bioreactors were run in batch mode and the PBMCs were pre-expanded for a varying period of time (5-7 days) in T-flasks before being seeded in the bioreactors at 1.5 x 10^5 cells ml^{-1}. Furthermore, the stirring speed was increased day by day and it is not clear whether the slower

proliferation at higher speed was due to the lack of nutrients or if it was a consequence of the increasing shear stress. Pluronic, which is known to improve cell viability under sparged conditions, was not employed in any of the undertaken experiments. The use of protective additives is mentioned in the future work, together with perfusion culture, optimal dO_2 and pH investigations, feeding strategies, and medium formulation.

Some of these parameters (pH, feeding strategy, dO_2, and temperature) have been later investigated by Bohnenkamp et al. (2002) in static T-flasks. The optimal conditions were then used to expand T-cells in a stirred-tank bioreactor. This study used PBMCs from healthy donors who tested positive for cytomegalovirus (CMV). The optimal pH range was found to be 7.0-7.3 in the static control. The optimal feeding regime was a daily half media exchange, achieving a higher cell density compared to a medium exchange every 2^{nd} or 3^{rd} day. The oxygen tension seemed to have an impact on T-cells proliferation, with 5% dO_2 resulting in the higher fold expansion, but with a comparable growth rate to the conditions grown at 25% and 50% dO_2. For the dO_2 testing a Cellferm-pro® system was used, which allowed for the online monitoring of pH, temperature and dO_2. The same system was also used for temperature testing in a range from 34°C to 40°C. The optimal temperature was found to be 38.5°, simulating a fever condition *in vivo*. For the assessment of the growth of T-cells in a stirred environment they used a conventional stirred 1 liter vessel by Applikon Biotek and a suspension bioreactor developed within their group. The PBMCs were activated for 4 days using

immobilised anti-CD3 mAbs, after the activation the two bioreactors were seeded. The seeding density was inconsistent between the two bioreactors. The Applikon Biotek bioreactor was seeded at 1.35 x 10^5 cells ml^{-1}, while the bioreactor developed by the group was seeded at 5 x 10^5 cells ml^{-1}. The fold expansion in the two systems was 44.4 and 30 fold respectively, after almost 10 days of culture. This study also confirmed the faster down-regulation of the IL-2R in the stirred environment compared to the static one. On the other hand, lower oxygen tension (5%) improved the fold increase of T-cells when compared to higher values (75%). However, the stirring speed used for the expansion of T-cells in the stirred-tank bioreactors was not reported.

Klarer et al. (2018) published a study reporting the growth of primary T-cells from healthy donors in an ambr® 15 high-throughput stirred-tank bioreactor. Negatively isolated $CD3^+$ cells from three different donors apheresis products were used in this work and static culture was compared to the stirred-tank bioreactor. The medium used in this study was the serum-free X-VIVO (Lonza) with the addition of 5% human AB serum and 100 IU ml^{-1} of IL-2. The T-cells were activated using 3:1 Dynabeads® to cells ratio. A fed batch feeding strategy was compared with a high (50% medium exchange per day) and low (35% medium exchange per day) perfusion mimic strategy. The impeller was stopped one hour before the medium removal and the medium exchanges were performed after cell sedimentation. This step caused a 4.84% loss of the cells per iteration. Two out of the three donors showed a significantly better growth under the high perfu-

sion feeding compared to the fed batch conditions. The third donor showed poor growth in all the expansion platforms. The pH in the bioreactors was controlled between 7.1-7.2 and the dO_2 was kept at 50% by headspace aeration. However, the stirring in the ambr® 15 bioreactor was only started on day 5 of culture and was set to 300 rpm in down-pumping mode. This study also shows that, although continuous stirring did not reduce the overall growth of the T-cells, the cells in static conditions displayed a higher growth rate in the first five days compared to the the one grown in stirred environment. The cultures were carried out for 13 days, however a halt in the T-cell growth was seen after day 9 for all the donors.

Ou et al. (2019) in their study reported the growth of primary human T-cells in a 2 liter stirred-tank bioreactor developed within the group. They report the comparison between different activation methods: 1:1 cell to Dynabeads® ratio and soluble anti-CD3 and anti-CD28 mAbs, claiming that T-cells activated using Dynabeads® show a significantly better proliferation and fold expansion. They also assessed the effect of double activation, showing that it achieved a higher fold expansion. The cells were activated 4 days prior to the inoculation in the bioreactor and the Dynabeads® were removed after 4 days prior to the inoculation. The volume in the bioreactor was 800 ml and operated in a fed batch mode; no further details about the feeding strategy are provided. The stirred-tank bioreactor was operated at 70 rpm, the pH set at 7.4 and dO_2 at 70% with gas sparging at 0.01 volume of liquid per minute (VVM). The final reported

cell density in the bioreactor after 4 days of culture was 6.40 x 10^6 cells ml^{-1}. The fold exchange was in the range of 132 to 1011-fold, however it was calculated from the day of thawing and activation, rather than from the day of the stirred-tank inoculation. These numbers could therefore be misleading. It is also unclear if the seeding density was re-adjusted to 0.5 x 10^6 cells ml^{-1} on the bioreactor inoculation day or if all the cells contained in the flask were transferred to the vessel regardless of the cell numbers. The medium used for the bioreactor culture was the CTS™ OpTmizer™ T-cell expansion medium, a complete serum-free and xeno-free medium developed by Thermo Fisher. No further information on the bioreactor used was provided in this paper nor further references to any other sources were given.

All these studies confirm that it is possible to grow T-cells in a stirred-tank bioreactor despite the general belief that T-cells are shear sensitive (Bohnenkamp et al., 2002; Carswell et al., 2000; van den Bos et al., 2014; Klarer et al., 2018; Ou et al., 2019). The two early studies highlight the dependence of IL-2R down-regulation in the stirring regime, compared to the static one, suggesting it has an effect on the growth of the cells (Bohnenkamp et al., 2002; Carswell et al., 2000). None of the two more recent papers have looked into the IL-2R down-regulation (Carswell et al., 2000; Bohnenkamp et al., 2002). However, the immunophenotype analysis at the end of the bioreactor culture showed no significant difference in CD4 and CD8 markers expression between the static and stirred environment (Klarer et al., 2018) and the proliferation of T-cells in

the stirred-tank was better than the one in the static conditions (Klarer et al., 2018; Ou et al., 2019). These two studies also used Dynabeads® for T-cell activation (although in different beads to cell ratio). T-cells activated using magnetic beads showed a higher proliferation rate compared to the one activated using soluble mAbs (Ou et al., 2019).

Although these papers give a great general proof of concept, no studies up to date have been carried out growing gene-modified CAR-T cells in stirred-tank bioreactors and examining their potency at the end of the process. Furthermore, the scalability between different bioreactors has not been assessed with this type of cells. Having a scale-down model that could be then scaled-up to commercial scale would immensely benefit the research and development of CAR-T therapies limiting the cost and the raw material needed.

1.5.5 Current challenges in the expansion process of CAR-T cell therapies

The current production of CAR-T therapies still needs to overcome different bottlenecks in order to reach a fully efficient commercial manufacturing process. This is highly due to the relatively small number of products requested and a highly personalised manufacturing process which significantly increases the overall cost. Different companies have put in place different approaches to bring the cost down, i.e. automation, development of closed all-in-one system, and scaling-up the process for allogeneic therapies.

Tyagarajan et al. (2019) recently published a paper on the manufacturing challenges faced during the KYMRIAH® clinical trials by Novartis. The process was developed at University of Pennsylvania and therefore the optimisation was mainly focused on the translation of the process from a single academic institution to manufacturing the same product for numerous clinical sites from two centralised manufacturing facilities. The main challenges in scaling out the production were in the standardisation and characterisation of the process and the product to ensure consistency, meet the different regulatory requirements that vary in different countries, substitute the manual processes with automated manufacturing steps to ensure reproducibility of the process, and manage the logistics in global clinical trials (Tyagarajan et al., 2019).

The production of CAR-T therapies needs to be performed in appropriate and costly clean room facilities, requiring frequent manipulation by highly skilled personnel. This increases the overall cost of manufacturing. An all-in-one closed system could present a solution that addresses not only the high cost, but also mitigates contamination risk and reduces the number of operators needed.

As discussed in the section above, the only currently available closed system product available for CAR-T therapies manufacturing is the CliniMACS Prodigy® produced by Miltenyi Biotec. Closed systems can be placed in a lower grade clean room (ISO 7 instead of ISO 5), which are less expensive to construct and to operate (Dai et al., 2019). However, the footprint of the CliniMACS Prodigy® system is considerable and

in order to produce multiple products for different patients in parallel you need multiple machines which adds to the overall capital costs which can be difficult for small to medium enterprises (SMEs) to bear.

The automation of the manufacturing process from start to end would help standardising the complex process. This could potentially contribute towards a more uniform final product. There are several systems on the market that allow for the automation of different steps of the process, but none of them are completely integrated, exception made for the CliniMACS Prodigy®.

Different manufacturing approaches have been undertaken by different companies and whilst there are systems on the market which currently enable the manufacture of small batch sizes of CAR-T cells, it is critical that manufacturing processes and platforms are developed to allow for a larger number of universal, off-the-shelf therapy doses. The possibility to manufacture multiple off-the-shelf product batches at once would reduce the waiting time for the therapy administration, which is critical for patients with acute malignancies, and would significantly reduce the cost of CAR-T therapies (Depil et al., 2020).

1.6 Research aim and objectives

Stirred-tank bioreactors are widely used for CHO and E. Coli cultures and they are well characterised from a biological perspective. Despite the amount of work carried out in stirred-tank bioreactors and the wide use of stirred vessels in the industry, there is limited work investigating the feasibility of manufacturing CAR-T cell products in stirred-tank bioreactors.

The research presented in this doctoral thesis focuses on the development of a robust and reproducible manufacturing process for CAR-T therapies in a stirred environment at different scales. Given the fact that stirred-tank are scalable expansion platforms, there is an opportunity for high-throughput screening of in process parameters in scale-down models. This would allow to optimise the manufacturing process bringing down the quantity of raw material needed and consequently the cost of research and development. Once the process has been optimised at small scale, it can be then scaled-up to 1L or larger volume stirred-tank bioreactors, which are essential for the manufacturing of allogeneic CAR-T therapies.

The research aim of this EngD thesis is to demonstrate the robust and reproducible manufacture of T-cell and CAR-T cells therapies in stirred-tank bioreactors.

In order to achieve this aim, the following research objectives were established:

- Demonstrate Jurkat E6.1 T-cell line can be grown in stirred-tank bioreactors under dynamic conditions.
- Establish a robust and reproducible expansion protocol for primary human T-cells and CAR-T cells from healthy donors in a stirred-tank bioreactor investigating a range of culture parameters including different agitation speeds.
- Investigate whether CAR-T cells grown in stirred-tank bioreactors retain the same quality attributes as the one grown under static conditions.
- Identify a suitable scale-down model that could be used to perform high-throughput screening.
- Scale the process to larger volumes (1L stirred-tank bioreactor) as a proof of concept for allogeneic therapies.

1.7 Outline of research chapters

The research presented in this doctoral thesis is split in three results chapters (Figure 1.4) as follows:

- Demonstrating T-cells expansion in a stirred tank bioreactor

The key work in this chapter demonstrates Jurkat E6.1 T-cell line can be grown in the ambr® 250 bioreactor under dynamic conditions. Furthermore, results demonstrating that primary T-cells from healthy donors can be grown in a stirred-tank bioreactor are presented. Two different vessels (baffled vs. unbaffled) are compared on a power per unit volume basis in terms of growth kinetics, metabolite profiles, and immunophenotype. The T-cells growth kinetics in stirred-tank bioreactors are compared to the T-cells growth kinetics in static T-flasks.

- Establishing the expansion of human CAR-T cells in stirred-tank bioreactors

In this chapter healthy donors primary T-cells are transduced using lentivral vector and the engineered CAR-T cells expanded in the ambr® 250 stirred-tank bioreactor using the unbaffled vessel. Different agitation speeds are investigated (up to 500 rpm) and results on the effect of shear stress on the growth, immunophenotype, and potency (*in vitro* cytotoxicity assay) of the final product are discussed.

- Scaling-up the manufacture of human primary T-cells in stirred-tank bioreactors

The key work presented in this chapter intends to identify a suitable scale-down model that can be used in CAR-T cells manufacturing for high-throughput screening. For this purpose, an initial screening experiment is performed in the ambr® 15 stirred-tank bioreactor investigating different agitation parameters and dissolved oxygen concentrations. The process is then scaled to 1 L as a proof of concept for allogeneic CAR-T therapies. The results obtained at 15 ml, 250 ml, and 1 L are compared in terms of growth kinetics and immunophenotype.

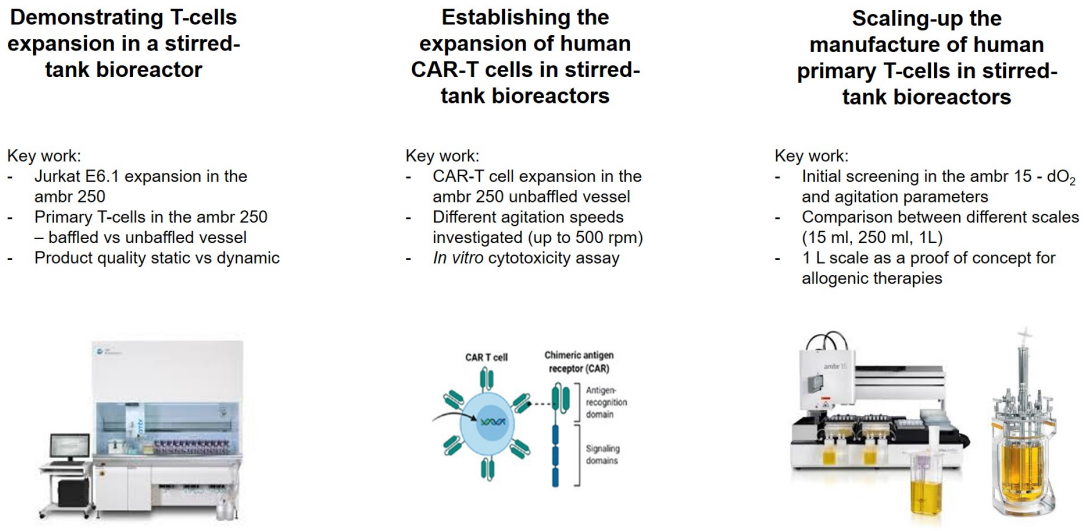

Figure 1.4: Summary of the three results chapters presented in this doctoral thesis.

Chapter 2

Materials and Methods

2.1 Jurkat E6.1 cell line

2.1.1 Banking of Jurkat E6.1 cells

A vial containing 5 x 10^6 cells was purchased from the European Collection of Authenticated Cell Cultures (ECACC, UK). The vial was thawed in a 37°C water bath and the content was added to 15 ml Falcon® conical tube (StemCell™ Technologies, UK) containing 5 ml of RPMI 1640 (Gibco™, Thermo Fisher Scientific, UK) medium supplemented with 10% (v/v) FBS (Thermo Fisher Scientific, UK) and 2mM L-Glutamine (Thermo Fisher Scientific, UK), referred to as complete RPMI (cRPMI) 1640 from now on. The cRPMI was pre-warmed to 37°C in the water bath. The cells were centrifuged at 350 x*g* for 5 minutes, the supernatant was aspirated, the cells were re-suspended in

10 ml of fresh cRPMI, and plated in a Nunc™ T-75 non-treated culture flask (Thermo Fisher Scientific, UK). The flask was then placed into a humidified incubator (PHC Europe B.V., UK) at 37°C and 5% CO_2. cRPMI medium was added to the flask every 2-3 days in order to maintain the cell concentration below 1 x 10^6 live cells ml^{-1} and split into multiple Nunc™ T-175 non-treated culture flasks (Thermo Fisher Scientific, UK) at need. The Jurkat E6.1 cell were expanded for 2 weeks, after which 5 x 10^6 cells were frozen down in 1 ml of 10% (v/v) dimethylsulphoxide (DMSO; Sigma-Aldrich Company Ltd., UK) in FBS using 1.2 ml Corning® cryogenic vials (Corning®, France). All steps were performed in a Class 2 Biological Safety Cabinet (BSC) under sterile conditions. The closed vials were appropriately labelled and put into a CoolCell™ LX Freexing Container (Sigma-Aldrich Company Ltd., UK) and placed in the freezer at -80°C. After 1 day in the freezer, the vials were moved inside a box in the liquid nitrogen tank for long term storage. Part of the cells was kept in culture and frozen after further expansion.

2.1.2 Jurkat E6.1 culture

A vial containing 5 x 10^6 Jurkat E6.1 was thawed at need, following the same procedure described in Section 2.1.1. The cells were plated in a Nunc™ T-75 non-treated flask containing 10 ml of cRPMI. The cells were then placed into a humidified incubator at 37°C and 5% CO_2 and diluted using fresh cRPMI every 2-3 days in order to keep the

cell concentration below 1 x 10^6 cells ml^{-1}. When the volume reached 50 ml the cell suspension was transferred to a Nunc™ T-175 non-treated flask. The cells were kept in culture until they reached the number of cells needed for the different experiments.

2.2 Human primary T-cells

Fresh whole blood or PBMCs from healthy donors were purchased from Cambridge Bioscience (Cambridge Bioscience, UK). The whole blood or PBMCs were processed straight upon delivery in order to isolate CD3 positive T-cells.

2.2.1 PBMCs isolation from whole blood

Whole blood samples were processed by diluting the 495 ml of blood in a 1:1 ratio in RPMI 1640 medium supplemented with 2% (v/v) FBS. 33 SepMate™-50 PBMC isolation tubes (StemCell™ Technologies Inc, UK) were filled with 15 ml of Lymphoprep™ solution (StemCell™ Technologies Inc, UK) each. 30 ml of whole blood was slowly pipetted using a 50 ml CLEARLine® serological pipette (Kisker Biotech GmbH & Co.KG, Germany) into each SepMate™-50 tube avoiding to mix the blood with the Lymphoprep™ solution. The tubes were then centrifuged at 1200 x*g* for 15 minutes. This resulted in a separation of different layers from top to bottom: plasma, PBMCs, density gradient medium, and red blood cells and granulocytes, as shown in Figure 2.1.

Figure 2.1: SepMate™-50 PBMC isolation tube after centrifuging. Different components of the whole blood have been separated forming 4 layers: plasma, PBMCs, density gradiend medium, and red blood cells and granulocytes.

Approximately 20 ml of plasma was carefully aspirated from each tube without disturbing the PBMCs layer. The rest of the plasma, together with the PBMCs layer was poured into a 1 L sterile bottle (Sigma-Aldrich Company Ltd., UK). The membrane inside the SepMate™-50 PBMC isolation tubes retained the density gradient medium, red blood cells, and granulocytes inside the tube. The cells were then diluted in RPMI 1640

medium containing 2% (v/v) FBS in order to make up 1 L of final solution. The solution was then pipetted into 50 ml conical centrifuge Falcon® tubes (Thermo Fisher Scientific, UK) and centrifuged at 500 x*g* for 10 minutes at 18°C. The supernatant was aspirated from each tube and the cell pellet re-suspended in 20 ml of RPMI 1640 medium containing 2% (v/v) FBS, pooling two Falcon® tubes into a single one. The same procedure was then repeated, centrifuging the cells at 400 x*g* for 10 minutes and the superantant was aspirated. The cell pellet was re-suspended in 20 ml of RPMI 1640 medium containing 2% (v/v) FBS and the content of two tubes was pooled into one. The last centrifugation step was performed at low speed (150 x*g*) for 10 minutes in order to remove platelet contamination. The superantant was removed by pouring and the PBMCs were re-suspended in RPMI 1640 medium and ready for the T-cell isolation step. The whole procedure was carried out inside a BSC under sterile conditions.

2.2.2 Primary T-cell isolation from PBMCs

Once the PBMCs were isolated from whole blood, or were directly purchased from Cambridge Bioscience, T-cell isolation was performed. In order to separate the T-cells form PBMCs the Pan T Cell Isolation Kit (Miltenyi Biotec, UK) was used together with LS Columns (Miltenyi Biotec, UK) and MidiMACS™ Separator (Miltenyi Biotec, UK) as per manufacturer's instruction. An isolation buffer containing 0.5% (w/v) bovine serum albumin (BSA; Sigma-Aldrich Company Ldt., UK) and 2 mM

ethylenediaminetetraacetic acid (EDTA; Thermo Fisher Scientific, UK) in phosphate-buffered saline (PBS; Thermo Fisher Scientific, UK) was prepared prior to the isolation and kept in the fridge at 4°C.

The PBMCs contained in a 50 ml Falcon® were counted and centrifuged at 350 x*g*, the supernatant was aspirated and the cell pellet was re-suspended in 40 µl of buffer per 10^7 cells. 10 µl of Pan T Cell Biotin-Antibody Cocktail (Milteny Biotec, Surrey, UK) per 10^7 total cells was then added to the same tube. The solution was mixed using a 1000 µl mechanical pipette (Sartorius Stedim Biotech, UK) and incubated for 5 minutes at 4°C. After this step 30 µl of isolation buffer per 10^7 total cells was added to the same tube, together with 20 µl of Pan T Cell MicroBead Cocktail per 10^7 total cells. The final solution was mixed using a 1000 µl mechanical pipette and incubated for 10 minutes at 4°C. While the cells were in the refrigerator, 4 LS Columns were placed on the MidiMACS™ Separator and rinsed with 3 ml of isolation buffer each. After 10 minutes, 1/4 of the cell suspension was pipetted onto each LS column. The flow-through, representing the enriched T-cells, was collected into four 50 ml Falcon® and each column was washed with 3 ml of buffer. The flow through from the wash was combined with the enriched T-cells and the 4 Falcon® tubes were pooled into one. All the procedures were performed in a Class 2 BSC under sterile conditions. A 200 µl sample was taken from the final T-cell solution for a cell count using the NucleoCounter® NC-3000™ (ChemoMetec A/S©, Denmark) using Via 1-Cassette™ (ChemoMetec A/S©, Denmark)

containing arcridine orange and DAPI stains.

2.2.3 Primary T-cell cryopreservation

Following the LS Columns isolation and cell counting, the suspension containing the enriched T-cells was spinned down for 5 minutes at 350 x*g*, the supernatant was discarded, and the cells re-suspended in an adequate volume of CryoStor® CS10 (STEMCELL Technologies Ltd., UK) in order to have 10^7 cells ml^{-1}. 1 ml of the T-cells solution was then pipetted into multiple 1.2 ml Corning® cryovials under sterile conditions inside a BSC. The closed vials were appropriately labelled, put into a CoolCell™ LX Freexing Container, and placed in the freezer at -80°C. After 1 day in the freezer, the vials were moved inside a box in the liquid nitrogen tank for long term storage.

2.2.4 Primary T-cell pre-expansion

Primary T-cells were pre-expanded for 7 days prior to inoculation in the different expansion platforms. One vial containing 10^7 T-cells was thawed at need in a 37°C water bath. Its content was pipetted into a 15 ml Falcon® containing 5 ml of cRPMI medium and centrifuged at 350 x*g* for 5 minutes. The supernatant was aspirated and the cell pellet was re-suspended in 10 ml of cRPMI medium supplemented with 30 IU ml^{-1} of IL-2 (Miltenyi Biotech Ltd., UK). The cells suspension was moved to a Nunc® T-75 culture flask and Dynabeads® in a 1:1 cells to beads ratio were added to it for T-cell

activation. The Dynabeads® were washed in 2 ml of 1 x PBS solution and re-suspended in 1 ml of cRPMI before adding them to the cell suspension. The flask was then placed at 37°C and 5% CO_2 in a humidified incubator. After 2 days the T-cells were transferred into a Nunc® T-175 non-treated flask and 30 ml of cRPMI medium supplemented with 1200 IU of IL-2 (in order to have a final concentration of 30 IU ml^{-1} of IL-2 in 40 ml). cRPMI 1640 medium was then added to the cells every 1-2 days in order to maintain the cell density in the range of 0.5-1.5 x 10^6 ml^{-1}. At day 7 the cells were re-activated and seeded in the wanted platforms (T-flask, spinner-flask (BellCo, USA), ambr® 250 bioreactor (Sartoirus Stedim Biotech, UK), and ambr® 15 bioreactor (Sartorius Stedim Biotech, UK)). In order to seed the 1 L UniVessel® (Sartorius Stedim Biotech, Germany) two vials containing 10^7 cells of primary T-cells were thawed and pre-expanded using the same procedure described above. This was due to the larger number of cells needed (200 x 10^6) for the inoculation of the 1 L UniVessel®.

2.3 Human primary CAR-T cells

Engineered CAR-T cells were used for experiments, when specified. The isolation, freezing, thawing, and activation procedures were carried out in the same way as for primary T-cells (Sections 2.2.1, 2.2.2, 2.2.3, and 2.2.4). One day after thawing and activation T-cells were transduced using lentiviral vectors produced in house using human embryonic kidney (HEK)293T cells.

2.3.1 Lentivirus production for CAR-T cell transduction

HEK293T cells were cultured in 20 cm round culture dishes (Thermo Fisher Scientific, UK), using Dulbecco's Modified Eagle Medium (DMEM; Gibco™, Thermo Fisher Scientifc, UK) supplemented with 10% (v/v) FBS. The dishes containing HEK293T were placed in a humidified incubator at 37°C and 5% CO_2 until 70% confluent. The medium was then changed to DMEM Advanced (Gibco™, Thermo Fisher Scientifc, UK) serum free medium. The cells were then transfected with packaging plasmids pMD2.G, pCMV-dR8.74 (Addgene plasmids #12259 and #2203; Addgene, Teddington, UK), and CD19-specific CAR plasmid (gifted by Martin Pule) using GeneJuice® transfection reagent (Merck Millipore Limited, UK). The CD19-specific CAR used in this work comprised an FMC63 scFv, a CD8 alpha stalk with a 41BB-CD3ζ endodomain, and it was transcriptionally lined to RQR8 containing the CD34 epitope (Philip et al., 2014).

The first lentivirus harvest was performed 48 hours after transfection. The medium was gently collected from each round culture dish using a 25 ml serological pipette, paying attention not to detach the HEK293T from the surface of the dish, and pooled into a 1 L sterile bottle and stored in the fridge at 4°C overnight. The medium in each dish was immediately replaced with fresh DMEM Advanced medium and a second lentivirus harvest was performed 72 hours after transfection (24 hours after the first harvest). The lentivirus collected from the two harvest points was combined into the

same 1 L flask and filtered by using a 0.45 μm filter (Sigma-Aldrich Company Ltd, UK). The lentivirus was aliquoted into 30 ml aliquotes and stored at -80°C until use.

2.3.1.1 Primary T-Cell transduction

On the day when primary T-cells were thawed a non-treated 6 well plate (Corning®, France) was coated with 1 ml of RetroNectin® (Takara, Japan) solution per well containing 20 μg ml^{-1} RetroNectin® in 1 x PBS. The plate was stored at 4°C overnight. Each well was consequently washed with sterile 1 x PBS and 0.5 ml of cell solution containing 1.5 x 10^6 activated T-cells in cRPMI was pipetted into each well. Each well was topped up with 4 ml of lentiviral vector and IL-2 was added in order to have 100 IU ml^{-1} IL-2 as a final concentration in each well. The plate was then placed into a centrifuge and spinnoculated for 40 minutes at 32°C at 1000 x*g*. After the spinnoculation the well plate containing the cells was put into a cell culture incubator at 37°C and 5% CO_2.

The transduced CAR-T cells were removed from RetroNectin® 24 hours after spinnoculation by vigorously pipetting with a P1000 mechanical pipette and transferred into a 50 ml Falcon® tube. The cells were centrifuged at 350 x*g* for 5 minutes and the supernatant was discarded. The CAR-T cells were re-suspended in fresh cRPMI supplemented with 30 IU ml^{-1} of IL-2 and transferred into a Nunc™ T-175 non-treated cell culture flask. The cells were then expanded as previously described for primary T-cells (Section 2.2.4). All the steps were performed in a Class 2 BSC under sterile conditions.

2.4 Expansion of T-cells in different expansion platforms

Jurkat E6.1 cells were seeded into different expansion platforms (T-flask and ambr® 250 bioreactor) once they were expanded to the wanted number.

Primary T-cells were re-activated with Dynabeads® and seeded into different expansion platforms (T-flask, spinner-flask, ambr® 250 bioreactor, ambr® 15 bioreactor, and 1 l UniVessel® bioreactor) as detailed in the sections below, after the 7 day pre-expansion.

Transduced CAR-T cells were reactivated with Dynabeads® and seeded into different expansion platforms (T-flask and ambr® 250 bioreactor) as detailed in the sections below, after trasduction and 7 days pre-expansion.

2.4.1 Nunc™ T-175 non-treated flask culture

Nunc™ T-175 non-treated flasks were used as a static control. The T-flasks containing the cell suspension were placed into a cell culture humidified incubator at 37°C and 5% CO_2. 1 ml daily samples were taken for cell counting and metabolite analysis. All the steps (sampling and medium additions) were carried out in a Class 2 BSC under sterile conditions.

2.4.1.1 Jurkat E6.1

After expansion Jurkat E6.1 were seeded in the T-175 flask at 0.1 cells ml^{-1} in 20 ml of cRPMI medium. Medium was added to each flask on day 3 (20 ml), 4 (10 ml), and 5

(10 ml).

2.4.1.2 Primary T-cells and CAR-T cells

Primary T-cells (transduced or non transduced) were seeded in a T-175 flask at 0.5 cells ml^{-1} in 20 ml of cRPMI medium supplemented with 30 IU ml^{-1} IL-2 after 7 days of pre-expansion. T-cells were re-activated using 1:1 cell to Dynabeads® ratio. The feeding strategy used was the same as for Jurkat E6.1 cells described in Section 2.4.1.1. Immunophenotype analysis was performed via flow cytometry on the day of the inoculation and 7 days after, at harvest.

2.4.2 Spinner-flask culture

A glass spinner-flask, with a vessel height and diameter of 135 mm and 60 mm respectively, was fitted with a magnetic horizontal stirrer bar (40 mm length) and a vertical paddle (50 mm diameter) was used for all the spinner-flask experiments. The horizontal magnetic stir bar was set 5 mm above the bottom of the spinner-flask. The spinner-flasks were autoclaved and inocluation was performed in a Class 2 BSC. The spinner-flasks were placed on a BellEnnium™ Compact 5-position magnetic stirrer platform (BellCo, USA) in a humidified incubator at 37°C and 5% CO_2 and set to agitate at 35 rpm.

2.4.2.1 Primary T-cells

After 7 days pre-expansion period, primary T-cells were seeded at 0.5 cells ml^{-1} in 50 ml of cRPMI medium supplemented with 30 IU ml^{-1} IL-2. T-cell were reactivated by using Dynabeads® in a 1:1 beads to cells ratio. Following inoculation, a cap on the spinner flask arm was loosened to allow gas exchange. Medium was added on day 3 and 4, 10 and 40 ml respectively, after which the maximum working volume of 100 ml was reached. cRPMI medium was supplemented with IL-2 in order to have a final concentration of 30 IU ml^{-1} in the medium at every medium addition. 1 ml samples were taken every day for cell counting and metabolite analysis. Flow cytometry analysis was performed on day 0 and at the end point of the experiment (7 days after inoculation).

2.4.3 ambr® 250 stirred-tank bioreactor culture

An ambr® 250 high throughput two bioreactors test system (Sartorius Stedim Biotech, UK) was used to culture T-cells (Figure 2.2).

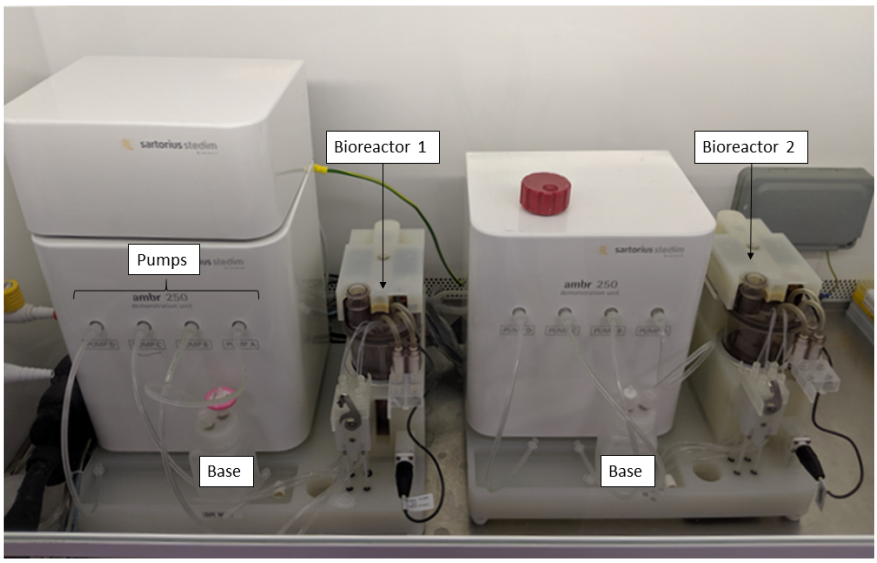

Figure 2.2: ambr® 250 stirred-tank two bioreactors test system used for the experiments. The bioreactor was placed into a BSC in order to allow opening the bioreactors for sample tanking and medium addition under sterile conditions.

Two types of single use bioreactors vessels, each of diameter T = 60 mm, were used. One vessel type, developed primarily for free suspension animal cell cultures, was equipped with two 3-segment, 30° pitched blade impellers (D = 26 mm) and four vertical baffles (width 6.25 mm). The other vessel type, developed for microcarrier culture of adherent cell types, was equipped with a single larger 3-segment, 45°C pitched blade impeller (D = 30 mm) and it was unbaffled (Figure 2.3). In both cases, the impellers pumped downwards and key culture parameters including pH, dO_2, temperature, and the headspace gas flow were measured continuously and monitored throughout the experiment.

Baffled Vessel		
Impeller diameter (3-pitched blade) (D)	26 mm	T/D = 2.3
Impeller height from bottom (C)	17 mm	C/D = 0.65
Impeller number	2	
Impeller spacing	30 mm	
No. of baffles	4	
Baffle width (W)	6.25 mm	W/T = 0.1

Unbaffled Vessel		
Impeller diameter (Elephant ear) (D)	30 mm	T/D = 2
Impeller height from bottom (C)	17 mm	C/D = 0.57
Impeller number	1	
No. of baffles	0	

Figure 2.3: ambr® 250 stirred-tank baffled (top) and unbaffled (bottom) vessels. The baffled vessel has two 3-segment, 30° pitched blade impellers and four vertical baffles. The unbaffled vessel has a single 3-segment, 45° pitched blade impeller and no baffles. T = diameter of the vessel (60 mm), D = diameter of the impeller, C = impeller height from the bottom, and W = baffle width.

Oxygen in the ambr® 250 was provided for cultivation by headspace aeration with the headspace flow regulated to 14.25 ml min^{-1} of N_2, with 21% O_2 and with an additional flow of CO_2 of 0.75 ml min^{-1}. These conditions were set to replicate the 5% CO_2 condition inside the incubator where the static controls were placed (T-175 flasks). After medium exchange on day 5, dO_2 was controlled at 60% by gas blending with oxygen.

80 ml of cRPMI medium was put into each vessel and and left to condition for at least 6 hours, after which a 2 ml sample was taken in order to measure the pH off-line. The measured pH value was then inserted into the software for each vessel individually.

After inoculation, 1 ml sample was taken from each vessel daily in order to perform cell counts and metabolite analysis. 1 ml medium samples were taken after each medium addition or exchange in order to run the metabolite analysis.

2.4.3.1 Jurkat E6.1

Jurkat E6.1 cells were seeded in the ambr® 250 unbaffled vessel at 0.1 cell ml^{-1} in 100 ml of cRPMI medium. 100 ml of cRPMI medium waw added on day 3 after inoculation, 50 ml was added on day 4, reaching the maximum volume (250 ml) inside the bioreactor vessels. On day 5 the impeller was stopped and the cells were left to sediment for 6 hours, after which 100 ml of medium was removed and replaced with fresh cRPMI.

2.4.3.2 Primary T-cells and CAR-T cells

One week after thawing a vial of 10 x 10^6 T-cells and their pre-expansion and transduction (in case of CAR-T cells), the cells were seeded into an ambr® 250 vessel at $0.5x10^6$ cells ml^{-1} in 100 ml of cRPMI medium supplemented with 30 IU ml^{-1} IL-2. The cells were reactivated using 1:1 Dynabeads® to cell ratio. The same feeding strategy was used as for Jurkat E6.1 cells described in Section 2.4.3.1. The medium used for primary T-cells and CAR-T cells was supplemented with enough IL-2 in order to have a final concentration of 30 IU ml^{-1} in the medium after each medium addition or exchange. In the first set of experiments (Chapter 3) the medium exchange was performed via sedimentation. The impeller was stopped for 6 hours, after which 100 ml of

medium was removed and replaced with fresh cRPMI medium supplemented with the appropriate amount of IL-2. In the following chapters the medium exchange was performed via centrifugation. 100 ml of cell suspension was removed without stopping the impeller. The cells were centrifuged at 350 x*g* for 10 minutes, re-suspended in 100 ml of fresh cRPMI medium supplemented with IL-2 and pipetted back into the bioreactor vessel. When specified, a pH control between 7.1-7.2 and a dO_2 control were set on day 0 and throughout the whole experiment duration. The upper pH limit was controlled via CO_2 addition via headspace aeration, while the lower limit was controlled with a 7.5% (w/v) sodium bicarbonate (Sigma-Aldrich Company Ltd., UK) in distilled water (Gibco™, Thermo Fisher Scientific, UK). The dO_2 was set at 50% and it was controlled by changing the oxygen and nitrogen inflow into the headspace aeration mix.

2.4.4 ambr® 15 stirred-tank bioreactor culture

An ambr® 15 high throughput, automated biroeactor systems (Sartorius Stedim Biotech, UK) with 12 independent vessels in each of the two culture stations and with a liquid handler was used for these studies (Figure 2.4).

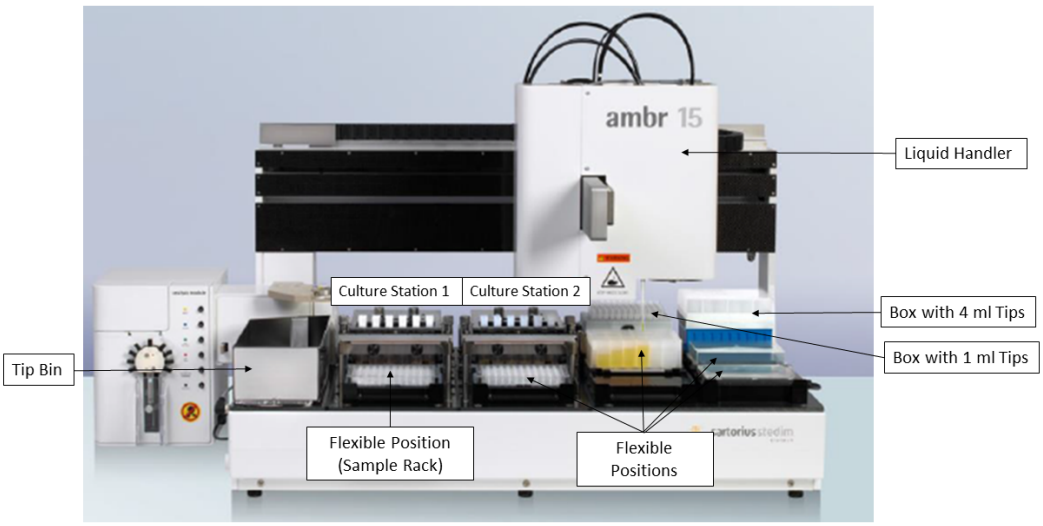

Figure 2.4: An ambr® 15 high-throughput stirred-tank bioreactor with two culture station and a liquid handler used in the experiments. The 6 flexible positions can accommodate the sample rack or other wells appositely designed for the system.

24 overlay vessels (no sparging) with a working volume of 10-15 ml and single-use pH and dO_2 sensors positioned at the bottom of the vessels were used for each experiment, 12 per each culture station. The vessels had a single pitched blade impeller (D = 11.2 mm) (Figure 2.5).

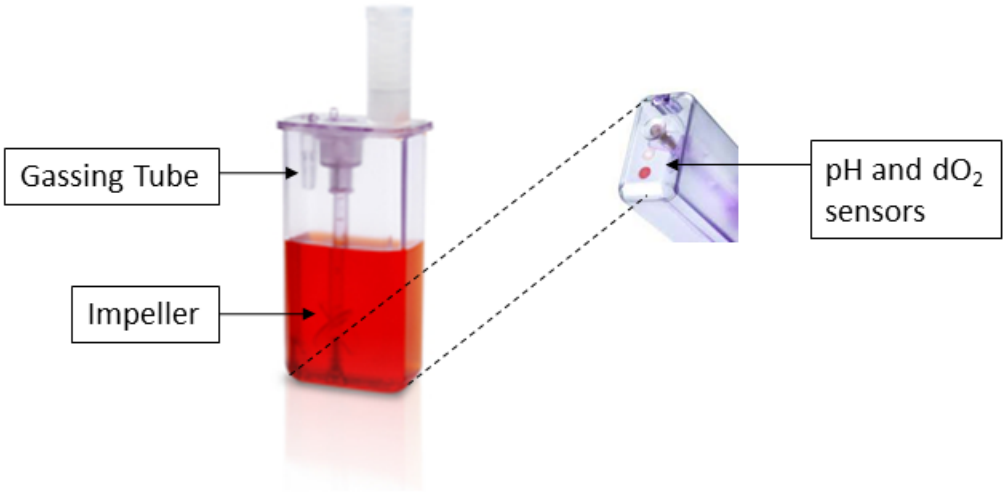

Figure 2.5: An ambr® 15 stirred-tank bioreactor vessel with an overlay gassing tube and a single impeller. Single use pH and dO_2 sensors are placed on the bottom of the vessel.

All the experiments were conducted in down-pumping mode and pH, temperature, dO_2 and headspace gas flow were measured and controlled throughout the experiments. The N_2 was set at 0.100 ml min^{-1} and the other gasses (CO_2 and O_2) were consequently regulated by the software in order to achieve the wanted dO_2 in each vessel. When the dO_2 was not controlled, the CO_2 was set to 5% and the O_2 to 21% of the total gas flow. pH upper limit was set at 7.2 and the lower limit at 7.1 for all the experiments. The upper limit was controlled by CO_2 inflow into the headspace, while the lower limit was controlled by 7.5% (w/v) sodium bicarbonate solution in distilled water, added to each vessel at need by the liquid handler. At the beginning of the runs 9 ml of cRPMI medium was put into each vessel using the automated liquid handler. The medium was

left to condition overnight and 3 ml from each vessel was collected by the liquid handler for pH sampling the following morning. The medium pH was measured off-line with and external pH probe and the value was inserted into the software for each vessel.

2.4.4.1 Primary T-cells

One run was performed using the ambr® 15 system with 24 bioreactors. The ambr® 15 bioreactor was placed into a Class 2 BSC in order to keep the culture sterile throughout the experiment. The target seeding density was of $0.5x10^6$ viable cells ml^{-1} in a total volume of 12 ml cRPMI medium supplemented with 30 IU ml^{-1} in each vessel. The daily sampling was performed using the liquid handler. 600 μl samples were taken from each vessel and placed into a different 1.5 ml Eppendorf tube® 3810X (Eppendorf, UK) previously placed on the sample rack and loaded onto the bioreactor hardware. Each 1.5 ml tube was mapped on the ambr software and uniquely assigned to a different vessel. 60-80 μl from each sample was used to determine the cell count and the viability, while the rest was used for metabolite analysis. 100% and 25% dilutions with fresh cRPMI medium containing the wanted amount of IL-2 in order to have a final concentration of 30 IU ml^{-1} were performed on day 3 and day 4 respectively, while a 40% medium exchange was carried out on day 5 in order to mimic the feeding regime in the ambr® 250 bioreactor. The dilutions were all performed by the liquid handler and a sample was taken before and after each medium addition/exchange.

2.4.5 1 L UniVessel® stirred-tank bioreactor culture

A 1 L UniVessel® Glass bioreactor (Sartorius Stedim Biotech, Germany), controlled through a DCU control tower (Sartorius Stedim Biotech, Germany) was used for scale-up studies (Figure 2.6).

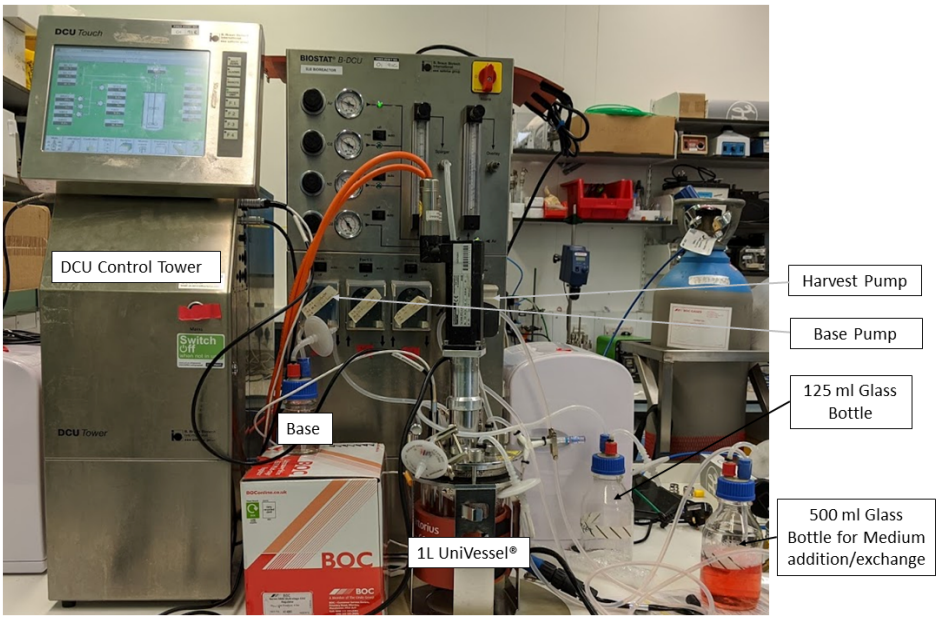

Figure 2.6: The 1 L UniVessel® glass bioreactor set-up. The base and the medium addition bottles were connected to the bioreactor through the base and the harvesting pump respectively.

The internal vessel diameter was T = 110 mm and the internal height was 180 mm. The vessel had a single 3-segment 30° pitched blade impeller (D=48 mm) and it was operated in down-pumping mode. The pH was measured throughout the experiment with the Easyferm K8 Plus/160 (Hamilton, USA) pH sensor. A calibration of the pH probe was performed at pH 4 and 7 prior to autoclaving the system before each run. The dO_2 was measured using a VisiFerm mA 160 H3 dO_2 optical sensor (Hamilton, USA).

The probe was calibrated before each run (with pure N_2 at 0% and with air at 100% dO_2). The total flow rate was set at 200 ml min^{-1} and the control tower was connected to air, O_2, CO_2 and N_2. The temperature was measured using the Pt100 probe with thermowell (Sartorius Stedim Biotech, Germany). The inflow gasses were controlled by the control tower in order to keep the dO_2 at the set point of 50%. The pH control was set between 7.1-7.2 and it was controlled by base addition (7.5% (w/v) sodium bicarbonate solution; lower limit) and CO_2 addition via gas blending (upper limit).

The 1 L vessel was connected to a 125 ml glass bottle (BellCo, USA) containing 80 ml of base and to a 500 ml glass bottle (BellCo, USA) for inoculation and medium addition or exchange. All connections were made using 3.2 mm Fisherbrand™ silicone pump tubing (Fisher Scientific, UK). Additionally, the sparger and headspace gas lines were connected to two different Midisart 2000 filters (Sartorius Stedim Biotech, Germany). The filters were covered using aluminium foil and the bioreactor and the bottles attached were autoclaved at 121°C. The bioreactor was then left to cool down overnight. Prior to inoculation, the base tube (connecting the 125 ml glass bottle to the bioreactor) was inserted into the base pump on the control tower, while the 500 ml medium bottle was inserted into the harvesting pump of the DCU tower.

2.4.5.1 Primary T-cells

In the runs performed with the 1 L UniVessel® the pH was controlled between 7.1 and 7.2 and dO_2 was set at 50% from inoculation to harvest. The impeller speed was set at

200 rpm in down-pumping mode. 400 ml of cell suspension with a target density of 0.5 x 10^6 viable cells ml^{-1} was pipetted into the 500 ml glass bottle and pumped into the bioreactor using the harvesting pump. The medium was supplemented with 30 IU ml^{-1} of IL-2. The daily sampling (1-2 ml) was performed through a single-use sampling port with needle-free septum (Sartorius Stedim Biotech, Germany) using a Luer-lok™ 50 ml syringe (Becton Dickinson, USA). 200 ml of the sample was used for the determination of the cell number and viability, while the rest was used for metabolite analysis.

The feeding strategy was kept proportional to the initial ambr® 250 and ambr® 15 runs. 400 ml of cRPMI medium were added on day 3 (100% dilution) and 200 ml (25% dilution) on day 4. Both medium additions were performed using the 500 ml glass bottle and the harvesting pump on the control tower. The medium was supplemented with IL-2 in order to have a final concentration of 30 IU ml^{-1} in the total volume inside the vessel after each addition. A 400 ml (40% of the total volume) medium exchange was performed on day 5. The medium was removed from the bioreactor via the harvesting pump and pumped into the 500 ml medium glass bottle. The bottle was then moved into a BSC (the tubing was long enough to enable this without disconnecting it form the bioreactor) and the cell suspension was put into eight 50 ml Falcon® tubes under sterile conditions. The tubes were then centrifuged at 350 *xg* for 10 minutes, the supernatant was discarded and the cells were re-suspended in 400 ml of fresh cRPMI containing 30000 IU ml^{-2}, pipetted into the sterile medium bottle and pumped back into the 1 L

vessel.

Flow cytometry analysis to determine the immunophenotype of the primary T-cells was performed on day 0 and day 7 (at harvest).

2.5 Calculation of the power input

The power input was calculated for each bioreactor at different speeds and filling volumes using the following equation:

$$P = P_o \rho N^3 D^5, \tag{2.1}$$

where P [W] is the power input, P_o is the power number [dimensionless], ρ [kg m^{-3}] is the density of the medium (here assumed to have the same physical properties as water), N [rev s^{-1}] is the impeller speed and D [m] is the impeller diameter.

2.6 Analytical techniques

Different analytical methods were used during the T-cell expansion in various platforms. Cell density and viability was assessed daily using the NucleoCounter® NC-3000™. Samples for medium analysis were taken on a daily basis and analysed using the CuBiAn HT270 Bioanalyser (Optocell GmbH & Co., KG, Germany). Flow cytometry to assess the T-cell immunophenotype and CAR expression of the T-cells was performed

on the day of the bioreactor inoculation and at harvest in the different expansion platforms used. Furthermore, potency assays (cyototxicity assay and cytometric bead array assay) were performed at the end of experiments when CAR-T cells were used.

2.6.1 Determination of cell density and viability

Cell counts and viability were determined using a NucleoCounter NC-3000 automated mammalian counter in combination with a Via-1 Cassette™ containing acridine orange and DAPI. A sample of at least 200 µl was taken daily form each expansion platform and put into a 1.5 Eppendorf tube®. The sample was then analysed using the NucleoCounter NC-3000 within the next 5 minutes. The Via-1 Cassette™ tip was immersed in the cell suspension and the sample was withdrawn by aspiration. Once the sample was loaded, the cassette was placed inside the NC-3000 and the analysis was started. The staining with acridine orange and DAPI was performed automatically by the NC-3000. The cell density and viability were displayed on the software and recorded for each sample.

2.6.2 Medium analysis and specific consumption rate

0.5-1 ml samples of spent medium were taken aseptically from each expansion platform for medium analysis on a daily basis and placed into 1.5 ml Eppendorf tubes® appropriately labelled. When medium addition or exchange were performed, the samples were taken before and after fresh medium was added. The medium samples were then placed

in a freezer at -20°C and stored for up to one month. Prior to analysis with the CuBiAn HT270 the samples were thawed at room temperature and mixed thoroughly with a P1000 mechanical pipette. The analysis of lactate [mmol l^{-1}] and glucose [mmol l^{-1}] were performed for all the samples. When specified, ammonia [mmol l^{-1}] and glutamine [mmol l^{-1}] concentrations in the medium were measured as well.

Once the metabolite data and viable cell number were collected, specific growth rate, doubling time, fold increase, and specific metabolite consumption rate were determined.

Specific growth rate

$$\mu = \frac{(\ln(\frac{C_x(t)}{C_x(0)}))}{\Delta t}, \tag{2.2}$$

where μ = specific growth rate [h^{-1}], $C_x(t)$ = the cell number at the end of the exponential growth phase, $C_x(0)$ = cell number at the start of the exponential growth phase, and Δt = duration of the exponential phase [h].

Doubling time

$$t_d = \frac{\ln 2}{\mu}, \tag{2.3}$$

where t_d = doubling time [h].

Fold expansion

$$FE = \frac{\text{Final viable cell number}}{\text{Initial viable cell number}} \tag{2.4}$$

Specific consumption rate

$$q_{met} = \frac{\mu}{C_x(0)} x \frac{C_{met(t)} - C_{met(0)}}{e^{\mu t} - 1}, \tag{2.5}$$

where q_{met} = specific consumption rate, $C_{met(t)}$ = metabolite concentration at the start of the exponential growth phase [mmol], $C_{met(0)}$ = metabolite concentration at the end of the exponential growth phase [mmol], and t = time [hr].

Lactate yield from glucose

$$\frac{Y_{lac}}{Glc} = \frac{\Delta[Lac]}{\Delta[Glc]}, \tag{2.6}$$

where $\frac{Y_{Lac}}{Glc}$ = lactate yield form glucose, Δ[Lac] = lactate production over a specific time period, and Δ[Glc] = glucose consumption over the same time period.

2.6.3 Flow cytometry

Immunophenotypic analysis of human primary T-cells was performed by flow cytometry after 7 days pre-expansion in T-Flask and at the end of the bioreactor culture, 7 days after inoculation. This was performed using BD LSRFortessa X-20 flow cytometer (BD Biosciences, UK) with five different lasers with excitation at 355, 405, 488, 561, and 640 nm.

2.6.3.1 Primary T-Cells

The T-cells, both pre-expansion and post harvest (day 7), were stained with the antibodies listed in Table 2.1 (BD Bioscience, UK).

The cell samples were washed twice with 1 x PBS and re-suspended in an antibody cocktail pre-prepared by adding each antibody to 50 µl of Brilliant Stain Buffer (BD Biosciences, UK) as per manufacturer's instructions. Cells were incubated with the antibodies at 4°C for 30 minutes. The cells were then washed with stain buffer (BD Biosciences, UK), supernatant was removed and the cells were fixed using a 1 x PBS solution containing 4% (v/v) paraformaldehyde (PFA; Sigma-Aldrich Company Ltd, UK).

Table 2.1: Antibodies used for flow cytometry staining. The name, clone, volume per test [µl], reactivity, and brand are listed for each antibody. All the antibodies were purchased from BD Biosciences, UK.

Name	**Clone**	**Volume per test [µl]**	**Reactivity**
BUV395 Mouse Anti-Human CD3	SP34-2	5	Human CD3
FITC Mouse Anti-Human CD4	RPA-T4	20	Human CD4
BUV737 Mouse Anti-Human CD8	SK1	5	Human CD8
BV421 Mouse Anti-Human CD197 (CCR7)	150503	5	Human CCR7
PE-Cy™7 Mouse Anti-Human CD45RO	UCHL1	5	Human CD45RO

After 15 minutes at 4°C, two final washes were performed using the stain buffer and

the tubes were kept in the fridge, wrapped in aluminum foil for no longer than 2 days, until flow cytometry analysis was performed. Staining specificity was confirmed using fluorescence minus one (FMO) controls for CCR7 and CD45RO for each sample. A minimum of 50,000 events were recorded for each sample and the data were analyzed using FlowJo™ computer software (BD Biosciences, UK). An example of the gating strategy is shown in Figure 2.7.

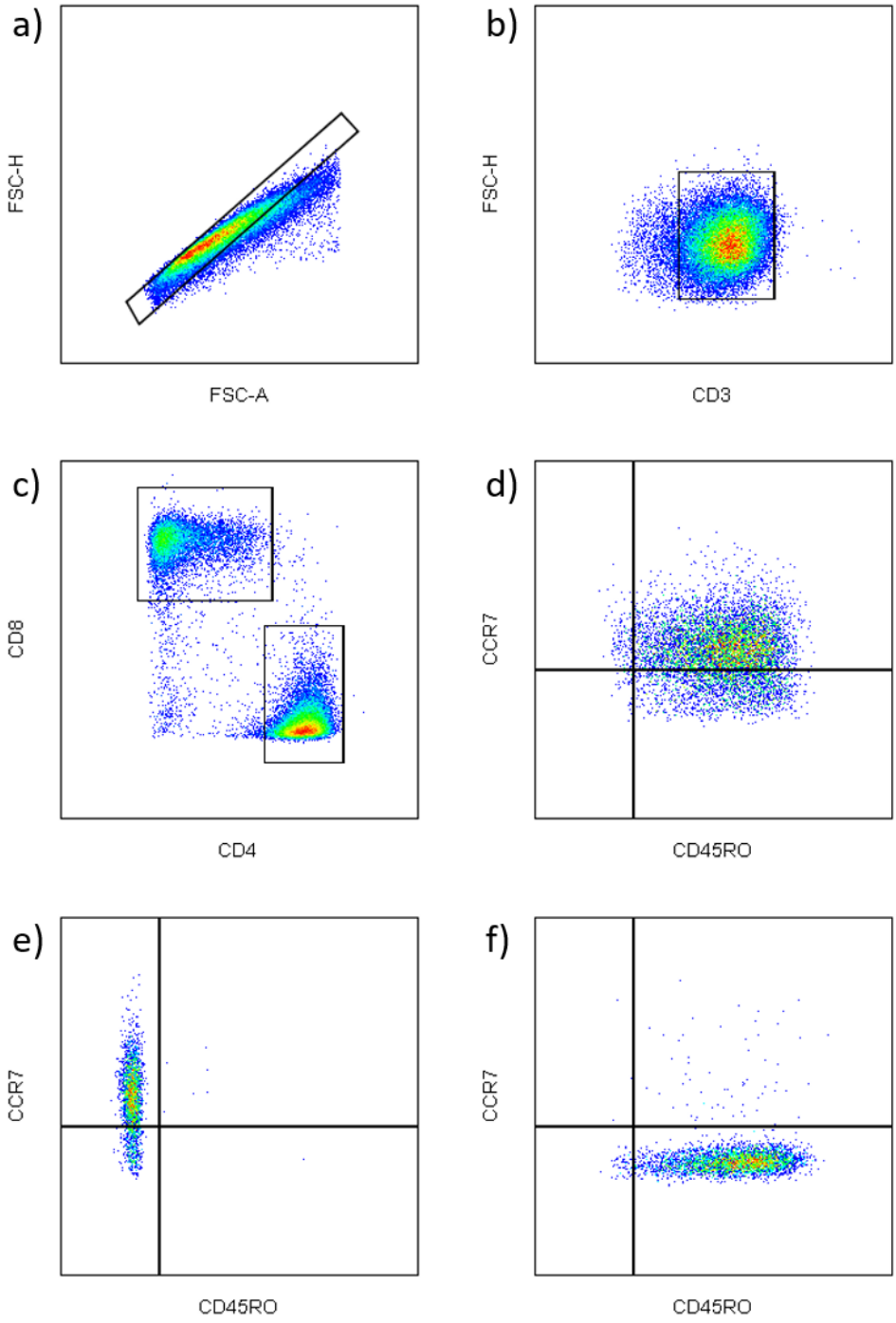

Figure 2.7: Gating strategy for immunophenotype analysis. (a) Single cells gating. (b) CD3 positive cells gating. (c) CD4 and CD8 positive T-cells. (d) CD8 positive T-cell subpopulations gated based on FMO controls. (e) FMO CD45RO control. (f) FMO CCR7 control.

2.6.3.2 CAR-T cells

In the experiments where CAR-T cells were used, the antibody panel used was the same as for the primary T-cells in order to determine the phenotypic composition of the cells (Table 2.1). Furthermore, another panel composed by: CD3-BUV396, CD4-FITC, CD8-BUV373 (BD Biosciences) and CD34-PE (Thermo Fisher Scientific, UK) was used to determine the CAR expression. Staining specificity was determined using FMO controls for CD34 for each sample. The samples were then prepared, acquired and analysed as described above (Section 2.6.3.1).

2.6.4 Cytotoxicity assay

2.6.4.1 Isolation of CAR-T Cells

Successfully transduced T-cells expressing the RQR8-FMC63-CAR were isolated at the end of the dynamic or static culture using the CD34 MicroBeads Kit (Miltenyi Biotech Ltd, UK) and LS columns (Miltenyi Biotech Ltd, UK) following the manufacturer's instructions. At the end of the isolation, the cells were re-suspended in cRPMI 1640 medium (without any IL-2) and kept in a humidified incubator at 37°C for 48 hours.

2.6.4.2 Plating cytotoxicity assay

Isolated CAR-T cells were then seeded at 1:1 effector:target (E:T) ratio, where Nalm6 cells, a B cell line expressing CD19 was used as the target. 5 x 10^4 Nalm6 target cells

were seeded per well in a 96 well plate (Thermo Fisher Scientific, UK) with the same number of CAR-T cells, in a total volume of 100 µl. Non transduced T-cells from the same donor were plated in co-culture with Nalm6 at a 1:1 E:T ratio as a negative control. CAR-mediated cytotoxicty was assessed 24 hours after seeding via flow cytometry analysis.

2.6.4.3 Flow cytometry

The cells were transferred into a V-shaped 96 well plate (Thermo Fisher Scientific, UK) and washed twice with 1 x PBS solution. 100 µl of stain buffer solution containing 6.25 µl of CD3-BUV395 ml^{-1} was added to each well and the cells were incubated in the fridge at 4°C for 30 minutes. The samples were then washed twice with stain buffer and re-suspended in 200 µl of 0.1% solution of SYTOX™ red dead cell stain (Thermo Fisher Scientific, UK) in stain buffer. The cells were then moved from the 96 V-shaped bottom well plate to mini FACS tubes (Corning®, France) and 25 µl of CountBright™ Absolute Counting Beads (Thermo Fisher Scientific, UK) was added to each mini FACS tube. The samples were then acquired on the BD LSRFortessa X20 flow cytometer.

2.6.4.4 Analysis of the cytotoxic ability of CAR-T cells

The samples were analysed using FlowJo™ computer software. Nalm6 were separated from T-cells based on the CD3+ staining on the control sample (Nalm6 cells co-cultured with non transduced T-cells). The live cells were then gated based on the SYTOX™ red

dead cell stain (Figure 2.8).

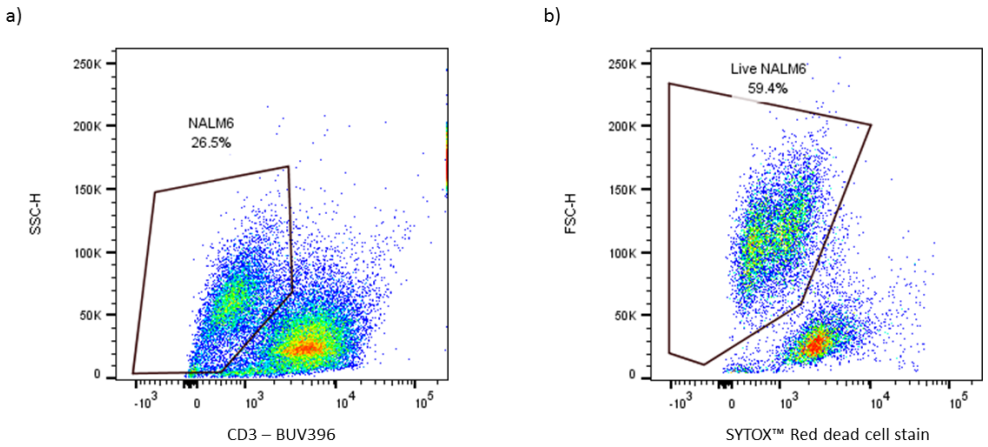

Figure 2.8: An example of the gating strategy used for the cytotoxic assay. a) The separation of Nalm6 cells from CD3+ T-cells. b) The separation of dead and live target cells (Nalm6) based on the SYTOX™ Red dead cell stain.

The percentage of remaining target (Nalm6) viable cell was calculated. Total number of viable cells

$$\text{Total number of viable cells} = \frac{\text{NVTCE}}{\text{NBE}} \text{x NB in } 25\mu\text{l}^2 \tag{2.7}$$

Remaining target viable cells

$$\text{Remaining target viable cells} = \frac{\text{Total number of viable cells (CART)}}{\text{Total number of viable cells (NT)}} \text{x } 100, \tag{2.8}$$

where NVTCE = number of viable target cell events, NBE = number of bead events,

and NB = number of beads.

2.6.5 Cytometric Bead Array (CBA) assay

The same plating procedure was followed as described for the cytotoxicity assay (Section 2.6.4), using isolated CAR-T cells and plating them at a 1:1 E:T ratio in a 96 well plate, using 5 x 10^4 Nalm6 cells per well. After 24 hours the plates were centrifuged at 200 *xg* in order to make the cells sediment and 70 μl of supernatant was removed and placed in a new V-shaped 96 well plate and placed in a -80°C freezer until the CBA human Th1/Th2/Th17 imunoassay (BD Biosciences, UK) was performed as per manufacturer's instructions. This assay allowed to detect the concentration [pg ml^{-1}] of the following cytokines in supernatant: IL-2, IL-4, IL-6, IL-10, TNF, INF-γ, and IL-17A.

Firstly, the human standards Th1/Th2/Th17 were prepared by reconstituting the lyophilised samples in 2 ml of assay diluent (both contained in the kit). The dilutions prepared were 1:2, 1:4, 1:8, 1:16, 1:32, 1:64, 1:128, and 1:256 together with a negative control. 10 μl of each Capture Beads (IL-2, IL-4, IL-6, IL-10, TNF, INF-γ, IL-17A) was then added to each sample (including the standards). Once the samples were ready to be analysed, they were placed in a clear round bottom 96 well plate (Corning®, France) and run on the BS FACSVerse™ cytometer (BD Bioscences, UK) and the data were analysed using BD FACSuite™ computer software (BD Bioscences, UK).

2.7 Statistical analysis

Data analysis was performed using GraphPad Prism 7 software (GraphPad, USA). Results are represented as mean $\pm$ standard deviation (SD). A one-way analysis of variance (ANOVA) test was used and values were considered statistically significant when probability (P) values were equal or below 0.05(*), 0.01(**), 0.001(***), or 0.0001(****).

Chapter 3

Demonstrating T-cells expansion in a stirred-tank bioreactor

3.1 Introduction

Static platforms (T-flasks, G-Rex and permeable bags) and rocking motion bioreactors are commonly used in the manufacturing of CAR-T cell therapies (Vormittag et al., 2018; Marsh et al., 2017b). Although T-cells are suspension cells, they are considered to be shear sensitive (van den Bos et al., 2014). This explains why little work has been done in stirred-tank bioreactors thus far (Klarer et al., 2018; Bohnenkamp et al., 2002; Carswell et al., 2000; Ou et al., 2019).

The purpose of this result chapter is to investigate the growth of T-cells in stirred-

tank bioreactors, given their proven scalability, extensive engineering and biological characterisation, and process monitoring and control capabilities which make them perfect candidates for large scale production (Q. A. Rafiq et al., 2016b). The bioreactor used in this study was the ambr® 250 bioreactor, a fully automated culture platform that enables the simultaneous operation of up to 24 bioreactors in parallel, each with a working volume range between 100-250 ml. This platform is suitable as a scale-down model for high-throughput screening and optimisation of culture parameters and reagents. Furthermore, it is a good candidate for the manufacturing of autologous CGTs, with its potential to scale-out and run more processes in parallel.

Preliminary results were gathered using Jurkat E6.1 cell line, an immortalised T-cell line originally obtained from the peripheral blood of a boy with T-cell leukemia (Abraham et al., 2004). The unbaffled vessel for the ambr® 250 bioreactor, developed for cells grown on microcarriers was used. Once proven that Jurkat E6.1 cells can be successfully grown in a stirred environment, primary human T-cells were used for further studies. First, the growth of these cells was investigated in a spinner-flask and later in the ambr® 250 stirred-tank bioreactor. Moreover, a comparison between two types of commercially available ambr® 250 vessels was carried out. The baffled vessel, commonly used for CHO culture (P. Xu et al., 2017) and unbaffled vessel, developed for adherent cells grown on microcarriers were compared in order to identify the best one for the expansion of T-cells.

3.2 Jurkat E6.1 in a stirred-tank bioreactor

The Jurkat E6.1 cell line has been used as a model for the growth of primary T-cells (Montano, 2014). In this chapter Jurkat E6.1 were used to gather preliminary results on the growth and viability of T-cells in a stirred environment. Static (T-flask) and dynamic environment (ambr® 250 stirred-tank bioreactor) were compared in terms of viable cells per millilitre, cell viability, fold expansion (Figure 3.1), specific growth rate, doubling time (Figure 3.2), pH and dO_2 profiles (Figure 3.4), and metabolite flux (Figure 3.5).

3.2.1 Jurkat E6.1 growth kinetics in a stirred environment

Figure 3.1a shows the number of viable cells per millilitre in the T-175 flask and in the ambr® 250 at 100 rpm in an unbaffled vessel (developed for cells grown with micro-carriers). The chosen stirring speed was the lowest at which the bioreactor could be operated (100 rpm), due to the concern of sheer stress damage to T-cells (van den Bos et al., 2014). The culture on day 0 was started with 100 ml in the bioreactor and 20 ml in the T-flask, with a seeding density of 0.1 x 10^6 live cells ml^{-1}. Medium was added on day 3 (100 ml in the ambr® 250 and 20 ml in the T-flask) and day 4 (50 ml in the ambr® 250 and 10 ml in the T-flask) in order to keep the cell density below 1 x 10^6 cells ml^{-1}. Once the volume in the vessel reached the maximum (250 ml), a 100 ml medium exchange was performed on day 5 in the ambr® 250 in order to provide fresh nutrients to the cells. 10 ml of cRPMI medium was added to the T-flasks on day 5. From day 5

onward, a 60% dO_2 control was set via gas blending.

The Jurkat E6.1 cells grew similarly in the two platforms with a final cell density of 3.89 ± 0.18 x 10^6 live cells ml^{-1} and 3.76 ± 0.08 x 10^6 live cells ml^{-1} in the ambr® 250 and T-175 flask respectively. The viability was slightly higher in the stirred-tank bioreactor compared to the static control (Figure 3.1b). However, the viability was above 95% at all times, showing that no damage was caused by the dynamic environment in the stirred-tank bioreactor. The drop in viability from day 6 to day 7 after seeding was likely due to a high density of cells in the medium and a lack of nutrients (discussed later). The fold expansion (Figure 3.1c), calculated using Equation (2.4), was 112.90 ± 2.55 in the T-flask (static control) and 97.25 ± 4.60 in the ambr® 250 bioreactor.

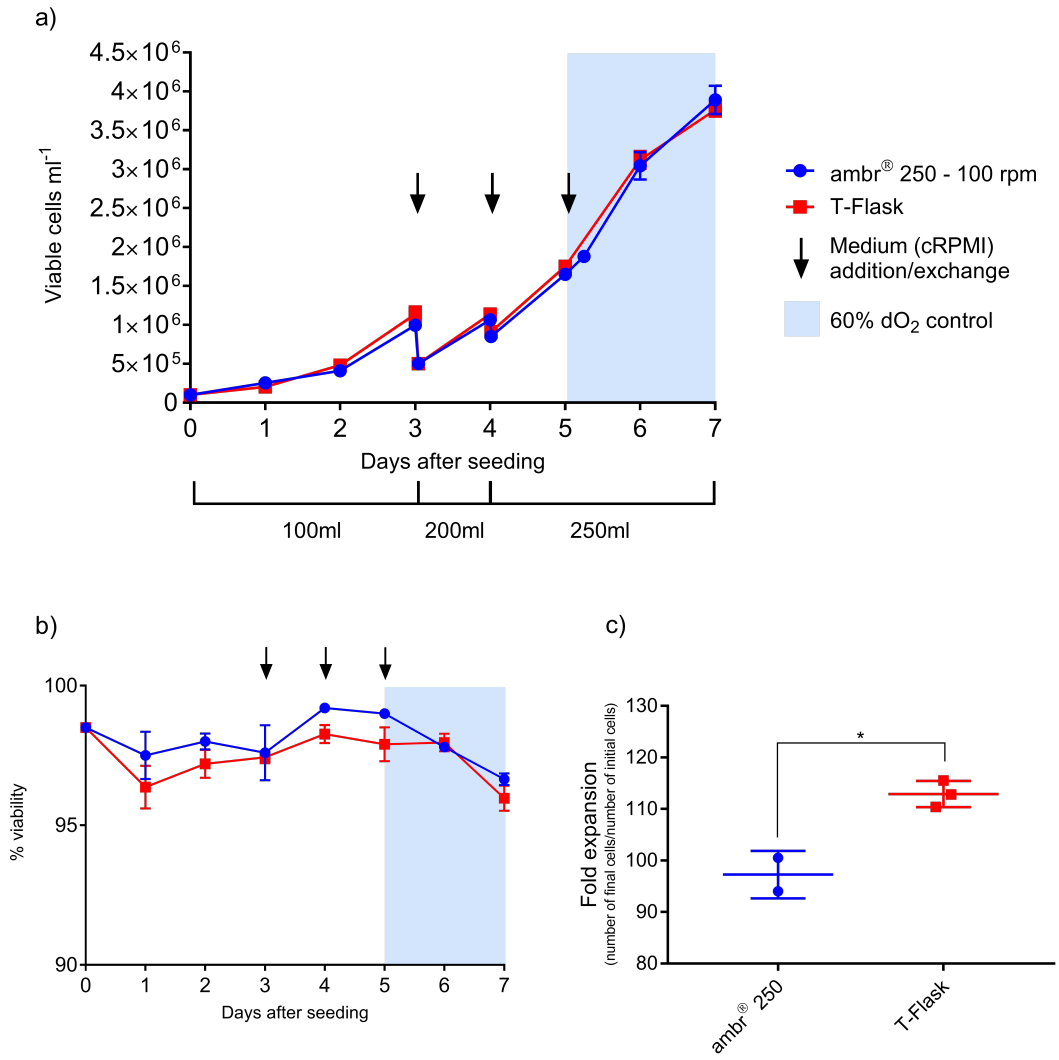

Figure 3.1: Growth of Jurkat E6.1 cell line over 7 days in T-175 flask and in an ambr® 250 bioreactor in the unbaffled vessel. The black arrows indicate medium addition or exchange on day 3, 4, and 5. 60% dO_2 control was started on day 5 after medium exchange. a) Viable cells ml^{-1} in 175 T-flasks (red; n=3) and ambr® bioreactor at 100 rpm (blue; n=2). The volumes at the bottom show the working volume on different days. Data shown as mean ± SD. b) Viability [%] over the 7 days of culture in the static (T-flask) and dynamic environment. c) The fold expansion [final number of cells/initial number of cells] for both expansion platforms. A one way ANOVA test was used and values were considered statistically significant when probability (P) values were equal or below 0.05(*), 0.01(**), 0.001(***), or 0.0001 (****).

The medium addition on day 5 in the flask increased the volume in the expansion platform (while no medium addition was performed in the ambr® 250) explains why there was a difference between the two vessels, although the viable cell concentrations were almost identical. A 20 ml medium exchange in the flasks would have made the dilutions between the two systems equal. However, since a dilution for the flask was performed on day 5 in the first experiment, the same feeding regime was kept for further experiments.

Nevertheless, the specific growth rate [h^{-1}] and the doubling time [h] were calculated for both platforms from day 2 to day 7 (Figure 3.2a,b). The linear regression for ln(cell number) versus time was performed and $R^2 > 0.9$ from day 2 to day 7, indicating the cells were in their exponential growth phase.

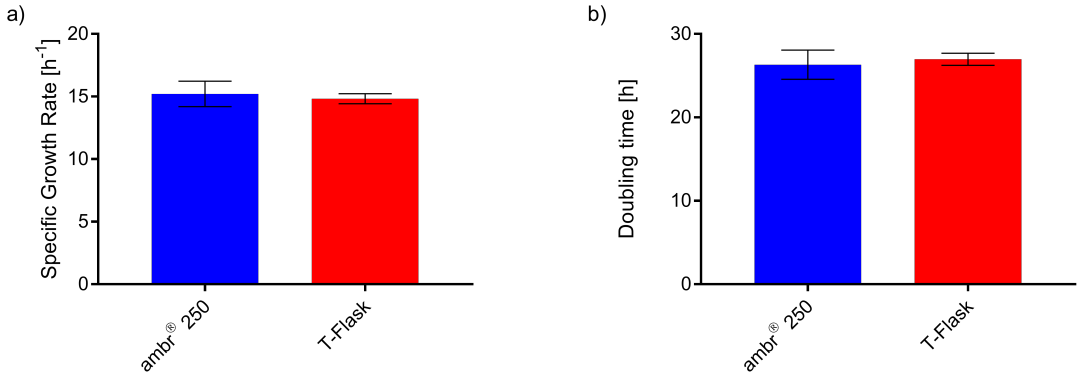

Figure 3.2: Growth kinetic parameters for Jurkat E6.1 cells grown in T-flask (static control; n=3) and ambr® 250 bioreactor at 100 rpm (n=2) for 7 days. The specific growth rate [h^{-1}] (a) and doubling time [h] (b) were calculated between day 2 at 7 when the cells were in their exponential phase of growth. Data shown as mean ± SD.

The specific growth rate was 14.82 ± 0.40 h^{-1} in the T-flask and 15.21 ± 1.02 h^{-1} in the ambr® 250 bioreactor. Doubling times were 26.96 ± 0.73 h and 26.31 ± 1.75 h in the T-flask and ambr® 250 respectively. Both values were very similar between the two platforms tested, indicating that the stirred environment did not have an impact on the growth kinetics of Jurkat E6.1 cells.

3.2.2 Cell sedimentation for medium exchange

In order to perform the medium exchange on day 5 in the ambr® 250 bioreactor, the impeller was stopped and the Jurkat cells were let to sediment. A 1 ml sample was taken each hour with a 5 ml steripipette paying attention not to mix the cell suspension, to assess the sedimentation rate of the cells (Figure 3.3).

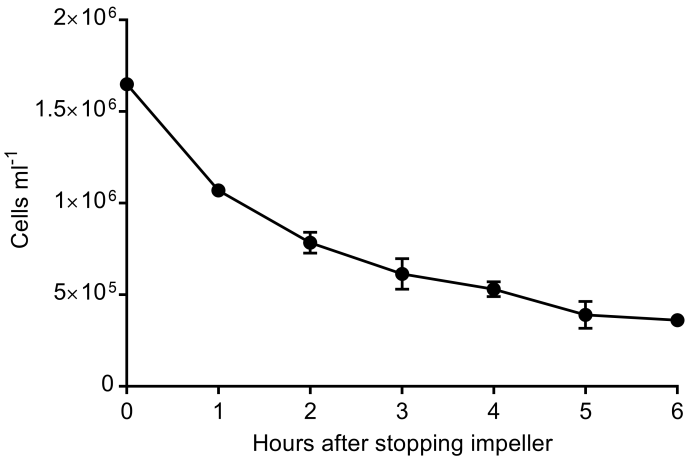

Figure 3.3: Cells ml^{-1} in the ambr® 250 bioreactor after stopping the impeller. The sampling was performed every hour until the sedimentation of the cells slowed down. Data shown as mean ± SD, n = 2.

The sample was taken always at the same vessel height, approximately $\sim$ 3.5 cm below the medium surface (being that the amount of medium that would have been removed with the medium exchange). 6 hours after stopping the impeller, the sedimentation rate slowed down (3.62 $\pm$ 0.97 x 10^5 cells ml^{-1} compared to 3.91 $\pm$ 0.73 x 10^5 cells ml^{-1} an hour earlier). The medium exchange was performed after 6 hours by removing 100 ml of cell suspension (approximately 4 x 10^6 total cells of 412 x 10^6 total cells in the bioreactor) and replacing it with 100 ml of fresh cRPMI. Once the impeller was re-started and a sample post medium exchange was taken, the number of cells resulted higher compared to 6 hours earlier (1.65 $\pm$ 0.18 x 10^6 before medium exchange and 1.88 $\pm$ 0.14 x 10^6 after medium exchange). Consequently, the proliferation in the 6 hours, while the impeller was stopped, was higher than the number of cells removed with the medium exchange.

The alternative to the medium exchange would have been to remove 100 ml of cell suspension, centrifuge it, re-suspend the cell pellet in fresh medium, and re-add it to the bioreactor. However, having in mind a fully automated process that could be carried out by the robotic arm alone, the sedimentation strategy for the medium exchange was preferred. Stopping the impeller, removing 100 ml of cell suspension, and replacing them with 100 ml of fresh medium can be all programmed via the ambr® software and executed by the robotic arm without the need of any human interaction with the system.

3.2.3 The impact of dissolved oxygen concentration and pH on Jurkat E6.1 growth

dO_2 and pH were monitored throughout the duration of the 7 days expansion in the bioreactor with the ambr® software (Figure 3.4). The spikes observed in the dO_2 profile are due to the feeding of the system, which required to open the cap of the bioreactor, while the dip was due to the stopping of the impeller on day 5. After the 100 ml medium exchange the dO_2 control was set at 60% until the end of the run. The k_La appeared to match the oxygen demand for the first 3 days resulting in a stable dO_2 at approximately 85%, until 100 ml of cRPMI medium were added. From day 3 to day 5 the dO_2 dropped form $\sim$ 85% to $\sim$ 40% (Figure 3.4a). The higher rate of fall in the dO_2 profile after day 3 was due to a lower rate of oxygen mass transfer from the headspace, due to the increased volume in the bioreactor and the increasing cell density, which led to a higher oxygen demand that could not be met. A 60% dO_2 control was therefore set on day 5 in order to compensate for the lower mass transfer and provide enough O_2 to the cells.

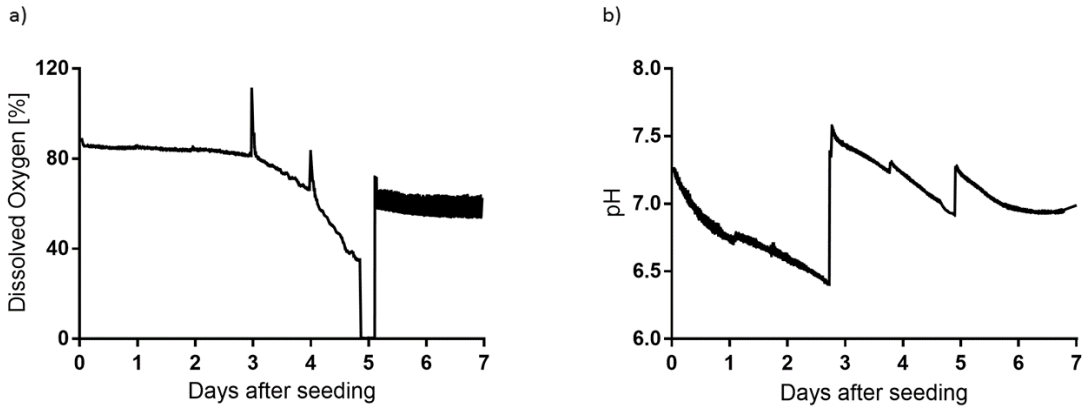

Figure 3.4: Dissolved oxygen percentage (a) and pH (b) readings in the ambr® 250 bioreactor during the culture of Jurkat E6.1 cells.

The pH profile (Figure 3.4b) correlates with the viable cell concentration and with the production and accumulation of lactate in the medium. The spikes in the pH profile are due to the medium additions (day 3 and 4) and medium exchange (day 5). The pH dropped from $\sim$ 7.3 on day 0 to $\sim$ 6.4 on day 3. After medium addition the pH reading went up to $\sim$ 7.6 and lowered to $\sim$ 7 on day 5 and 7. Notably, there was a plateau in the pH during the last day of bioreactor culture, which might indicate a slow down in the proliferation of the Jurkat E6.1 cells and a limited lactate production, as discussed later.

3.2.4 Metabolite analysis

The levels of glucose and lactate in the medium were measured off-line on a daily basis using the CuBiAn HT270 bio-analyser for the static and dynamic conditions (Figure 3.5). The glucose concentration (Figure 3.5a) in the fresh cRPMI medium was $\sim$ 10 mmol l^{-1} at day 0. The level of glucose in the medium dropped according to the cell growth and it was replenished on days 3, 4, and 5 with medium addition or exchange, as previously indicated. The level of glucose on day 6 was low both in the ambr® 250 and T-flask (1.63 $\pm$ 0.06 mmol l^{-1} and 0.54 $\pm$ 0.03 mmol l^{-1} respectively). Jurkat E6.1 cells ran out of glucose between day 6 and 7 as the reading on day 7 was 0 mmol l^{-1} in both platforms. The lack of glucose in the medium could potentially limit their proliferation. There were no significant differences in glucose concentration between the static and dynamic conditions up to day 5 (Figure 3.5a), when the level of glucose was slightly higher in the ambr® 250 due to the medium exchange. Both platforms run out of glucose between day 6 and 7. A feeding strategy based on the concentration of glucose could be applied in order to boost the cell proliferation. Supplying fresh medium containing glucose on day 6 would avoid the cells to suffer from glucose deprivation and slow down their growth.

The lactate production reflected the cell growth (Figure 3.5b). Higher the cell density, higher the lactate production and accumulation in the medium. The drops in the lactate concentration were due to medium addition or exchange on day 3, 4, and 5. From

day 6 to day 7 the amount of lactate produced was very limited, which relates to the lack of glucose in the medium and to the plateau in the pH profile. The lactate concentration did not show any major differences between the static and dynamic conditions up to day 4. Despite these slight differences from day 4 onward, the lactate concentration was almost the same on day 7, 15.13 $\pm$ 0.07 mmol l^{-1} in the ambr® 250 and 15.10 $\pm$ 0.09 mmol l^{-1} in the static control (T-175 flask). It has been shown that lactate levels over 20 mmol l^{-1} can inhibit the growth of primary T-cells, due to the lowering of the pH (Fisher, 2007). However, in this study none of the conditions reached this limit, suggesting that the lactate levels should not inhibit Jurkat growth.

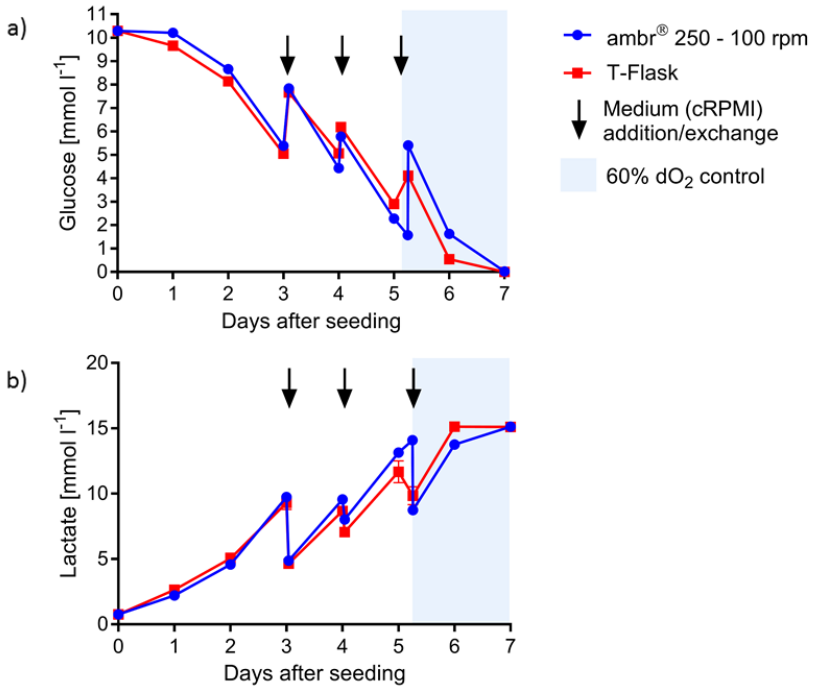

Figure 3.5: Metabolites concentrations for the ambr® 250 and the T-175 flask as static control. Data shown mean $\pm$ SD, n=2 for the ambr® 250 and n=3 for the T-flask. (a) Glucose concentration [mmol l^{-1}]. (b) Lactate concentration [mmol l^{-1}].

The medium exchange in the ambr® 250 bioreactor increased the glucose concentration to 5.40 ± 0.01 mmol l^{-1} compared to the T-flask after medium addition on day 5 (4.11 ± 0.15 mmol l^{-1}). Jurkat E6.1 in the T-flask were likely to run out of glucose earlier than the one cultured in the ambr® 250 bioreactor. The glucose deprivation could further limit their growth. To have more comparability between the two systems, a 20 ml medium exchange should have been performed in the T-flask as well. Furthermore, the level of lactate in the medium did not reach the level of T-cell growth inhibition (20 mmol l^{-1}) (Figure 3.5b), therefore the lower proliferation between day 6 and 7 (Figure 3.1), reflected by a plateau in the pH (Figure 3.4a), was most likely due to a lack of glucose.

The specific consumption rate for glucose and lactate were calculated for the T-flask and ambr® 250 bioreactor (Figure 3.6a,b).

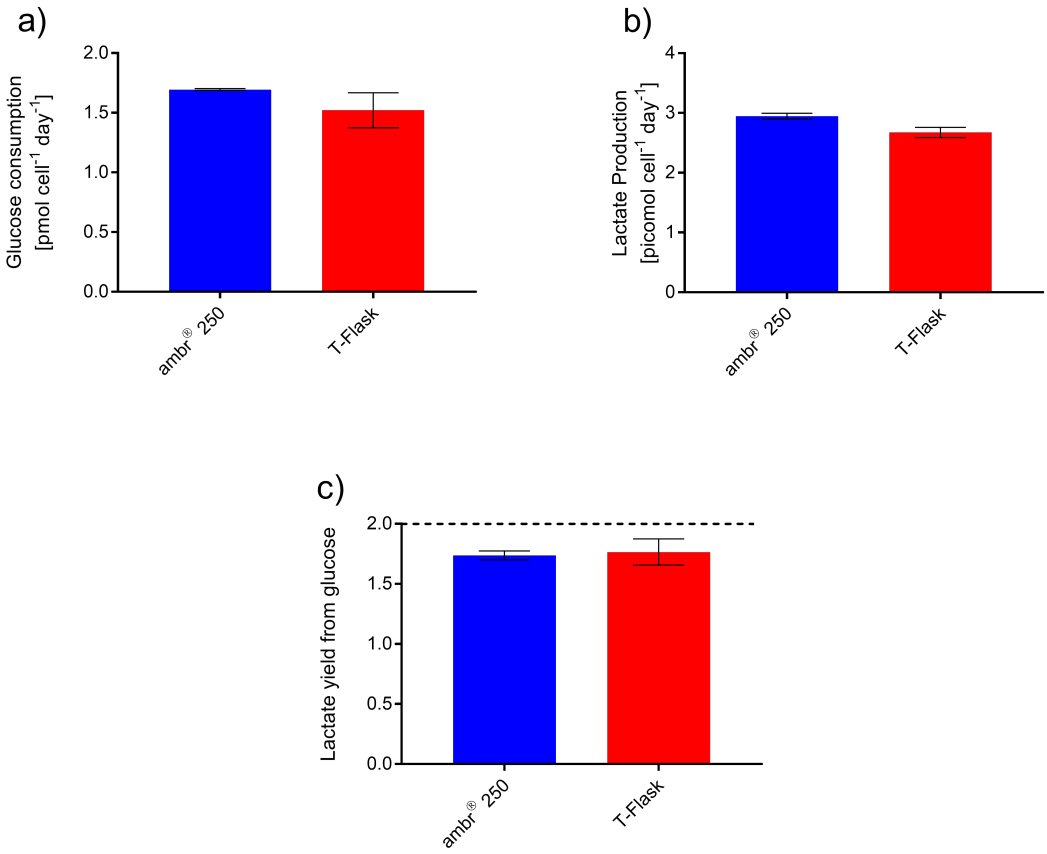

Figure 3.6: Specific consumption and production rates [picomol cell^{-1} day^{-1}] for glucose and lactate. Data shown as mean ± SD, n=3 for T-flask and n=2 for ambr® 250. (a) Glucose specific consumption rate in the culture medium in the static and dynamic condition. (b) Lactate specific production rate in the culture medium for both conditions. (c) Yields of lactate from glucose for the T-flasks and ambr® 250 vessels. Reference line at 2 is the maximum theoretical yield of lactate from glucose.

The consumption rates were calculated from day 2 to day 7 when the growth of the cells was considered to be in the exponential phase. Glucose consumption rate was 1.52 ± 0.15 pmol cell^{-1} day^{-1} in the T-flask (static control) and 1.69 ± 0.01 pmol cell^{-1} day^{-1} in the ambr® 250 bioreactor (Figure 3.6a). The rate of glucose consumption was comparable ($P > 0.05$) in the two system, suggesting that the stirred environment had

no impact on the glucose metabolism of Jurkat cells. The lactate production rate was 2.67 $\pm$ 0.08 pmol cell^{-1} day^{-1} in the T-flask and 2.94 $\pm$ 0.05 pmol cell^{-1} day^{-1} in the ambr® 250 bioreactor (Figure 3.6b). Once again, no significant difference ($P > 0.05$) was seen in the lactate production rate between the two culture platforms.

The lactate yield from glucose was 1.76 $\pm$ 0.11 for the T-flask and 1.74 $\pm$ 0.04 for the ambr® 250 bioreactor (Figure 3.6c). Both values were lower than the maximum theoretical yield of lactate from glucose of 2 mol mol^{-1}, suggesting that the cells could be consuming glucose via aerobic glycolisis rather than using the oxidative phosphorylation (OXPHOS) pathway (Vander Haiden 2009, Glacken 1988). When glucose is being metabolised via aerobic glycolysis, 1 mol of glucose results in 2 mol of ATP and 2 mol of lactate (Warburg, 1956). Aerobic glycolysis, which consists in the oxidation of glucose through glycolisis even when sufficient oxygen is present, has been identified as a trademark of tumour cells (Hanahan and Weinberg, 2011).

These findings are in line with the previously discussed results (similar growth and viable cell concentration in the two platforms), indicating that the stirred environment did not have an impact on Jurkat E6.1 growth kinetics and did not alter the glucose and lactate metabolisms of the cells.

3.3 Primary human T-cells in a stirred environment

After the successful results obtained with the Jurkat E6.1 cell line, the focus was moved on to primary human T-cells in a stirred environment (spinner-flask and ambr® 250). The first run with primary T-cells was performed in a spinner flask. After that an ambr® 250 bioreactor was used and two commercially available vessels, the baffled (used for CHO cells) and unbaffled one (developed for hMSCs grown on microcarriers) were compared in terms of rpm and power per unit volume. Primary T-cells were isolated from PBMCs and pre-expanded in T-flask placed into a humidified incubator in order to have enough cells for the inoculation 7 days from thawing. The first experiment with primary T-cells was performed in a glass spinner-flask. 0.5 x 10^6 cells ml^{-1} were needed for each bioreactor in 100 ml of cRPMI supplemented with 30 IU ml^{-1} of IL-2. Two vessels could be run in parallel on the ambr® 250 system. The growth (Figure 3.8), pH, dO_2 (Figure 3.11), and metabolite flux (Figure 3.12), were monitored over the 7 days of culture.

3.3.1 Primary T-cell growth kinetics in a spinner-flask

Spinner-flasks are commonly used as a small scale model for larger stirred-tank bioreactors. Although they are uncontrolled in terms of pH and dO_2, they are used as the first step for culturing new cell types in a dynamic environment (Hewitt et al., 2011; Q. A. Rafiq et al., 2013b). Therefore, an experiment in a spinner flask was conducted first in

order to gather preliminary data (Figure 3.7). The human primary T-cells cultured in the spinner-flask at 35 rpm did not show any significant growth, resulting in a final cell number of 0.18 x 10^6 viable cells ml^{-1} after 7 days.

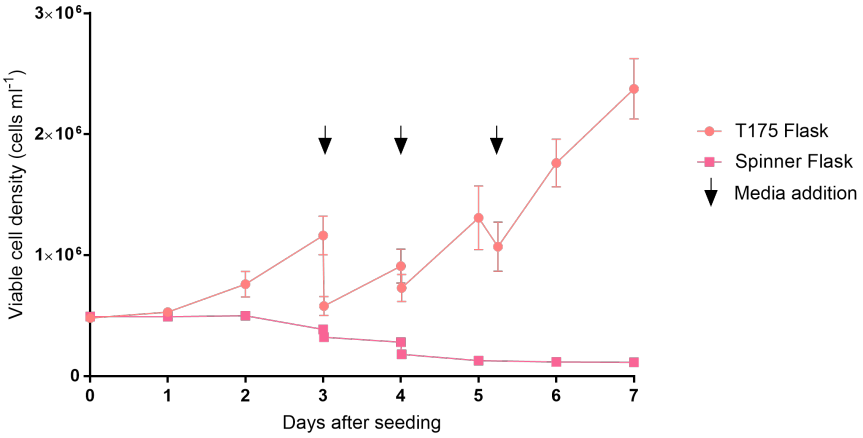

Figure 3.7: Viable cells ml^{-1} in the T-flask (n=3) and in a spinner-flask (n=1) at 35 rpm over 7 days. The black arrows indicate the medium addition for both systems on day 3 (20 ml in the T-175 flask and 10 ml in the spinner-flask) and day 4 (10 ml in the T-175 flask and 40 ml in the spinner-flask), while the last arrow on day 5 indicates a medium addition for the T-175 flask only. Data for the T-175 flask are shown as mean $\pm$ SD.

Due to the poor growth, the feeding regime was adapted in order not to dilute the cells too much, which could have had a negative impact on their proliferation. However, the T-cell proliferation was poor even in the first three days when the cells were not diluted at all, proving that the main cause for such low growth was not due to the concentration after dilution. These preliminary results could support the contention that T-cells are very 'shear sensitive'.

However, careful observation of the impeller, showed that most of the magnetic Dynabeads® were attached to it. The Dynabeads®, used for cell activation, have a

magnetic core, as does the bar connected to the impeller paddle in the spinner-flask, enabling the impeller paddle to be driven by a rotating magnet at the base. It would seem that because the Dynabeads® were magnetically attached to the impeller spinner bar, the Dynabeads® were not well mixed in the culture vessel and did non interact effectively with the T-cells, which would be dispersed throughout the medium, leading to poor activation, and consequently, poor proliferation.

3.3.2 Primary T-cell growth kinetics in a stirred-tank bioreactor

The growth kinetics in the two ambr® 250 vessels (baffled and unbaffled), the static condition in the ambr® 250 unbaffled vessel, and the static condition (T-flask) are shown in Figure 3.8.

The first vessel tested was the baffled vessel with two impellers at 100 rpm (Run 1), which has been widely utilised for ambr® 250 Chinese Hamster Ovary (CHO) suspension culture (Xu et al., 2017). During the first 3 days of culture when the volume in the vessel was 100 ml, only the lower impeller was submerged in the culture medium; after the 100 ml medium addition on day 3, both impellers were submerged. These conditions resulted in a final cell density $0.91 \pm 0.07 \times 10^6$ viable cells ml^{-1} which was significantly lower than the $2.38 \pm 0.25 \times 10^6$ viable cells ml^{-1} obtained for the static T-flask control.

Due to the poor performance and general belief that the region near the baffles in

baffled bioreactors is one of high shear which is not present if baffles are not installed, it was decided to investigate the use of the single-impeller, unbaffled ambr® 250 vessel configuration at the lowest speed (Run 2; Figure 3.8). This condition led to a higher final cell density of 3.62 $\pm$ 0.23 x 10^6 viable cells^{-1} compared to the static control and Run 1. The improvement from Run 1 to Run 2 might be attributed to the change in the fluid dynamic between the two vessels. However, there were two differences between the fluid dynamic regimes in Run 1 and Run 2. Not only have the baffles been removed in Run 2, in addition, because the impeller diameter and power number were greater, so was the specific power input (P/M), which defines the small-scale turbulence structure generally considered to impart the stress on cells in stirred bioreactors (Nienow, 1998). The specific power input, once the filling volume reached 250 ml on day 4, increased from 3.1 x 10^{-4} W kg^{-1} in Run 1 to 9.3 x 10^{-4} W kg^{-1} in Run 2 (Figure 3.9a).

In order to explore all the possibilities, a single run under static conditions (0 rpm) was conducted in the ambr® 250 unbaffled vessel (Static; Figure 3.8). The impeller was set at 200 rpm 5 minutes before taking the sample and stopped right after the sampling was performed. This Static run yielded a final cell density of 1.73 x 10^6 viable cells ml^{-1}, which was higher compared to the final cell density in Run 1 (0.91 $\pm$ 0.07 x 10^6 viable cells ml^{-1}). It can be noted how the performance in the initial stages of the expansion (up to day 3) was comparable to Run 2 and T-flasks, suggesting that the stirring at 100 rpm in the unbaffled vessel did not improve the T-cell growth in the initial stages of the

culture.

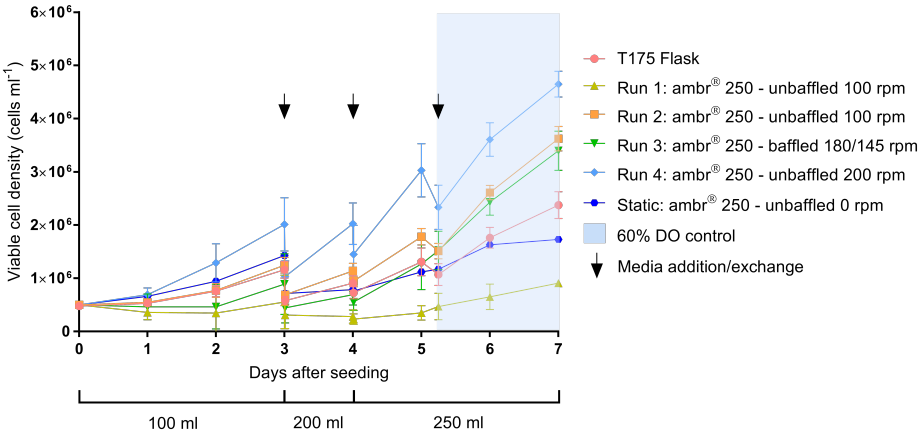

Figure 3.8: Viable cells ml^{-1} in the T-flask, baffled and unbaffled vessels in an ambr® at different speeds (n=3) and under static conditions (0 rpm; n=1). Data shown as mean ± SD. The black arrows indicate a medium addition (day 3 and 4) and exchange (day 5). 60% dO_2 control was introduced after medium addition on day 5.

Due to the considerations that increased P/M led to a better performance, the following run (Run 3), was carried out using a higher speed in the baffled two-impeller vessel (the same vessel used in Run 1), in order to match the specific power input obtained in Run 2 (9.3 x 10^{-4} W kg^{-1}) at 100 rpm. This meant operating the two-impellers baffled vessel at 180 rpm for the initial stages of the culture when the filling volume was 100 ml and only one of the two impellers was submerged. The speed was then reduced to 145 rpm when the volume was increased to 200 ml (day 3) and both impellers were submerged. The same speed was kept after the volume was increased to 250 ml on day 4. Culture under these conditions resulted in a final cell density of 3.34 ± 0.37 x 10^6 viable cells ml^{-1} (Figure 3.8), which was comparable with the cell density obtained with the single-impeller, unbaffled vessel in Run 2, both of which were higher than the final

cell density obtained in the static T-flask control. These results suggested that the baffles were not the reason for the poor performance in Run 1 (two-impeller, baffled vessel at 100 rpm).

Given the increase in final cell density achieved with the higher agitation speed in Run 3 compared with Run 1, it was decided to increase the impeller agitation speed further to 200 rpm in the single-impeller unbaffled vessel (Run 4). This configuration resulted in a P/M of 74 x 10^{-4} W kg^{-1} (Figure 3.9a) which yielded the highest cell density of 4.65 $\pm$ 0.24 x 10^{6} viable cells ml^{-1} at harvest.

The growth kinetics are further illustrated in Figure 3.9b, where the fold expansion for all the conditions investigated is shown. Run 1 (two-impeller, baffled vessel at 100 rpm) resulted in a significantly lower ($P < 0.0005$) fold expansion at the harvest point (4.58 $\pm$ 0.33) compared with all the other expansion platform tested. Both Run 2 (single-impeller, unbaffled vessel at 100 rpm) and Run 3 (two-impeller, baffled vessel at 180/145 rpm) resulted in a higher fold expansion of 18.1 $\pm$ 1.2 and 17.1 $\pm$ 1.7, respectively in comparison with the T-flask control. Given the highest final cell density was achieved in Run 4 (single-impeller unbaffled vessel at 200 rpm), this condition showed the greatest fold expansion of 23.2 $\pm$ 1.3, which was significantly larger ($P < 0.001$) than that of the T-flask static control which yielded a fold expansion of 15.2 $\pm$ 3.1.

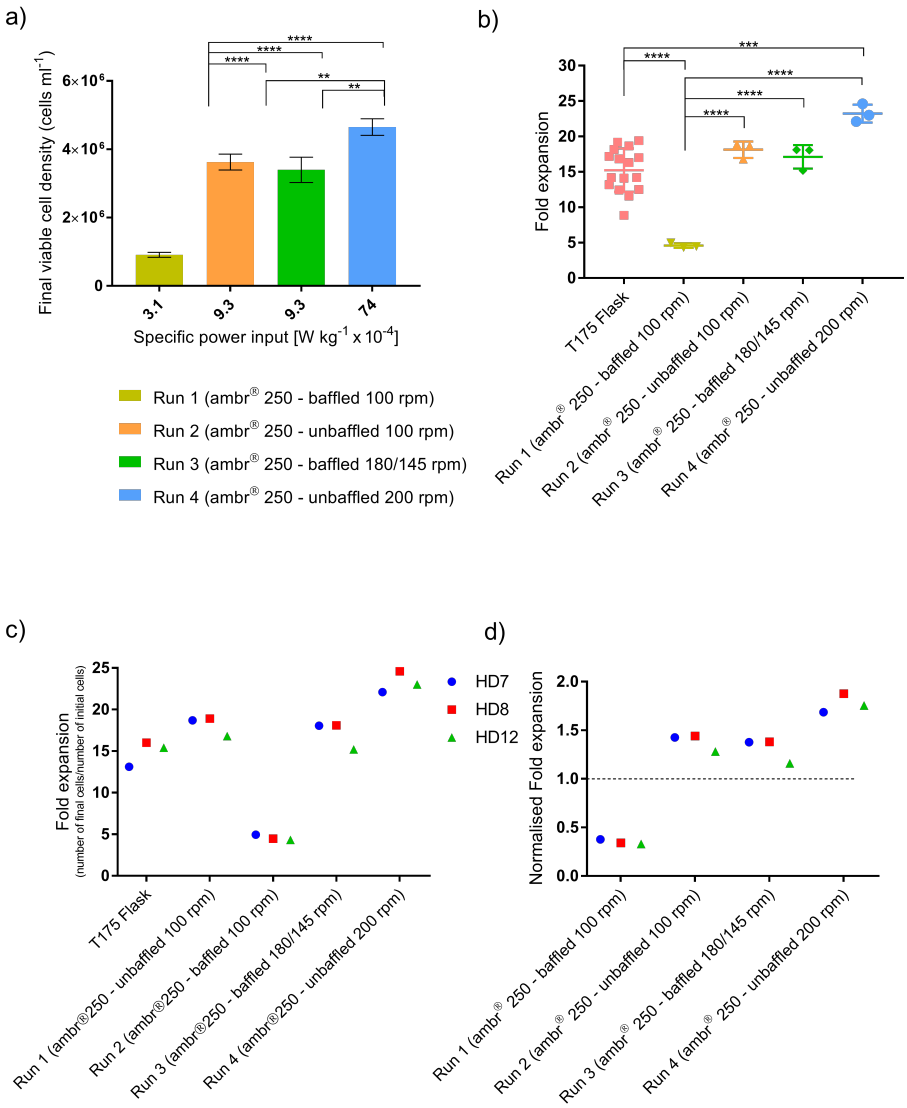

Figure 3.9: Growth kinetics of primary human T-cells in different expansion platforms. A one way ANOVA test was performed. Statistical significance is shown when probability (P) values were equal or below 0.05 (*), 0.01(**), 0.001(***), or 0.0001 (****). (a) Final viable cell density (cells ml^{-1}) at day 7 plotted against the specific power input (W kg^{-1} x 10^{-4}) for each condition. Data shown as mean ± SD. (b) Fold expansion (total number of viable cells at day 7/total number of viable cells at seeding) in all the different conditions. Data shown as mean ± SD. (c) Fold expansion for each donor (HD7, HD8, and HD12) in each expansion platform. (d) Fold expansion for each donor (HD7, HD8, and HD12) in the ambr® 250 bioreactors normalised with the fold expansion for the same donor in T-175 flasks. The reference dotted line at 1 shows the equivalence in fold expansion between the static control (T-175 flask) and the condition tested.

To assess the inter-donor reproducibility, each donor was analyzed separately (Figure 3.9c) and normalized to its own T-175 flask fold expansion (Figure 3.9d). All the conditions, except the baffled vessel at 100 rpm (0.39 ± 0.03), performed better than the T-Flask (reference line at normalized fold expansion = 1), as illustrated in Figure 3.9d. This analysis also demonstrated a high reproducibility between the 3 donors in all the systems tested, with the higher coefficient of variation (%CV) being 10.25% in the T-175 flask, suggesting that the automated ambr® 250 system could reduce the donor-to-donor variability.

Specific growth rate and doubling time were calculated for all the conditions (Figure 3.10). Both parameters were calculated between day 2 and 7 when the T-cells were growing exponentially (the linear regression for ln(cell number) versus time was performed and $R^2 > 0.9$). This was true for all the conditions (static and dynamic) exception made for Run 1. In this case the cells never reached the exponential phase (ln(cell number) plotted versus time always resulted in an $R^2 < 0.9$). Therefore, no conclusions could be drawn for that particular condition and this explains the large error bars for Run 1.

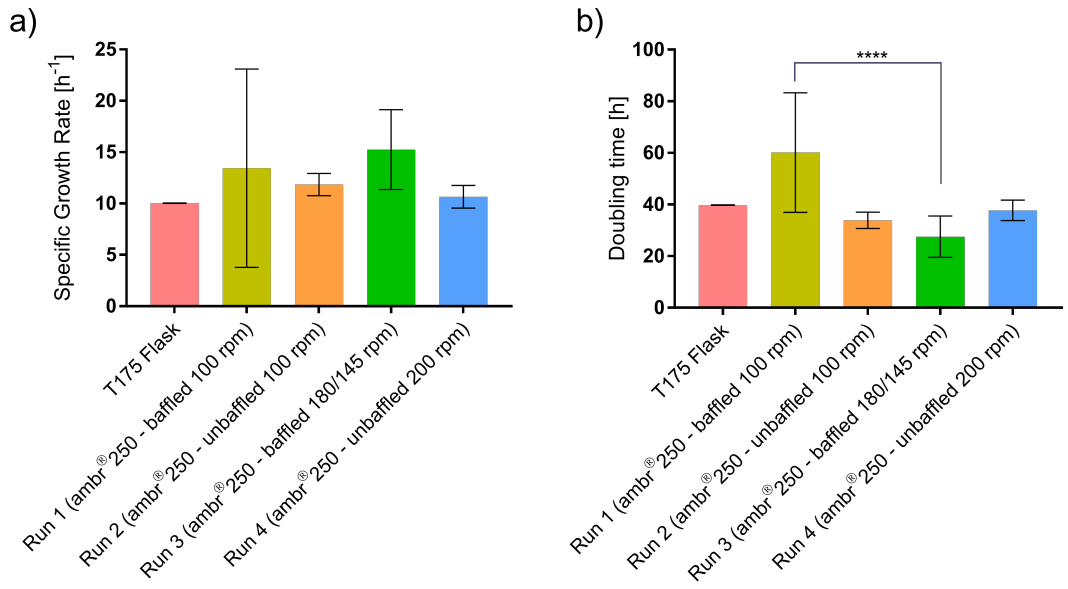

Figure 3.10: Growth kinetics parameters for human primary T-cells grown in T-flask (n=3) and ambr® 250 bioreactor (n=3). Both parameters were calculated between day 2 and day 7 when the cells were in the exponential phase of growth. Data shown as mean ± SD. A one way ANOVA test was performed. Statistical significance is shown when probability (P) values were equal or below 0.05 (*), 0.01(**), 0.001(***), or 0.0001(****). (a) Specific growth rate [h^{-1}]. (b) Doubling time [h].

The specific growth rate was comparable ($P > 0.05$) between the T-flask (static control) and Runs 2-4 (Figure 3.10a). However, the growth rate in the static control (10.03 ± 0.02 h^{-1}) was slightly lower compared to the conditions in the ambr® 250 bioreactor. Figure 3.10b shows the doubling time of the primary T-cells. The doubling time for the T-flask (39.82 ± 0.10 h) was slightly higher compared to Run 2 (33.89 ± 3.19 h), Run 3 (25.55 ± 8.02 h), and Run 4 (37.74 ± 3.78 h), showing a faster proliferation in the ambr® 250 bioreactors than in the static control, justifying the higher

cell concentration at harvest (day 7).

3.3.3 pH and dissolved oxygen concentrations

The pH and dO_2 were monitored throughout the duration of the 7 day expansion with the ambr® software (Figure 3.11). The spikes observed in the dO_2 profiles are due to the feeding of the system, which required the opening of the cap of the bioreactor (which was housed in a biological safety cabinet). For all runs, the impeller was stopped on day 5 for 6 hours, in order to let the cells sediment and allow a 100 ml medium exchange, after which a dO_2 control as 60% was started. The feeding protocol was kept the same as for the Jurkat E6.1 cells in order to be able to compare the two sets of experiments without inducing new variables in the process.

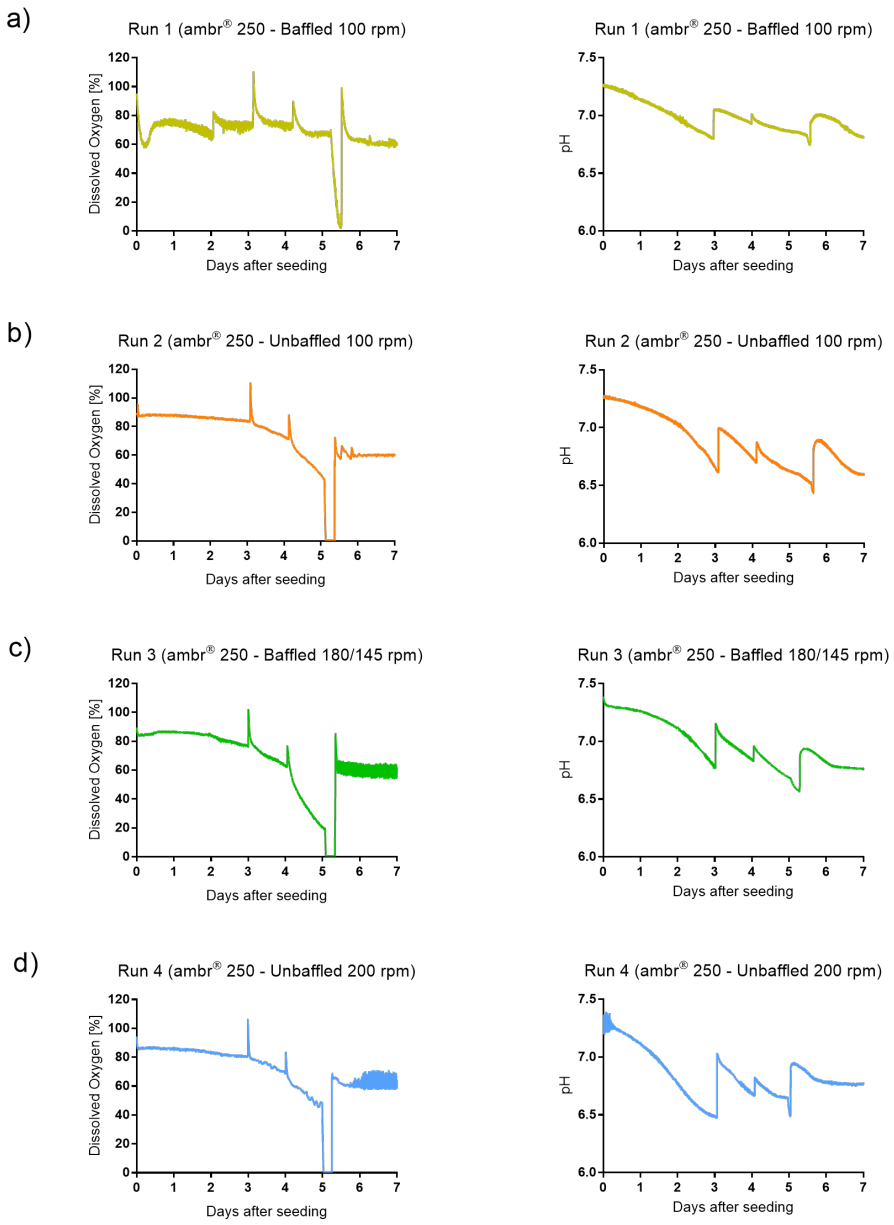

Figure 3.11: Representative dissolved oxygen (dO_2; left hand side) and pH (right hand side) trends under different agitation and fill conditions in the two ambr® 250 vessels over 7 days. In all runs, dO_2 control at 60% was introduced at Day 5 after the impeller was stopped for 6 hr (dO_2 at 0%) to let the cells sediment and perform a 100 ml medium exchange. (a) Run 1 – in the baffled vessel at 100 rpm. (b) Run 2—in the unbaffled vessel at 100 rpm. (c) Run 3—in the baffled vessel at 180/145 rpm (the speed was changed on Day 3). (d) Run 4—in the unbaffled vessel at 200 rpm.

The two-impeller baffled vessel at 100 rpm (Run 1) displayed a rapid lowering of the dO_2 (from 80% to 60%) when compared with other runs (Figure 3.11a). This drop was probably due to a very low k_La at such a low agitation intensity. The dO_2 then increased to $\sim$ 75% on day 2, perhaps because of cell death during the adaptation period so that the oxygen demand of the cells could be met, and then remained stable up to day 5 since cell numbers hardly increased. Agitation was then stopped and dO_2 fell to zero. Upon restarting, it was controlled at 60% by gas blending. This last sequence occurred in every run.

The starting dO_2 in Runs 2-4 was $\sim$ 85% and it remained stable for the first 3 days with the agitation intensity leading to a k_La seemingly matching the oxygen demand of the cells. After more medium was added and steady cell growth from day 3 to day 5, the oxygen demand of the cells could no longer be met and a drop occurred to $dO_2 \sim 40\%$ in Run 2 (Figure 3.11b), to 20% in Run 3 (Figure 3.11c), and to 50% in Run 4 (Figure 3.11d).

The pH profile (Figure 3.11) correlates with the viable cell concentration and with the lactate production and accumulation as discussed below. The spikes in the pH measurments are due to medium addition and exchange (day 3, 4, and 5).

The pH readings in Run 1 (two-impeller baffled vessel at 100 rpm) showed higher readings compared with the other conditions, due to the lower number of viable cells in the system and a consequent lower lactate production (discussed below). Runs 2 and

4 (single impeller unbaffled vessel conditions at 100 and 200 rpm, respectively; Figure 3.11c,d right hand side) showed minimal differences in terms of pH profile, with the lowest point being $\sim$ 6.5 on day 3 and 5. Finally, the slope of the pH profile in the last hours of the cell culture for Run 3 (two-impeller baffled vessel at 180/145 rpm; Figure 3.11c) and Run 4 (unbaffled vessel at 200 rpm; Figure 3.11d) may indicate that the cell expansion slowed down during this period.

3.3.4 The interaction between agitation, Dynabeads, and cell growth

As discussed previously (Section 3.3.1), primary human T-cells in the spinner flask did not grow as expected, due to the Dynabeads® being attached to the impeller and not interacting with the cells. A poor result compared with the static T-flask control and ambr® static control (0 rpm) was also found in Run 1 (two-impeller, baffled vessel at 100 rpm). Due to the prevailing concerns regarding agitation speed and potential for fluid dynamic stresses on T-cells, the lowest possible agitation speed the system could accommodate was used (100 rpm). After this first run, it would have been easy to conclude that T-cells prefer to be grown in static conditions and are very sensitive to fluid dynamic stress which were preventing growth. By persevering using the newer, larger diameter single-impeller in the unbaffled vessel (Run 2), a higher level of cell growth was obtained compared with both Run 1 and the static controls both in T-flask and in the ambr®. Run 3 in the baffled vessel and Run 4 in the unbaffled vessel, both at speeds

higher than those used initially in the respective vessels, led to improved performance as shown in Figure 3.8.

The fact that these increases in speed led to an improved performance in Run 3 compared with Run 1 and ambr® 250 Static condition, and in Run 4 compared with Run 2, strongly suggests that the problems contributing to poor growth in Run 1 was due to some phenomenon other than fluid dynamic stress. One possibility is that at 100 rpm in Run 1, the Dynabeads® were not interacting with the cells due to poor suspension, resulting in inadequate T-cell activation. A key reason for this hypothesis is the poor performance in the spinner flask where the magnetic core of the beads was causing them to attach to the magnetic spinner rather than be fully suspended in the culture medium. This hypothesis was further reinforced by the Static run in the ambr® 250 vessel and by the T-flask performance, where neither cells nor Dynabeads® were suspended and they were in contact even without motion. However, when the Dynabeads® were not suspended and cells were (Run 1), contact was very poor.

In addition, though the Dynabeads® are very small (a few microns in size) they are rather dense (SG $\sim$ 1.4), much denser than microcarriers (SG $< \sim$ 1.1). It is well established that the increase in speed required to just completely suspend particles (commonly designated as N_{JS}) of greater density is much higher than that required to accommodate particles of larger sizes (A. Nienow, 1968; Zwietering, 1958). The Dynabeads® are about $\sim$ 4.5 μm in diameter. Thus, the relatively high density and the

small size of the beads (which makes observation of suspension difficult) both suggest that at the lower agitation speed, the particles were not well suspended. This explanation for the poor performance in Run 1 (two-impeller, baffled vessel at 100 rpm) is further reinforced by the improved performance with increased impeller speed for the two-impeller, baffled vessel in Run 3 (180/145 rpm) and again for the unbaffled vessel between Run 2 (100 rpm) and Run 4 (200 rpm). Using multiple, identical donor material and consistent culture parameters with the exception of agitation speed, a substantial increase in the final cell density with increasing agitation was observed.

3.3.5 Agitation intensity and cell growth

The presence of the magnetic field in the spinner-flask and the magnetic core of the Dynabeads® clearly explains the attachment of the beads to the spinner stirrer bar. This attachment also was the reason for poor culture performance in the spinner flask and it was not related in any way to the fluid dynamic environment present.

To make a comparison of, and explain the difference in the culture performance in the two configurations of the stirred ambr® 250 bioreactor vessels (baffled and unbaffled), where the only difference between the various runs was the fluid dynamic environment, it is helpful to compare the specific power input which is numerically equivalent to the mean specific energy dissipation rate. The power input is given by Equation 2.1. The specific power is then P/M [W kg^{-1}] where M [kg] is the mass of medium in the

bioreactor (A. Nienow, 1998) which in each run varies with the time as described in Table 3.1.

Table 3.1: Different conditions tested in the ambr® bioreactors, each indicating the working volumes, number of impellers submerged by the medium and correspondent speed and specific power input at different times throughout the experiments.

	Run 1	**Run 2**	**Run 3**	**Run 4**
Vessel Type	Baffled	Unbaffled	Baffled	Unbaffled
Starting Volume Day 1-3	100 ml			
Impeller agitation speed (rpm) x 10^{-4} W kg^{-1} from Day 1 to 3	100/3.8	100/23	180/22	200/184
Number of impellers submerged in the culture medium Day 1-3	1	1	1	1
Working Volume Day 3-4	200 ml			
Impeller agitation speed (rpm) x 10^{-4} W kg^{-1} from Day 3 to 4	100/3.8	100/12	145/12	200/92
Number of impellers submerged in the culture medium Day 3-4	2	1	2	1
Working Volume Day 4-7	250 ml			
Impeller agitation speed (rpm) x 10^{-4} W kg^{-1} from Day 4 to 7	100/3.1	100/9.3	145/9.3	200/74
Number of impellers submerged in the culture medium Day 4-7	2	1	2	1

In Run 1 (two-impeller baffled vessel at 100 rpm), P/M was very low, much lower than would normally be found in free suspension culture (Alvin W Nienow, 2006a). However, since the dO_2 did not drop below $\sim$ 60%, the fact that the cells hardly grew could not be attributed to inadequate mass transfer. At the higher speed in Run 3 (two-

impeller baffled vessel operating at 180/145 rpm), initially P/M = 2.2 x 10^{-3} W kg^{-1}, which was still low for free suspension culture, but within the range used. In Run 3, the cells grew relatively well, which certainly did not suggest that the problem at the lower speed (Run 1) was due to fluid dynamic stresses damaging cells.

After day 4, when the volume was increased to 250 ml, the specific power decreased and the rate of decrease of dO_2 significantly increased to reach a value of $\sim$ 20% at day 5, going back to 60% when dO_2 control was set (Figure 3.11c). The higher rate of fall in the dO_2 profile was due to the lower rate of O_2 mass transfer from the headspace and the increasing cell density at the latter stage of culture leading to a higher oxygen demand.

Comparing Runs 2 and 3, the P/M value tracks extremely closely between both runs, as indeed was the intention. As can be seen, in that case, all measured parameters in the majority of cases were remarkably similar. In both cases, the culture performance was superior to that obtained in the static T-flask control.

In Run 4, the P/M value (74 x 10^{-4} W kg^{-1}) was typical of that found in commercial processes across many scales in free suspension culture (Nienow, Scott et al., 2013) and the cell growth was the highest by a considerable margin. There was no indication of 'shear sensitivity'. To assess the likelihood of fluid dynamic stress damaging cells, the usual approach was to compare the size of the cell to that of the Kolmogorov scale of turbulence, λ_K:

$$\lambda_K = (\varepsilon_{T\,max}/\upsilon^3)^{-1/4}, \tag{3.1}$$

where $\varepsilon_{T\,max}$ [W kg^{-1}] is the maximum specific energy dissipation rate close to the impeller and υ [m^2 s^{-1}] is the kinematic viscosity. If $\lambda_K >$ size of the cell, it should not be damaged. The precise value of the maximum to the mean specific energy dissipation rate (=P/M) has proved difficult to measure (Gabriele et al., 2009), but based on literature, a reasonable but high value to assess the likelihood of damage can be assumed. Thus, assuming that $\varepsilon_{T\,max}$ is 50 times the mean specific energy dissipation rate (=P/M) for the geometry question (Alvin W Nienow et al., 2016), then λ_K = 32 μm ≫ size of T-cell. Thus, damage would not be expected based on this analysis of the impact of turbulence on cells.

This discussion strengthens further the earlier suggestion that the reason for the poor performance at the lowest P/M, Run 1 (3.1 x 10^{-4} W kg^{-1}), was due to the inability of the agitation to suspend the Dynabeads®. At the higher P/M investigated, Run 4 (74 x 10^{-4} W kg^{-1}), it was shown that the Kolmogrov scale was greater than the size of the T-cells. It was also seen that the higher P/M, the better the performance. It is worth nothing in this instance, it was not a lack of oxygen transfer that prevented the cells growing at the lowest P/M, nor was the dO_2 a problem at the higher speed. Higher speeds increase many mixing parameters, but the current results indicate that it is better cell-bead contact that gives better performance. This relationship suggests that

the interaction between Dynabeads® and cell is related to the frequency with which each is brought into contact with the other. Even though the Reynolds number here ($\sim$ 3,000) at the highest P/M was less than the value at which the turbulence is fully established, it has been found that analysis based on the assumption of turbulent flow work well for hMSCs grown on microcarriers at similar Reynolds numbers (Alvin W Nienow et al., 2016). Under turbulent flow conditions, the higher the specific energy dissipation rate, the greater the rate of contact of particles (Davies, 2012; Levich, 1962), so the concept that higher P/M values led to greater interaction between cells and Dynabeads® and improved culture seems reasonable. In addition, higher agitation intensity above the minimum required for suspension, N_{NJ}, leads to a more homogeneous distribution of particles throughout the medium (A. Nienow, 1997), thus further improving the contact between Dynabeads® and cells.

Computational Fluid Dynamic (CFD) simulation studies have been widely used to determine the flow patterns and local liquid velocities in stirred tank bioreactors. This has been performed for the ambr® 250 unbaffled vessel bioreactor as a single-phase (liquid only) simulation (Rotondi et al., 2021). However, for the work presented in this thesis, the suspensions of Dynabeads® in the ambr® 250 vessel, would need to be considered as a two-phase simulation, adding a layer of complexity to the simulation. Although the average size of the Dynabeads® is known, the density of the Dynabeads® is unknown and changes throughout the volume of the beads, from a high density mag-

netic core, to a less dense polymeric coating. This makes it hard to have a good approximation of the overall density of the magnetic beads, which plays a determinant role in the CFD simulation. Small changes in particle density can have a big impact on the outcome of the model. This adds additional complexity when trying to estimate the minimum impeller speed required for Dynabeads® suspension. Furthermore, the experimental validation of the CFD model would require advanced techniques (e.g. electrical resistance tomography) due to the small size of the Dynabeads®. Nonetheless, a single-phase CDF modelling could help to identify if there are parts in the bioreactor that are not homogeneously mixed at lower speed, which could potentially have an impact on the cell to beads interaction.

3.3.6 Metabolite concentrations

The levels of glucose, lactate, and ammonia were measured off-line on a daily basis (Figure 3.12). The glucose concentration (Figure 3.12a) reflected the trends previously described in terms of cell growth. The condition which resulted in the lowest final cell density (Run 1) had the highest amount of glucose remaining in the medium samples, correlating well with the cell growth kinetic data. The condition which resulted in the highest final cell density (Run 4), resulted in a lower glucose concentration in the medium when compared with the other conditions analysed.

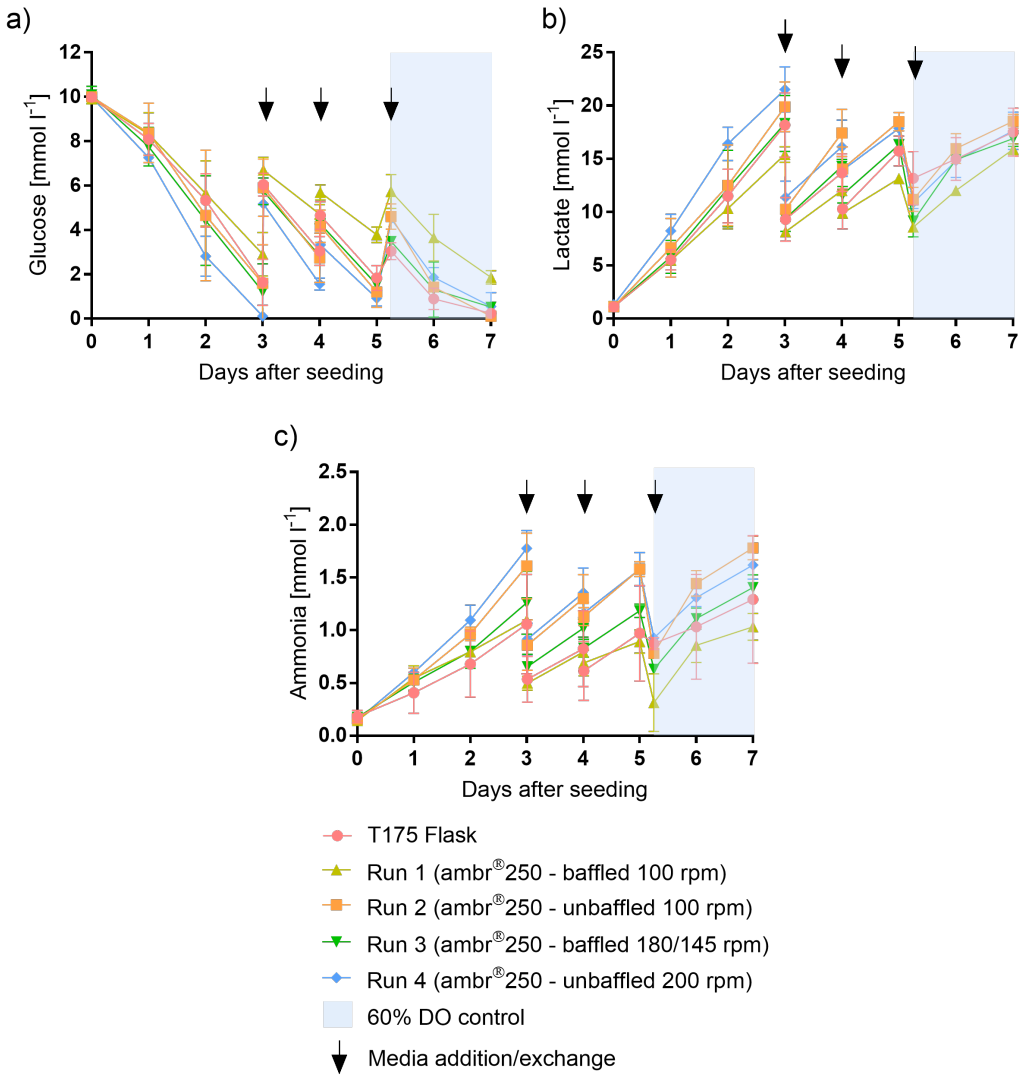

Figure 3.12: Metabolite concentration profiles under the different agitation in the two ambr® 250 vessels over 7 days and in T-175 flasks as a static control. The black arrows indicate a medium addition/exchange. Data shown as mean ± SD, n=3. (a) Glucose concentration [mmol l^{-1}] in the culture medium in the different expansion systems. (b) Lactate concentration [mmol l^{-1}] in the culture medium in all the examined conditions. (c) Ammonia concentration [mmol l^{-1}] in the culture medium in the different expansion systems.

The lactate concentration was higher in the best performing condition (Run 4), which reached the highest cell density. This was evident in the first three days of culture after which the lactate accumulation was similar to the other conditions. On the other hand, the worst performing condition in terms of cell growth (Run 1) showed the lowest accumulation of lactate in the medium (Figure 3.12b). Ammonia production followed the same trend as lactate production, showing a higher accumulation of ammonia in the medium for the fastest growing condition (Run 4) especially in the first 3 days of culture (Figure 3.12c). Run 1 was the condition with the lowest ammonia concentration at harvest.

The specific consumption or production rates for glucose, lactate, and ammonia were calculated for T-flask and the different conditions in the bioreactor (Figure 3.13). It was assumed that the cells were in the exponential phase of growth between day 2 and 7, which was the case for all the conditions except for Run 1. In Run 1 the cells growth kinetic was hardly exponential, therefore no conclusions could be drawn from this condition. The specific consumption rate for glucose, showed how cells in the ambr® 250 bioreactor consumed a larger amount of glucose, although no significant difference ($P > 0.05$) was detected. It is known that the consumption of glucose is higher for activated and faster growing T-cells (Frauwirth et al., 2004). This explains the higher glucose consumption rate for Run 2 (1.71 ± 0.18 pmol cell^{-1} day^{-1}), Run 3 (1.91 ± 0.66 pmol cell^{-1} day $^{-1}$), and Run 4 (1.15 ± 0.16 pmol cell^{-1} day^{-1}) compared

to the T-flask (static control; 0.45 ± 0.10 pmol cell^{-1} day^{-1}). Similarly, the conditions with the higher glucose consumption rate, resulted in a higher lactate production rate. The cells cultured in the static T-flask showed a lower accumulation of glucose (0.68 ± 0.29 pmol cell^{-1} day^{-1}) compared to Run 2 (3.62 ± 1.25 pmol cell^{-1} day^{-1}), Run 3 (3.87 ± 2.07 pmol cell^{-1} day^{-1}), and Run 4 (1.81 ± 0.67 pmol cell^{-1} day^{-1}).

Activated T-cells are known to require an increased source of energy to proliferate, which was reflected in an increase in the uptake of glucose and production of lactate (Wahl et al., 2010). Ammonia specific consumption rate mimicked the trend discussed for lactate accumulation, the cells cultured in the ambr® 250 showed a higher ammonia production rate compared to the static control, due to their faster proliferation (Figure 3.13d).

Finally, the yield of lactate from glucose is presented in Figure 3.13c. There was no significant difference in the yield of lactate from glucose in all the conditions analysed which resulted in values ranging from 1.51 ± 0.39 to 2.09 ± 0.55 (except for Run 1; 3.28 ± 2.07 due to the non exponential growth of the cells), which was close to 2 mol mol^{-1}, the maximum theoretical yield of lactate from glucose. This result suggests that there was no impact on the primary T-cells metabolic profile caused by the dynamic environment.

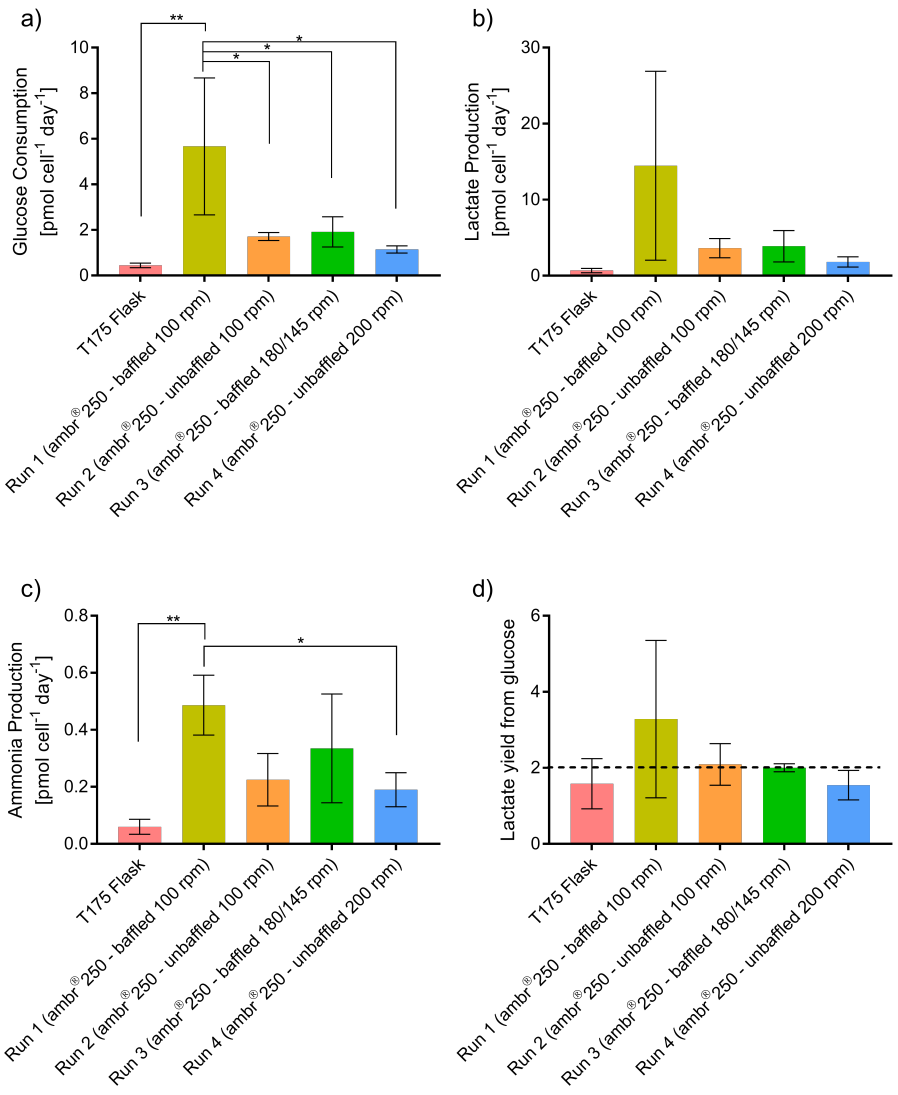

Figure 3.13: Specific consumption/production rates [picomol cell^{-1} day^{-1}] for glucose, lactate and ammonia were calculate from day 2 to day 7 of culture. Data shown mean ± SD, n=3. A one way ANOVA test was performed. Statistical significance is shown when probability (P)values were equal or below 0.05 (*), 0.01(**), 0.001(***), or 0.0001(****). (a) Glucose specific consumption rate in the culture medium in the different expansion systems. (b) Lactate specific production rate in the culture medium in all the examined conditions. (c) Ammonia specific production rate. (c) Yields of lactate from glucose. Reference line at 2 is the maximum theoretical yield of lactate from glucose.

3.3.7 The impact of agitated stirred-tank bioreactor culture on cell quality

Flow cytometric analysis was performed at the beginning and at the end of the expansion in the bioreactors. The $CD8^+$ subpopulation was then gated for naïve (CCR7+ CD45RO-), central memory (CCR7+ CD45RO+), effector memory (CCR7- CD45RO+), and terminally differentiated (CCR7- CD45RO-) T- cells, based on FMO controls . The CD4 to CD8 T-cell ratio was taken as an indicator of the quality of the final product (Figure 3.14).

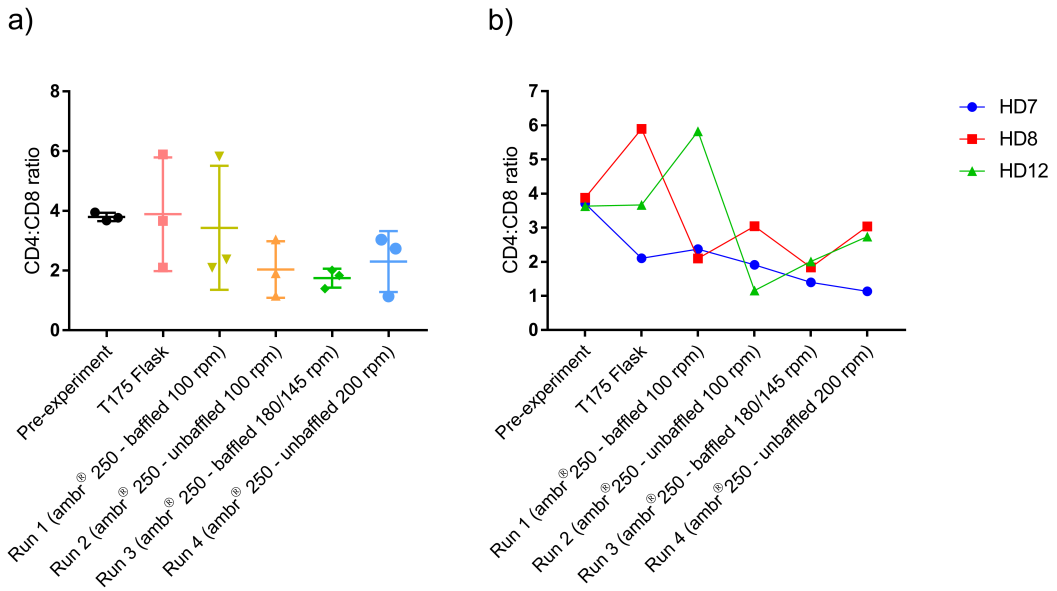

Figure 3.14: Phenotypic characterisation of primary T-cells when seeded in the bioreactor (pre-experiment) and post-harvest in the different agitation and fill conditions in the two ambr® 250 vessels over 7 days and in T175 flasks as a static control. (a) CD4:CD8 ratio in each expansion vessel. (b) CD4:CD8 ratio for each donor in different vessels individually.

It can be seen from Figure 3.14 that the ratio of CD4:CD8 was higher at the beginning of the culture (3.89 $\pm$ 1.90), while after the culture in the ambr® 250 bioreactor, it lowered towards the desired 1:1 value for Run 2-4. At the same time, a lower variability between the three different donors was shown after the expansion in the ambr® 250 stirred-tank bioreactor vessels compared with the T-flask static control (Figure 3.14), with the exception of Run 1, where the cells were not properly activated. Each donor was then plotted individually (Figure 3.14b) in order to assess the donor-to-donor variability.

All there donors showed a similar CD4:CD8 ratio after pre-expansion. HD7 showed a similar trend in all the expansion platforms, with the lowest CD4:CD8 ratio being 1.13 in Run 4 and the highest being 2.37 in Run 1. HD8 showed a slightly higher CD4:CD8 compared to HD7, with a ratio of 5.88 in the static control. This trend only occurred for this particular donor. Finally, for HD12 the highest CD4:CD8 ratio was seen in Run 1 (CD4:CD8 ratio of 5.82). Notably, for all three donors the CD4:CD8 ratio in Run 2, 3 and 4 was lower compared to the pre-expansion one.

Moreover, the $CD8^+$ T lymphocyte subpopulation was analysed in terms of naïve, central memory, effector memory, and terminally differentiated T-cells. Figure 3.15a and b show $CD8^+$ T central memory and effector memory subpopulations (the amount of naïve and terminally differentiated T-cells was lower than 5% in all samples).

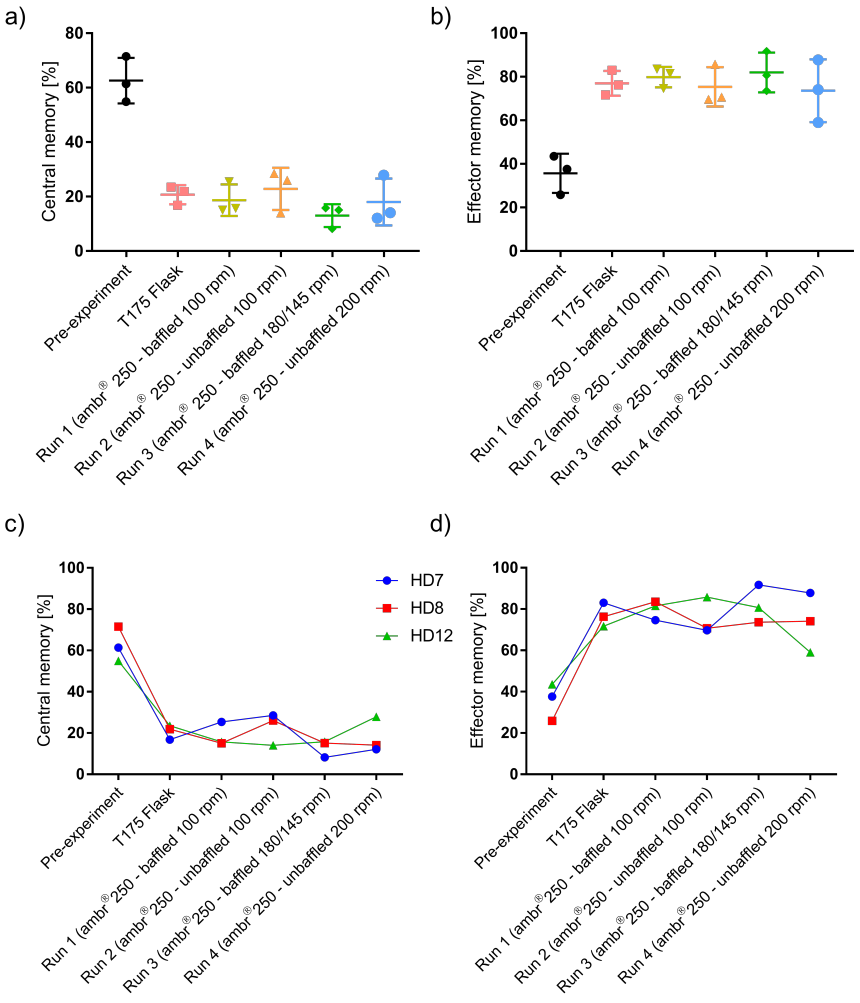

Figure 3.15: Phenotypic characterisation of primary T-cells when seeded in the bioreactor (pre-experiment) and post-harvest in the different agitation and fill conditions in the two ambr® 250 vessels over 7 days and in T175 flasks as a static control. Data shown mean ± SD. (a) $CD8^+$ T central memory ($CCR7^+$ $CD45RO^+$) subpopulation percentage of the cells. (b) $CD8^+$ T effector memory ($CCR7^-$ $CD45RO^+$) subpopulation percentage of the cells. (c) The three donors used (HD7, HD8, HD12) are plotted individually to show the $CD8^+$ T central memory percentage in each culture vessel. (d) The three donors used (HD7, HD8, HD12) are plotted individually to show the $CD8^+$ T effector memory percentage in each culture vessel.

The central memory subpopulation was higher in the pre-experiment sample (62.61 $\pm$ 10.58%) compared with all the other conditions. On the other hand, the effector memory cells increased from 35.69 $\pm$ 10.98% to $\sim$ 80% after 7 days expansion in the different systems. Notably, no significant difference was found in the T-cell subpopulation profiles between the static T-flask control and the various ambr® 250 stirred-tank bioreactor runs. All the three donors tested show a similar trend in the different expansion platforms in terms of central and effector memory subpopulations (Figure 3.15c,d).

Although it was demonstrated that primary human T-cells from multiple donors can be grown more effectively in an ambr® 250 stirred-tank bioreactor in comparison with a static T-flask control, it is necessary to take into account any impact on cell quality. This was ascertained by assessing cellular immunophenotype. CD4:CD8 T-cell ratio and $CD8^+$ T-cell subpopulations were further analysed before inoculation and post-harvest in terms of naïve, central memory, effector memory, and terminally differentiated T-cells. With respect to the CD4:CD8 T-cell ratio, ideally an equal amount of $CD4^+$ and $CD8^+$ T-cells would be present in the final composition (Turtle et al., 2016). From the data obtained, there was a greater level of consistency between replicates with Runs 2-4 in comparison with the static T-flask control. This difference may be indicative of the benefits of automation and improved process monitoring and control associated with automated bioreactor platforms as shown previously for human mesenchymal stem cell/microcarrier cultures in the ambr® 15 microbioreactor system (Q. A. Rafiq et al.,

2017).

Naïve and central memory T-cells have a higher persistence when re-infused into the patient (Sommermeyer et al., 2016), therefore, a higher percentage of these cells and a lower percentage of T-cells in more differentiated stages are desirable in the final product for immunotherapy applications. Figure 3.15 shows $CD8^+$ T central memory and effector memory subpopulations. Although the expanded cells appeared to have a more differentiated phenotype, importantly, this was the case irrespective of the culture platform used or agitation conditions. The tendency of the cells to differentiate toward the effector memory phenotype can be explained by the prolonged expansion protocol (14 days in total including cell pre-expansion before bioreactor inoculation), double activation (at thawing and before inoculation in the bioreactor and T-flask), and the use of IL-2 in the medium, which was shown to provoke differentiation if used for lengthy periods (Crompton et al., 2014; Cha et al., 2010). Using a shorter expansion protocol (seeding freshly isolated cells in the ambr® 250 bioreactor) and replacing the IL-2 with different interleukins (IL-7, IL-15, and IL-21), would help to maintain a more undifferentiated phenotype of the cells (Sabatino et al., 2016; N. Singh et al., 2016).

These data suggest that further optimization of the culture process (both static T-Flask and stirred-tank bioreactor culture) is required to facilitate the production of the desired T-cell subset. However, with the potential for high-throughput development using systems like the ambr® 250 bioreactor, this investigation paves the way for the

design of experiment approaches to be used to streamline T-cell manufacturing optimization efforts. Importantly, cell differentiation was not impacted by the agitation regime, presenting a similar phenotype to the static controls, thereby, suggesting that an agitated culture environment does not impact the cell differentiation, whilst achieving, in certain conditions, an increased fold expansion.

3.4 Conclusions

The focus of the study was to establish whether human T-cells could be cultured in stirred-tank bioreactor systems, which have proven scalability and process control capability (Q. A. Rafiq et al., 2016b). The general belief that T-cells are shear sensitive (van den Bos et al., 2014) has limited the use of such systems and favoured static expansion platforms (i.e., T-flasks, permeable bags and G-Rex). In this study, however, it has been demonstrated that Jurkat E6.1 cell line as well as primary human T-cells not only can be grown in stirred-tank bioreactors, but that higher impeller agitation speeds improve proliferation with no adverse impact on the quality of the cells. Jurkat E6.1 cell line was used for initial proof of concept studies, however to better understand the growth dynamic of human primary T-cells, these cells were isolated from whole blood or PBMCs for further experiments. This provided a more reliable set of data to build on for future studies.

Importantly, from the data obtained, there is no indication that T-cells prefer being

grown under static conditions or are sensitive to fluid dynamic stresses within a stirred-tank bioreactor system at the agitation speeds investigated (100 - 200 rpm). The immunophenotype analysis of the primary T-cells at the end of the bioreactor runs did not show any differences between the static and dynamic conditions. Furthermore, there was no evidence of an alteration of the metabolism of the T-cells in the stirred-tank compared to the T-flask.

Primary T-cells grow better under higher agitation speeds, and in all but one investigation (Run 1), resulted in a higher final cell density compared to the T-flask static control where dO_2 control could not be used. All the runs in the ambr® 250 under dynamic conditions performed better than the ambr® 250 Static run, where the dO_2 control was kept above 60% after day 5 as in all the other conditions. The only condition that under-performed compared to the Static run in the ambr® was Run 1, where it is believed that the poor cell-to-bead interaction due to the cells being suspended, but not the Dynabeads, lead to poor activation and poor T-cell growth.

The different feeding strategy on day 5 needs to be taken into consideration: medium exchange in the ambr® 250 and medium addition in the T-flask. However, the cell concentration was considerably higher in Run 4 before the medium exchange was performed, suggesting that the higher cell concentration at harvest was not due to the difference in the feeding strategy. Furthermore, the 60% dO_2 control in the ambr® 250 from day 5 has to be taken into consideration, as it might have favoured the T-cells pro-

liferation, although the initial study in the ambr® 250 under static conditions suggests differently.

Currently, the precise mode of action in stirred environments is not well understood and requires more investigation. But the concept that impeller agitation damages T-cells preventing their culture in stirred-tank bioreactors is incorrect. Even at the present agitation intensities, when the beads are suspended, the performance in the stirred-tank bioreactors is better than in the T-flask. The Static run in the ambr® 250 highlights the importance of the bead-to-cell interaction and how no agitation is better to poor agitation if beads are not well suspended with the cells (Run 1). The final product quality after cultivation is essentially the same, independently of the configuration used. The higher the agitation intensity used, the better the result. Furthermore, the analysis of the Kolmogorov microscale suggests that even better results might be obtained with even higher agitation intensities by enhancing cell-Dynabeads® interactions without cell damage.

Chapter 4

Establishing the expansion of human CAR-T cells in stirred-tank bioreactors

4.1 Introduction

This chapter investigates the feasibility of expanding CAR-T cells in stirred-tank bioreactors. Once proven that human primary T-cells can be grown in stirred-tank bioreactors (Chapter 3) and that the final cell quality was comparable to the T-cells grown under static conditions, the next step was to culture transduced CAR-T cells under dynamic

conditions.

CAR-T therapies for clinical trials are mostly manufactured in static vessels or in rocking motion bioreactors (Vormittag et al., 2018). No study has been reported on CAR-T cells in stirred-tank bioreactors thus far. In Chapter 3 100 and 200 rpm speeds were tested using primary non transduced T-cells. The hypothesis behind the better performance at the higher speed (200 rpm) was that the magnetic beads were better suspended and therefore the T-cells at this speed were better activated. At a 100 rpm, when the Dynabeads® were not suspended and the interaction between cells and beads was lower, the final cell density was also lower.

Building on previous results, where the higher agitation speed led to higher cell density at harvest, increasing agitation speeds were investigated, up to 500 rpm, corresponding to a specific power input of 1164 x 10^{-4} W kg^{-1}. When manufacturing CAR-T therapies, the quality attributes of the cells at the end of the process need to be assessed in order to determine whether the cells retain their potency or whether CAR shedding might occur due to shear stress at increased speeds.

4.2 Stirring speed and Kolmogorov scale in the ambr 250 stirred-tank bioreactor

CAR-T cells were grown in an ambr® 250 stirred-tank bioreactor at 100, 200, 300, 400 and 500 rpm and compared to the static control (T-flask). The 100 and 200 rpm speeds were the same tested in Chapter 3 for non transduced human primary T-cells. In Chapter 3 it was demonstrated that T-cells are able not only to withstand the hydrodynamic forces in a stirred-tank bioreactor, but also that they reach a significantly higher ($P < 0.05$) fold expansion compared to static culture (T-flask). However, given that the results previously presented suggested that the 200 rpm condition resulted in a higher growth compared to the 100 rpm agitation speed, it was decided to investigate higher speeds.

The Kolmogorov scale of turbulence (λ_K) was calculated and used as a criterion to assess the likelihood of fluid dynamic stress damaging T-cells at different speeds. If $\lambda_K >$ than the cells size, then the cells should not be damaged. λ_K was calculated for different speed using equation 3.1. The maximum specific dissipation rate close to the impeller (ε_{Tmax}) has proven to be difficult to calculate (Gabriele et al., 2009). However, based on literature, it was considered to be 50 times the mean specific dissipation rate (Alvin W Nienow et al., 2016). υ was considered to be the kinematic viscosity of water at 37°C (0.69 x 10^{-6} m^2 s^{-1}). The λ_K values calculated for different speeds (100-700 rpm) are shown in Table 4.1. At 500 rpm $\lambda_K \sim$ 16 μm which is slightly larger than the size of a CAR-T cell, generally considered to be $\sim$ 12-15μm (data not shown; retrieved

from the NucleoCounter® 3000). For speeds higher than 500 rpm the λ_K was considered to be comparable to the CAR-T cells size and was therefore assumed that at 600 rpm the T-cells would likely be damaged by the fluid dynamic stresses. Therefore speeds above 500 rpm were not investigated.

Table 4.1: Specific dissipation rates and Kolmogorov scale of turbulence (λ_K) at different speeds (100-700 rpm) in the ambr® 250 stirred-tank bioreactor unbaffled vessel.

Speed [rpm]	Specific dissipation rate [W kg^{-1}]	λ_K [μm]
100	9.3	$\sim$ 52
200	74	$\sim$ 31
300	251	$\sim$ 23
400	595	$\sim$ 18
500	1164	$\sim$ 16
600	2007	$\sim$ 13
700	3187	$\sim$ 12

4.3 Investigating the growth kinetics of CAR-T cells at higher speeds

The viable cell concentration was assessed on a daily basis across the tested conditions (Figure 4.1a). At the lowest speed (100 rpm, 9.3 x 10^{-4} W kg^{-1}), a final density of 3.76 $\pm$ 0.69 x 10^6 viable cells ml^{-1} was obtained. This speed resulted in the lowest cell density at harvest amongst the agitation conditions tested in the ambr® 250 stirred-tank bioreactor, but still higher than the viable cell count at harvest in the static control (2.57 $\pm$ 1.38 x 10^6 viable cells ml^{-1}). Better CAR-T cell growth was observed when the

agitation speed was increased to 200 rpm with a final cell density of 4.99 $\pm$ 0.77 x 10^6 viable cells ml^{-1}. The trend confirmed the previous results for non transduced T-cells presented in Chapter 3 and showed that increasing the speed and P/M leads to a higher proliferation.

Although speeds higher than 200 rpm did not lead to significantly higher levels of proliferation, likely due to nutrient limitations in the medium (discussed later), CAR-T cells viability at harvest was greater than 90% for all speeds (Figure 4.1), suggesting that the cells were not adversely impacted by the higher agitation rates and associated fluid dynamic stresses. Importantly, it was noted that the cells were able to proliferate and remain $>$ 85% viable at all agitation intensities up to 500 rpm (P/M as high as 1164 x 10^{-4} W kg^{-1}). These results clearly show that the CAR-T cells are not as sensitive to fluid dynamic stresses as generally believed (van den Bos et al., 2014) and therefore, they can be successfully grown in stirred-tank bioreactors. The final cell yield at 300, 400, and 500 rpm were 5.07 $\pm$ 0.21, 5.00 $\pm$ 0.39, and 4.81 $\pm$ 0.79 x 10^6 viable cells ml^{-1} respectively.

The doubling time and cumulative population doublings for each condition are shown in Figure 4.1a and b. The doubling times were calculated from day 2 to day 7, when the cells were in their exponential growth phase and no significant difference ($P > 0.05$) between the dynamic and static conditions was detected. However, the condition with the lowest doubling time was found to be CAR-T cells grown at 200 rpm (36.11 $\pm$ 2.16

h), while the CAR-T cells grown at 500 rpm displayed the highest doubling time (44.58 $\pm$ 7.39 h) (Figure 4.1b). The cumulative population doublings indicate the number of times the cell population has doubled throughout the culture. The trend was similar to the one seen for the growth curve, where the static control had the lowest number of cumulative doublings throughout the 7 days of culture (8.21 $\pm$ 1.88). The CAR-T cells grown at 100 rpm showed slightly higher cumulative population doublings (9.58 $\pm$ 0.75) compared to the static control. The conditions grown at 200, 300, 400, and 500 rpm showed almost identical cumulative population doublings being 10.61 $\pm$ 0.53, 10.78 $\pm$ 0.16, 10.77 $\pm$ 0.23, and 10.53 $\pm$ 0.55 respectively.

Overall, the doubling time and cumulative population doublings for the 200, 300, 400 and 500 rpm agitation speeds were found to be very similar (Figure 4.1). This indicates that no improvement in terms of cell proliferation was achieved by increasing the stirring speed over 200 rpm, which is the estimated speed at which the Dynabeads® (T-cell activation beads) are well suspended and interact with the T-cells in efficient way (Costariol et al., 2019).

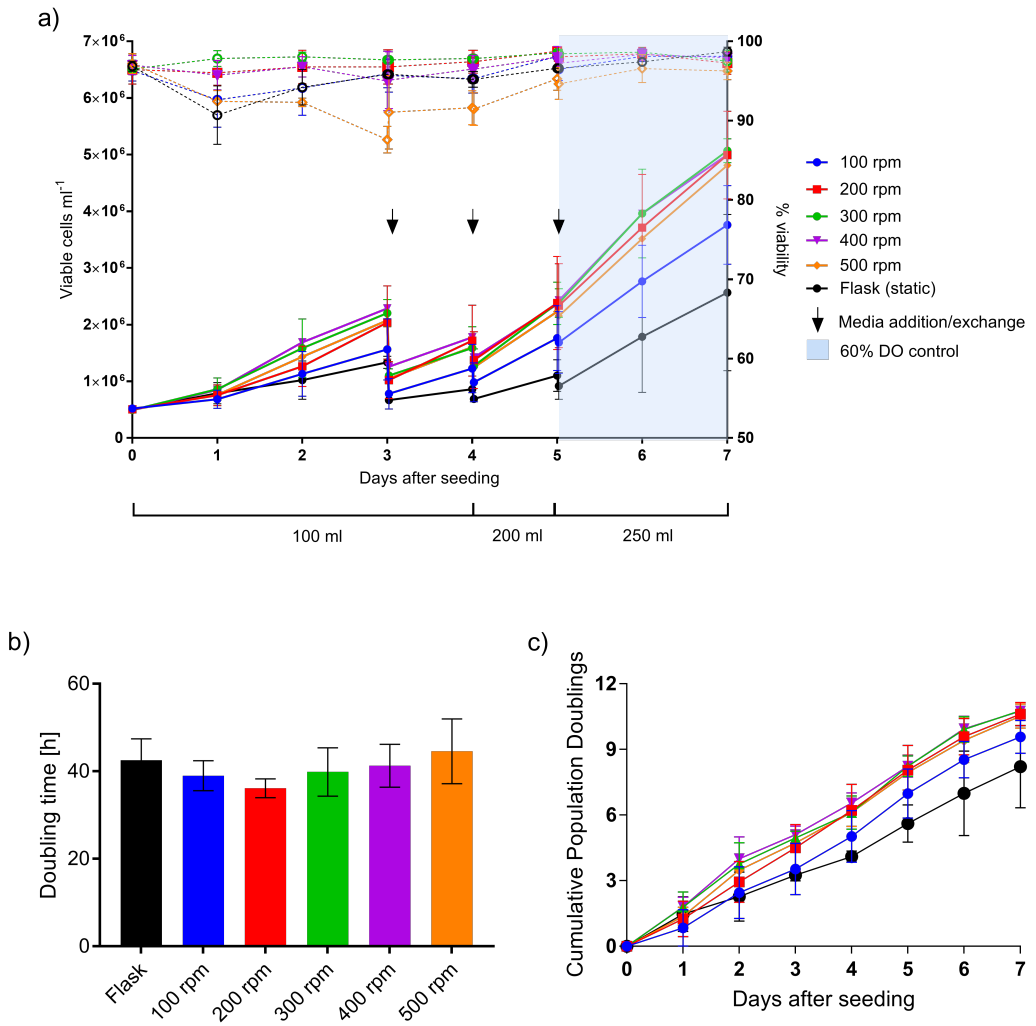

Figure 4.1: The growth kinetics for CAR-T cells grown at different speeds and in the static control. Data shown as mean ± SD with all 3 donors. Only 2 donors were used for the static control (HD12 and HD16). (a) The growth of CAR-T cells and percentage viability from three donors (HD12, HD16 and HD18) over 7 days in the unbaffled ambr® 250 at different agitation speeds. The black arrow indicates the medium addition on day 3 (100 ml), day 4 (50 ml) and a medium exchange (100 ml) on day 5. (b) Doubling time for CAR-T cells grown at different speeds and in the static control (T-flask). No significant difference ($P > 0.05$) was detected between the conditions using a One-way ANOVA test. (c) Cumulative population doublings for CAR-T cell grown at different speeds in the ambr® 250 and in the T-flask (static control).

Similar results were found for the fold expansion (Figure 4.2a), where the lowest fold expansion amongst the ones tested in the ambr® 250 unbaffled vessel was at 100 rpm (18.22 ± 0.42) and the highest one was the fold expansion at 300 rpm (25.70 ± 1.21). However, there was no significant difference ($P > 0.05$) between the various speeds tested.

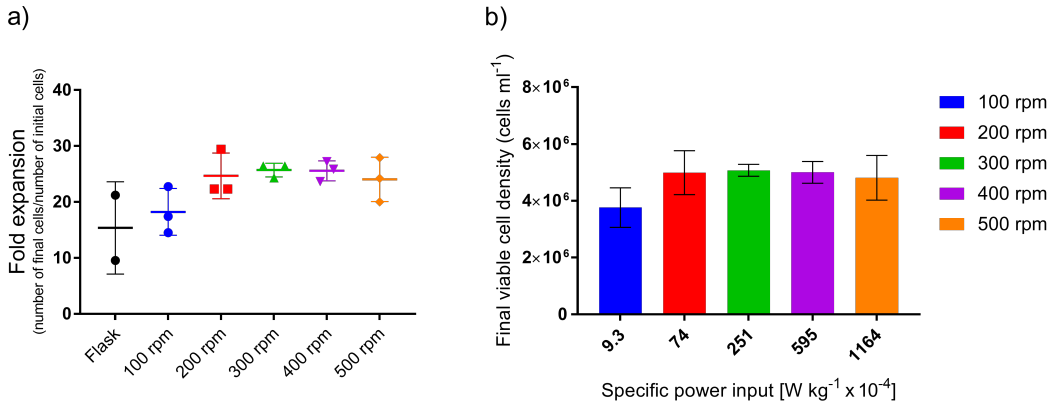

Figure 4.2: After 7 days culture in the unbaffled ambr® 250 at different agitation speeds and different culture parameters were analysed. Data shown as mean ± SD with all 3 donors. Only 2 donors were used for the static control (HD12 and HD16). a) Fold expansion (total number of viable cells on day 7/total number of viable cells at seeding). Each symbol represents one donor (star = HD12; circle = HD16, square = HD16). b) Final viable cell density (cells ml^{-1}) at day 7 plotted against the specific power input [W kg^{-1} x 10^{-4}] at the end of each run. No significant difference ($P > 0.05$) was detected between the conditions using a One-way ANOVA test.

There was no statistically significant difference ($P > 0.05$) in the CAR-T yield at day 7 at any of the speeds tested (Figure 4.2b), even though the range of final specific power inputs was broad (from 9.3 to 1164 x 10^{-4} W kg^{-1}). It was speculated in Chapter 3 that if the improvement in cell yield from 100 rpm to 200 rpm was due to enhanced contact due to increasing turbulence between cells and Dynabeads®, further increases

in P/M would lead to further improvement. However, despite the increase from 200 rpm to 500 rpm (P/M from 7 x 10^{-4} W kg^{-1} to 1164 x 10^{-4} W kg^{-1}), each of these cultures performed similarly with respect to growth kinetics, suggesting that sufficient suspension of the Dynabeads® has been achieved at 200 rpm (Figure 4.2b).

As reported above, at 500 rpm and P/M of 1164 x 10^{-4} W kg^{-1}, λ_K was $\sim$ 16 μm, which is approximately the size of CAR-T cells. Thus, though higher speeds might lead to a deterioration in performance, the lack of damage up to 500 rpm is not contrary to what is expected from the turbulence theory. The lack of sensitivity to fluid dynamic stresses shown by CAR-T cells over the tested range of agitation speeds, suggests that if higher cell densities can be achieved through enhanced feeding strategies, higher k_La values could be obtained to meet the increased oxygen demand. The same applies for larger volumes stirred-tank bioreactors, where headspace aeration could not be sufficient for a high cell density. However, the k_La could be increased by increasing the stirring speed up to a P/M of 1164 x 10^{-4} W kg^{-1}, as proven in this doctoral thesis. Furthermore, results have shown that Dynabeads® are well suspended and efficiently activate the cells at 200 rpm. Although this activation method is widely used, the beads need to be removed at the end of the culture. Therefore investigating alternative activation methods that are easier to suspend (i.e. TransAct™) could give a better insight on whether higher speeds are needed to improve the proliferation of CAR-T cells or if they can be grown at lower speeds with comparable results.

4.4 Metabolite concentrations

The levels of glucose, lactate, glutamine, and ammonia in the medium were measured off-line on a daily basis (Figure 4.3). For the runs at speeds of 200 rpm and above which exhibited similar growth, the metabolites measured in the medium followed similar trends. In each case, the medium was depleted of glucose and glutamine by day 3, which was probably the cause for the reduced growth rate at this time point (Figure 4.6, right hand side). The glucose and glutamine concentrations were consistently depleted throughout the course of the culture despite the regular medium exchanges/additions on day 3, 4 and 5. The glucose and glutamine concentrations were close to 0 mmol l^{-1} on day 6, and were completely depleted in the medium by day 7 in all conditions. The glucose concentration dropped below 2 mmol l^{-1} on day 5 (before the medium exchange) and day 6 (Figure 4.3). It is likely that cultures with higher viable cells ml^{-1} (200 rpm and higher speeds) run out of glucose and glutamine earlier than the ones with less cells ml^{-1} (100 rpm). However, due to the nature of off-line daily sampling, this could not be detected. The same trend was seen in the work published by A. Amini et al. (2020), where fastest growing T-cells rapidly consumed all the available glucose from the medium, despite a perfusion mimic feeding strategy. On the other hand Klarer et al. (2018) prevented the depletion of glucose from the medium by using the X-VIVO™ 10 medium, which contains $\sim$ 25 mmol l^{-1} of glucose compared to the $\sim$ 11 mmol l^{-1} of glucose present in the RPMI 1640.

Once CAR-T cells are activated, they undergo extensive proliferation and significant changes in their metabolism. They switch from a catabolic metabolism to an anabolic one in order to support the proliferation and new biomass formation (Windt et al., 2012). Furthermore, the uptake of glucose and glutamine from the medium is essential for proliferation and expression of effector functions, such as cytokine production and cytolytic molecules secretion. Both nutrients are therefore crucial for T-cell expansion. The drop in glutamine and glucose concentrations could be a potential explanation to why, at higher speeds, the cells did not reach higher cell densities. The complete depletion of the metabolites indicates a need to optimise the feeding strategy in order to avoid a possible growth rate limitation with respect to nutrient provision or switch to other commercially available medium with a higher content of glucose. Culture under such conditions would establish whether higher speeds can improve the proliferation of CAR-T cells, as it has been shown that fluid dynamic stresses do not adversely impact it up to 500 rpm in the ambr® 250 bioreactor.

With glucose becoming a limiting factor, the lactate production also slowed down (Figure 4.3a,b). The levels of lactate reached the maximum concentration on day 3 for all conditions ($\sim$ 20 mmol l^{-1}). The medium additions/exchange on day 3, 4 and 5 diluted the concentration of lactate to lower levels. It can be noted how the lactate production slowed down on the last day of culture (Figure 4.3b), probably due to the lack of glucose and glutamine available in the medium, as mentioned above. The level of

lactate in the medium was higher than the one reported by Hollyman et al. (2009), which reached $\sim$ 14 mmol l^{-1} in a rocking motion bioreactor and Gagliardi et al. (2019) who reported $\sim$ 15 mmol l^{-1} of lactate in a gas permeable bag at day 7. A. Amini et al. (2020) reported a level of lactate in the medium of $\sim$ 17 mmol l^{-1} with primary T-cells in a shaken microbioreactor. The rocking motion bioreactor and the shaken microbioreactor were both operated in perfusion or perfusion mimic mode, which allowed to partially remove the lactate accumulated in the culture medium and keep it at a stable level. The viable cell number in the gas permeable bag at day 7 was $\sim$ 0.4 x 10^8, while there were $\sim$ 12.5 x 10^8 total cells in the ambr 250 at day 7. This explains the higher amount of lactate accumulation in the medium despite the medium dilutions and exchange.

During rapid cell proliferation, glutamine uptake results in intracellular nitrogen building up and is secreted as ammonia in order to avoid toxic effects on the cells (Windt et al., 2012). The highest ammonia concentration detected in the medium was $\sim$ 2 mmol l^{-1} (Figure 4.3d). A study conducted by Luo et al. (2014), showed that 2.5 mmol l^{-1} of ammonia slowed the proliferation of dendritic cell, while 3 mmol l^{-1} was proven to have a negative impact on mesenchymal stem cells proliferation by Schop et al. (2009). The level of ammonia detected in this work was lower, however it is not clear whether 2 mmol l^{-1} could have an inhibitory effect on CAR-T cells, as no literature was found on this matter.

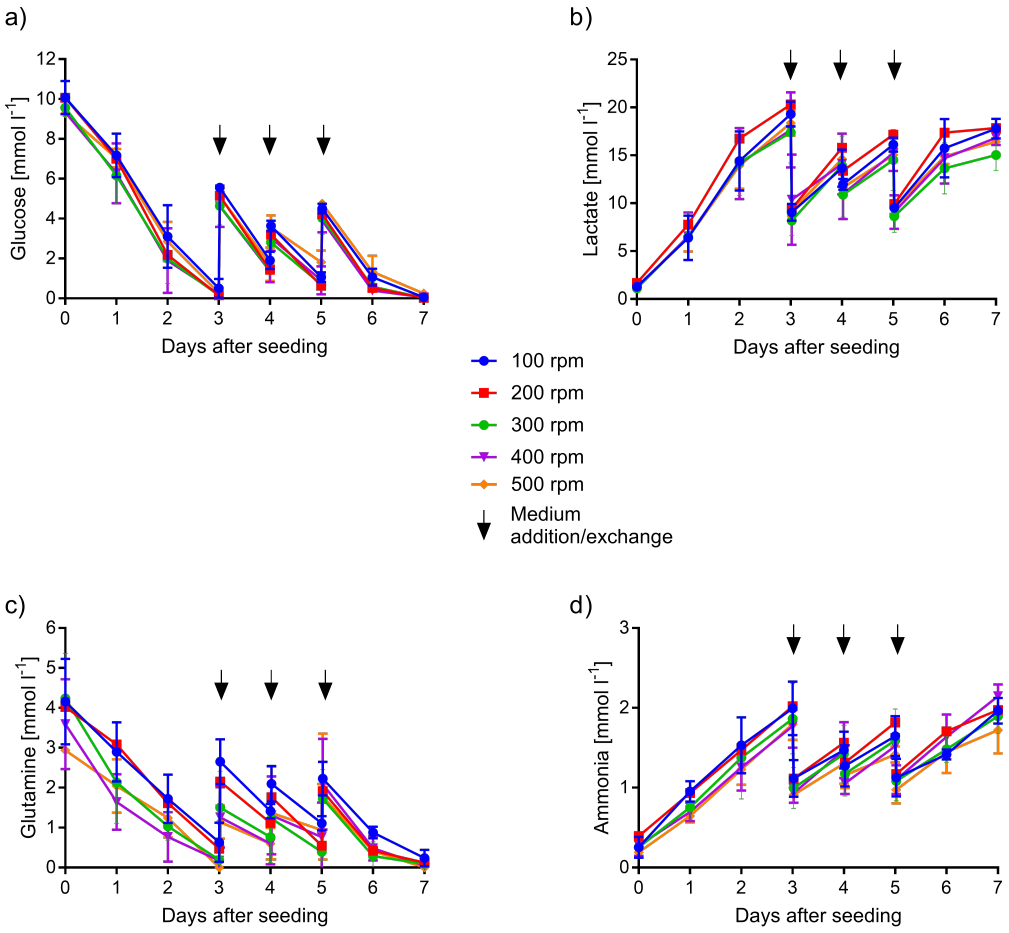

Figure 4.3: Metabolite concentration [mmmol l^{-1}] profiles from the day of inoculation to the end of the culture (day 7) in the ambr® 250 unbaffled vessel at different impeller speeds. The black arrows indicate a medium addition on day 3 and 4 and a medium exchange on day 5. Data shown as ± SD, n=3. (a) Glucose concentration. (b) Lactate concentration. (c) Glutamine concentration. (d) Ammonia concentration.

4.4.1 Specific production and consumption rates

Specific metabolite consumption and production rates were calculated for glucose and lactate respectively from day 2 to day 7, when the CAR-T cells were in their exponential growth phase, and on a daily basis (Figure 4.4a, b, c, d). It can be noted that for both glucose and lactate, the 100 rpm agitation intensity resulted in higher consumption/production rates, although not significantly ($P > 0.05$), compared to the other agitation conditions from day 2-7 (1.47 ± 0.36 pmol cell^{-1} day^{-1} for glucose and 2.40 ± 0.63 pmol cell^{-1} day^{-1} for lactate) (Figure 4.4a, c). Similarly, the consumption and production rates for glucose and lactate calculated on a daily basis showed higher values for the lowest speed from day 3 onward (Figure 4.4b, d). However, none of these values were significantly different ($P > 0.05$) compared to other speeds. The higher consumption/production rate for CAR-T cells grown at 100 rpm was to be expected given this is a per cell metric. In the higher speed conditions, there was an increase in the overall cell density, that resulted in a lower specific consumption or production rate, given the concentration of the available metabolite was the same to start with. When there were fewer cells in the vessel (100 rpm), but the available metabolites were the same, the consequence was that the uptake resulted higher given the greater availability of glucose per cell in that condition. In the other conditions (200-500 rpm), where the metabolites were depleted faster, a lower glucose consumption rate needed to be accounted for on day 3 and 4 in particular, which made the consumption rate calculated from day 2 to day 7

lower (Figure 4.4a, b). Similar results were found by A. Amini et al. (2020) with non transduced T-cells in a shaken microbioreactor, where T-cells grown at lower shaking speeds had a higher glucose uptake and slower proliferation.

The production of lactate is highly correlated to glucose consumption (Buck et al., 2015). It is therefore understandable that the same pattern was seen in the specific lactate production, where the amount of lactate produced per cell resulted higher at lower speeds (Figure 4.4c, d). However, none of the conditions showed a significantly higher ($P > 0.05$) production rate for lactate. Furthermore, low pH are believed to inhibit the production of lactate in T-cell culture, which could be another reason for the lower specific production of lactate from day 3 onward (Calcinotto et al., 2012).

The lactate yield from glucose was calculated in order to assess the efficiency of the CAR-T cells metabolism to convert glucose into energy (Figure 4.4e, f). The most efficient way to consume glucose is through the OXPHOS metabolic pathway, which yields 30-38 ATP molecules per mole of glucose consumed (Hanga et al., 2017). The alternative pathway, called aerobic glycolysis or 'The Warbug Effect', it is far less efficient yielding only 2 ATP per mole of glucose consumed and 2 moles of lactate as a byproduct (Warburg, 1956). In this study the lactate yield from glucose calculated from day 2 to day 7 was found to be close to the theoretical limit of 2 mmol $mmol^{-1}$ for all the assessed speeds (Figure 4.4e). This suggested that the CAR-T cells were metabolising glucose via the inefficient aerobic glycolysis rather than through OXPHOS. Activated

T-cells are known to undergo a metabolic reprogramming towards aerobic glycolysis (Buck et al., 2015; Maciolek et al., 2014). The percentage of T effector memory cells in the culture (discussed later) could have an impact on the lactate yield from glucose, as T effector memory cells are known to process glucose mainly through aerobic glycolysis (Bantug et al., 2018). However, no significant difference ($P > 0.05$) was found in the lactate yield from glucose across the range of speeds tested, indicating that the increasing stirring speed did not have a significant impact on the glucose and lactate metabolism of the CAR-T cells. The results on day 7 (Figure4.4f) show a higher lactate yield from glucose mainly due to the low content of glucose in the medium between day 6 and 7.

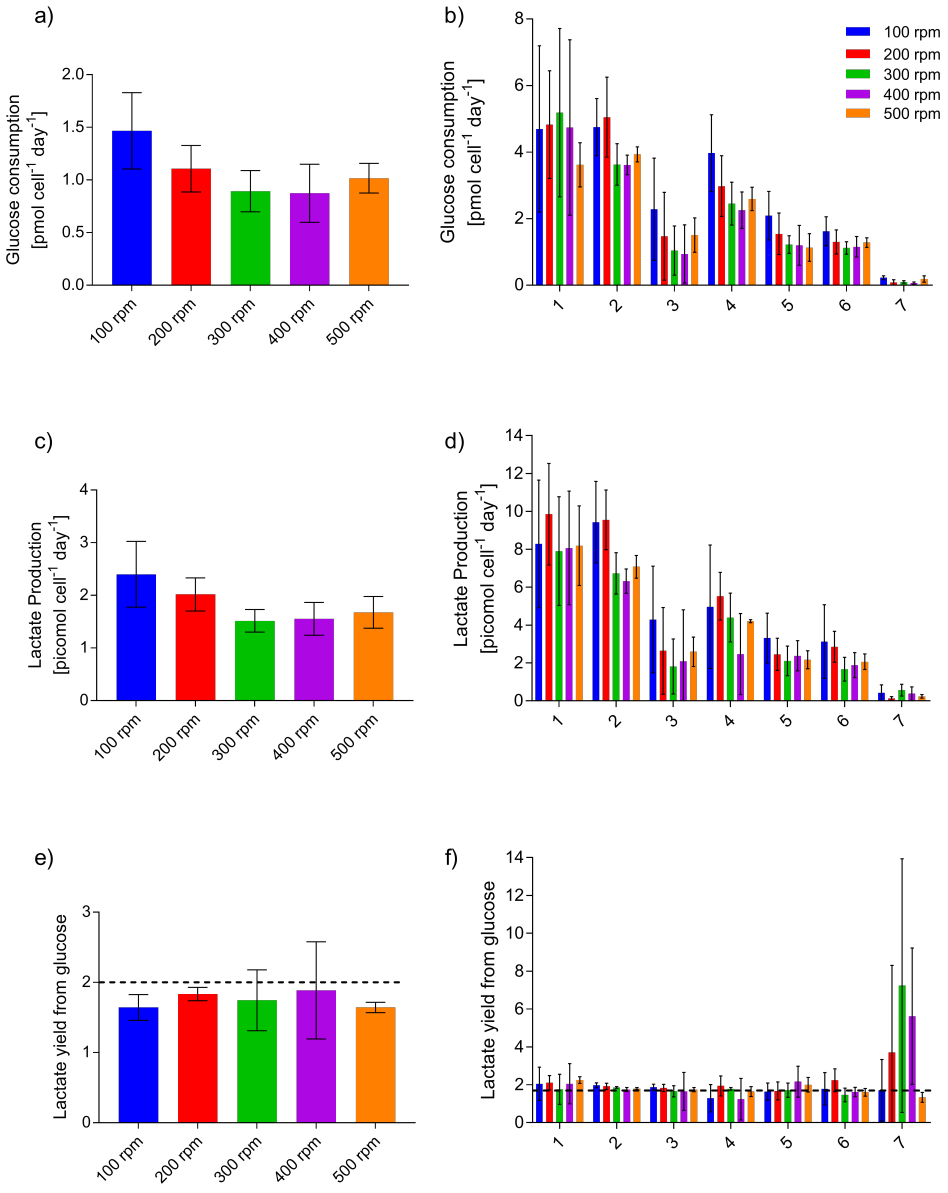

Figure 4.4: Specific consumption or production rates for CAR-T cells production under different agitation conditions (100 - 500 rpm) in the ambr® 250 stirred-tank bioreactor. All data shown as $\pm$ SD, n=3. No significant difference ($P > 0.05$) was detected between different conditions using a One-way ANOVA test. (a) Glucose consumption rate [pmol cell^{-1} day^{-1}] from day 2 to day 7. (b) Glucose day by day consumption rates. (c) Lactate production rate [pmol cell^{-1} day^{-1}] from day 2 to day 7. (d) Lactate day by day production rates. (e) Yields of lactate from glucose from day 2 to 7. Reference line at 2 is the maximum theoretical yield of lactate from glucose. (f) Yields of lactate from glucose on a daily basis. Reference line at 2 is the maximum theoretical yield of lactate from glucose.

Glutamine and ammonia specific consumption and production rates are shown in Figure 4.5. The specific glutamine consumption rate calculated from day 2 to day 7 (Figure 4.5a) showed a similar trend to glucose, it was lower at higher speeds. The glutamine consumption rate was 0.57 $\pm$ 0.17 pmol cell^{-1} day^{-1} at 100 rpm, while it dropped to 0.31 $\pm$ 0.1 pmol cell^{-1} day^{-1} at the highest speed (500 rpm). Once again, this lowering was likely due to an early depletion of glutamine in the medium, caused by an higher number of cells in the 300 - 500 rpm conditions, while the consumption rate at 200 rpm (0.44 $\pm$ 0.08) was between the lowest speed (100 rpm) and the higher speeds. The same trend was detected on a daily basis (Figure 4.5b), where the lowest speed showed a higher consumption rate from day 3 onward. However, there was no significant difference ($P > 0.05$) between the tested conditions. Ammonia specific production rate calculated between day 2 and 7 (Figure 4.5c) did not show any significant difference ($P > 0.05$) amongst the tested conditions. The values ranged from 0.16 $\pm$ 0.03 pmol cell^{-1} day^{-1} at 500 rpm to 0.22 $\pm$ 0.06 pmol cell^{-1} day^{-1} at 100 rpm. The daily analysis for the ammonia production rate (Figure 4.5d) exhibited a consistently decreasing ammonia production, however no significant difference ($P > 0.05$) was detected between different conditions. These results suggest that the stirring speed did not have a significant impact on the consumption of glutamine and production of ammonia in CAR-T cells grown in the ambr® 250 stirred-tank bioreactor.

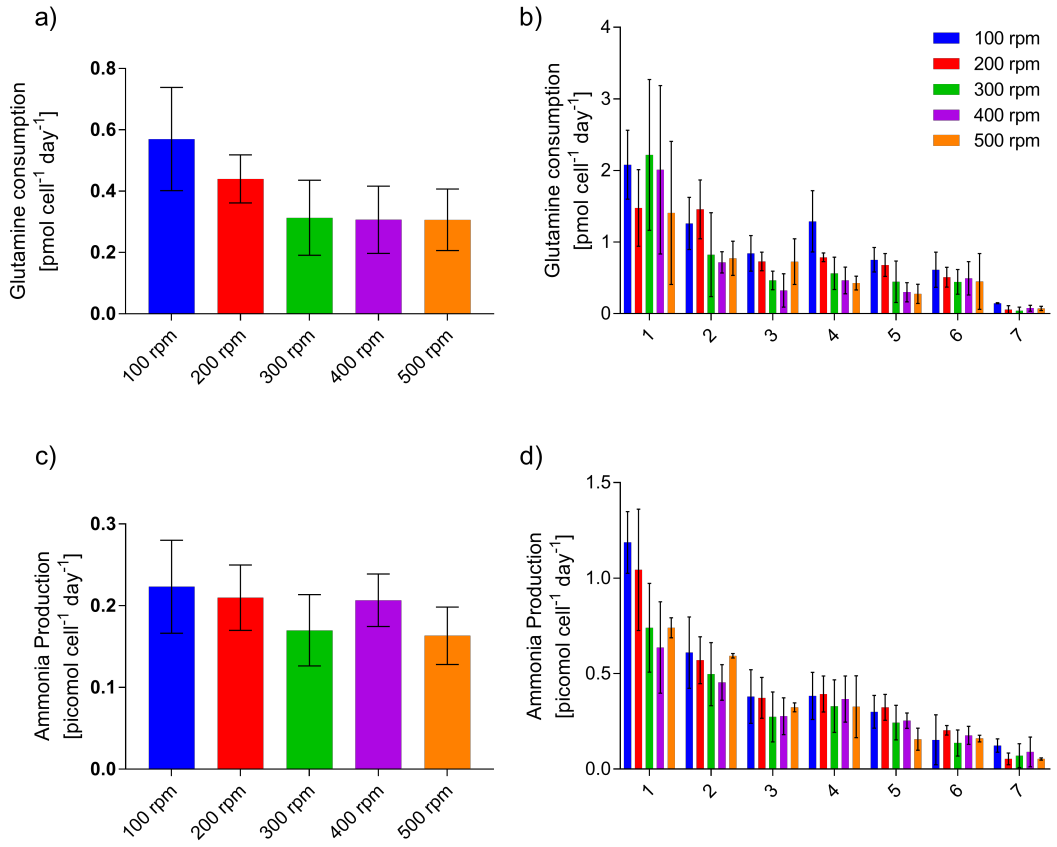

Figure 4.5: Specific consumption or production rates for CAR-T cells production under different agitation conditions in the ambr® 250 stirred-tank bioreactors. Data shown as ± SD, n=3. A one way ANOVA test was performed. No significant difference ($P > 0.05$) was detected between different conditions using a One-way ANOVA test. (a) Glutamine consumption rate [pmol cell^{-1} day^{-1}] from day 2 to day 7. (b) Glutamine day by day consumption rates. (c) Ammonia production rate [pmol cell^{-1} day^{-1}] from day 2 to day 7. (d) Ammonia day by day production rates.

4.5 pH and dissolved oxygen concentration

pH and dO_2 are two of the key parameters in cell culture and manufacturing of therapeutics products and they were monitored throughout the duration of the 7 days CAR-T expansion using the ambr® bioreactor controller software (Figure 4.6). The spikes observed in the dO_2 profiles are due to the opening of the bioreactor cap to allow for medium additions and exchange. For all runs, a dO_2 control by gas blending at 60% was started on day 5 after a 100 ml medium exchange, keeping the experimental set up consistent with the experiments presented in Chapter 3. The dO_2 control was active only when the monitored dO_2 dropped below 60%, but did not lower the dO_2 to 60%.

The dO_2 (Figure 4.6a-e, left hand side) was $\sim$ 85% at inoculation in all the conditions (100 - 500 rpm). This value fell slightly over the first 3 days at 100 rpm, but remained stable during this time at the higher speeds. After medium addition on day 3, a drop in dO_2 occurred, due to an increase in volume (from 100 to 200 ml) and due to an increased cell concentration at the lowest speed (100 rpm), condition in which the k_La was lowest and could not meet the oxygen demand of the proliferating CAR-T cells. At 200 rpm and above, since the cell density and hence the oxygen uptake rates were approximately the same for these agitation speeds, the drop in dO_2 was less pronounced as the speed is increased. This difference was probably due to the higher k_La resulting from the increase in the agitation speed. At day 5, when the dO_2 control at 60% became operational, this value was held at all speeds as indicated in the dO_2 profiles. However,

at 400 rpm the oscillations caused by the oxygen control were smaller indicating that the control was really needed only towards the end of the culture, due to the high viable cell density reached (Figure 4.6d). At 500 rpm the dO_2 from day 5 on was still slightly above 60% due to the higher k_La and therefore the dO_2 control was not activated. However, the overall culture performance was still comparable to the other conditions.

It can be concluded that dO_2 did not play a determinant role in this scenario, as the profiles did not show any significant differences between the different speeds (Figure 4.6a-e).

pH profiles (Figure 4.6a-e, right hand side) were very similar across all the speeds, correlating with the viable cell concentration and with the lactate production and accumulation in the medium. The rapid increase in the pH profiles indicated the points at which medium additions or exchanges occurred (day 3, 4 and 5). There was a slight increase or a plateau in the pH prior to the medium addition on day 3 for all the conditions, exception made for the highest speed (500 rpm).

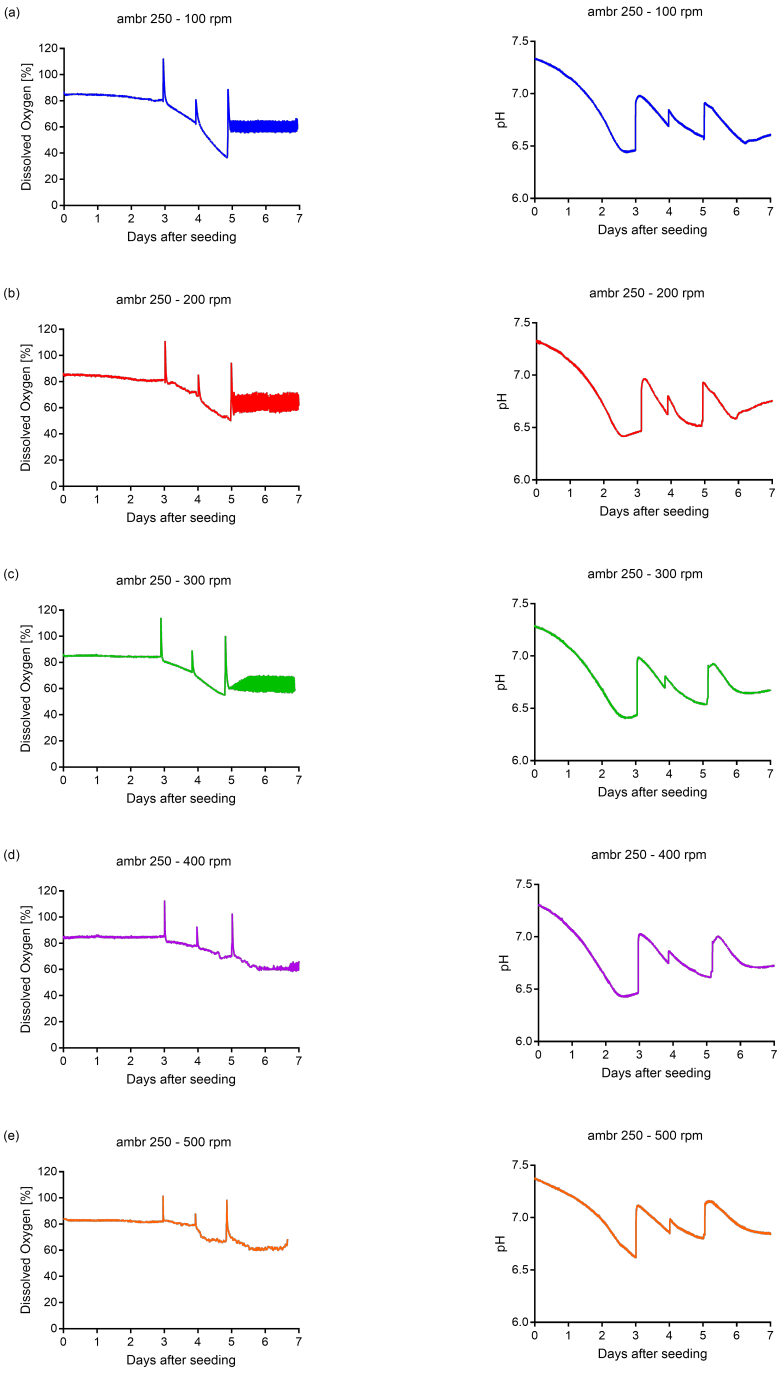

Figure 4.6: Representative dissolved oxygen (dO_2; left hand side and pH (right hand side) trends under different agitation as the medium volume increases in the ambr® 250 unbaffled vessel over 7 days. In all runs dO_2 control at 60% was introduced at day 5 after medium exchange. (a) 100 rpm. (b) 200 rpm. (c) 300 rpm. (d) 400 rpm. (e) 500 rpm.

It has been shown that lactic acid production causes a fall in the pH profile and can impair proliferation in mammalian cell cultures if pH reaches values lower than 6.6-6.8 (Konakovsky et al., 2016; W. M. Miller et al., 2000). The lower pH consequently restricts the formation of lactic acid and its accumulation in the medium (Erra Diaz et al., 2018). The plateau in the pH may therefore indicate that CAR-T cells run out of glucose and glutamine which, combined with the low pH, limited their proliferation and lactate production. The same effect could be seen in the last day of culture, when once again, the glutamine and glucose levels were down to zero. The lowest pH was $\sim$ 6.4 on day 3 in the runs at 100-400 rpm (Figure 4.6a,b,c,d), while it was slightly higher ($\sim$ 6.6) for the 500 rpm (Figure 4.6e). Such low pH values have been reported to slow down the growth of T-cells and believed to down regulate the specific lactate production (Calcinotto et al., 2012).

4.6 Assessment of cell quality and functionality

Although the final cell yield is relevant for CAR-T therapies, expanded CAR-T cells need to be able to efficiently target tumour cells once reinfused into the patient. Once the target dose has been reached, it is crucial to assess their immunophenotypes and cytotoxicity at the end of the culture.

4.6.1 Immunophenotypic analysis and CAR expression

The immunophenotypic profile of CAR-T cells was assessed via flow cytometry analysis at the beginning (pre-experiment) and at the end of the expansion in the ambr® 250 bioreactor and in the T-flask, used as a static control (Figure 4.7). The CD4:CD8 ratio (Figure 4.7a) was higher in the static control (3.1 ± 0.7) compared to the ambr® 250 at different speeds, where it reached values closer to the desired 1:1 ratio (Turtle et al., 2017). The result shown by the static control was not in line with previous studies found in literature, where $CD4^+$ T-cells number lowered during expansion, while $CD8^+$ T-cell percentage increased (W. Zhang et al., 2018). However, the difference between the pre-experiment and flask sample was not significant ($P > 0.05$). IL-2 was used as medium supplement in all the experiments, however different interleukins could help to lower the CD4:CD8 ratio. It has been previously reported that T-cells cultured with IL-7 and IL-15 showed a higher proportion of $CD8^+$ T-cells, which would lower the CD4:CD8 ratio towards the desired value of 1 (Cha et al., 2010; Turtle et al., 2017).

The CD8 positive subpopulation of CAR-T cells was further analysed in terms of naïve, central memory, effector memory, and terminally differentiated T-cells. It has been demonstrated that a higher proportion of naïve and central memory T-cells in the final product help to improve the persistence of CAR-T therapies *in vivo* (Sommermeyer et al., 2016). The amount of naïve and terminally differentiated T-cells was lower than 5% in all samples (data not shown). The central memory subpopulation was higher

in the pre-experiment sample (39.6 $\pm$ 3.8 %) compared to the samples post-expansion (Figure 4.7b). Although it is known that T-cells differentiate during expansion and therefore prolonged culture periods will see a decrease in T central memory cells, it has been suggested that the use of IL-7 and IL-15 should result in a higher percentage of T central memory cells compared to T-cells cultured with IL-2 (Cha et al., 2010). The results presented in this doctoral thesis are in line with the study by Gagliardi et al. (2019), where after 11 days of culture $\sim$ 20% of the T-cells showed a central memory phenotype, although different expansion platforms were used (i.e. G-Rex and gas permeable bags). Furthermore, A. Amini et al. (2020) reported a similar T central memory percentage (between $\sim$ 20 and 35%) in a shaken microbioreactor at 100 and 200 rpm. The effector memory percentage increased over the 7 days culture, both in the static control (T-flask) and in the ambr® 250, showing no significant difference ($p > 0.05$) between the final product in the static and dynamic conditions. These results are in line with data found in literature, where the percentage of effector memory T-cells in a shaken bioreactor was reported to be between 60 and 70% (A. Amini et al., 2020). As demonstrated in Chapter 3, the proportion of the T-cell subpopulations at the end of the culture was not affected by agitation for speeds up to 200 rpm. In this case the same can be stated for speeds up to 500 rpm, as no significant difference ($p > 0.05$) was found between the static condition and the dynamic ones.

It can be concluded that the expanded cells showed a more differentiated pheno-

type, with less central memory cells (Figure 4.7b) and higher percentage of effector memory cells (Figure 4.7c). However, it is important to note that this was irrespective of culture platform (static T-flask or stirred-tank bioreactor). These findings were expected due to the prolonged expansion protocol (14 days in total), the use of IL-2 in the medium, and a double activation of T-cells (when thawed and on day 0). The fact that there was no significant difference between the static and dynamic conditions suggests that fluid dynamic stresses associated with higher agitation speeds did not impact the immunophenotypic profile of CAR-T cells.

In order to limit the differentiation of the T-cells, a shorter protocol should be put in place and the IL-2 replaced with different interleukins (IL-7, IL-15, and IL-21), which have been proven to help maintain the undifferentiated phenotype of T-cells (Sabatino et al., 2016; N. Singh et al., 2016). Furthermore, cells grown with IL-7 and IL-15 (10 ng ml^{-1} each) showed a higher efficacy *in vivo* compared to T-cells cultured with IL-2 (Cha et al., 2010).

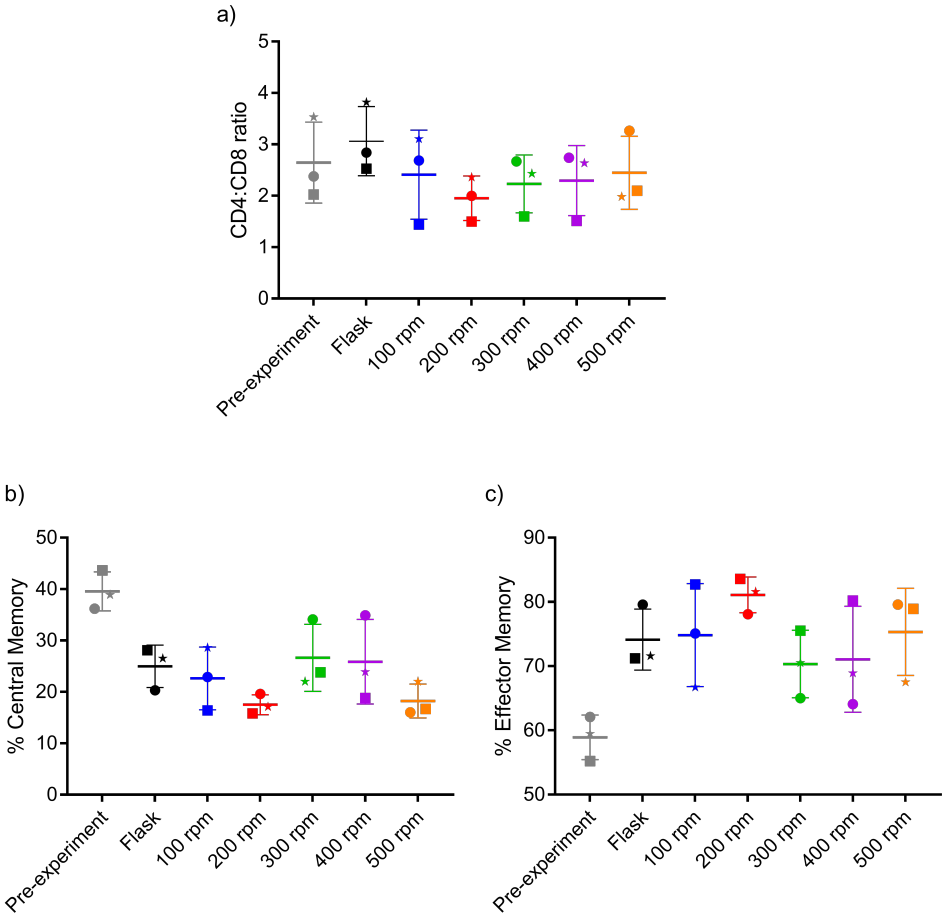

Figure 4.7: Phenotypic characterisation of primary CAR-T cells when seeded in the bioreactor (Day 0 - grey) and post-harvest at different agitation conditions in the ambr® 250 unbaffled vessels and in T-175 flasks (static control) after 7 days of expansion. Data shown as ± SD, n=3. No significant difference ($P > 0.05$) was detected between different conditions using a One-way ANOVA test. Each symbol represents one donor (HD12 = star; HD16 = circle; HD18 = square). (a) CD4:CD8 ratio. (b) $CD8^+$ T central memory ($CCR7^+$ $CD45RO^+$) subpopulation percentage of the cells. (c) $CD8^+$ T effector memory ($CCR7^-$ $CD45RO^+$) subpopulation percentage in all the analysed conditions.

The expression of the CAR receptor was assessed by flow cytometry at seeding (day 0) and at the end of the 7 days expansion in the bioreactors and in the static control (Figure 4.8). The CAR expression at day 7 was normalised to the expression at day 0 for each different donor and condition assessed. This was necessary due to a variable transduction efficiency for each run ranging from 20 to 50%. The percentage of T-cells expressing the CAR in all the analysed conditions did not show any significant difference ($P > 0.05$) compared to the static control, suggesting that the fluid dynamic stresses induced by the stirring regime did not cause CAR shedding. However, at 500 rpm the percentage of cells expressing the anti-CD19 CAR was slightly lower (although not statistically significant ($P > 0.05$)) than in all other conditions (Figure 4.8). This difference might be an indication that, as hinted at by the estimate of the Kolmogorov eddy size at this speed, fluid dynamic stresses start to have an impact on the CAR receptor. Further investigations at a higher speed would be needed in order to prove this hypothesis.

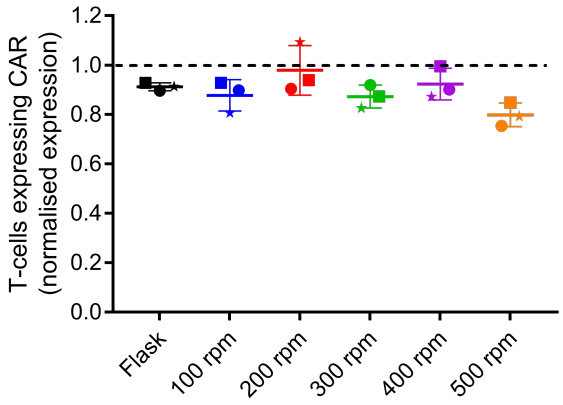

Figure 4.8: Normalised CAR expression at the end of 7 days expansion in the ambr® 250 unbaffled vessels and in T-175 flasks (static control). Each run has been normalised to the starting CAR expression obtained for the specific condition at inoculation (day 0). Reference line at 1 shows the equivalence in CAR expression between day 0 and day 7. Each symbol represents one donor (HD12 = star; HD16 = circle; HD18 = square). Data shown as ± SD, n=3. No significant difference ($P > 0.05$) was detected between different conditions using a One-way ANOVA test.

4.6.2 *In vitro* cytotoxicity assay

Anti-CD19 CAR-T cell functionality was assessed by performing an *in vitro* cytotoxicity assay using Nalm6 (CD19 positive cells) as target cells (Figure 4.9). This assay, also called killing assay, is commonly used to assess the capability of expanded CAR-T cells to recognise and kill tumour cells *in vitro* (Zaritskaya et al., 2010; W. Zhang et al., 2018). CAR-T cytolytic activity was retained in all culture conditions and it was comparable or better than that exhibited by the static CAR-T control (9.68 ± 2.71% remaining target cells) with less than 8% of the target Nalm6 cells remaining after 24 hours across all conditions in the ambr® 250 stirred-tank bioreactor. In detail 6.27 ± 1.48% Nalm6

were alive when co-cultured with CAR-T cells expanded at 100 rpm in the ambr® 250, 6.83 ± 2.68% when co-cultured with CAR-T cells expanded at 200 rpm, 7.95 ± 5.91% when co-cultured with CAR-T cells expanded at 300 rpm, and 5.85 ± 2.13% when co-cultured with CAR-T cells grown at 400 rpm. Although the normalised CAR expression was found to be lower at 500 rpm, once the CAR-T cells were isolated, they showed a low percentage of remaining target cells (7.80 ± 2.05%) proving that they retained their cytolytic function *in vitro* (Figure 4.9). These results are comparable to data presented in published studies using the same CAR plasmid to transduce human primary T-cells (Stavrou et al., 2018).

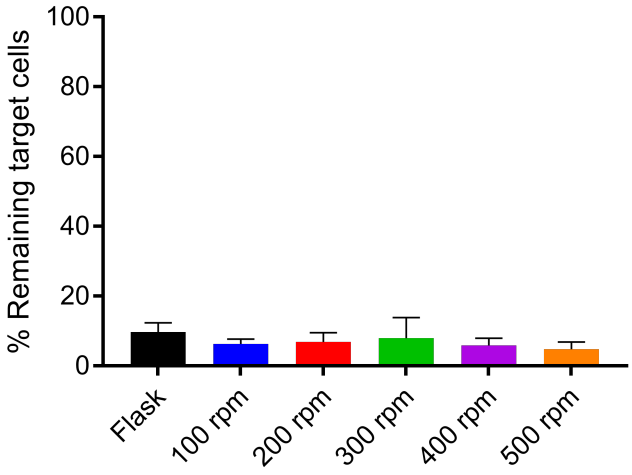

Figure 4.9: Percentage of remaining target cells (Nalm6) from the cytotoxicity assay performed with CAR-T cells grown at different agitation conditions in the ambr® 250 unbaffled vessels and in T-175 flasks (static control). Data shown as ± SD, n=3. No significant difference ($P > 0.05$) was detected between different conditions using a One-way ANOVA test. .

4.6.3 Cytokine secretion

In addition to the immunophenotypic profile and cytotoxicity assay, the culture supernatant was used to perform a CBA assay and analyse the cytokines released in the medium after co-culturing anti-CD19 CAR T-cells with CD19 expressing cells (Figure 4.10 and 4.11). The CBA assay is generally used to confirm the functionality of CAR-T cells against tumour cells expressing the CD19 receptor *in vitro*, verifying and confirming the cytotoxicity data results.

This assay detects cytokines such as Interferon-gamma (INF-γ), Tumour Necrosis Factor (TNF), and IL-2. These pro-inflammatory cytokines are known to be produced by the T helper 1 (Th1) subset, but also by $CD8^+$ CAR-T cells. As shown in Figure 4.10a, INF-γ was released in all the conditions with no statistically significant difference ($P > 0.05$) between the static and dynamic conditions. The same result was found for the TNF secretion, where no significant difference ($P > 0.05$) was found amongst the different conditions (Figure 4.10b). IL-2, an indicator of CAR-T cell proliferation, but also secreted for T-cell survival and differentiation (W. Zhang et al., 2018), was also detected in the supernatant with no statistically significant difference ($P > 0.05$) between the static and dynamic conditions (Figure 4.10c).

The limit of the CBA assay is at 5000 pg ml^{-1} of detected cytokine; for levels higher than that, the software extrapolates the value. It can be however stated, that the concentration of IL-2 was higher than 5000 pg ml^{-1} for all the conditions, although the plotted

values might not be accurate (Figure 4.10c).

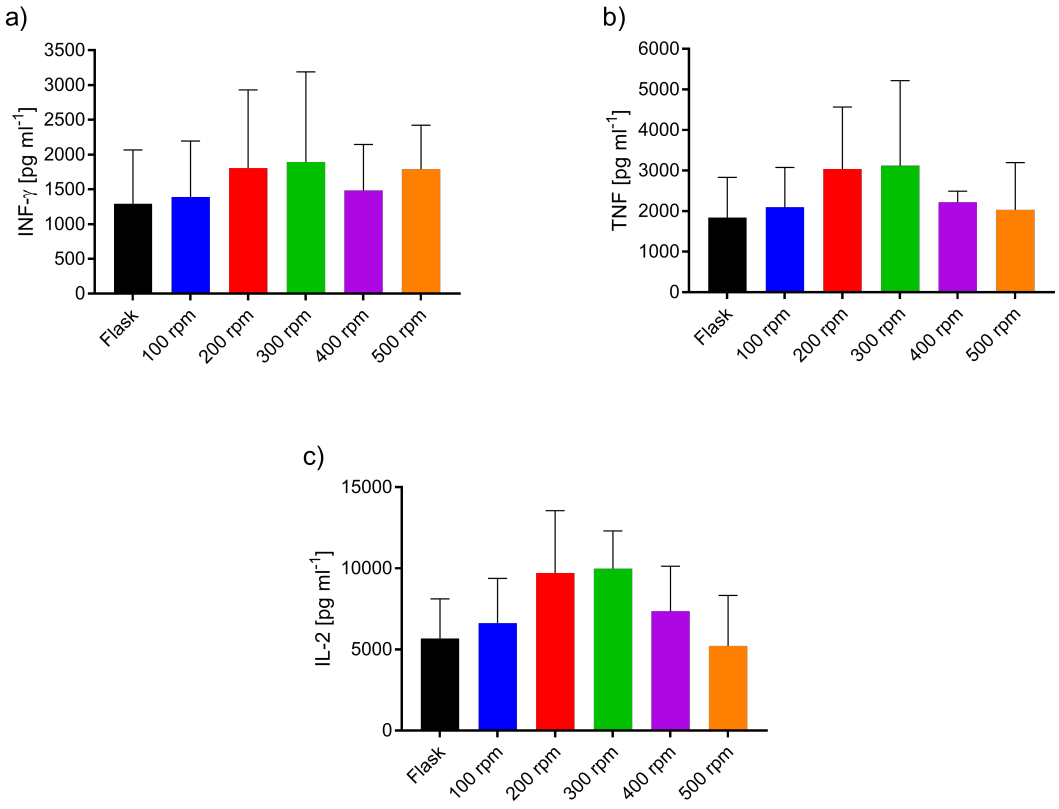

Figure 4.10: Quantitative analysis of cytokines secreted [pg ml^{-1}] by T helper 1 cells in the supernatant medium for CAR-T cells grown at different agitation speeds and in T-175 flasks (static control) when exposed to NALM6 cells. Data shown as $\pm$ SD, n=3. A one way ANOVA test was performed. No significant difference ($P > 0.05$) was detected between different conditions using a One-way ANOVA test. (a) INF-γ concentration. (b) TNF concentration. (c) IL-2 concentration.

Although for all the analysed cytokines, the trend was similar, there was a higher level of cytokine secreted by CAR-T cells grown at 200 and 300 rpm. The levels of INF-γ were in line with those found in previous work (Cha et al., 2010; Kochenderfer et al., 2012), when CAR-T cells were co-cultured with leukemia cells, giving once again

the confirmation of their functionality and cytolytic abilities. INF-γ secretion upon stimulation of CAR-T cells is routinely used in potency assay during clinical trials (Gee, 2018). Th1 cells have been shown to be more effective in the induction of anti-tumour cell-mediated immunity *in vivo* (Nishimura et al., 2000).

The CBA assay was also used to detect cytokines typically secreted by T helper 2 (Th2) and T helper 17 (Th17) subsets. These cytokines are IL-4, IL-6, IL-10, and IL-17A (Figure 4.11). The quantity of IL-4, IL-6 and IL-10 secreted by Th2 cells are shown in Figure 4.11a,b,c. Their levels in the medium were detected at a much lower concentration compared to INF-γ, TNF, and IL-2, in line with what was reported in other studies (W. Zhang et al., 2018). However, there was no significant difference ($P > 0.05$) between the different conditions, with the exception of IL-10 (Figure 4.11c), where CAR-T cells grown at 500 rpm secreted a significantly higher ($P < 0.05$) amount of cytokine compared to the other conditions. IL-10 is a regulatory cytokine mainly secreted by T regulatory cells and it has immunosuppressive functions (Plitas et al., 2016). This result suggested that a more vigorous agitation promoted the differentiation of T-cells towards a T regulatory phenotype (Kofler et al., 2011), however further studies are needed in order to confirm this finding. No significant difference ($P > 0.05$) was detected in IL-17A secretion for the CAR-T cells cultured in different conditions (Figure 4.11d), suggesting that the agitation did not promote differentiation into Th17 subset. The levels of IL-17A are in line with the one reported in other studies (Pucino et al.,

2019).

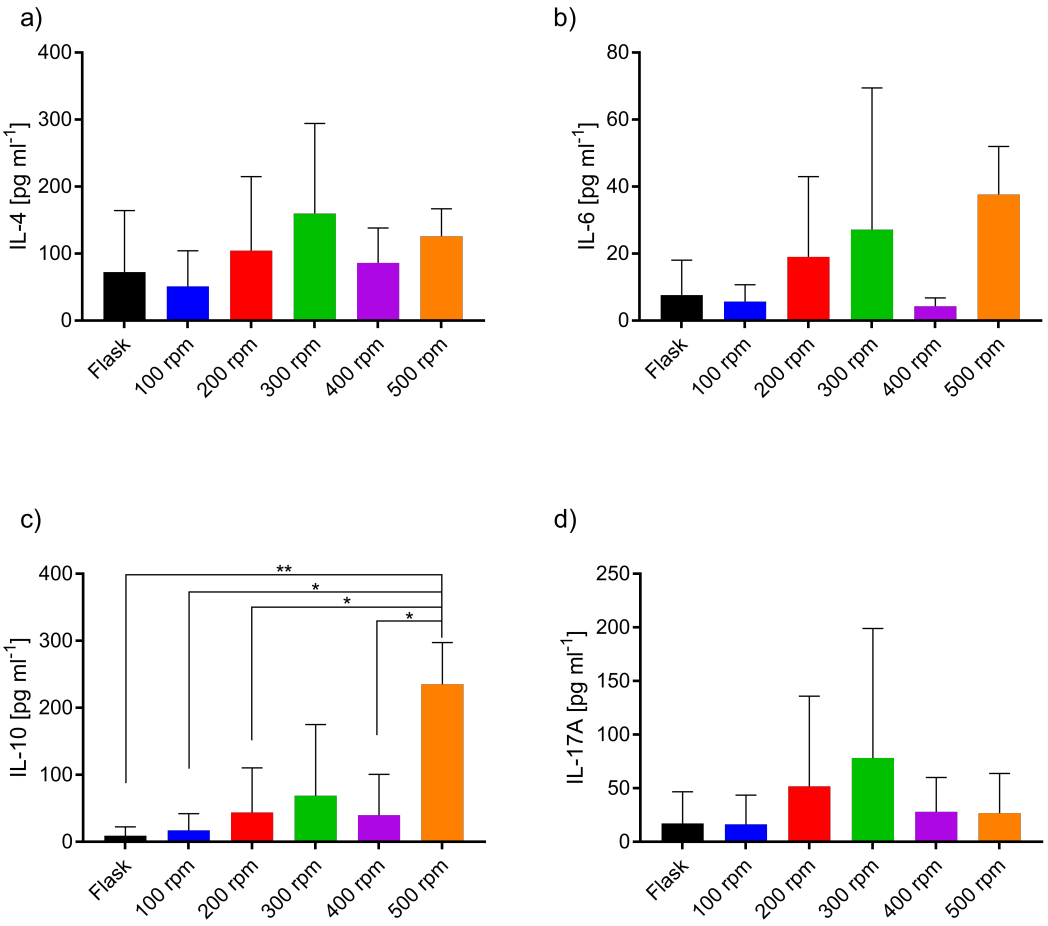

Figure 4.11: Quantitative analysis of cytokines secreted [pg ml^{-1}] by T helper 2 and T helper 17 cells in the supernatant medium for CAR-T cells grown at different agitation speeds and in T-175 flasks (static control) when exposed to Nalm6 cells. Data shown as ± SD, n=3. A one way ANOVA test was performed. Statistical significance is shown when probability (P) values were equal or below 0.05 (*), 0.01(**), 0.001(***), or 0.0001(****). (a) IL-4 concentration. (b) IL-6 concentration. (c) IL-10 concentration. (d) IL-17A concentration.

4.7 Manufacturing platforms for CAR-T cell production

No existing literature on CAR-T cells expanded in stirred-tank bioreactors has been found. However, the final cell yield and growth kinetics obtained in the stirred-tank bioreactor were compared to other routinely used CAR-T cell expansion platforms (e.g. gas permeable bags, G-Rex, rocking motion bioreactors, and CliniMACS Prodigy®) (Vormittag et al., 2018). Although it was challenging to find peer reviewed papers that report the detailed manufacturing process for CAR-T therapies, some data on final cell yields across different platforms were retrieved.

4.7.1 Static culture systems

G-Rex and gas permeable bags are static platforms generally used for the manufacture of CAR-T cell products for phase I/II clinical trials (Vormittag et al., 2018). Tumaini et al. (2013) reported a 8-14 fold expansion in permeable bags for CAR-T cells using a 13 days expansion protocol. The medium used was AIM V™ serum-free medium supplied by Gibco, supplemented with 5% AB serum, 1% Gluta-Max and 300 IU ml^{-1} IL-2. Two of the samples used were from patients, while one was from a healthy donor.

In the G-Rex system with a gas-permeable membrane at the bottom, a fold expansion up to 42 has been reported in 6-well plates (Gagliardi et al., 2019). However, this

only occurred when CAR-T cells were seeded at low seeding density (0.06 x 10^6 cells cm^{-2}). For higher seeding density (1 x 10^6 cells cm^{-2}) the fold expansion was $\sim$ 20. The length of the culture was 11-14 days in TexMACS™ GMP medium produced by Miltenyi Biotec supplemented with IL-7 and IL-15. The activation of the T-cells was performed with soluble anti-CD3 and anti-CD28 antibodies.

Both these studies, report a lower fold expansion compared to the ambr® 250 stirred-tank bioreactor ($\sim$ 25 fold expansion at 300 rpm), exception made for the condition seeded at very low density. The expansion period in the cited studies was 6 to 7 days longer than the one described in this thesis and the medium and medium supplements were different. Due to the nature of the G-Rex vessel, where the cells sit on the bottom of it on the permeable membrane, it is hard to compare the initial cell densities, as in the G-Rex this is reported on cells per unit of area, while in stirred-tank or rocking motion bioreactors the cells are in suspension and the seeding density is given in cells per millilitre.

Although static platforms are easy and straightforward to use, both these platforms require frequent manipulations by trained operators in biosafety cabinets (Vormittag et al., 2018; Q. A. Rafiq et al., 2015). Furthermore these static platforms are not scalable, meaning that a single dose might require multiple gas permeable bags or G-Rex platforms to be produced impacting on the cost of the product (Mizukami et al., 2020). Another drawback is that these static expansion system do not have in-process controls,

which are present in stirred-tank bioreactors and other bioreactors in general. The higher fold expansion in a shorter time, clearly demonstrates the better performance of stirred-tank bioreactors, where agitated culture conditions enable an enhanced mass transfer and homogeneous nutrient distribution throughout the culture medium.

4.7.2 Rocking motion bioreactors and Prodigy CliniMACS system

Rocking motion bioreactors and CliniMACS Prodigy® systems are more comprehensive than static platforms, with in-process control systems and dynamic culture options (Xiuyan Wang et al., 2016). Hollyman et al. (2009) achieved a cell density at harvest of 13.2-31 x 10^6 cells ml^{-1} (87 to 668 fold expansion) in a rocking motion bioreactor (WAVE EHT, GE Healthcare) after 13-18 days of culture. This resulted in significantly higher cell densities compared to the ones achieved in the stirred-tank bioreactor at 300 rpm (best growing condition), which was $\sim$ 5 x 10^6. The culture medium used in their study was X-VIVO™ 15 serum-free chemically defined medium produced by Lonza supplemented with 5% AB serum and 100-500 IU ml^{-1} of IL-2.

Different studies were found on the expansion of CAR-T cells using a CliniMACS Prodigy®, reporting a fold expansion ranging from 16 to 81 and 8-13 days of expansion (W. Zhang et al., 2018; Zhu et al., 2018; Lock et al., 2017; Aleksandrova et al., 2019). All these studies used TexMACS™ GMP medium. The medium was supplemented with 3-5% human AB-serum in all cases and different concentrations of IL-2 or IL-7 and IL-

15 were added to the medium for CAR-T cell culture. Furthermore, all of these studies used TransAct™ particles for T-cell activation.

The results obtained by Hollyman et al. (2009) were significantly higher than the one presented in this chapter. However, the expansion process reported in literature consisted of a 6-11 days longer culture period and a feeding strategy based on perfusion (from 200 ml to 1600 ml of medium were exchanged over 24h), which enabled to remove waste products and provide a continuous supply of glucose, glutamine, and other supplements necessary for T-cell growth. Klarer et al. (2018) have shown how a perfusion feeding yielded higher cell densities compared to a fed batch feeding, which was used in this thesis. Although the final cell density achieved in the rocking motion bioreactor by Hollyman et al. (2009) was higher, the perfusion feeding strategy and prolonged expansion protocol most likely played a crucial role in the CAR-T cells proliferation, making it hard to directly compare their results with the ones presented in this doctoral thesis. The range of fold expansion in the CliniMACS Prodigy® was very broad. The 25 fold expansion achieved in the stirred-tank bioreactor at 300 rpm falls in that range. However, the culture medium, medium supplements, and the activation reagents differ from the one used in this thesis. Although the CliniMACS Prodigy® allows for a closed process from cell isolation to expansion, it is only suitable for a scale-out strategy rather than scale-up due to the limited size of the culture vessel (250 ml). On the other hand, rocking motion bioreactors allow for increased scale with dif-

ferent modes of operation, e.g. perfusion. Stirred-tank bioreactors are already widely used as cell expansion platforms for different autologous and allogeneic applications, with scales varying from 100 ml to $>$ 20,000 L for large-scale recombinant protein production using CHO cells and other mammalian cell types (Alvin W Nienow, 2006b; Costariol et al., 2020). They have also been used at scale for human mesenchymal stem cells culture on microcarriers and have been extensively used in the biologic industry, which led to an extensive characterisation for cell production and a proven track record for large-scale industrial manufacture (Alvin W Nienow, 2006b; Alvin W Nienow et al., 2016; Q. A. Rafiq et al., 2013a). This usage increases the likelihood of adoption for therapeutic development by companies who have these manufacturing platforms in place and reduces the risk associated with using such platforms for commercial manufacture. Furthermore, stirred-tank bioreactors have the advantage that, unlike rocking motion bioreactors, they have small-scale models, such as the ambr® 15 and 250, and the DASbox system, which can be operated at low volumes (15 - 250 ml). These small scale stirred-tank bioreactors allow multiple processes to be run in parallel, increasing the parameters tested, process understanding and reducing development time frames during process development.

4.7.3 Improvements for a more efficient culture in stirred-tank bioreactors

Due to the different culture parameters (i.e. activation methods, medium, feeding strategy, length of expansion, medium supplements) it was not possible to make a direct comparison with the data found in literature. However, it can be seen how the rocking-motion bioreactor had the highest fold expansion, mainly due to the perfusion feeding strategy. Bioreactors give the opportunity to monitor and control key culture parameters, such as pH and dO_2, which can improve the growth kinetics of T-cells (Klarer et al., 2018; A. Amini et al., 2020). This is why, stirred-tank bioreactors have an advantage compared to static culture vessels, not only they allow for better mass transfer, but also allow to monitor key culture parameters which play a crucial role in CAR-T cell expansion.

Even though the current expansion protocol was not optimised, and higher cell number could potentially be achieved, the final cell yield in the best growing condition (300 rpm) was $\sim$ 12.5 x 10^8 viable cell ml^{-1} after 7 days expansion. With a transduction efficiency as low as 20.5%, the number of CAR positive viable T-cells at harvest would be 2.56 x 10^8, which falls in the range of target doses current administered to patients in the FDA approved CAR-T therapies. This makes the ambr® 250 automated stirred-tank bioreactor potentially suitable for the manufacturing of personalised medicines. Moreover, platforms such as the ambr® 250, which allow for the simultaneous operation of

24 independent bioreactors, enable a level of throughput and flexibility not currently seen in existing manufacturing platforms. With the move towards allogeneic CAR-T production, stirred-tank bioreactors also have proven scalability and it is not difficult to foresee multiple doses of allogeneic treatments being manufactured in $>$ 5 L stirred-tank bioreactors, with the potential for further scalability. However, further studies on the comparability between small scale and large scale bioreactors in terms of cell yields and cell functionality are needed.

Dynabeads®, antibody coated paramagnetic beads, are widely used in the CAR-T therapy manufacture to activate the cells. However, these beads cannot be left in the final product, but need to be removed prior to final formulation, which adds a step to the already complex manufacturing process. In this study, the stirring speeds investigated were in the range of 100 rpm to 500 rpm, showing the final product quality and potency was not impacted by the increased agitation. The best condition in terms of final cell density was found to be the one at 300 rpm, with little or no difference to the cell yield at 200, 400, and 500 rpm. The hypothesis was that at low speed (100 rpm) the paramagnetic beads were not well suspended and did not interact efficiently with the CAR-T cells (Costariol et al., 2019). In order to verify and confirm this hypothesis, alternative activation methods, such as TransAct™ CD3/CD28 polymeric nanomatrix coated particles could be used. These particles are mostly used in the CliniMACS Prodigy® system in conjunction with the TexMACS™ medium, all produced by Miltenyi Biotec

(W. Zhang et al., 2018; Zhu et al., 2018; Lock et al., 2017; Aleksandrova et al., 2019). These particles are smaller than Dynabeads®, easier to suspend and degradable, with no need for the removal step at the end of the expansion process. TransAct™ could be used to assess whether the slower growth at 100 rpm compared to higher speeds was only due to the suspension of the Dynabeads®. However, controversial studies have been found in literature and it is not clear if the activation of the CAR-T cells with TransAct™ is comparable to the one achieved with Dynabeads® (Mock et al., 2016; Wang et al., 2015).

The medium used in this thesis was RPMI 1640 supplemented with 10% FBS, 2mM L-Glutamine, and 30 IU ml^{-1} IL-2. Medvec et al. (2018) reported a higher population doubling for CAR-T cells cultured with AIM V™ and X-VIVO™ 15 medium supplemented with human serum compared to CAR-T cells grown in RPMI 1640 (although the vessel used for T-cell expansion was not reported). TexMACS™ medium was found to achieve a lower fold expansion than the X-VIVO™ 15 medium, however the study was performed with cytokines induced killer cells (Castiglia et al., 2018), and no direct comparison with RPMI 1640 was found in literature. RPMI 1640 could be one of the limiting factors for the expansion of CAR-T cells. Switching to a different medium, with higher glucose content would avoid the depletion of glucose throughout the culture. Furthermore, animal supplements (e.g. FBS) cannot be used in clinical trials and for commercialised products, therefore a switch to serum free medium or human AB

serum would be beneficial. The amount of IL-2 used in the above cited studies was also significantly higher than the one used in the ambr® 250 process, which could have an effect on T-cell proliferation (Hollyman et al., 2009).

4.8 Conclusions

This work proved the production of CAR-T cells in a stirred-tank bioreactor is feasible. Building on previous work with primary T-cells (Chapter 3), the study investigated a range of agitation intensities from 100 rpm (9.3 x 10^{-4} W kg^{-1}) up to 500 rpm (1164 x 10^{-4} W kg^{-1}) to understand the impact on CAR-T cells growth kinetics and quality.

Agitated stirred-tank bioreactor conditions resulted in higher final cell densities than the static T-flask controls, with equivalent cell quality and potency. It was found that an increase from 100 rpm to 200 rpm (74 x 10^{-4} W kg^{-1}) led to higher cell yields ($\sim$ 4 x 10^6 cells ml^{-1} compared to $\sim$ 5 x 10^6 cells ml^{-1}, respectively), which is in line with the previous findings with primary T-cells (Chapter 3). Similar cell densities were obtained from the 200, 300, 400 and 500 rpm agitation intensities, suggesting that once the Dynabeads® are well suspended, the increase in the agitation speed does not improve final cell yield. However, all speeds gave higher cell densities than the static T-flask control ($\sim$ 2.5x10^6 cells ml^{-1}). Furthermore, higher speeds did not impact the final product quality and might be needed in order to improve gas transfer at higher scales for allogeneic therapies. It was therefore important to show there was no cell damage at

higher speeds.

Importantly, it was demonstrated that for all agitation rates tested, the quality and functionality of the CAR-T cells was retained, with a cytolytic functionality greater than 90% after 24 hours, thereby proving that fluid dynamic stresses do not affect the CAR-T cell efficacy to target and kill the leukaemia cells *in vitro*. Furthermore no significant differences ($P > 0.05$) were found between samples in terms of metabolism for glucose, lactate, glutamine, and ammonia. However, an optimised feeding strategy or different medium formulations would need to be implemented for further studies to avoid complete depletion of nutrients in the medium, which may limit the growth of CAR-T cells. Furthermore, alternative activation methods could be tested to better understand whether a better activation at lower speeds (i.e., 100 rpm) could lead to a more substantial growth, as hypothesised.

Stirred-tank bioreactors bring different advantages to the process. Firstly, they allow for on-line monitoring of different culture parameters, such as pH and dO_2 and for a more homogeneous culture condition compared to static platforms. Secondly, they are already widely used in the biopharma industry and have a well established supply chain, reducing supply risk at scale, which is a constraint for the current alternative technologies, which often rely on single source suppliers and low product manufacturing volumes (e.g. CliniMACS Prodigy®). Lastly, they have suitable scale-down models (15-250 ml scale), which significantly reduce the cost for process development and al-

low for high-throughput screening of different reagents and conditions.

Chapter 5

Scaling-up the manufacture of human primary T-cells in stirred-tank bioreactors

5.1 Introduction

Autologous CAR-T therapies are currently manufactured in small scale bioreactors or static expansion flasks and bags (Vormittag et al., 2018). However, with the field showing increasing interest in allogeneic CAR-T therapies there is a need to scale-up the expansion process to larger scale bioreactors, decreasing the footprint in expensive clean

rooms, and lowering the cost of the manufacturing process. The scale needed for allogeneic CAR-T therapies would be the limited by number of T-cells that can be isolated per donor ($\sim$ 500 - 5000 x 10^6 total T-cells after leukopak processing and gene editing), which can be expanded in 2-10 L volumes. However, it is still important and necessary to find suitable scale-down models that would allow for high-throughput screening without incurring in prohibitive raw materials cost. Stirred-tank bioreactors are well established in the pharmaceutical industry and their availability at different scales (from few milliliters to 2000 L) makes them suitable for various manufacturing processes that may require larger volumes (Alvin W Nienow, 2006b; Schirmer et al., 2020).

Having successfully cultured primary T-cells and engineered CAR-T cells in an ambr® 250 bioreactor (Chapter 3 and Chapter 4), the following step was to find suitable scale-down and scale-up models for the expansion process. This chapter aims to identify whether the scaling-up of the expansion process for T-cells is feasible. Starting from a screening experiment in the small scale high-throughput ambr® 15 stirred-tank bioreactor, the best expansion outcome in terms of final yield and immunophenotype was then scaled-up to an ambr® 250 stirred-tank bioreactor and to a 1 L UniVessel® stirred-tank bioreactor. Primary human T-cells were used to demonstrate the comparability between the three scales (15 ml, 250 ml, and 1 L). The scale-up was performed based on the P/M, which has proven to be a valid comparability parameter between different geometries (baffled vs. unbaffled vessel) in the ambr® 250 stirred-tank bioreactor,

as discussed in Chapter 3 (Costariol et al., 2019). The results were compared in terms of growth kinetics, final cell yield, metabolite profiles, and final product composition.

5.2 Initial screening in the ambr 15 bioreactor

An ambr® 15 was used for the initial screening of different culture parameters. This small scale high-throughput stirred-tank bioreactor has been extensively used for different mammalian cells culture, such as CHO cells, hMSCs, and primary T-cells (Alvin W Nienow et al., 2016; Rameez et al., 2014; Warr, 2020; Klarer et al., 2018). The ambr® 15 bioreactor allows up to 48 vessels to be run in parallel, as well as allowing for temperature, dO_2, pH monitor and control throughout the culture, which is rarely possible in other small-scale systems or in static culture flasks.

Different dO_2 were tested in order to investigate the effect on T-cell growth. The ambr® 15 high-throughput stirred-tank bioreactor allows to independently set the dO_2 levels (uncontrolled, 25%, 50%, and 75% dO_2) for each vessel. The 25% dO_2 is believed to be similar to the oxygen tension in lymphoid tissues (Carswell et al., 2000). The higher dO_2 levels were chosen to allow a wider screening range. Previous studies suggest that neutral pH at lower dO_2 (5-50% dO_2) better promotes T-cell growth (Bohnenkamp et al., 2002; A. Amini et al., 2020). In order to reduce the variability, pH was fixed between 7.1-7.2 in all the experiments. The pH was chosen based on previous work by Bohnenkamp et al. (2002), suggesting that the optimal pH range for

T-cells growth is between 7.0 and 7.3, while lower pH might have and adverse effect (Calcinotto et al., 2012). Furthermore, the same pH range was used in Chapter 4 and the data did not suggest such pH to have an unfavorable effect on CAR-T cell growth.

5.2.1 Growth kinetics

The uncontrolled dO_2 condition, where the dO_2 was monitored, but not set at any value, was run at two speeds (300 and 450 rpm) and was compared to 25, 50 and 75% dO_2 at 450 rpm (Figure 5.1). The 300 rpm run was performed to confirm the hypothesis that lower speeds and lower P/M achieve a lower growth presumably due to poor Dynabeads® suspension (Costariol et al., 2019). As expected, the T-cells grown in uncontrolled dO_2 resulted in a lower cell yield at harvest at both speeds (2.92 ± 0.73 x10^6 viable cells ml^{-1} at 300 and 3.53 ± 0.55 x10^6 viable cells ml^{-1} at 450 rpm) compared to the conditions grown at 450 rpm and set dO_2. Therefore, no other condtions were tested at 300 rpm. At 450 rpm the final cell concentrations were 4.77 ± 0.24 x10^6 viable cells ml^{-1} at 25% dO_2, 4.60 ± 0.32 x10^6 viable cells ml^{-1} at 50% dO_2, and 4.50 ± 0.31 x10^6 viable cells ml^{-1} at 75% dO_2.

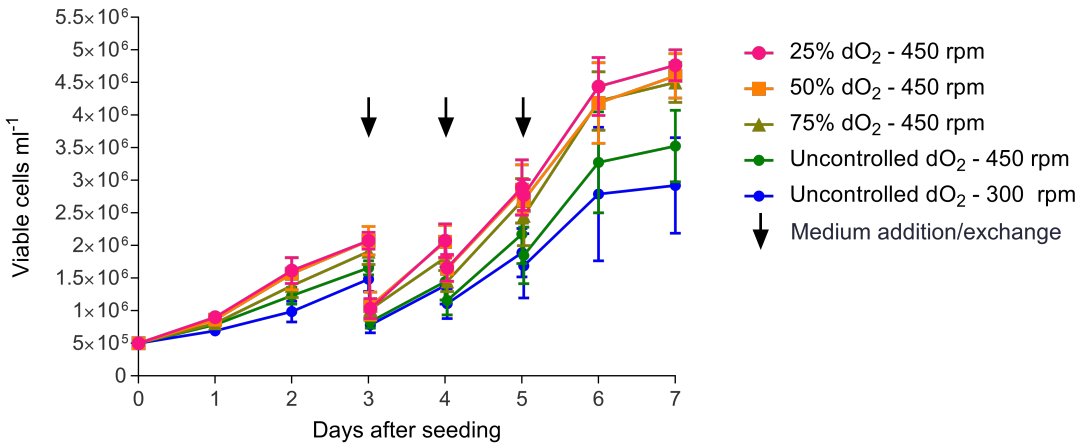

Figure 5.1: Initial screening experiment performed in an ambr® 15 stirred-tank bioreactor. Viable cells ml^{-1} for each of the tested conditions. The black arrows indicate medium addition/exchange. All data are shown as mean ± SD, n=3.

The dO_2 trends of the two uncontrolled conditions at 300 and 450 rpm are shown in Figure 5.2. The dO_2 profiles at the two speeds almost overlapped, ranging from 90% at the beginning of the expansion to 50% at the end of the culture.

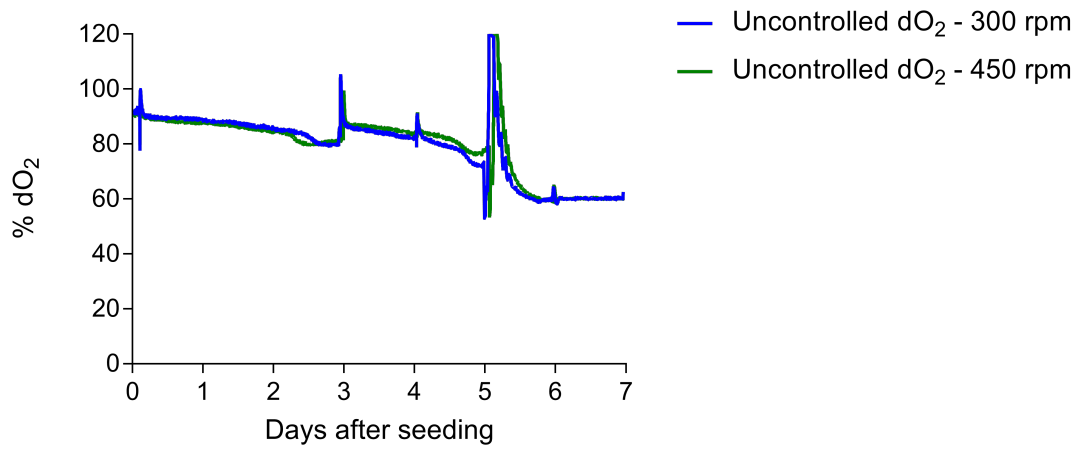

Figure 5.2: Representative dO_2 trend of the uncontrolled conditions at 300 rpm and 450 rpm in the ambr® 15 bioreactor.

Given that the pH was fixed between 7.1 and 7.2 in all the experiments and the dO_2 profiles of the uncontrolled conditions were similar at both speeds, it can be hypothesised that the better performance of the cultures at 450 rpm was only due to an enhanced mixing, as previously reported for the ambr® 250 stirred-tank bioreactor (Costariol et al., 2019). The higher speed might lead to a better suspension of the Dynabeads® and to an increased activation and proliferation of the T-cells. The 300 rpm speed in the ambr® 15 resulted in a P/M of 28 x 10^{-4} W kg^{-1}, which was lower than the P/M needed to suspend the Dynabeads® reported in Chapter 3 (74 x 10^{-4} W kg^{-1}). On the other hand, at 450 rpm the P/M in the ambr® 15 was 95 x 10^{-4} W kg^{-1}, which was higher than the P/M needed to suspend the paramagnetic beads. This adds strength the hypothesis that Dynabeads® were not well suspended at lower speeds and need an enhanced mixing and higher P/M in order to interact with the cells and activate them efficiently (Costariol et al., 2019).

At 450 rpm the uncontrolled dO_2 condition showed a higher fold expansion (16.47 $\pm$ 2.56), although not significantly ($P > 0.05$), to the condition grown at uncontrolled dO_2 at 300 rpm (13.65 $\pm$ 3.43), confirming that higher stirring speed results in better final yield in terms of viable cell numbers (Figure 5.3). All the conditions run at controlled dO_2 (25%, 50%, and 75%) and 450 rpm resulted in a significantly higher ($P < 0.05$) fold expansion compared to the condition grown at 300 rpm (Figure 5.3a).

The fold expansion achieved by the T-cells grown at 25% dO_2 was 22.26 $\pm$ 1.11

and resulted slightly higher, although not significantly ($P > 0.05$), compared to the 50% and 75% dO_2 conditions, which had a fold expansion of 21.50 ± 1.60 and 21.01 ± 1.44 respectively. This results are in line with previously published studies, where primary T-cells grown at lower dO_2 showed a higher final cell yield (A. Amini et al., 2020). The doubling time calculated from day 2 to day 7, when the cells were in their exponential growth phase, ranged between 39.63 ± 1.15 hours (75% dO_2 at 450 rpm) and 42.34 ± 1.11 hours (uncontrolled dO_2 at 450 rpm) as shown in Figure 5.3b. There was no significant difference ($P > 0.05$) in the doubling time across the tested conditions. The cumulative population doublings shown in Figure 5.3c reflected the data displayed on the growth curve graph (Figure 5.1), showing a slow down in the growth from day 6 to day 7 probably due to a lack of nutrients in the medium (data not shown).

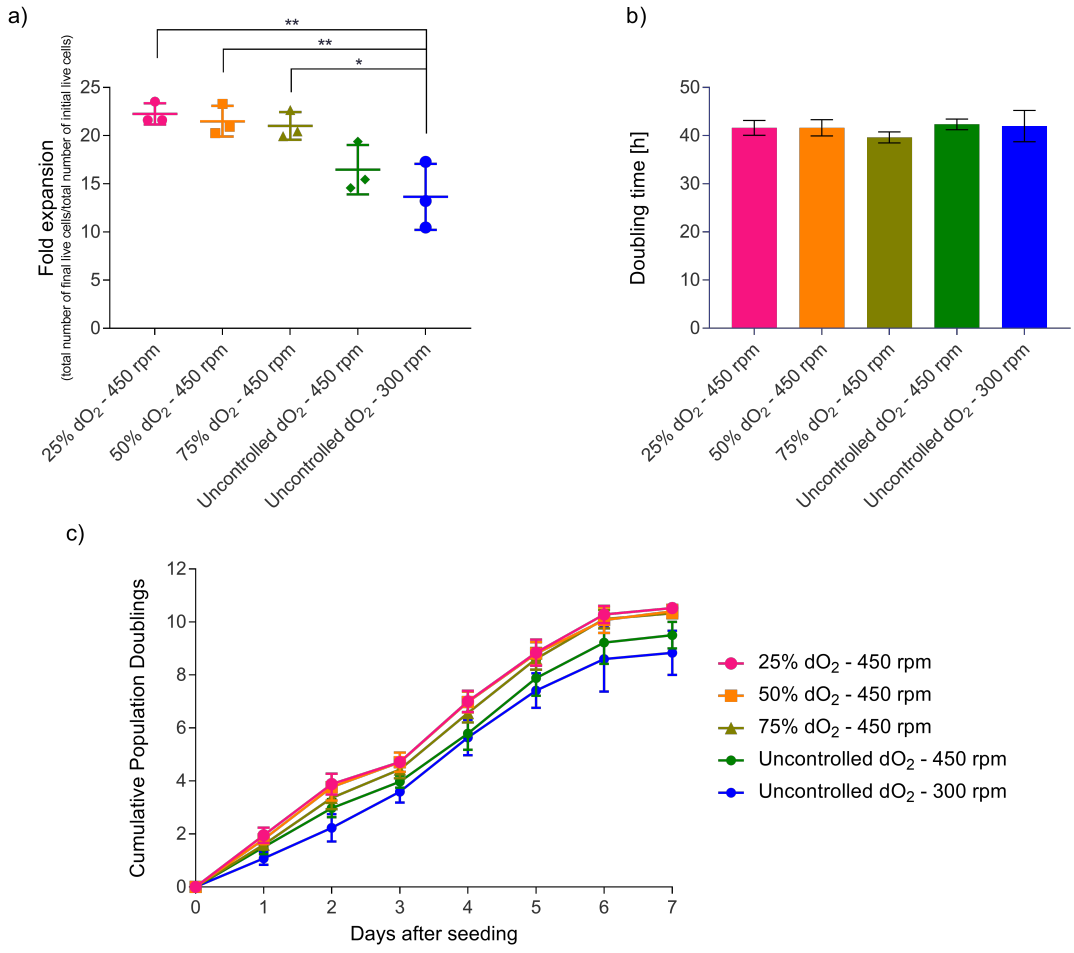

Figure 5.3: Growth of primary human T-cells in an ambr® 15 high-throughput bioreactor at different dO_2 and speeds (300 and 450 rpm). (a) Fold expansion for each of the tested conditions. A one-way ANOVA test was run and statistical significance is shown when probability (P) values were equal or below 0.05 (*), 0.01(**), 0.001(***), or 0.0001 (****). (b) Doubling time [h]. No significant difference ($P > 0.05$) was detected between the conditions using a one-way ANOVA test. (c) Cumulative population doublings.

5.2.2 Immunophenotypic analysis

The T-cells immunphenotype was investigated at seeding and after 7 days expansion in the ambr® 15 stirred-tank bioreactor via flow cytometry analysis (Figure 5.4). The T-cells were stained for CD4 and CD8 markers. The CD8 expressing T-cells were further divided in naïve ($CCR7^+$ $CD45RO^-$), central memory ($CCR7^+$ $CD45RO^+$), effector memory ($CCR7^-$ $CD45RO^+$) and terminally differentiated ($CCR7^-$ $CD45RO^-$) T-cells.

Studies have suggested that the CD4:CD8 ratio in the final product should be ~ 1 (Turtle et al., 2016). The CD4:CD8 ratio lowered towards 1 after 7 days expansion in the ambr® 15 bioreactor (Figure 5.4a). It can be noted the high consistency of the CD4:CD8 ratio between the different conditions, suggesting that the dO_2 did not have a major impact on this parameter.

The 25% dO_2 condition showed a lower percentage of T central memory cells (20.83 $\pm$ 5.05 %) and a higher percentage of T effector memory cells (74.2 $\pm$ 6.40 %) compared to the other conditions (Figure 5.4b,c). Similar results were reported in previous studies, where low dO_2 coupled with low pH (6.9), showed a lower percentage of T central memory compared with conditions grown at higher dO_2 (A. Amini et al., 2020). This suggests that the lower dO_2 levels promote T-cells differentiation towards an effector memory phenotype, which is short lived and has a lower persistence once reinfused into the patient compared to less differentiated T central memory cells (Petiti et al., 2020).

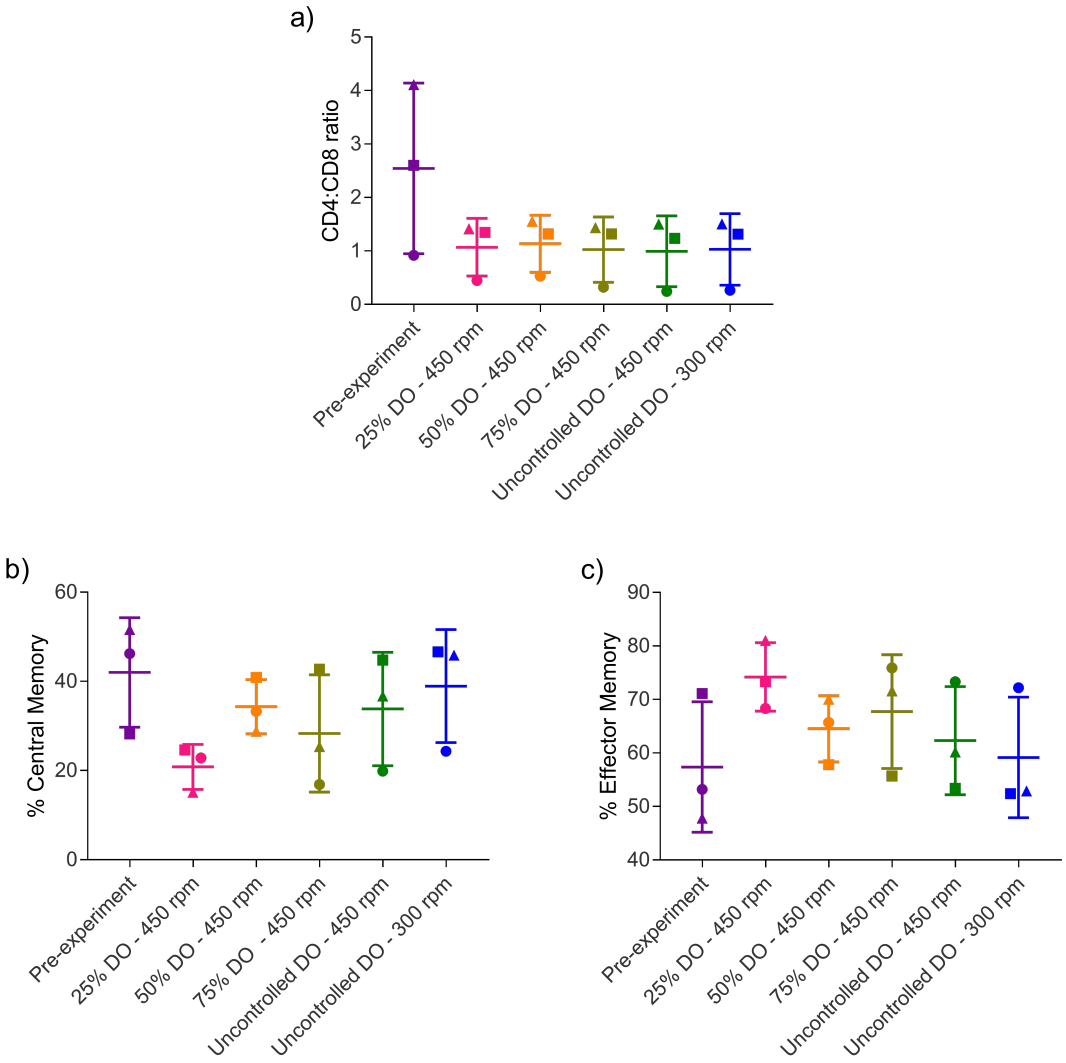

Figure 5.4: Immunophenotype analysis of the T-cells grown under different dO_2 and speed conditions. No significant difference ($P > 0.05$) was detected between the postharvest conditions using a One-way ANOVA test. (a) CD4:CD8 ratio. (b) Percentage of T central memory cells ($CCR7^+$ $CD45RO^+$). (c) Percentage of T effector memory cells ($CCR7^-$ $CD45RO^+$).

5.2.3 Identifying the best culture condition to scale-up

After the initial screening in the ambr® 15 bioreactor it was decided to use the higher stirring speed, 450 rpm, for the scale-up study. This decision was based on the significantly higher ($P < 0.05$) fold expansion achieved at 450 rpm. The different dO_2 conditions had all comparable growth, but the 25% one showed a lower percentage of T central memory cells at harvest, which is not desirable in the final product (Sabatino et al., 2016). It was therefore decided to use 50% dO_2 for the scale-up study, as it was the second best condition in terms of fold expansion, but had a higher percentage of T central memory cells compared to the 25% dO_2 condition. Therefore the 450 rpm with 7.1-7.2 pH control and 50% dO_2 control was scaled-up on a P/M basis to the 250 ml and 1 L scale (Figure 5.5).

Figure 5.5: Three stirred-tank bioreactors at different scale used for the scale-up studies. A small-scale ambr® 15 high-throughput bioreactor (15 ml), a 250 ml ambr® 250 stirred-tank bioreactor, and a 1 L glass UniVessel®. All the bioreactors are produced by Sartorius Stedim Biotech.

5.3 Comparison between different scales

The comparison between different stirred-tank bioreactors scales can be performed based on different parameters, such as k_La (volumetric mass transfer coefficient), impeller tip speed, impeller shear rate (γ), mixing time, and P/M (Garcia-Ochoa et al., 2009; Micheletti et al., 2006; Xing et al., 2009). As discussed in Chapter 3 the comparability between the baffled and unbaffled studies were carried out on a P/M bases and yielded comparable results. It was therefore decided to use the same parameter for the comparison between the different scales (15 ml, 250 ml, and 1 L). P/M takes in consideration both the mixing and mass transfer characteristics and has been used for scaling-up processes in different stirred-tank bioreactors (Micheletti et al., 2006; Rocha-Valadez et al., 2006). The power numbers (P_0) used to calculate the P/M for the different bioreactors are shown in Table 5.1.

Table 5.1: Power numbers for the different systems used in the scale up study (ambr® 15, ambr® 250 unbaffled vessel and 1 L reusable UniVessel®).

Bioreactor	Power number	Source
ambr® 15	2.10	Alvin W Nienow et al., 2013
ambr® 250	2.07	Costariol et al., 2019
1 L UniVessel®	0.7	Sartorius Stedim Biotech

5.3.1 Energy dissipation rate, specific power input, and tip speed

In order to calculate the energy dissipation rate and P/M, which are numerically equivalent, the Equation 2.1 was used. The medium was assumed to have the same density

as water (998 kg m^{-3}). The speed for each bioreactor was fixed for the duration of the experiment, as well as the dO_2 and pH control, at 50% and between 7.1 and 7.2, respectively. The P/M weighted average was calculated taking into consideration the length of the culture at different P/M over the 7 days experiments (Table 5.2).

Table 5.2: P/M for the different systems used in the scale up study (ambr® 15, ambr® 250 unbaffled vessel and 1 L reusable UniVessel®) at different filling volumes and the P/M average weighted over 7 days of culture. The speed was kept constant from day 0 throughout day 7.

	ambr® 15	**ambr® 250**	**1 L UniVessel®**
Speed [rpm] *Day 0-7*	450	200	200
Volume [ml] *Day 0-3*	12	100	400
P/M [x 10^{-4} W kg^{-1}] *Day 0-3*	119	186	165
Volume [ml] *Day 3-4*	13	200	800
P/M [x 10^{-4} W kg^{-1}] *Day 3-4*	110	93	82
Volume [ml] *Day 4-7*	15	250	1000
P/M [x 10^{-4} W kg^{-1}] *Day 4-7*	95	74	66
P/M [x 10^{-4} W kg^{-1}] weighted average over 7 days	**107**	**125**	**111**

It has been shown in previous chapters (Chapter 3 and Chapter 4) that a P/M of 74 x 10^{-4} W kg^{-1} was able to appropriately suspend the Dynabeads® enhancing the bead-to-cell interaction (Costariol et al., 2019). Furthermore, P/M greater than 74 x 10^{-4} W kg^{-1} (corresponding to 200 rpm in the ambr® 250) did not seem to have a significant impact on the proliferation of the T-cells (Costariol et al., 2020). The initial screening in the ambr® 15 showed better results at 450 rpm compared to the lower speed. It was therefore decided to keep the speed at 450 rpm for the ambr® 15 and select appropriate speeds based on the P/M comparison for the ambr® 250, which resulted in 200 rpm, and

1 L UniVessel®, run at 200 rpm as well (Table 5.2).

The weighted average power inputs over the 7 days were 107 x 10^{-4} W kg^{-1} for the ambr® 15, 125 x 10^{-4} W kg^{-1} for the ambr® 250, and 111 x 10^{-4} W kg^{-1} for the UniVessel®, which gave a good comparability between the three systems. All the P/M were above 74 x 10^{-4} W kg^{-1} at which the Dynabeads® seemed to be well suspended (Costariol et al., 2019; Costariol et al., 2020), therfore an increase in the stirring speed did not seem to be necessary.

Although the P/M was used as the scale-up parameter, the impeller tip speed, which can be assumed proportional to the shear stress exerted to the cells (K. G. Clarke, 2013), was also calculated using the following equation:

$$v_{tip} = \pi DN, \tag{5.1}$$

where v_{tip} [m s^{-1}] is the impeller tip speed, D [m] is the impeller diameter, and N [rev s^{-1}] is the impeller speed. The tip speeds for each bioreactor used in the scale-up study are listed in 5.3. It is to be noted, that the tip speed was constant throughout the duration of the experiment, as the impeller speed was not changed.

Table 5.3: Tip speed for the different systems used in the scale up study (ambr® 15, ambr® 250 unbaffled vessel and 1 L reusable UniVessel®).

	Impeller diameter [m]	**Impeller speed [rpm]**	**Tip speed [m s^{-1}]**
ambr® 15	0.011	450	0.259
ambr® 250	0.030	200	0.314
1L UniVessel®	0.048	200	0.502

5.3.2 Growth kinetics

The viable cell concentrations throughout 7 days of expansion for the three tested stirred-tank bioreactors (ambr® 15, ambr® 250, and 1 L UniVessel®) at different scales are shown in Figure 5.6. The experiments were conducted with the same three donors across the three tested platforms. The ambr® 15 vessel operated at 450 rpm resulted in a final cell density of 4.60 $\pm$ 0.34 x 10^6 viable cells ml^{-1}. The ambr® 250 unbaffled vessel with a stirring speed of 200 rpm, yielded 4.22 $\pm$ 0.36 x 10^6 viable cell ml^{-1} at day 7. Finally, the 1 L UniVessel® resulted in a final cell density of 4.24 $\pm$ 0.65 x 10^6 viable cell ml^{-1}.

The final viable cell count per millilitre for the three vessels was within the 4.22-4.60 x 10^6 range. This suggests that high-throughput screening of different medium, medium supplements, and culture parameters such as dO_2 and pH could be performed at small scale (15 ml), lowering the cost of each run and increasing the number of parameters that can be tested in parallel (the system allows up to 48 bioreactors in a single run). After identifying the best condition, this could be reproduced at the 1 L scale yielding comparable results in terms of final cell density for potential allogeneic CAR-T therapies production.

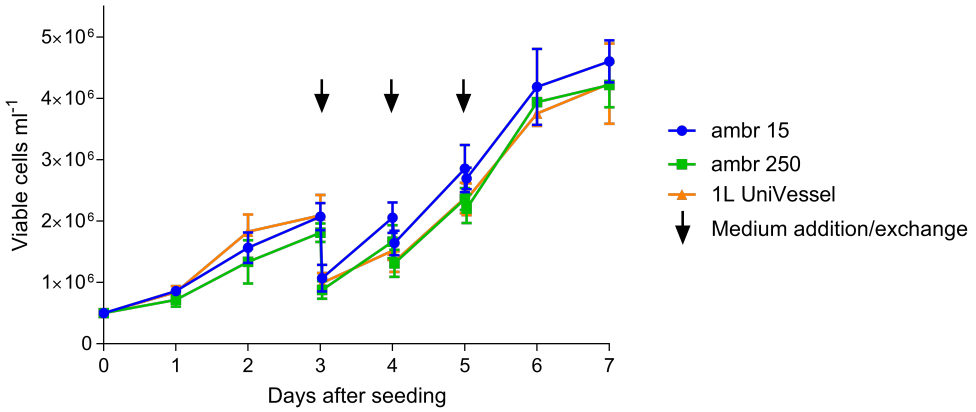

Figure 5.6: The viable cell concentration of primary T-cells from multiple donors (n = 3) over 7 days in the ambr® 15, ambr® 250 and UniVessel® stirred-tank bioreactors. The black arrow indicates a medium addition on days 3 and 4 and a medium exchange on day 5. Data show mean ± SD, n = 3.

Figure 5.7 shows the fold expansion, doubling time and cumulative population doublings for each of the three bioreactors used in this study. The fold expansion (Figure 5.7a) was highly consistent across the three stirred-tank bioreactors, resulting in 21.25 ± 1.58 in the ambr® 15, 21.10 ± 1.81 in the ambr® 250, and 21.20 ± 3.27 in the UniVessel®. This highlights the comparability between the different scales (15 ml, 250 ml and 1 L) in terms of final cell yield and fold expansion.

The doubling times calculated from day 2 to day 7, when the T-cells were in their exponential growth phase, are shown in Figure 5.6b. It can be noted how the UniVessel® resulted in a higher doubling time (48 ± 7.81 h), although not significantly ($P > 0.05$), to the two ambr systems (41.63 ± 1.70 in the ambr® 15 and 40.27 ± 5.36 in the ambr® 250). It can be hypothesised that the higher doubling time at 1 L scale was mainly due to

the depletion of glucose and glutamine between day 2 and 3 (discussed later in Section 5.3.3). This was reflected in a higher, although not statistically significant ($P > 0.05$), doubling time on day 3 (138.72 ± 130.10 h in the 1 L UniVessel® compared to 71.65 ± 34.70 h and 72.01 ± 56.38 h in the ambr® 15 and ambr® 250, respectively) for primary T-cells in the UniVessel® (Figure 5.7c). Higher doubling times across all platforms can be noted on day 7 as well, which overlaps with the depletion of glucose in the medium (discussed later in Section 5.3.3), suggesting the lack of nutrients had a negative impact on T-cell growth.

The cumulative population doubling shows the total number of times the cells have doubled in culture from day 0 to day 7 (Figure 5.7d). The slower growth between days 2-4 in the 1 L UniVessel® was reflected in the cumulative population doublings, showing a decrease in the plotted slope between the data points at day 2 and 3, and day 3 and 4. Nevertheless, the final cumulative population doublings were comparable between the tested vessels resulting in 10.41 ± 0.24, 10.12 ± 0.28, and 10.11 ± 0.50 cumulative population doublings for the ambr® 15, ambr® 250, and 1 L UniVessel® respectively.

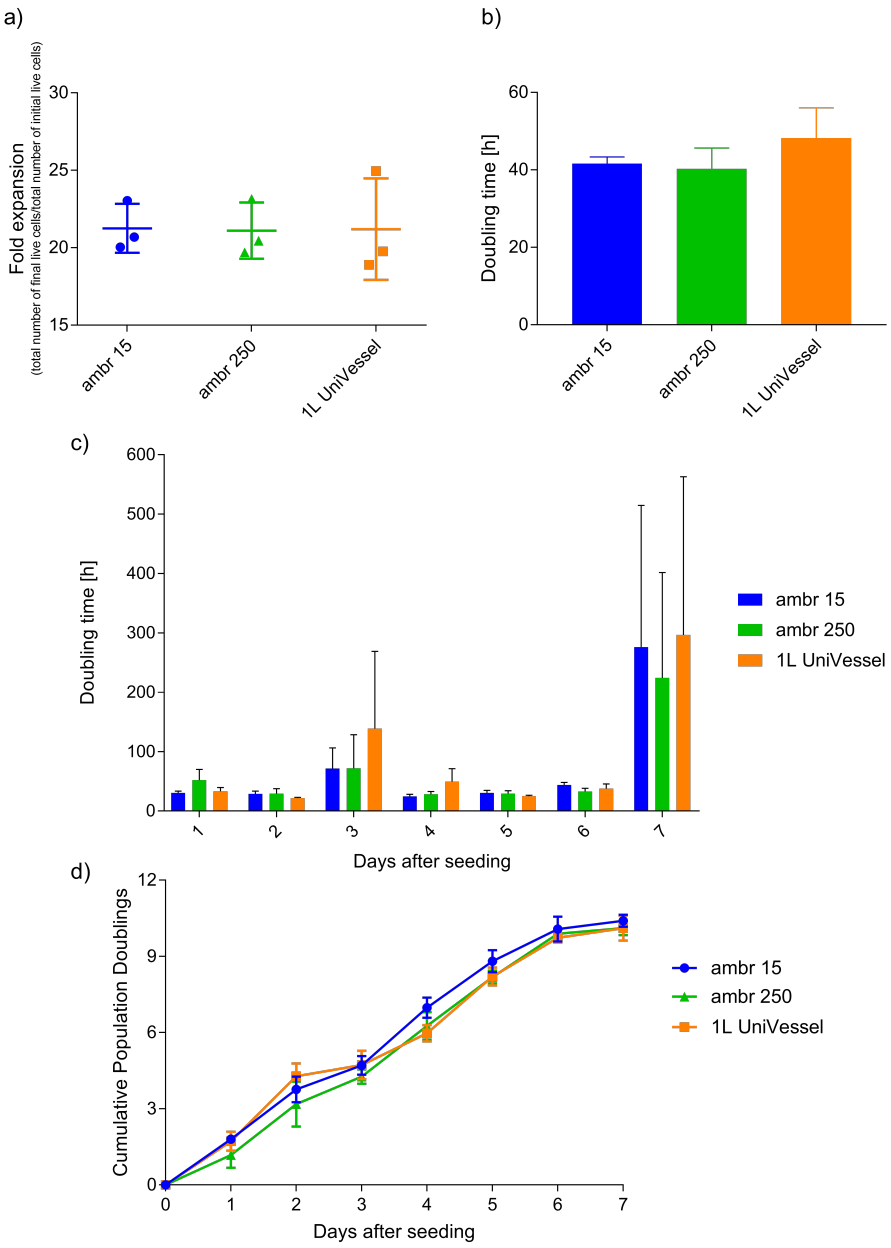

Figure 5.7: The growth kinetics for T-cells grown in the ambr® 15, ambr® 250 and UniVessel® stirred-tank bioreactors. Data show as mean ± SD, n = 3. No significant difference ($P > 0.05$) was detected between the tested conditions using a one-way ANOVA test. (a) Fold expansion. (b) Doubling time [h] calculated from day 2 to day 7. (c) Doubling time [h] shown day by day. (d) Cumulative population doublings.

All the analysed culture parameters demonstrated that the three stirred-tank bioreactors across different scales yielded comparable results over 7 days of culture. The scalability was therefore confirmed in terms of growth kinetics and final cell densities. Due to a lack of literature reporting T-cell growth in stirred-tank bioreactors, it was difficult to compare these results with existing work, mainly due to different platforms and feeding strategies used. However, the fold expansion and growth kinetics parameters were in line with results on T-cells grown in stirred-tank bioreactors presented in this thesis in Chapter 3 (Costariol et al., 2019).

5.3.3 Metabolite concentrations across different scales

The metabolites concentration for each run and platform were taken off-line on a daily basis during 7 days of bioreactor culture. Glucose, lactate, glutamine, and ammonia were monitored throughout the experiment (Figure 5.8). All the metabolites showed a consistent trend across the different stirred-tank bioreactors and across the three donors tested. Furthermore, the metabolite profiles correlated well with the respective growth curves, where increased cell concentration showed a higher amount of lactate and ammonia in the medium and a concomitant lower concentration of glucose and glutamine.

Activated T-cells undergo a metabolic switch from a catabolic metabolism to an anabolic one increasing the glucose uptake for faster proliferation (Windt et al., 2012). The glucose concentration in the culture medium decreased rapidly during the culture

and resulted completely depleted in the ambr® 15 and in the 1 L UniVessel® by day 2 (Figure 5.8a). The measured concentration of glucose in the ambr® 250 at day 2 was also very low, resulting in 0.75 ± 1.23 mmol l^{-1} and reached 0 mmol l^{-1} by day 3. This correlated with the decreased proliferation rate and increased doubling time in the UniVessel® and it indicated that the slower growth could be attributed to the lack of nutrients. In the ambr® 15 vessel the growth rate seemed less affected from the lack of glucose between day 2 and 3 (Figure 5.6), although the doubling time showed an increase on day 3 in both ambr® systems (Figure 5.7c). The spikes in the glucose concentration on days 3, 4, and 5 indicate a medium addition or exchange, replenishing the levels of metabolites in the medium. Once glucose run out on day 6, there were no further medium addition nor exchanges, meaning that the cells did not have any glucose in the last 24 hours of culture. This was reflected in a decreased proliferation rate (Figure 5.6) and in higher doubling times on day 7 (Figure 5.7c). In literature, T-cells showed a high consumption of glucose and complete depletion of the nutrient even when the feeding strategy was switched to a semi-perfusion mode (A. Amini et al., 2020). However, improvement of the feeding strategy or a switch to a medium with higher glucose content (e.g., X-Vivo™ 10) should prevent glucose from becoming a limiting factor in the culture and help to investigate whether the final cell number could have been further improved.

The lactate concentrations across the three stirred-tank bioreactors displayed similar

trends (Figure 5.8b), with peaks on day 3, 4, 5, and 6, the same days on which the glucose in the medium resulted completely depleted. Lactate profiles showed a strong correlation with the T-cell viable concentrations, as expected (Grist et al., 2018). The highest level of lactate was reached in the 1 L UniVessel® on day 3 (20.82 ± 0.67 mmol l^{-1}). Once the glucose was completely depleted on day 6, the level of lactate in the medium did not increase in any of the vessels. It is known that proliferating T-cells only divert pyruvate into lactate when the energy requirements are met, therefore it was not surprising that once the glucose has been completely depleted from the medium, the level of lactate did not increase (Maciolek et al., 2014). The final lactate concentrations in the medium were 17.32 ± 0.49 mmol l^{-1} in the ambr® 15, 17.48 ± 0.31 mmol l^{-1} in the ambr® 250, and 19.04 ± 0.68 mmol l^{-1} in the 1 L UniVessel®. In all the cases the final concentration of lactate in the medium was lower than the 20 mmol l^{-1} reported by Fischer et al. (2007) and believed to have a major impact on T-cell proliferation when cells were exposed to it for 24 hours. Grist et al. (2018) report lactate levels of $\sim$ 15 mmol l^{-1} in T-cells culture with no remarks to cell death. Therefore, it can be hypothesised that lactate levels did not have a major impact on T-cell proliferation and viability. The 20 mmol l^{-1} limit was reached only in the 1 L UniVessel® on day 3, however the cells were exposed to it for less than 24 hours (Figure 5.8b).

Glutamine concentrations for the three expansion vessels (ambr® 15, ambr® 250, and 1 L UniVessel®) are shown in Figure 5.8c. The level of glutamine rapidly decreased

during the culture resulting in $\sim$ 0.5 on day 2 and run out in all the platforms by day 3. The glutamine was replenished with the medium additions on day 3, 4 and 5 and completely consumed by the T-cells by day 6. There was no glutamine present in the medium in the last day of culture. The lack of glutamine is known to have an inhibitory impact on T-cell growth, explaining the lower growth rate of the T-cells on the last day of culture (Maciolek et al., 2014).

The ammonia levels in the medium are shown in Figure 5.8d. This metabolite is correlated with the consumption of glutamine and conversion of it into glutamate and α -keto-glutamate (Hanga et al., 2017). The trend seen in ammonia levels was consistent between the three scales of stirred-tank bioreactors used. The ammonia produced by the T-cells was diluted with the addition of new medium on days 3, 4 and 5, reaching a peak before the medium addition on day 3 and on the last day of culture (day 7). The highest level of ammonia in the medium for the ambr® 15 was detected on day 7 (2.13 $\pm$ 0.10 mmol l^{-1}). For the ambr® 250 the peak in ammonia concentration was reached on the last day of culture (1.95 $\pm$ 0.10 mmol l^{-1}), while for the 1 L scale UniVessel® the maximum concentration was detected on day 3 (2.13 $\pm$ 0.02 mmol l^{-1}). No work has been found in the literature on the effect of ammonia concentration in the medium which inhibits T-cell growth. However, Schop et al., 2009 report that ammonia concentrations below 3 mmol l^{-1} do not have an impact on the growth of mesenchymal stem cells. Therefore, the slower proliferation on the last day of culture can be primarily attributed

to the depletion of glucose and glutamine, rather than to the accumulation of ammonia in the medium. The depletion of glucose and glutamine together with a high levels of lactate and ammonia are not optimal for T-cell growth, however medium and feeding optimisation were beyond the scope of this work.

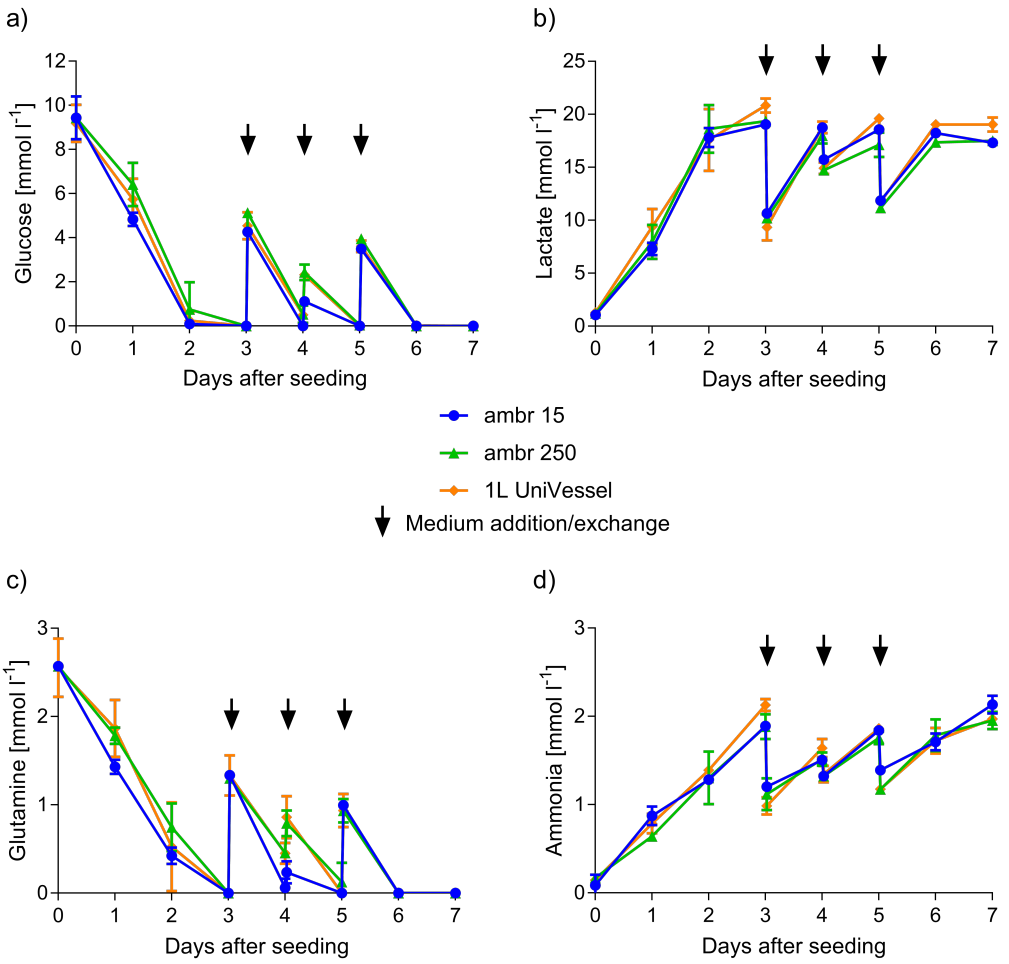

Figure 5.8: Metabolite concentration profiles in the ambr® 15, ambr® 250 and 1 L UniVessel®. The black arrows indicate a medium addition/exchange. Data show as mean ± SD, n = 3. (a) Glucose concentration [mmol l^{-1}]. (b) Lactate concentration [mmol l^{-1}]. (c) Glutamine concentration [mmol l^{-1}]. (d) Ammonia concentration [mmol l^{-1}].

5.3.3.1 Specific metabolite production and consumption rates

Glucose consumption, lactate production and lactate yield from glucose were calculated for each bioreactor from day 2-7 and on a daily basis (Figure 5.9).

The glucose consumption was significantly higher ($P < 0.05$) for the cells grown in the ambr® 250 (1.17 $\pm$ 0.23 pmol cell^{-1} day^{-1}) compared to the smaller scale ambr® 15 (0.68 $\pm$ 0.08 pmol cell^{-1} day^{-1}) (Figure 5.9a). None of the bioreactors showed significantly different values ($P > 0.05$) compared to the 1 L UniVessel® (0.95 $\pm$ 0.05 pmol cell^{-1} day^{-1}). The glucose consumption measured on a daily basis showed a high consumption (above 4 pmol cell^{-1} day^{-1}) in the first two days of culture. The low consumption rates seen on day 3 and 7 reflected the depletion of glucose in the medium. On day 4 and day 5 the glucose consumption rate in the ambr® 15 was significantly lower ($P < 0.05$) compared to the larger scale bioreactors. This reflected the fact that the concentration of glucose in the ambr® 15 was lower compared to the ambr® 250 and 1 L UniVessel® (Figure 5.8a) and explained why the glucose consumption from day 2 to day 7 in the ambr® 15 resulted lower. It also confirmed the hypothesis that the glucose in the ambr® 15 was depleted earlier than in the larger vessels.

The lactate production rate resulted significantly lower ($P < 0.05$) in the ambr® 15 (1.32 $\pm$ 0.24 pmol cell^{-1} day^{-1}) compared to the 1 L UniVessel® (2.13 $\pm$ 0.33 pmol cell^{-1} day^{-1}) (Figure 5.9b). The lower production of lactate in the ambr® 15 correlated with the lower specific glucose consumption rate discussed previously. However, this

was not the case for the 1 L stirred-tank bioreactor, where a higher lactate production rate hinted to a more inefficient glucose consumption. When looking at the lactate production rate on a daily basis (Figure 5.9d), it can be noted how the production rate in the ambr® 15 was significantly lower ($P < 0.05$) compared to the 1 L UniVessel® on days 4 and 5. These are the same days when the consumption of glucose was lower, due to a lower concentration of glucose present in the medium, showing the correlation between glucose consumption and lactate production. The lactate production rate on day 7 showed negative results in the ambr® 15, implying that the lactate was being consumed by the T-cells. However, the value was so close to 0 (-0.19 $\pm$ 0.02 pmol cell^{-1} day^{-1}), that this was probably due to measurement inaccuracy.

In order to asses the efficiency of the T-cells to metabolise glucose into energy, the yield of lactate from glucose was calculated (Figure 5.9e,f). The oxidative phosphorilation (OXPHOS) metabolic pathway yields 30-38 ATP per mole of glucose consumed and it is the most efficient way for energy production (Hanga et al., 2017). On the other hand, aerobic glycolysis, also known as 'The Warburg Effect', produces only 2 molecules of ATP and yields 2 moles of lactate every mole of glucose consumed (Warburg, 1956). Despite the aerobic glycolysis being less efficient, it provides important metabolic intermediates for cell growth and proliferation (Buck et al., 2015). The calculated yield of lactate from glucose for the ambr® 15 and 1 L UniVessel® were ~ 2, which suggested that the cells were consuming glucose via the less efficient anaerobic

glycolisis pathway. In the ambr® 250 vessel the lactate yield from glucose was significantly lower ($P < 0.05$) compared to the 1 L UniVessel®, resulting in 1.4 ± 0.12 and 2.25 ± 0.33 respectively. The higher level of anaerobic glycolysis detected in the larger vessel could be due to the higher number of T effector memory type, as they process glucose preferentially through glycolysis (Bantug et al., 2018). It is known that activated and actively proliferating cells undergo metabolic reprogramming, and switch to aerobic glycolisis (Maciolek et al., 2014; Buck et al., 2015).

The day by day lactate yield from glucose (Figure 5.9f) showed higher values on day 3, in particular for the ambr® 250 vessel (4.58 ± 6.65), indicating an inefficient way of glucose consumption. This could be due to the complete depletion of glucose in the medium. Day 7 values were 0, due to the lack of glucose in the medium.

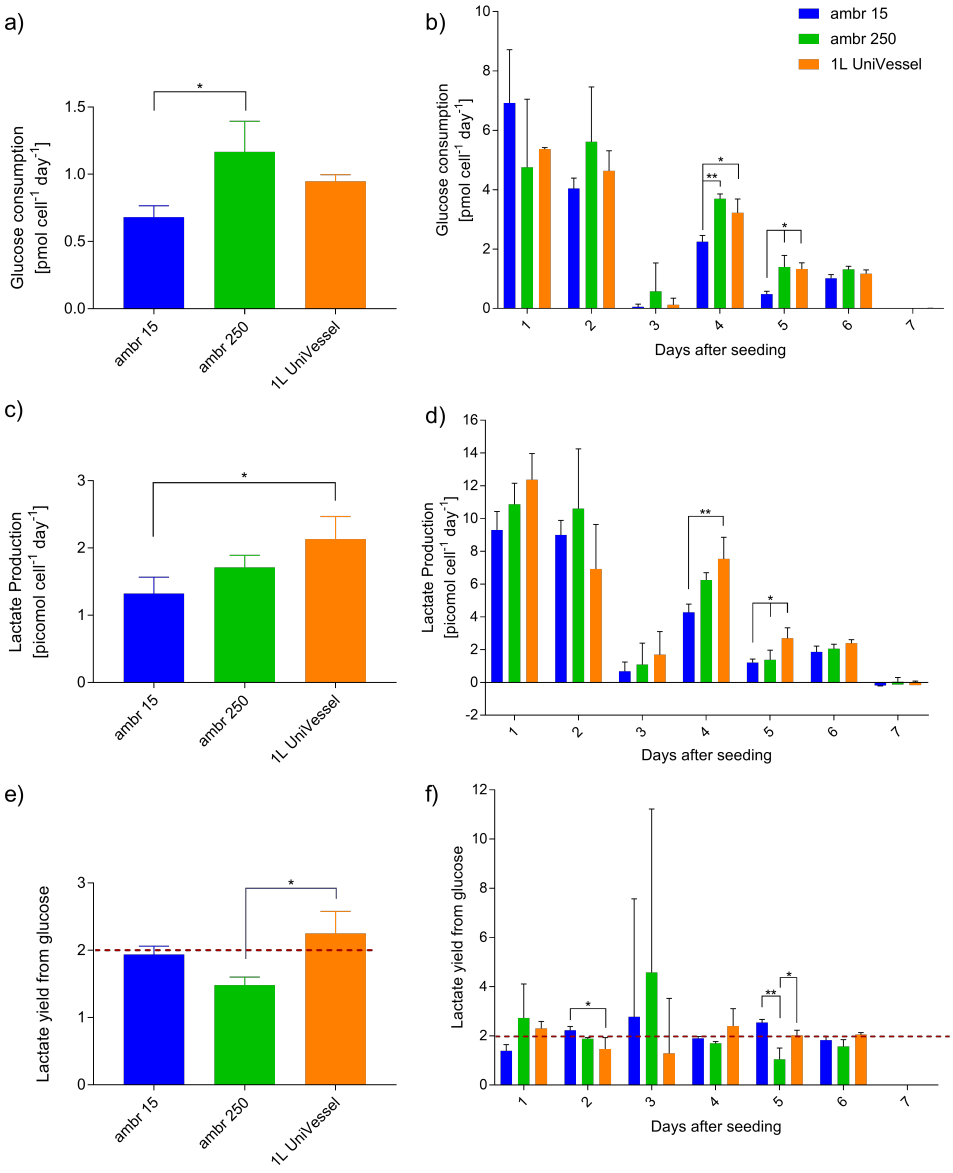

Figure 5.9: Specific consumption/production rates calculated from day 2 to day 7 and on a daily basis in the ambr® 15, ambr® 250 and 1 L UniVessel®. A one way ANOVA test was performed. Statistical significance is shown when probability (P) values were equal or below 0.05 (*), 0.01(**), 0.001(***), or 0.0001 (****). Data shown as mean ± SD (n=3). (a) Glucose consumption rate [pmol cell^{-1} day^{-1}] day 2-7. (b) Glucose consumption rate [pmol cell^{-1} day^{-1}] on a daily basis. (c) Lactate production rate [pmol cell^{-1} day^{-1}] day 2-7. (d) Lactate production rate [pmol cell^{-1} day^{-1}] on a daily basis. (e) Lactate yield from glucose day 2-7. The reference line at 2 is the maximum theoretical yield of lactate from glucose. (f) Lactate yield from glucose on a daily basis. The reference line at 2 is the maximum theoretical yield of lactate from glucose.

The specific glutamine consumption and ammonia production rates are shown in Figure 5.10. Glutamine is used by proliferating T-cells in conjunction with glucose as an energy source (Carr et al., 2010). There was no significant difference ($P > 0.05$) between the glutamine consumption rates calculated form day 2 to day 7 at the three different scales (Figure 5.10a). The values were 0.22 ± 0.01 pmol cell^{-1} day^{-1}, 0.29 ± 0.06 pmol cell^{-1} day^{-1}, and 0.27 ± 0.06 pmol cell^{-1} day^{-1} for the ambr® 15, 250 and 1 L UniVessel® respectively. The day by day glutamine consumption rate showed a higher consumption during the first two days, when the glutamine concentration in the medium was higher (Figure 5.8c). Lower glutamine consumption was seen on days 3-6, when the metabolite was completely depleted in the medium. No glutamine consumption was detected on day 7, due to the lack of glutamine in the medium in all the platforms.

The main source for ammonia build up is the amino acids metabolism, mainly glutamine, in proliferating cells. High levels of ammonia (higher than 3 mmol l^{-1}) in the medium are believed to be inhibitory for mammalian cell growth (M. Schneider et al., 1996). The ammonia production rate did not show significant difference ($P > 0.05$) between the three scales of stirred-tank bioreactors used in this study. The production rate was 0.16 ± 0.023 pmol cell^{-1} day^{-1} in the ambr® 15, 0.20 ± 0.02 pmol cell^{-1} day^{-1} in the ambr® 250, and 0.21 ± 0.01 pmol cell^{-1} day^{-1} in the 1 L UniVessel®. The day by day analysis of the ammonia production showed a significantly lower ($P < 0.05$) production rate in the ambr® 15 compared to the larger scale bioreactors. Similarly, on day 4, the

ammonia production rate was significantly lower ($P < 0.05$) in the ambr® 15 compared to the 1 L UniVessel®. There was ammonia production detected on day 7, suggesting that the T-cells were still breaking down amino acids other than glutamine, which was completely depleted, producing ammonia (M. Schneider et al., 1996).

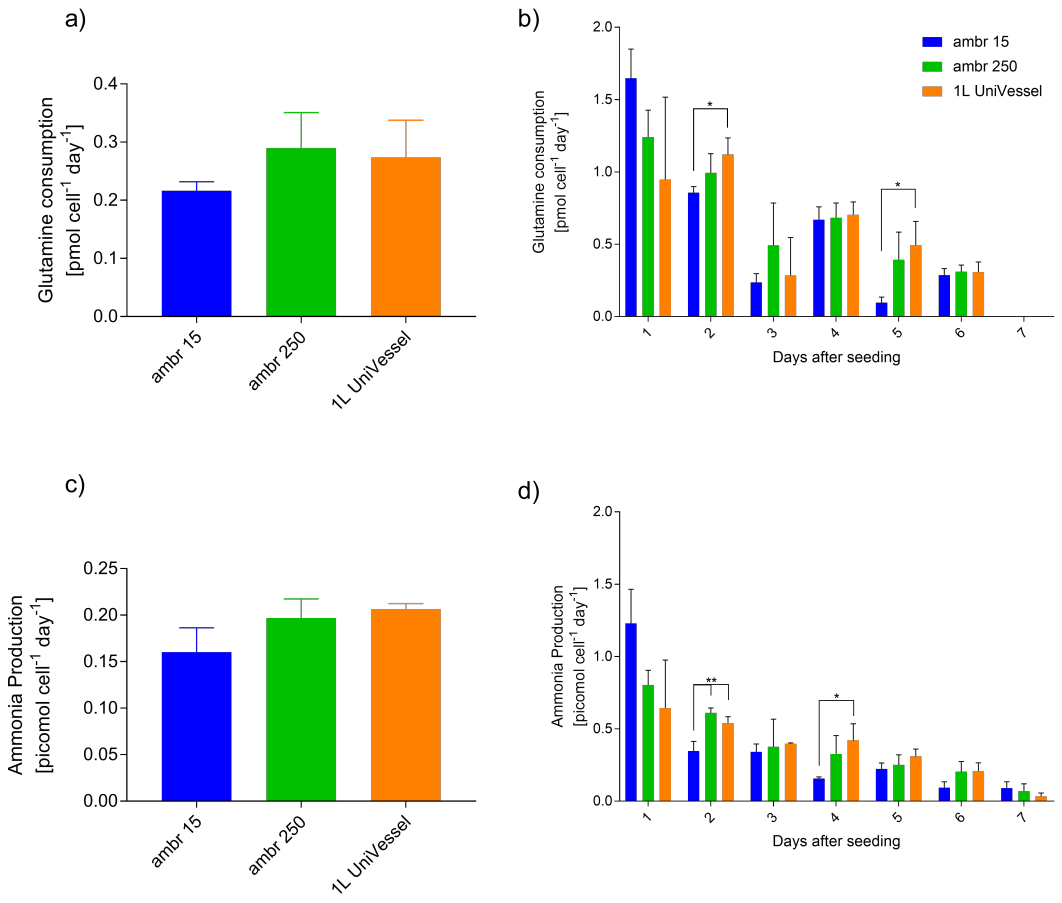

Figure 5.10: Specific consumption/production rates calculated from day 2 to day 7 and on a daily basis in the ambr® 15, ambr® 250 and 1 L UniVessel®. A one way ANOVA test was performed. Statistical significance is shown when probability (P) values were equal or below 0.05 (*), 0.01(**), 0.001(***), or 0.0001 (****). Data shown as mean ± SD (n=3). (a) Glutamine consumption rate [pmol cell^{-1} day^{-1}] day 2-7. (b) Glutamine consumption rate [pmol cell^{-1} day^{-1}] on a daily basis. (c) Ammonia production rate [pmol cell^{-1} day^{-1}] day 2-7. (d) Ammonia production rate [pmol cell^{-1} day^{-1}] on a daily basis.

5.3.4 Cell quality across different scales

Cell quality is of primary importance in CAR-T therapies, therefore the immunophenotype of the T-cells was assessed at the beginning and after the expansion in the three stirred-tank bioreactors (Figure 5.11 & 5.12). CD3 positive T-cells were first analysed in terms of CD4 and CD8 expressing cells percentage. The $CD8^+$ T-cell subpopulation was then analysed in terms of naïve, central memory, effector memory, and terminally differentiated T-cells.

The percentage of $CD4^+$ expressing T-cells at seeding was slightly higher (73 ± 5.63 %) to all the postharvest conditions (Figure 5.11a). One of the donors (HD9) used in this experiment showed a low amount of CD4 positive cells after 7 days expansion in the ambr® 15 (32.2 %) and ambr® 250 (24.3 %). However, this did not occur in the larger 1 L UniVessel® stirred-tank bioreactor, which could be linked to a higher tip speed in this particular bioreactor. The $CD8^+$ population of T-cells was higher for that specific donor (HD9) in the ambr® 15 (60.5 %) and ambr® 250 (61.5 %) (Figure 5.11b). This resulted in a low CD4:CD8 ratio for that particular donor (HD9) in the two smaller scale stirred-tank bioreactors (Figure 5.11c). Donor to donor variability in the CD4:CD8 ratio has been reported in literature before (A. Amini et al., 2020).

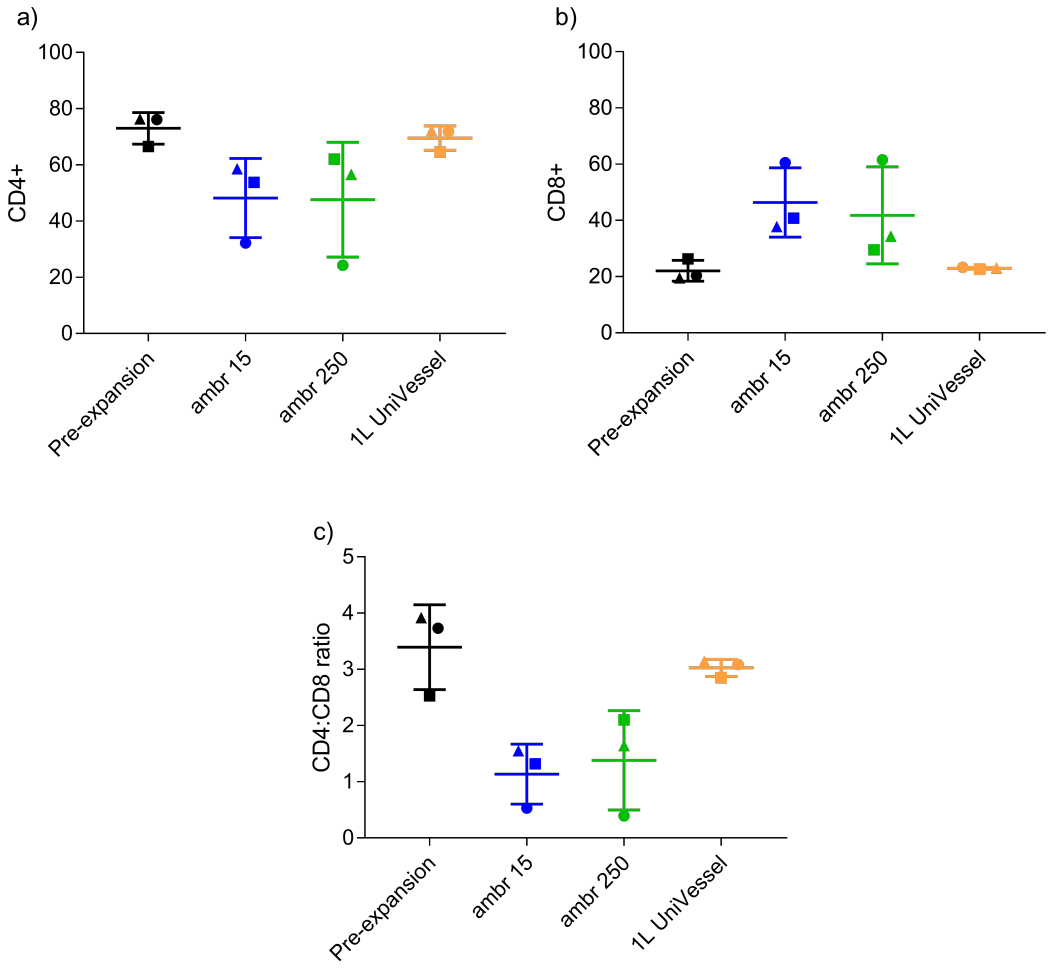

Figure 5.11: Phenotypic characterisation of primary T-cells in terms of CD4 and CD8 postive cells when seeded in the bioreactor (pre-expansion - black) and postharvest in the ambr® 15, ambr® 250 and 1 L UniVessel®. A one way ANOVA test was performed and no statistical significance ($P > 0.05$) was detected. Data shown as mean $\pm$ SD (n=3). Different donors are represented with different shapes (HD9 - circle, HD12 - square, HD17 - triangle). (a) $CD4^+$ subpopulation percentage of the cells. (b) $CD8^+$ subpopulation percentage of the cells. (c) CD4:CD8 ratio.

It can be noted how the CD4:CD8 ratio postharvest in the ambr® 15 and 250 results closer to 1 compared to the pre-expansion one. However the CD4:CD8 ratio in the 1 L UniVessel® remains $\sim$3. It has been suggested, in literature, that a CD4:CD8 ratio

closer to 1 is desirable in the final product (Turtle et al., 2016). Different parameters may have an impact on T-cell growth and final product composition and it is therefore hard to identify which one played a critical role in this experiment. However, the larger scale bioreactor did not promote the lowering of the CD4:CD8 ratio, although to fully understand the reason behind this further studies would need to be undertaken. This is mainly due to the low percentage of CD8 positive T-cells, which did not increase during the expansion step (Figure 5.11b). It can be noted that the 1 L UniVessel® showed the highest consistency in the phenotype between the three donors (Figure 5.11). The coefficient of variation in the 1 L UniVessel® was 6.27% for CD4, 1.53% for the CD8, and 1.53% for the CD4:CD8 ratio.

The percentage of T central memory and T effector memory cells are shown in Figure 5.12. The naïve and terminally differentiated T-cells were also analysed (data not shown), and their percentage was lower than 5% for all the samples. Less differentiated T-cells phenotypes, such as naïve and central memory T-cells are desirable for a higher *in vivo* persistence once reinfused into the patient (Sommermeyer et al., 2016). Figure 5.12a shows the percentage of central memory T-cells. As discussed previously in Chapter 3, the expanded cells showed a lower percentage of T central memory cells when compared to the pre-expansion samples. This can be explained by a long expansion protocol (14 days), the use of IL-2 in the medium, and a double activation using Dynabeads® (Costariol et al., 2019; Crompton et al., 2014).

In the pre-expansion sample 46.1 $\pm$ 10.55 % of the T-cells had a central memory phenotype (CCR7$^+$ CD45RO$^+$). The percentage dropped to 34.33 $\pm$ 6.12 % in the ambr® 15, 27.1 $\pm$ 10.23 % in the ambr® 250, and 18.47 $\pm$ 9.41 % in the 1 L UniVessel®. The largest vessel resulted in the lower, although not significantly ($P > 0.05$), percentage of T memory cells. Further studies with a higher number of donors would need to be undertaken in order to understand whether the larger volume could have an impact on the differentiation of T-cells.

Figure 5.12b shows the percentage of CD8$^+$ T effector memory subpopulation. There was no significant difference ($P > 0.05$) between the three vessels tested. The percentages were 64.5 $\pm$ 6.19 % in the ambr® 15, 70.23 $\pm$ 9.58 % in the ambr® 250, and 68.97 $\pm$ 10.08 % in the 1 L UniVessel®. It can be noted how the HD12 donor (represented with a square) tended to have the lower number of effector memory across the tested samples, however this trend was found to be inverted in the 1 L UniVessel®, with the HD12 donor having the higher number of effector memory cells. As mentioned above, the higher level of anaerobic glycolysis could be due to a higher percentage of T effector memory cells in the 1 L UniVessel®. Furthermore, the higher impeller tip speed and higher shear stress could have an impact on the T-cell differentiation. However, this was not the case on day 7, but a day by day immunophenotypic characterisation would have helped to understand this phenomena better.

The higher number of effector memory cells after the 7 days expansion in the stirred-

tank bioreactors was to be expected. It is a challenge to keep T-cell in their less differentiated phenotype, furthermore the prolonged expansion (14 days), activation and IL-2 supplement were not ideal to keep the cells in a less differentiate state.

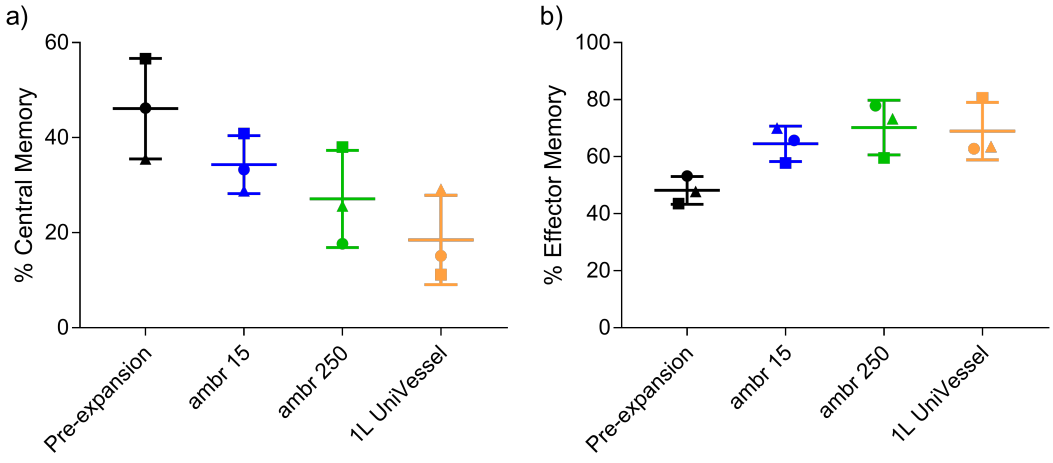

Figure 5.12: Phenotypic characterisation of primary T-cells when seeded in the bioreactor (pre-expansion - black) and postharvest in the ambr® 15, ambr® 250 and 1 L UniVessel®. A one way ANOVA test was performed and no statistical significance ($P > 0.05$) was detected. Data shown as mean $\pm$ SD (n=3). Different donors are represented with different shapes (HD9 - circle, HD12 - square, HD17 - triangle). (a) $CD8^+$ T central memory ($CCR7^+$ $CD45RO^+$) subpopulation percentage of the cells. (b) $CD8^+$ T effector memory ($CCR7^-$ $CD45RO^+$) subpopulation percentage of the cells.

5.4 The importance of scale-down models

This study highlighted the reproducibility in terms of T-cells growth between different scales (15 ml, 250 ml and 1 L) in stirred-tank bioreactors. This allows for the process development to be undertaken at smaller scales, which brings numerous advantages. Firstly, the raw materials needed are significantly reduced when running processes at a

few milliliters. The ambr® 15 stirred-tank bioreactor has a starting volume of 10 ml and allows for 48 bioreactors to be run in parallel, which makes it an optimal candidate for screening studies that would take several months at larger scales, reducing the time for the products to reach to clinical trials. Secondly, the cost of goods would be reduced due to the lower amount of starting material needed. This includes medium and medium supplements which can be highly expensive, especially in GMP settings. Finally, this system operates with an automatic liquid handler, reducing the operators interactions to the minimum and providing the possibility to interlink the bioreactor with other technologies. This would help to automate the whole process and reduce the variability introduced by human operators.

The ambr® 15 high-throughput bioreactor is one of the few small-scale bioreactors equipped with pH and dO_2 sensors and with an impeller. It also allows to control these two parameters, along with temperature, independently for each of the 48 bioreactors. Most of the other scale-down models are shaken chambers (i.e., micro-Matrix manufactured by Applikon® Biotechnology), or do not allow for the screening of culture parameters (i.e. shake flasks, static well plates) (Rameez et al., 2014). This makes the comparability between different scales extremely hard and it is unlikely that a process established in such small-scale vessels, can be easily translated to larger scales.

The ambr® 15 stirred-tank bioreactor has already been used for different mammalian cells (i.e., primary T-cells, CHO, and hMSCs), proving itself suitable for var-

ious processes (Klarer et al., 2018; Alvin W Nienow et al., 2016; Q. A. Rafiq et al., 2016a), however prior to this study no data on T-cells growth at different scales were reported (Rameez et al., 2014). Studies where the ambr® 15 has been compared with larger stirred-tank bioreactors (not manufactured from Sartorius Stedim Biotech) for the growth of CHO cells to produce mAbs have been reported. They proved a good comparability in terms of cell growth, titer and product quality, based on tip speed comparison, with 2-7 L stirred-tank bioreactors (Hsu et al., 2012; Moses et al., 2012).

Similar results were obtained with primary T-cells in the work presented in this chapter, where the comparability in terms of growth and product quality was good across different scales. It is therefore possible to high-throughput screening at smaller scale and scale-up the optimised process to a larger scale stirred-tank bioreactor, obtaining reproducible results.

5.5 Stirred-tank bioreactors for allogeneic CAR-T therapies

This chapter proves that human primary T-cells can be grown up to 1 L scale in stirred-tank bioreactors. This becomes particularly relevant for allogeneic CAR-T therapies, which are becoming increasingly popular (Depil et al., 2020). Allogeneic therapies aim to reduce the cost of the manufacturing process, being able to produce multiple

batches per run. Furthermore, having an available 'off-the-shelf' product will allow to promptly administer the therapy to the patient, without having to wait for the extended manufacturing time.

Although one autologous dose can be produced in the ambr® 250 stirred-tank bioreactor, this bioreactor is not suitable for GMP use. The volume of the ambr® 250 is comparable to the CliniMACS Prodigy® system, which is currently used for CAR-T therapies production in different clinical trials (Autolus Therapeutics plc, 2018). However, the Prodigy® system does not allow for scale-up, but was only designed to scale-out the process by running multiple systems in parallel, which is not ideal in an allogeneic setting. For allogeneic purposes the number of bioreactors could be significantly decreased, while increasing the volume and batch numbers produced for each bioreactor, resulting in a smaller footprint in the expensive clean room space.

In order to have a cost effective process for the development and manufacture of allogeneic CAR-T therapies, scalable and robust expansion platforms are required. Although it is not yet clear at which scale these therapies could be produced, using scalable stirred-tank bioreactors will allow for an easy increase in scale with reproducible results, where needed as demonstrated in this results chapter. It is unlikely that the volumes needed will reach the ones currently used in mAbs production (2000 L), due to the nature of primary cells, which have a limited life-span and proliferation capability. However, processes are likely to be run at 1-10 L scales. This is the range of volumes

at which rocking-motion bioreactors are currently operated. However, rocking-motion bioreactors require a large starting volume, for which a pre-expansion in static culture flasks is necessary. Furthermore the process in the bags is not easy to scale-up (Eibl et al., 2009; Hanson et al., 2009).

Primary T-cells have been grown to high densities in rocking motion bioreactors using a perfusion based feeding strategy to continuously supplement nutrients to the cells and remove the waste products from the medium. The continuous perfusion feeding strategy, combined with up to 500 U ml^{-1} IL-2, enabled to reach a cell density of 31 x 10^6 cells ml^{-1}. The CAR-T cells showed *in-vitro* and *in-vivo* cytotoxicity against Raji-19 cell line expressing CD19 (Hollyman et al., 2009). Another study reports T-cells densities up to 10^7 cells ml^{-1} (Xiuyan Wang et al., 2016). However little comments were made on the phenotypic profile of the T-cells. Growing T-cells to such a high density requires a constant supply of glucose, achieved throughout continuous perfusion, furthermore the gas exchange needs to satisfy the cells oxygen demand. For this reason, headspace aeration might not be sufficient at larger scales and high cell densities (Hollyman et al., 2009). Furthermore, prolonged culture times, high IL-2 levels, and insufficient nutrients in high density cultures, might have an impact on the CAR-T cell potency and functionality. High cell densities in an allogeneic setting would allow for more doses to be produced simultaneously. However, the immunophenotypic profile and the potential exhaustion of the CAR-T cells due to the lack of nutrients, oxygen,

and extended proliferation time need to be kept in consideration. It is known that less differentiated T-cell subset (i.e. naïve and central memory T-cells) persist longer *in-vivo* after infusion (S. Rafiq et al., 2020).

An ideal expansion vessel would have a low starting volume and allow for all the manufacturing steps to occur without user interaction needed. The CliniMACS Prodigy® is the only fully closed system currently available on the market. However, having an all-in-one system reduces the flexibility of the manufacturing process and presents supply chain risks, relying on a single supplier for the whole process. Therefore, different closed systems that can be interlinked, might be a good solution for an increased flexibility and assurance of supply. Stirred-tank bioreactors are a good candidate for the expansion step and can easily be connected with other systems via sterile tube welding. They also allow for a flexible feeding strategy that can go from batch to perfusion mode, depending on the cell demand for nutrients. The monitoring of critical culture parameters, such as pH, temperature, and dO_2 is also important for a successful CAR-T therapy production. The work presented in this thesis demonstrates the potential of stirred-tank bioreactors in terms of T-cells expansion. The high comparability across different scales using primary T-cells shows great hope for the manufacture and process development of CAR-T therapies.

5.6 Conclusions

The initial screening in the ambr® 15 confirmed the hypothesis formulated in the previous chapters suggesting that low speeds (300 rpm in the ambr® 15) and low specific power inputs (28 x 10^{-4} W kg^{-1}) do not allow for a good suspension of Dynabeads®. This has a negative impact on T-cell proliferation due to a limited bead-to-cell interaction and activation. Amongst the screened conditions, the one cultured at 50% dO_2 showed a good growth with a better postharvest phenotype compared to the 25% dO_2 condition. This is why the 50% dO_2 was kept across different bioreactors to scale-up the expansion process.

The scale-up study between the ambr® 15, ambr® 250, and 1 L UniVessel® proved high consistency between the systems in terms of T-cell growth. The metabolite data was also highly reproducible across the tested scales (15 ml, 250 ml, and 1 L). However, nutrients depletion could be limiting the expansion of T-cells. The feeding strategy would need to be further improved, or a different medium with a higher content of glucose could be tested in further studies. There were no major differences in terms of metabolite consumption/production rates across different scales, suggesting that larger volumes and different geometries do not have a significant impact on the T-cell metabolism.

The immunophenotype analysis did not show significant differences ($P > 0.05$) in terms of final product composition. However, the 1 L UniVessel® displayed a more dif-

ferentiated phenotype, although not significantly different ($P > 0.05$), at the end of the culture. More replicates with different donors across the three platforms would provide a better insight to whether the vessel has a significant impact on T-cell differentiation.

In conclusion, the ambr® 15 bioreactors was a good scale-down model and can be used for high-throughput screening of different process parameters. The final cell yield and growth kinetics were comparable across the different scales tested, proving that the expansion process can be scaled-up to 1 L stirred-tank bioreactors based on the specific power input.

Chapter 6

Conclusions and Future Work

6.1 Conclusions

The increased number of FDA approved CAR-T products and ongoing clinical trials highlight the growing interest in the CGT field (Panagopoulou et al., 2019; Vormittag et al., 2018). Despite the significant clinical results and the possibility to treat previously incurable diseases, the manufacturing process for CAR-T cell therapies still needs improvement. Thus far the demand and doses produced have been limited, but with an increasing amount of products reaching the market, the number of requested doses will rapidly increase and the current manufacturing process is not designed to fulfil such needs. Current products are mainly manufactured in static vessels or rocking motion bioreactors, which have limited scaling-up capabilities (Vormittag et al., 2018). Static

vessels hardly allow for online monitoring of the critical culture parameters (e.g. pH, dO_2), while other systems, such as the CliniMACS Prodigy® have been designed to scale-out the process using multiple systems at once, rather than scaling-up the process, which will be an essential requirement for allogeneic therapies (Depil et al., 2020).

The main purpose of this doctoral thesis was to demonstrate that the expansion of primary CAR-T cells in stirred-tank bioreactors at different scales is possible. This will allow for a robust and standardised manufacturing process and a faster and more efficient development of CAR-T therapies towards commercialisation. Furthermore, stirred-tank bioreactors could be interlinked with different systems, which would make the whole manufacturing process automated, allowing for higher flexibility on the consumables used.

In order to achieve the final goal, the work was broken down into different aims, which were successfully addressed and culminated in an expansion process for CAR-T therapies in stirred-tank bioreactors. Furthermore, it was proven that the process is scalable and reproducible in a larger 1 L stirred-tank bioreactor.

Firstly, Jurkat E6.1 cell line was used to demonstrate T-cells can be grown in a stirred environment. Once this was proven successful, the work focused on primary T-cells and engineered CAR-T cells. Secondly, the growth of T-cells and CAR-T cells was compared under static and dynamic conditions. Critical culture parameters, such as stirring speed up to 500 rpm were investigated. Finally, the process was carried out at different

scales, from 15 ml to 1 L stirred-tank bioreactors, showing a high comparability across the tested scales.

The work presented in this doctoral thesis proves not only that the stirring environment improves the growth of T-cells compared to static T-flasks, but also that at higher stirring speeds (200 rpm) T-cell proliferation is improved. The hypothesis formulated was that at lower speed (100 rpm) the Dynabeads®, para-magnetic beads used to activate T-cells, were not well suspended and did not interact in an effective manner with the T-cells, leading to poor activation and proliferation. However, once the speed was high enough to suspend the Dynabeads® (i.e. 200 rpm) a further increase in the stirring speed did not lead to a better proliferation. On the other hand, it was important to prove that CAR-T cells are not as sensitive to shear stress as generally believed, but they can withstand high P/M without any consequences on their viability, proliferation and potency.

The hypothesis of poor Dynabeads® suspension at lower speeds was also seen in the high-throughput stirred-tank ambr® 15 bioreactor. At 300 rpm (corresponding to $\sim$ 100 rpm in the ambr® 250 in terms of P/M) the T-cells proliferation was lower compared to the higher speed (450 rpm) and higher P/M. This suggests that for speeds that result in a P/M equal to or lower than 74 x 10^{-4} W kg^{-1}, the Dynabeads® are not well suspended and the bead-to-cell interaction is not efficient, leading to poor proliferation.

Successfully transduced CAR-T cells were grown in an ambr® 250 bioreactor. At

the end of the expansion process, not only the CAR-T cells reached a higher cell yield compared to the static control, but they also retained their *in vitro* cytotoxic ability, which was comparable to the one displayed by cells grown in static T-flasks. It can be therefore stated that the shear stress does not have any adverse impact on the final CAR-T product potency, although further studies *in vivo* would be needed to confirm this statement.

Given the increasing importance of allogeneic CAR-T therapies, it was proven that the process performed at 250 ml, could be reproduced at larger scale (1 L UniVessel® stirred-tank bioreactor). At the same time, the importance to have a small-scale model was taken into account and an ambr® 15 high-throughput stirred-tank bioreactor was used for this scope. The scale-up study was performed based on the P/M and the selected speeds were 450 rpm in the ambr® 15, 200 rpm in the ambr® 250 and in the 1 L UniVessel® stirred-tank bioreactors. The three scales tested (15 ml, 250 ml, and 1 L) gave comparable results in terms of cell yield, phenotype, and metabolite profiles, proving that the process could be scaled-up for allogeneic CAR-T therapies and that the ambr® 15 and 250 bioreactors can be used as a process development tool in order to limit the raw materials needed and reduce the cost of goods at early development stages.

The feeding strategy was kept constant throughout the experiments, from Jurkat E6.1 cell line, to primary T-cells to CAR-T cells in order to have a better comparability and consistency across the performed experiments. However, it was not optimised, and

as discussed, the nutrients were depleted throughout the culture. This could be a factor limiting the cell expansion that needs to be taken in consideration for future studies.

Overall, this work demonstrates the suitability of stirred-tank bioreactors for the manufacturing of CAR-T cell products. As previously discussed, stirred-tank bioreactors have numerous advantages, such as online monitoring of different culture parameters, they improve the homogeneity of the culture environment and the mass transfer, they come at different scales, and they have scale-down models which are crucial for process development. Stirred-tank bioreactors are widely used in the biopharmaceutical industry and particularly suitable for larger scale production, as in the case of allogeneic CAR-T therapies.

6.2 Future work

This doctoral thesis has demonstrated that CAR-T therapies can be efficiently expanded in stirred-tank bioreactors and that the expansion process under dynamic conditions improves the final cell yield compared to static culture conditions. Stirred-tank bioreactors allow for online monitoring of culture parameters and the T-cell expansion process has proven to be scalable from 15 ml to 1 L bioreactors. Despite the results and novelty of the work presented in this doctoral thesis, different challenges still need to be addressed as identified below.

- Further **optimisation of in process parameters** such as stirring speed, dO_2, pH would be needed in order to find the optimal expansion condition not only in terms of cell yield, but also in terms of final product composition and potency.

- A **perfusion based feeding strategy** should be tested to see whether higher cell numbers could be achieved in a shorter time. Different chemically defined medium currently used in clinical trials and for the manufacture of approved CAR-T therapies should be tested in order to eliminate the variability introduced by animal products (e.g., FBS). In order to do that in an efficient manner, a design of experiments (DoE) approach should be considered and experiments carried out in an ambr® 15 bioreactor, allowing to run 48 stirred-tank bioreactors in parallel.

- Once the optimum medium and optimal process parameters are selected at a small

scale, the **process can be scaled-up** to 250 ml and 1 L stirred tank bioreactors, as demonstrated in this doctoral thesis (Chapter 5).

- The importance of suspending Dynabeads® and having them interact with the cells has been widely discussed in this thesis. However, it would be interesting to **test different commercially available activation methods** and how they behave at different stirring speeds. Furthermore, an in depth analysis of the activation markers would confirm the hypothesis formulated in this thesis, stating that lower P/M do not suspend the magnetic beads, which leads to a poor cell-to-bead interaction and an inefficient activation.

- Further **scale-up studies using engineered CAR-T cells** should be performed in order to confirm the reproducibility of the process at different scales. At the same time the pre-expansion step should be avoided, as it leads to unwanted T-cell differentiation. Starting with freshly isolated T-cells will give a better understanding of the final product composition and which parameters might have an impact on it. Once the process has been fully established, it would be ideally tested with patient material. In order for the process to be successful it would need to comply with the FDA guidelines on the release of CAR-T products, such as 70% viability.

- On the other hand, with the focus on allogeneic CAR-T therapies, further **studies at larger scale ($>$ 5 L)** should be performed. There might be an oxygen limitation using headspace aeration in larger stirred-tank bioreactors, therefore the impact of

sparging on CAR-T cell expansion should be investigated.

- In addition, **non-viral gene editing** could be tested and integrated in the expansion process, using an electroporation machine that would ideally have the possibility to interlink with stirred-tank bioreactors making it possible to have a closed process.

- Although the potency of CAR-T cells has been assessed via *in vitro* cytotoxicity assay, these results need to be confirmed *in vivo* on **animal models**. Due to the complexity and ethical concerns of this work, only CAR-T cells grown in carefully selected and optimised conditions should be tested *in vivo*.

References

Abraham, Robert T and Arthur Weiss (2004). “Jurkat T cells and development of the T-cell receptor signalling paradigm”. In: *Nature Reviews Immunology* 4.4, pp. 301–308.

Abramson, Jeremy S, Leo I Gordon, Maria Lia Palomba, Matthew Alexander Lunning, Jon E Arnason, Andres Forero-Torres, Michael Wang, David G Maloney, Alison Sehgal, Charalambos Andreadis, et al. (2018). *Updated safety and long term clinical outcomes in TRANSCEND NHL 001, pivotal trial of lisocabtagene maraleucel (JCAR017) in R/R aggressive NHL.*

Aleksandrova, Krasimira, Jana Leise, Christoph Priesner, Anette Melk, Fanni Kubaink, Hinrich Abken, Andreas Hombach, Murat Aktas, Mike Essl, Iris Bürger, et al. (2019). “Functionality and cell senescence of CD4/CD8-selected CD20 CAR T Cells manufactured using the automated CliniMACS Prodigy® Platform”. In: *Transfusion Medicine and Hemotherapy* 46.1, pp. 47–54.

Almeida, Luis, Matthias Lochner, Luciana Berod, and Tim Sparwasser (2016). “Metabolic pathways in T cell activation and lineage differentiation”. In: *Seminars in immunology*. Vol. 28. 5. Elsevier, pp. 514–524.

Amini, Arman, Vincent Wiegmann, Hamza Patel, Farlan Veraitch, and Frank Baganz (2020). “Bioprocess considerations for T cell therapy: Investigating the impact of agitation, dissolved oxygen and pH on T cell expansion and differentiation”. In: *Biotechnology and bioengineering*.

Anwer, Faiz, Al-Aman Shaukat, Umar Zahid, Muhammad Husnain, Ali McBride, Daniel Persky, Melissa Lim, Nida Hasan, and Irbaz Bin Riaz (2017). “Donor origin CAR T cells: graft versus malignancy effect without GVHD, a systematic review”. In: *Immunotherapy* 9.2, pp. 123–130.

Appay, Victor, Rene AW van Lier, Federica Sallusto, and Mario Roederer (2008). “Phenotype and function of human T lymphocyte subsets: consensus and issues”. In: *Cytometry Part A* 73.11, pp. 975–983.

Autolus Therapeutics plc (2018). “Autolus and Miltenyi Biotec sign strategic supply agreement”. In: [Online; https://autolus.gcs-web.com/node/6141/pdf; accessed 6-March-2020].

Bagley, Stephen J and Donald M O’Rourke (2020). “Clinical investigation of CAR T cells for solid tumors: lessons learned and future directions”. In: *Pharmacology & Therapeutics* 205, p. 107419.

Bajgain, Pradip, Roopa Mucharla, Usanarat Anurathapan, Natalia Lapteva, Ann M Leen, Helen E Heslop, Cliona M Rooney, and Juan F Vera (2012). *Optimizing the Manufacture of CAR-T Cells for Clinical Applications*.

Bajgain, Pradip, Roopa Mucharla, John Wilson, Dan Welch, Usanarat Anurathapan, Bitao Liang, Xiaohua Lu, Kyle Ripple, John M Centanni, Christine Hall, et al. (2014). "Optimizing the production of suspension cells using the G-Rex "M" series". In: *Molecular Therapy-Methods & Clinical Development* 1, p. 14015.

Bantug, Glenn R, Lorenzo Galluzzi, Guido Kroemer, and Christoph Hess (2018). "The spectrum of T cell metabolism in health and disease". In: *Nature Reviews Immunology* 18.1, p. 19.

Barba, Vassia (2019). "CAR-Ts that grow on trees: Automating cell therapy manufacturing". In: *BioPharma-Reporter.com*. [Online; https://www.biopharma-reporter.com/Article/2019/06/11/I
s-Cocoon-manufacturing-platform-at-BIO; accessed 10-May-2020].

Berger, Carolina, Michael C Jensen, Peter M Lansdorp, Mike Gough, Carole Elliott, and Stanley R Riddell (2008). "Adoptive transfer of effector CD8+ T cells derived from central memory cells establishes persistent T cell memory in primates". In: *The Journal of clinical investigation* 118.1, pp. 294–305.

Blaeschke, Franziska, Dana Stenger, Theresa Kaeuferle, Semjon Willier, Ramin Lotfi, Andrew Didier Kaiser, Mario Assenmacher, Michaela Döring, Judith Feucht, and Tobias Feuchtinger (2018). "Induction of a central memory and stem cell mem-

ory phenotype in functionally active CD4+ and CD8+ CAR T cells produced in an automated good manufacturing practice system for the treatment of CD19+ acute lymphoblastic leukemia". In: *Cancer Immunology, Immunotherapy* 67.7, pp. 1053–1066.

Boehmer, Harold von (1990). "Developmental biology of T cells in T cell-receptor transgenic mice". In: *Annual review of immunology* 8.1, pp. 531–556.

Bohnenkamp, H., U. Hilbert, and T. Noll (2002). "Bioprocess development for the cultivation of human T-lymphocytes in a clinical scale". In: *Cytotechnology* 38.1, pp. 135–145.

Braendstrup, Peter, Bruce L Levine, and Marco Ruella (2020). "The long road to the first FDA-approved gene therapy: chimeric antigen receptor T cells targeting CD19". In: *Cytotherapy*.

Brentjens, Renier J, Marco L Davila, Isabelle Riviere, Jae Park, Xiuyan Wang, Lindsay G Cowell, Shirley Bartido, Jolanta Stefanski, Clare Taylor, Malgorzata Olszewska, et al. (2013). "CD19-targeted T cells rapidly induce molecular remissions in adults with chemotherapy-refractory acute lymphoblastic leukemia". In: *Science translational medicine* 5.177, 177ra38–177ra38.

Brentjens, Renier J, Isabelle Riviere, Jae H Park, Marco L Davila, Xiuyan Wang, Jolanta Stefanski, Clare Taylor, Raymond Yeh, Shirley Bartido, Oriana Borquez-Ojeda, et al. (2011). "Safety and persistence of adoptively transferred autologous CD19-targeted

T cells in patients with relapsed or chemotherapy refractory B-cell leukemias". In: *Blood, The Journal of the American Society of Hematology* 118.18, pp. 4817–4828.

Brudno, Jennifer N and James N Kochenderfer (2019). "Recent advances in CAR T-cell toxicity: mechanisms, manifestations and management". In: *Blood reviews* 34, pp. 45–55.

Buck, Michael D, David O'sullivan, and Erika L Pearce (2015). "T cell metabolism drives immunity". In: *Journal of Experimental Medicine* 212.9, pp. 1345–1360.

Busch, Dirk H, Simon P Fräßle, Daniel Sommermeyer, Veit R Buchholz, and Stanley R Riddell (2016). "Role of memory T cell subsets for adoptive immunotherapy". In: *Seminars in immunology*. Vol. 28. 1. Elsevier, pp. 28–34.

Calcinotto, Arianna, Paola Filipazzi, Matteo Grioni, Manuela Iero, Angelo De Milito, Alessia Ricupito, Agata Cova, Rossella Canese, Elena Jachetti, Monica Rossetti, et al. (2012). "Modulation of microenvironment acidity reverses anergy in human and murine tumor-infiltrating T lymphocytes". In: *Cancer research* 72.11, pp. 2746–2756.

Carmelo, Joana G, Ana Fernandes-Platzgummer, Joaquim MS Cabral, and Claudia Lobato da Silva (2014). "Scalable ex vivo expansion of human mesenchymal stem/stromal cells in microcarrier-based stirred culture systems". In: *Stem Cells and Good Manufacturing Practices*. Springer, pp. 147–159.

Carr, Erikka L, Alina Kelman, Glendon S Wu, Ravindra Gopaul, Emilee Senkevitch, Anahit Aghvanyan, Achmed M Turay, and Kenneth A Frauwirth (2010). "Glutamine uptake and metabolism are coordinately regulated by ERK/MAPK during T lymphocyte activation". In: *The Journal of Immunology* 185.2, pp. 1037–1044.

Carswell, Kathleen S and Eleftherios T Papoutsakis (2000). "Culture of human T cells in stirred bioreactors for cellular immunotherapy applications: Shear, proliferation, and the IL-2 receptor". In: *Biotechnology and bioengineering* 68.3, pp. 328–338.

Castiglia, Sara, Aloe Adamini, Deborah Rustichelli, Laura Castello, Katia Mareschi, Giuseppe Pinnetta, Marco Leone, Alessandra Mandese, Ivana Ferrero, Giulia Mesiano, et al. (2018). "Cytokines induced killer cells produced in good manufacturing practices conditions: identification of the most advantageous and safest expansion method in terms of viability, cellular growth and identity". In: *Journal of translational medicine* 16.1, p. 237.

Cha, Esther, Laura Graham, Masoud H Manjili, and Harry D Bear (2010). "IL-7+ IL-15 are superior to IL-2 for the *ex vivo* expansion of 4T1 mammary carcinoma-specific T cells with greater efficacy against tumors *in vivo*". In: *Breast cancer research and treatment* 122.2, pp. 359–369.

Cheadle, Eleanor J, Hannah Gornall, Vania Baldan, Vivien Hanson, Robert E Hawkins, and David E Gilham (2014). "CAR T cells: driving the road from the laboratory to the clinic". In: *Immunological reviews* 257.1, pp. 91–106.

Chen, Allen Kuan-Liang, Yi Kong Chew, Hong Yu Tan, Shaul Reuveny, and Steve Kah Weng Oh (2015). "Increasing efficiency of human mesenchymal stromal cell culture by optimization of microcarrier concentration and design of medium feed". In: *Cytotherapy* 17.2, pp. 163–173.

Chicaybam, Leonardo, Andressa Laino Sodre, Bianca Azevedo Curzio, and Martin Hernan Bonamino (2013). "An efficient low cost method for gene transfer to T lymphocytes". In: *PloS one* 8.3.

Clarke, Kim Gail (2013). *Bioprocess engineering: An introductory engineering and life science approach*. Elsevier.

ClinicalTrials.gov (2020). In: [Online; clinicaltrials.gov; accessed 7-February-2020].

Costariol, Elena, Marco Rotondi, Arman Amini, Christopher J Hewitt, Alvin W Nienow, Thomas RJ Heathman, Martina Micheletti, and Qasim A Rafiq (2019). "Establishing the scalable manufacture of primary human T-cells in an automated stirred-tank bioreactor". In: *Biotechnology and bioengineering* 116.10, pp. 2488–2502.

Costariol, Elena, Marco C Rotondi, Arman Amini, Christopher J Hewitt, Alvin W Nienow, Thomas RJ Heathman, and Qasim A Rafiq (2020). "Demonstrating the Manufacture of Human CAR-T Cells in an Automated Stirred-tank Bioreactor". In: *Biotechnology Journal*, p. 2000177.

Crompton, Joseph G, Madhusudhanan Sukumar, and Nicholas P Restifo (2014). "Uncoupling T-cell expansion from effector differentiation in cell-based immunotherapy". In: *Immunological reviews* 257.1, pp. 264–276.

Cruz, Conrad Russell Y, Kenneth P Micklethwaite, Barbara Savoldo, Carlos A Ramos, Sharon Lam, Stephanie Ku, Oumar Diouf, Enli Liu, A John Barrett, Sawa Ito, et al. (2013). "Infusion of donor-derived CD19-redirected virus-specific T cells for B-cell malignancies relapsed after allogeneic stem cell transplant: a phase 1 study". In: *Blood, The Journal of the American Society of Hematology* 122.17, pp. 2965–2973.

Dai, Xiaofeng, Yi Mei, Jianqi Nie, and Zhonghu Bai (2019). "Scaling up the manufacturing process of adoptive T cell immunotherapy". In: *Biotechnology journal* 14.4, p. 1800239.

Davies, John Tasman (2012). *Turbulence phenomena: an introduction to the eddy transfer of momentum, mass, and heat, particularly at interfaces*. Elsevier.

Davila, Marco L, Isabelle Riviere, Xiuyan Wang, Shirley Bartido, Jae Park, Kevin Curran, Stephen S Chung, Jolanta Stefanski, Oriana Borquez-Ojeda, Malgorzata Olszewska, et al. (2014). "Efficacy and toxicity management of 19-28z CAR T cell therapy in B cell acute lymphoblastic leukemia". In: *Science translational medicine* 6.224, 224ra25–224ra25.

DeFrancesco, Laura (2016). *Juno's wild ride*.

Depil, S, P Duchateau, SA Grupp, G Mufti, and L Poirot (2020). "'Off-the-shelf' allogeneic CAR T cells: development and challenges". In: *Nature Reviews Drug Discovery*, pp. 1–15.

Edelstein, Michael L, Mohammad R Abedi, Jo Wixon, and Richard M Edelstein (2004). "Gene therapy clinical trials worldwide 1989–2004—an overview". In: *The Journal of Gene Medicine: A cross-disciplinary journal for research on the science of gene transfer and its clinical applications* 6.6, pp. 597–602.

Eibl, Regine, Sören Werner, and Dieter Eibl (2009). "Bag bioreactor based on wave-induced motion: characteristics and applications". In: *Disposable bioreactors*. Springer, pp. 55–87.

Elsallab, Magdi, Bruce L Levine, Alan S Wayne, and Mohamed Abou-El-Enein (2020). "CAR T-cell product performance in haematological malignancies before and after marketing authorisation". In: *The Lancet Oncology* 21.2, e104–e116.

Enblad, Gunilla, Hannah Karlsson, Gustav Gammelgård, Jessica Wenthe, Tanja Lövgren, Rose Marie Amini, Kristina I Wikstrom, Magnus Essand, Barbara Savoldo, Helene Hallböök, et al. (2018). "A phase I/IIa trial using CD19-targeted third-generation CAR T cells for lymphoma and leukemia". In: *Clinical Cancer Research* 24.24, pp. 6185–6194.

Epidemiology and Cancer Statistics Group (2019). "Summary information about haematological malignancies". In: [Online; https://www.hmrn.org/statistics/disorders; accessed 5-March-2020].

Erra Diaz, Fernando, Ezequiel Dantas, and Jorge Geffner (2018). "Unravelling the interplay between extracellular acidosis and immune cells". In: *Mediators of inflammation* 2018.

ESCGT (2016). "Gene and cell therapy glossary". In: [Online; https://www.esgct.eu/useful-information/gene-and-cell-therapy-glossary.aspx; accessed 6-April-2020].

Evers, Dorothea, Jaap Jan Zwaginga, Janneke Tijmensen, Rutger A Middelburg, Masja de Haas, Karen MK de Vooght, Daan van de Kerkhof, Otto Visser, Nathalie CV Péquériaux, Francisca Hudig, et al. (2017). "Treatments for hematologic malignancies in contrast to those for solid cancers are associated with reduced red cell alloimmunization". In: *haematologica* 102.1, pp. 52–59.

Eyquem, Justin, Jorge Mansilla-Soto, Theodoros Giavridis, Sjoukje JC van der Stegen, Mohamad Hamieh, Kristen M Cunanan, Ashlesha Odak, Mithat Gönen, and Michel Sadelain (2017). "Targeting a CAR to the TRAC locus with CRISPR/Cas9 enhances tumour rejection". In: *Nature* 543.7643, pp. 113–117.

Fekete, Natalie, Ariane V Béland, Katie Campbell, Sarah L Clark, and Corinne A Hoesli (2018). "Bags versus flasks: a comparison of cell culture systems for the production of dendritic cell–based immunotherapies". In: *Transfusion* 58.7, pp. 1800–1813.

Fesnak, Andrew and Una O'Doherty (2017). "Clinical development and manufacture of chimeric antigen receptor T cells and the role of leukapheresis". In: *European Oncology & Haematology* 13.1, pp. 28–34.

Filley, Anna C, Mario Henriquez, and Mahua Dey (2018). "CART immunotherapy: development, success, and translation to malignant gliomas and other solid tumors". In: *Frontiers in oncology* 8, p. 453.

Fischer, Karin, Petra Hoffmann, Simon Voelkl, Norbert Meidenbauer, Julia Ammer, Matthias Edinger, Eva Gottfried, Sabine Schwarz, Gregor Rothe, Sabine Hoves, et al. (2007). "Inhibitory effect of tumor cell–derived lactic acid on human T cells". In: *Blood* 109.9, pp. 3812–3819.

Flora Southey (2018). "Thermo Fisher and Juno sign seven-year CAR-T tech deal". In: *BioPharma-reporter.com*. [Online; https://www.biopharma-reporter.com/Article/2018/01/03/Thermo-Fisher-and-Juno-sign-seven-year-CAR-T-tech-deal; accessed 6-March-2020].

Food and Drug Administration (2019). "Approved Cellular and Gene Therapy Products". In: [Online; https://www.fda.gov/vaccines-blood-biologics/cellular-gene-therapy-products/approved-cellular-and-gene-therapy-products; accessed 5-February-2020].

Frauwirth, Kenneth A and Craig B Thompson (2004). "Regulation of T lymphocyte metabolism". In: *The Journal of Immunology* 172.8, pp. 4661–4665.

Frey, Noelle V, Pamela A Shaw, Elizabeth O Hexner, Saar Gill, Katherine Marcucci, Selina M Luger, James K Mangan, Stephan A Grupp, Shannon L Maude, Solveig

Ericson, et al. (2016). *Optimizing chimeric antigen receptor (CAR) T cell therapy for adult patients with relapsed or refractory (r/r) acute lymphoblastic leukemia (ALL).*

Gabriele, A, AW Nienow, and MJH Simmons (2009). "Use of angle resolved PIV to estimate local specific energy dissipation rates for up-and down-pumping pitched blade agitators in a stirred tank". In: *Chemical Engineering Science* 64.1, pp. 126–143.

Gagliardi, Christine, Mariam Khalil, and Aaron E Foster (2019). "Streamlined production of genetically modified T cells with activation, transduction and expansion in closed-system G-Rex bioreactors". In: *Cytotherapy* 21.12, pp. 1246–1257.

Gandhi, Roopali, Alice Laroni, and Howard L Weiner (2010). "Role of the innate immune system in the pathogenesis of multiple sclerosis". In: *Journal of neuroimmunology* 221.1-2, pp. 7–14.

Garcia-Ochoa, Felix and Emilio Gomez (2009). "Bioreactor scale-up and oxygen transfer rate in microbial processes: an overview". In: *Biotechnology advances* 27.2, pp. 153–176.

Gardner, Rebecca A, Olivia Finney, Colleen Annesley, Hannah Brakke, Corinne Summers, Kasey Leger, Marie Bleakley, Christopher Brown, Stephanie Mgebroff, Karen S Kelly-Spratt, et al. (2017). "Intent-to-treat leukemia remission by CD19 CAR T cells of defined formulation and dose in children and young adults". In: *Blood* 129.25, pp. 3322–3331.

Gattinoni, Luca, Christopher A Klebanoff, Douglas C Palmer, Claudia Wrzesinski, Keith Kerstann, Zhiya Yu, Steven E Finkelstein, Marc R Theoret, Steven A Rosenberg, and Nicholas P Restifo (2005). "Acquisition of full effector function in vitro paradoxically impairs the in vivo antitumor efficacy of adoptively transferred CD8+ T cells". In: *The Journal of clinical investigation* 115.6, pp. 1616–1626.

Gattinoni, Luca, Enrico Lugli, Yun Ji, Zoltan Pos, Chrystal M Paulos, Máire F Quigley, Jorge R Almeida, Emma Gostick, Zhiya Yu, Carmine Carpenito, et al. (2011). "A human memory T cell subset with stem cell-like properties". In: *Nature medicine* 17.10, p. 1290.

Gattinoni, Luca, Daniel J Powell, Steven A Rosenberg, and Nicholas P Restifo (2006). "Adoptive immunotherapy for cancer: building on success". In: *Nature Reviews Immunology* 6.5, pp. 383–393.

Gee, Adrian P (2018). "GMP CAR-T cell production". In: *Best Practice & Research Clinical Haematology* 31.2, pp. 126–134.

GEN (2016). "Point-of-Care Gene Therapy Is Out of the Box". In: *Genetic Engineering and Biotechnology News*. [Online; https://www.genengnews.com/topics/drug-discovery/point-of-care-gene-therapy-is-out-of-the-box/; accessed 10-May-2020].

Geyer, Mark B and Renier J Brentjens (2016). "Current clinical applications of chimeric antigen receptor (CAR) modified T cells". In: *Cytotherapy* 18.11, pp. 1393–1409.

Gilbert, Mark J (2017). "Severe neurotoxicity in the phase 2 trial of JCAR015 in adult B-ALL (ROCKET study): analyses of patient, protocol and product attributes". In: *Proceedings from the Society for Immunotherapy of Cancer*, pp. 8–12.

Golchin, Ali and Tahereh Zarnoosheh Farahany (2019). "Biological products: cellular therapy and FDA approved products". In: *Stem Cell Reviews and Reports* 15.2, pp. 166–175.

Gonzalez, Sergio, Araceli Naranjo, Lisa M Serrano, Wen-Chung Chang, Christine L Wright, and Michael C Jensen (2004). "Genetic engineering of cytolytic T lymphocytes for adoptive T-cell therapy of neuroblastoma". In: *The Journal of Gene Medicine: A cross-disciplinary journal for research on the science of gene transfer and its clinical applications* 6.6, pp. 704–711.

Grist, James T, Lorna B Jarvis, Zoya Georgieva, Sara Thompson, Harpreet Kaur Sandhu, Keith Burling, Ashley Clarke, Sarah Jackson, Mark Wills, Ferdia A Gallagher, et al. (2018). "Extracellular lactate: a novel measure of T cell proliferation". In: *The Journal of Immunology* 200.3, pp. 1220–1226.

GSK (2016). "GSK and Miltenyi Biotec establish cell and gene therapy collaboration". In: [Online; https://www.gsk.com/en-gb/media/press-releases/gsk-and-miltenyi-biotec-establish-cell-and-gene-therapy-collaboration/; accessed 6-March-2020].

Guedan, Sonia, Avery D Posey Jr, Carolyn Shaw, Anna Wing, Tong Da, Prachi R Patel, Shannon E McGettigan, Victoria Casado-Medrano, Omkar U Kawalekar, Mireia

Uribe-Herranz, et al. (2018). “Enhancing CAR T cell persistence through ICOS and 4-1BB costimulation”. In: *JCI insight* 3.1.

Hacein-Bey-Abina, Salima, Christof Von Kalle, Manfred Schmidt, Francoise Le Deist, Nicolas Wulffraat, Elisabeth McIntyre, Isabelle Radford, Jean-Luc Villeval, Christopher C Fraser, Marina Cavazzana-Calvo, et al. (2003). “A serious adverse event after successful gene therapy for X-linked severe combined immunodeficiency”. In: *New England journal of medicine* 348.3, pp. 255–256.

Hanahan, Douglas and Lisa M Coussens (2012). “Accessories to the crime: functions of cells recruited to the tumor microenvironment”. In: *Cancer cell* 21.3, pp. 309–322.

Hanga, Mariana P, Halina Murasiewicz, Andrzej W Pacek, Alvin W Nienow, Karen Coopman, and Christopher J Hewitt (2017). “Expansion of bone marrow-derived human mesenchymal stem/stromal cells (hMSCs) using a two-phase liquid/liquid system”. In: *Journal of Chemical Technology & Biotechnology* 92.7, pp. 1577–1589.

Hanson, Michael A, Kurt A Brorson, Antonio R Moreira, and Govind Rao (2009). “Comparisons of optically monitored small-scale stirred tank vessels to optically controlled disposable bag bioreactors”. In: *Microbial Cell Factories* 8.1, p. 44.

Heathman, Thomas RJ, Veronica AM Glyn, Andrew Picken, Qasim A Rafiq, Karen Coopman, Alvin W Nienow, Bo Kara, and Christopher J Hewitt (2015). “Expansion, harvest and cryopreservation of human mesenchymal stem cells in a serum-

free microcarrier process". In: *Biotechnology and bioengineering* 112.8, pp. 1696–1707.

Hewitt, Christopher J, Ken Lee, Alvin W Nienow, Robert J Thomas, Mark Smith, and Colin R Thomas (2011). "Expansion of human mesenchymal stem cells on microcarriers". In: *Biotechnology letters* 33.11, p. 2325.

Hippel, James (2018). "Bio-Techne to acquire Quad Technologies". In: *PRNewswire*.

Hollyman, Daniel, Jolanta Stefanski, Mark Przybylowski, Shirley Bartido, Oriana Borquez-Ojeda, Clare Taylor, Raymond Yeh, Vanessa Capacio, Malgorzata Olszewska, James Hosey, et al. (2009). "Manufacturing validation of biologically functional T cells targeted to CD19 antigen for autologous adoptive cell therapy". In: *Journal of immunotherapy (Hagerstown, Md.: 1997)* 32.2, p. 169.

Hou, Bin, Yao Tang, Wenhan Li, Qingnuo Zeng, and Dongmin Chang (2019). "Efficiency of CAR-T therapy for treatment of solid tumor in clinical trials: a meta-analysis". In: *Disease markers* 2019.

Hsu, Wei-Ting, Rigzen PS Aulakh, Donald L Traul, and Inn H Yuk (2012). "Advanced microscale bioreactor system: a representative scale-down model for bench-top bioreactors". In: *Cytotechnology* 64.6, pp. 667–678.

Huang, Xin, Hongfeng Guo, Johnthomas Kang, Suet Choi, Tom C Zhou, Syam Tammana, Christopher J Lees, Zhong-Ze Li, Michael Milone, Bruce L Levine, et al. (2008). "Sleeping Beauty transposon-mediated engineering of human primary T

cells for therapy of CD19+ lymphoid malignancies". In: *Molecular Therapy* 16.3, pp. 580–589.

Jacobson, Caron, Amy Emmert, and Meredith B Rosenthal (2019). "CAR T-cell therapy: A microcosm for the challenges ahead in Medicare". In: *Jama* 322.10, pp. 923–924.

Jenkins, Michael J and Suzanne S Farid (2018). "Cost-effective bioprocess design for the manufacture of allogeneic CAR-T cell therapies using a decisional tool with multi-attribute decision-making analysis". In: *Biochemical Engineering Journal* 137, pp. 192–204.

Juillerat, Alexandre, Alan Marechal, Jean Marie Filhol, Yannick Valogne, Julien Valton, Aymeric Duclert, Philippe Duchateau, and Laurent Poirot (2017). "An oxygen sensitive self-decision making engineered CAR T-cell". In: *Scientific reports* 7.1, pp. 1–8.

Kaartinen, Tanja, Annu Luostarinen, Pilvi Maliniemi, Joni Keto, Mikko Arvas, Heini Belt, Jonna Koponen, Angelica Loskog, Satu Mustjoki, Kimmo Porkka, et al. (2017). "Low interleukin-2 concentration favors generation of early memory T cells over effector phenotypes during chimeric antigen receptor T-cell expansion". In: *Cytotherapy* 19.6, pp. 689–702.

Kaiser, AD, M Assenmacher, B Schröder, M Meyer, R Orentas, U Bethke, and B Dropulic (2015). "Towards a commercial process for the manufacture of genetically modified T cells for therapy". In: *Cancer gene therapy* 22.2, pp. 72–78.

Kakarla, Sunitha and Stephen Gottschalk (2014). "CAR T cells for solid tumors: armed and ready to go?" In: *Cancer journal (Sudbury, Mass.)* 20.2, p. 151.

Kebriaei, Partow, Helen Huls, Harjeet Singh, Simon Olivares, Matthew Figliola, Sourindra Maiti, Su Shihuang, Pappanaicken R Kumar, Bipulendu Jena, Marie Andree Forget, et al. (2014). *Adoptive therapy using sleeping beauty gene transfer system and artificial antigen presenting cells to manufacture T cells expressing CD19-specific chimeric antigen receptor*.

Kebriaei, Partow, Harjeet Singh, M Helen Huls, Matthew J Figliola, Roland Bassett, Simon Olivares, Bipulendu Jena, Margaret J Dawson, Pappanaicken R Kumaresan, Shihuang Su, et al. (2016). "Phase I trials using Sleeping Beauty to generate CD19-specific CAR T cells". In: *The Journal of clinical investigation* 126.9, pp. 3363–3376.

Khalil, Danny N, Sadna Budhu, Billel Gasmi, Roberta Zappasodi, Daniel Hirschhorn-Cymerman, Tamar Plitt, Olivier De Henau, Dmitriy Zamarin, Rikke B Holmgaard, Judith T Murphy, et al. (2015). "The new era of cancer immunotherapy: manipulating T-cell activity to overcome malignancy". In: *Advances in cancer research*. Vol. 128. Elsevier, pp. 1–68.

Kisielow, Pawel and Harald Von Boehmer (1995). “Development and selection of T cells: facts and puzzles”. In: *Advances in immunology* 58, pp. 87–209.

Klarer, Alex, David Smith, Ryan Cassidy, TRJ Heathman, and QA Rafiq (2018). “Demonstrating scalable T-cell expansion in stirred-tank bioreactors”. In: *Bioprocess International* 16.6, pp. 6–14.

Kochenderfer, James N, Mark E Dudley, Steven A Feldman, Wyndham H Wilson, David E Spaner, Irina Maric, Maryalice Stetler-Stevenson, Giao Q Phan, Marybeth S Hughes, Richard M Sherry, et al. (2012). “B-cell depletion and remissions of malignancy along with cytokine-associated toxicity in a clinical trial of anti-CD19 chimeric-antigen-receptor-transduced T cells”. In: *Blood, The Journal of the American Society of Hematology* 119.12, pp. 2709–2720.

Kofler, David M, Markus Chmielewski, Gunter Rappl, Anja Hombach, Tobias Riet, Annette Schmidt, Andreas A Hombach, Clemens-Martin Wendtner, and Hinrich Abken (2011). “CD28 costimulation Impairs the efficacy of a redirected t-cell antitumor attack in the presence of regulatory t cells which can be overcome by preventing Lck activation”. In: *Molecular therapy* 19.4, pp. 760–767.

Konakovsky, Viktor, Christoph Clemens, Markus Michael Müller, Jan Bechmann, Martina Berger, Stefan Schlatter, and Christoph Herwig (2016). “Metabolic control in mammalian fed-batch cell cultures for reduced lactic acid accumulation and improved process robustness”. In: *Bioengineering* 3.1, p. 5.

Lanier, Lewis L (2013). “Shades of grey—the blurring view of innate and adaptive immunity”. In: *Nature Reviews Immunology* 13.2, p. 73.

Lee, Daniel W, James N Kochenderfer, Maryalice Stetler-Stevenson, Yongzhi K Cui, Cindy Delbrook, Steven A Feldman, Terry J Fry, Rimas Orentas, Marianna Sabatino, Nirali N Shah, et al. (2015). “T cells expressing CD19 chimeric antigen receptors for acute lymphoblastic leukaemia in children and young adults: a phase 1 dose-escalation trial”. In: *The Lancet* 385.9967, pp. 517–528.

Levich, Veniamin Grigorevich (1962). “Physicochemical hydrodynamics”. In:

Levine, BL (2015). “Performance-enhancing drugs: design and production of redirected chimeric antigen receptor (CAR) T cells”. In: *Cancer gene therapy* 22.2, pp. 79–84.

Li, SD and L Huang (2006). “Gene therapy progress and prospects: non-viral gene therapy by systemic delivery”. In: *Gene therapy* 13.18, pp. 1313–1319.

Lichtman, Marshall A (2008). “Battling the hematological malignancies: the 200 years’ war.” In: *Oncologist* 13.2.

Ligtenberg, Maarten A, Dimitrios Mougiakakos, Madhura Mukhopadhyay, Kristina Witt, Alvaro Lladser, Markus Chmielewski, Tobias Riet, Hinrich Abken, and Rolf Kiessling (2016). “Coexpressed catalase protects chimeric antigen receptor-redirected T cells as well as bystander cells from oxidative stress-induced loss of antitumor activity”. In: *The Journal of Immunology* 196.2, pp. 759–766.

Lim, Okjae, Mi Young Jung, Yu Kyeong Hwang, and Eui-Cheol Shin (2015). "Present and future of allogeneic natural killer cell therapy". In: *Frontiers in immunology* 6, p. 286.

Lock, Dominik, Nadine Mockel-Tenbrinck, Katharina Drechsel, Carola Barth, Daniela Mauer, Thomas Schaser, Carolin Kolbe, Wael Al Rawashdeh, Janina Brauner, Olaf Hardt, et al. (2017). "Automated manufacturing of potent CD20-directed chimeric antigen receptor T cells for clinical use". In: *Human gene therapy* 28.10, pp. 914–925.

Ludwig, Josh and Mark Hirschel (2020). "Methods and process optimization for large-scale CAR T expansion using the G-Rex cell culture platform". In: *Chimeric Antigen Receptor T Cells*. Springer, pp. 165–177.

Luo, Can, Guobo Shen, Ning Liu, Fengming Gong, Xiawei Wei, Shaohua Yao, Dan Liu, Xiu Teng, Ning Ye, Nan Zhang, et al. (2014). "Ammonia drives dendritic cells into dysfunction". In: *The Journal of Immunology* 193.3, pp. 1080–1089.

Luster, Andrew D (2002). "The role of chemokines in linking innate and adaptive immunity". In: *Current opinion in immunology* 14.1, pp. 129–135.

Maciolek, Jason A, J Alex Pasternak, and Heather L Wilson (2014). "Metabolism of activated T lymphocytes". In: *Current opinion in immunology* 27, pp. 60–74.

Majzner, Robbie G and Crystal L Mackall (2019). "Clinical lessons learned from the first leg of the CAR T cell journey". In: *Nature medicine* 25.9, pp. 1341–1355.

Mali, Prashant, Luhan Yang, Kevin M Esvelt, John Aach, Marc Guell, James E DiCarlo, Julie E Norville, and George M Church (2013). "RNA-guided human genome engineering via Cas9". In: *Science* 339.6121, pp. 823–826.

Manuri, Pallavi V Raja, Matthew H Wilson, Sourindra N Maiti, Tiejuan Mi, Harjeet Singh, Simon Olivares, Margaret J Dawson, Helen Huls, Dean A Lee, Pulivarthi H Rao, et al. (2010). "piggyBac transposon/transposase system to generate CD19-specific T cells for the treatment of B-lineage malignancies". In: *Human gene therapy* 21.4, pp. 427–437.

Marin, Virna, Irene Pizzitola, Valentina Agostoni, Greta Maria Paola Giordano Attianese, Helene Finney, Alastair Lawson, Martin Pule, Raphael Rousseau, Andrea Biondi, and Ettore Biagi (2010). "Cytokine-induced killer cells for cell therapy of acute myeloid leukemia: improvement of their immune activity by expression of CD33-specific chimeric receptors". In: *Haematologica* 95.12, pp. 2144–2152.

Marin Morales, Jose Manuel, Nadine Munch, Katja Peter, Daniel Freund, Uta Oelschlagel, Kristina Holig, Thea Bohm, Anne-Christine Flach, Jorg Keaaler, Ezio Bonifacio, et al. (2019). "Automated clinical grade expansion of regulatory T cells in a fully closed system". In: *Frontiers in immunology* 10, p. 38.

Marsh, Douglas TJ, Gary J Lye, Martina Micheletti, Akinlolu OO Odeleye, Andrea Ducci, and Matthew D Osborne (2017a). "Fluid dynamic characterization of a laboratory scale rocked bag bioreactor". In: *AIChE Journal* 63.9, pp. 4177–4187.

— (2017b). “Fluid dynamic characterization of a laboratory scale rocked bag bioreactor”. In: *AIChE Journal* 63.9, pp. 4177–4187.

Martinez, Marina and Edmund Kyung Moon (2019). “CAR T cells for solid tumors: new strategies for finding, infiltrating, and surviving in the tumor microenvironment”. In: *Frontiers in immunology* 10.

Maude, Shannon L, Noelle Frey, Pamela A Shaw, Richard Aplenc, David M Barrett, Nancy J Bunin, Anne Chew, Vanessa E Gonzalez, Zhaohui Zheng, Simon F Lacey, et al. (2014). “Chimeric antigen receptor T cells for sustained remissions in leukemia”. In: *New England Journal of Medicine* 371.16, pp. 1507–1517.

Medvec, Andrew R, Christopher Ecker, Hong Kong, Emily A Winters, Joshua Glover, Angel Varela-Rohena, and James L Riley (2018). “Improved expansion and in vivo function of patient T cells by a serum-free medium”. In: *Molecular Therapy-Methods & Clinical Development* 8, pp. 65–74.

Micheletti, M, T Barrett, SD Doig, F Baganz, MS Levy, JM Woodley, and GJ Lye (2006). “Fluid mixing in shaken bioreactors: Implications for scale-up predictions from microlitre-scale microbial and mammalian cell cultures”. In: *Chemical Engineering Science* 61.9, pp. 2939–2949.

Miller, William M, HW Blanch, and CR Wilke (2000). “A kinetic analysis of hybridoma growth and metabolism in batch and continuous suspension culture: effect of nu-

trient concentration, dilution rate, and pH". In: *Biotechnology and bioengineering* 67.6, pp. 853–871.

Milone, Michael C and Una O'Doherty (2018). "Clinical use of lentiviral vectors". In: *Leukemia* 32.7, pp. 1529–1541.

Miltenyi Biotec GmbH (2018). "MolMed and Miltenyi Biotec: EMA approves the utilization of the CliniMACS Prodigy® equipment". In: [Online; https://www.miltenyibiotec.com/US-en/about-us/newsroom/press-releases/molmed-and-miltenyi-biotec-ema-approves-the-utilization-of-the-clinimacs-prodigy-r-equipment.html; accessed 6-March-2020].

Mizukami, Amanda and Kamilla Swiech (2020). "Platforms for Clinical-Grade CAR-T Cell Expansion". In: *Chimeric Antigen Receptor T Cells*. Springer, pp. 139–150.

Mock, Ulrike, Lauren Nickolay, Brian Philip, Gordon Weng-Kit Cheung, Hong Zhan, Ian CD Johnston, Andrew D Kaiser, Karl Peggs, Martin Pule, Adrian J Thrasher, et al. (2016). "Automated manufacturing of chimeric antigen receptor T cells for adoptive immunotherapy using CliniMACS prodigy". In: *Cytotherapy* 18.8, pp. 1002–1011.

Monjezi, R, C Miskey, T Gogishvili, M Schleef, M Schmeer, H Einsele, Z Ivics, and M Hudecek (2017). "Enhanced CAR T-cell engineering using non-viral Sleeping Beauty transposition from minicircle vectors". In: *Leukemia* 31.1, pp. 186–194.

Montano, Monty (2014). *Translational biology in medicine*. Elsevier.

Morgan, Richard A, James C Yang, Mio Kitano, Mark E Dudley, Carolyn M Laurencot, and Steven A Rosenberg (2010). "Case report of a serious adverse event following the administration of T cells transduced with a chimeric antigen receptor recognizing ERBB2". In: *Molecular Therapy* 18.4, pp. 843–851.

Moses, Sarath, Matthew Manahan, Alexandre Ambrogelly, and Wai Lam W Ling (2012). "Assessment of AMBRTM as a model for high-throughput cell culture process development strategy". In:

Mulligan, Richard C (1993). "The basic science of gene therapy". In: *Science* 260.5110, pp. 926–932.

Neelapu, Sattva S, Frederick L Locke, Nancy L Bartlett, Lazaros J Lekakis, David B Miklos, Caron A Jacobson, Ira Braunschweig, Olalekan O Oluwole, Tanya Siddiqi, Yi Lin, et al. (2017). "Axicabtagene ciloleucel CAR T-cell therapy in refractory large B-cell lymphoma". In: *New England Journal of Medicine* 377.26, pp. 2531–2544.

Neelapu, Sattva S, Sudhakar Tummala, Partow Kebriaei, William Wierda, Cristina Gutierrez, Frederick L Locke, Krishna V Komanduri, Yi Lin, Nitin Jain, Naval Daver, et al. (2018). "Chimeric antigen receptor T-cell therapy-assessment and management of toxicities". In: *Nature reviews Clinical oncology* 15.1, p. 47.

Newick, Kheng, Shaun O'Brien, Edmund Moon, and Steven M Albelda (2017). "CAR T cell therapy for solid tumors". In: *Annual review of medicine* 68, pp. 139–152.

Nienow, Alvin W (2006a). “Reactor engineering in large scale animal cell culture”. In: *Cytotechnology* 50.1-3, p. 9.

— (2006b). “Reactor engineering in large scale animal cell culture”. In: *Cytotechnology* 50.1-3, p. 9.

— (2015). “Mass transfer and mixing across the scales in animal cell culture”. In: *Animal Cell Culture*. Springer, pp. 137–167.

Nienow, Alvin W, Christopher J Hewitt, Thomas RJ Heathman, Veronica AM Glyn, Goncalo N Fonte, Mariana P Hanga, Karen Coopman, and Qasim A Rafiq (2016). “Agitation conditions for the culture and detachment of hMSCs from microcarriers in multiple bioreactor platforms”. In: *Biochemical Engineering Journal* 108, pp. 24–29.

Nienow, Alvin W, Christopher D Rielly, Kathryn Brosnan, Neil Bargh, Kenneth Lee, Karen Coopman, and Christopher J Hewitt (2013). “The physical characterisation of a microscale parallel bioreactor platform with an industrial CHO cell line expressing an IgG4”. In: *Biochemical engineering journal* 76, pp. 25–36.

Nienow, AW (1968). “Suspension of solid particles in turbine agitated baffled vessels”. In: *Chemical Engineering Science* 23.12, pp. 1453–1459.

— (1997). “The suspension of solid particles”. In: *Mixing in the process industries* 2.

— (1998). “Hydrodynamics of stirred bioreactors”. In:

Nishimura, Takashi, Minoru Nakui, Marimo Sato, Kenji Iwakabe, Hidemitsu Kitamura, Masashi Sekimoto, Akio Ohta, Toshiaki Koda, and Shinichiro Nishimura (2000). "The critical role of Th1-dominant immunity in tumor immunology". In: *Cancer chemotherapy and pharmacology* 46.1, S52–S61.

Oliver, Amanda J, Peter KH Lau, Ashleigh S Unsworth, Sherene Loi, Phillip K Darcy, Michael H Kershaw, and Clare Y Slaney (2018). "Tissue-dependent tumor microenvironments and their impact on immunotherapy responses". In: *Frontiers in immunology* 9, p. 70.

Ou, Jianfa, Yingnan Si, Yawen Tang, Grace E Salzer, Yun Lu, Seulhee Kim, Hongwei Qin, Lufang Zhou, and Xiaoguang Liu (2019). "Novel biomanufacturing platform for large-scale and high-quality human T cells production". In: *Journal of biological engineering* 13.1, p. 34.

Pampusch, Mary S, Kumudhini Preethi Haran, Geoffrey T Hart, Eva G Rakasz, Aaron K Rendahl, Edward A Berger, Elizabeth Connick, and Pamela J Skinner (2020). "Rapid Transduction and Expansion of Transduced T Cells with Maintenance of Central Memory Populations". In: *Molecular Therapy-Methods & Clinical Development* 16, pp. 1–10.

Panagopoulou, Theano I and Qasim A Rafiq (2019). "CAR-T immunotherapies: Biotechnological strategies to improve safety, efficacy and clinical outcome through CAR engineering". In: *Biotechnology advances*.

Park, Jae Hong, Isabelle Riviere, Xiuyan Wang, Terence Purdon, Michel Sadelain, and Renier J Brentjens (2016). *Impact of disease burden on long-term outcome of 19-28z CAR modified T cells in adult patients with relapsed B-ALL.*

Petiti, Luca and Luigia Pace (2020). "The persistence of stemness". In: *Nature Immunology* 21.5, pp. 492–494.

Pharmaceutical Technologies (2017). "Juno Therapeutics Explores CAR-T Trial Deaths". In: [Online; https://www.pharmaceutical-technology.com/comment/juno-therapeutics-explores-car-t-trial-deaths/; accessed 5-March-2020].

Philip, Brian, Evangelia Kokalaki, Leila Mekkaoui, Simon Thomas, Karin Straathof, Barry Flutter, Virna Marin, Teresa Marafioti, Ronjon Chakraverty, David Linch, et al. (2014). "A highly compact epitope-based marker/suicide gene for easier and safer T-cell therapy". In: *Blood, The Journal of the American Society of Hematology* 124.8, pp. 1277–1287.

Plitas, George, Catherine Konopacki, Kenmin Wu, Paula D Bos, Monica Morrow, Ekaterina V Putintseva, Dmitriy M Chudakov, and Alexander Y Rudensky (2016). "Regulatory T cells exhibit distinct features in human breast cancer". In: *Immunity* 45.5, pp. 1122–1134.

Poirot, Laurent, Brian Philip, Cécile Schiffer-Mannioui, Diane Le Clerre, Isabelle Chion-Sotinel, Sophie Derniame, Pierrick Potrel, Cécile Bas, Laetitia Lemaire, Roman Galetto, et al. (2015). "Multiplex genome-edited T-cell manufacturing platform for

"off-the-shelf" adoptive T-cell immunotherapies". In: *Cancer research* 75.18, pp. 3853–3864.

Porter, David L, Bruce L Levine, Michael Kalos, Adam Bagg, and Carl H June (2011). "Chimeric antigen receptor–modified T cells in chronic lymphoid leukemia". In: *N engl j Med* 365, pp. 725–733.

Ptáčková, Pavlina, Jan Musil, Martin Štach, Petr Lesny, Šárka Němečková, Vlastimil Král, Milan Fábry, and Pavel Otáhal (2018). "A new approach to CAR T-cell gene engineering and cultivation using piggyBac transposon in the presence of IL-4, IL-7 and IL-21". In: *Cytotherapy* 20.4, pp. 507–520.

Pucino, Valentina, Michelangelo Certo, Vinay Bulusu, Danilo Cucchi, Katriona Goldmann, Elena Pontarini, Robert Haas, Joanne Smith, Sarah E Headland, Kevin Blighe, et al. (2019). "lactate Buildup at the site of chronic inflammation Promotes Disease by inducing cD4+ T cell Metabolic rewiring". In: *Cell metabolism* 30.6, pp. 1055–1074.

Pule, Martin A, Barbara Savoldo, G Doug Myers, Claudia Rossig, Heidi V Russell, Gianpietro Dotti, M Helen Huls, Enli Liu, Adrian P Gee, Zhuyong Mei, et al. (2008). "Virus-specific T cells engineered to coexpress tumor-specific receptors: persistence and antitumor activity in individuals with neuroblastoma". In: *Nature medicine* 14.11, p. 1264.

Qasim, Waseem, Hong Zhan, Sujith Samarasinghe, Stuart Adams, Persis Amrolia, Sian Stafford, Katie Butler, Christine Rivat, Gary Wright, Kathy Somana, et al. (2017). "Molecular remission of infant B-ALL after infusion of universal TALEN gene-edited CAR T cells". In: *Science translational medicine* 9.374, eaaj2013.

Rafiq, Qasim A, Kathryn M Brosnan, Karen Coopman, Alvin W Nienow, and Christopher J Hewitt (2013a). "Culture of human mesenchymal stem cells on microcarriers in a 5 l stirred-tank bioreactor". In: *Biotechnology letters* 35.8, pp. 1233–1245.

Rafiq, Qasim A, Karen Coopman, Alvin W Nienow, and Christopher J Hewitt (2013b). "A quantitative approach for understanding small-scale human mesenchymal stem cell culture–implications for large-scale bioprocess development". In: *Biotechnology journal* 8.4, pp. 459–471.

— (2016a). "Systematic microcarrier screening and agitated culture conditions improves human mesenchymal stem cell yield in bioreactors". In: *Biotechnology journal* 11.4, pp. 473–486.

Rafiq, Qasim A, Mariana P Hanga, Thomas RJ Heathman, Karen Coopman, Alvin W Nienow, David J Williams, and Christopher J Hewitt (2017). "Process development of human multipotent stromal cell microcarrier culture using an automated high-throughput microbioreactor". In: *Biotechnology and bioengineering* 114.10, pp. 2253–2266.

Rafiq, Qasim A, Thomas RJ Heathman, Karen Coopman, Alvin W Nienow, and Christopher J Hewitt (2016b). "Scalable manufacture for cell therapy needs". In: *Bioreactors,(Wiley-VCH Verlag GmbH & Co. KGaA 113–146*.

Rafiq, Qasim A and Christopher J Hewitt (2015). "Cell therapies: why scale matters". In: *Pharmaceutical Bioprocessing* 3.2, pp. 97–99.

Rafiq, Sarwish, Christopher S Hackett, and Renier J Brentjens (2020). "Engineering strategies to overcome the current roadblocks in CAR T cell therapy". In: *Nature reviews Clinical oncology* 17.3, pp. 147–167.

Raje, Noopur, Jesus Berdeja, Yi Lin, David Siegel, Sundar Jagannath, Deepu Madduri, Michaela Liedtke, Jacalyn Rosenblatt, Marcela V Maus, Ashley Turka, et al. (2019). "Anti-BCMA CAR T-cell therapy bb2121 in relapsed or refractory multiple myeloma". In: *New England Journal of Medicine* 380.18, pp. 1726–1737.

Ramamoorth, Murali and Aparna Narvekar (2015). "Non viral vectors in gene therapy-an overview". In: *Journal of clinical and diagnostic research: JCDR* 9.1, GE01.

Rameez, Shahid, Sigma S Mostafa, Christopher Miller, and Abhinav A Shukla (2014). "High-throughput miniaturized bioreactors for cell culture process development: Reproducibility, scalability, and control". In: *Biotechnology progress* 30.3, pp. 718–727.

Ren, Jiangtao, Xiaojun Liu, Chongyun Fang, Shuguang Jiang, Carl H June, and Yangbing Zhao (2017). "Multiplex genome editing to generate universal CAR T cells resistant to PD1 inhibition". In: *Clinical cancer research* 23.9, pp. 2255–2266.

Richman, Sarah A, Selene Nunez-Cruz, Babak Moghimi, Lucy Z Li, Zachary T Gershenson, Zissimos Mourelatos, David M Barrett, Stephan A Grupp, and Michael C Milone (2018). "High-affinity GD2-specific CAR T cells induce fatal encephalitis in a preclinical neuroblastoma model". In: *Cancer immunology research* 6.1, pp. 36–46.

Rocha-Valadez, J Antonio, Marlene Estrada, Enrique Galindo, and Leobardo Serrano-Carreón (2006). "From shake flasks to stirred fermentors: Scale-up of an extractive fermentation process for 6-pentyl-α-pyrone production by Trichoderma harzianum using volumetric power input". In: *Process Biochemistry* 41.6, pp. 1347–1352.

Rosenberg, Steven A, Paul Aebersold, Kenneth Cornetta, Attan Kasid, Richard A Morgan, Robert Moen, Evelyn M Karson, Michael T Lotze, James C Yang, Suzanne L Topalian, et al. (1990). "Gene transfer into humans—immunotherapy of patients with advanced melanoma, using tumor-infiltrating lymphocytes modified by retroviral gene transduction". In: *New England Journal of Medicine* 323.9, pp. 570–578.

Rotondi, Marco, Ned Grace, John Betts, Neil Bargh, Elena Costariol, Barney Zoro, Christopher J Hewitt, Alvin W Nienow, and Qasim A Rafiq (2021). "Design and

development of a new ambr250® bioreactor vessel for improved cell and gene therapy applications". In: *Biotechnology Letters*, pp. 1–14.

Sabatino, Marianna, Jinhui Hu, Michele Sommariva, Sanjivan Gautam, Vicki Fellowes, James D Hocker, Sean Dougherty, Haiying Qin, Christopher A Klebanoff, Terry J Fry, et al. (2016). "Generation of clinical-grade CD19-specific CAR-modified CD8+ memory stem cells for the treatment of human B-cell malignancies". In: *Blood, The Journal of the American Society of Hematology* 128.4, pp. 519–528.

Sadelain, Michel, Renier Brentjens, and Isabelle Riviere (2013). "The basic principles of chimeric antigen receptor design". In: *Cancer discovery* 3.4, pp. 388–398.

Sadelain, Michel, Renier Brentjens, and Isabelle Rivière (2009). "The promise and potential pitfalls of chimeric antigen receptors". In: *Current opinion in immunology* 21.2, pp. 215–223.

Salas-Mckee, January, Weimin Kong, Whitney L Gladney, Julie K Jadlowsky, Gabriela Plesa, Megan M Davis, and Joseph A Fraietta (2019). "CRISPR/Cas9-based genome editing in the era of CAR T cell immunotherapy". In: *Human vaccines & immunotherapeutics* 15.5, pp. 1126–1132.

Salmikangas, Paula, Niamh Kinsella, and Paul Chamberlain (2018). "Chimeric antigen receptor T-cells (CAR T-cells) for cancer immunotherapy–moving target for industry?" In: *Pharmaceutical research* 35.8, p. 152.

Sarah Nam Jeff Smith, Guang Yang (2019). “Unlocking the full potential of CAR-T cell therapies requires investment in four areas”. In: [Online; https://www.mckinsey.com/industries/pharmac and-medical-products/our-insights/driving-the-next-wave-of-innovation-in-car-t-cell-therapies; accessed 5-March-2020].

Schirmer, Cedric, Jan Müller, Nina Steffen, Sören Werner, Regine Eibl, and Dieter Eibl (2020). “How to produce mAbs in a cube-shaped stirred single-use bioreactor at 200 L scale”. In: *Animal Cell Biotechnology*. Springer, pp. 169–186.

Schirmer, Cedric, Thomas Nussbaumer, Reto Schöb, Ralf Pörtner, Regine Eibl, and Dieter Eibl (2018). “Development, engineering and biological characterization of stirred tank bioreactors”. In: *Biopharmaceuticals. InTech, London*, pp. 87–108.

Schneider, Markus, Ian W Marison, and Urs von Stockar (1996). “The importance of ammonia in mammalian cell culture”. In: *Journal of biotechnology* 46.3, pp. 161–185.

Schop, Deborah, Frank W Janssen, Linda DS van Rijn, Hugo Fernandes, Rolf M Bloem, Joost D de Bruijn, and Riemke van Dijkhuizen-Radersma (2009). “Growth, metabolism, and growth inhibitors of mesenchymal stem cells”. In: *Tissue Engineering Part A* 15.8, pp. 1877–1886.

Schuster, Stephen J, Jakub Svoboda, Elise A Chong, Sunita D Nasta, Anthony R Mato, Özlem Anak, Jennifer L Brogdon, Iulian Pruteanu-Malinici, Vijay Bhoj, Daniel

Landsburg, et al. (2017). “Chimeric antigen receptor T cells in refractory B-cell lymphomas”. In: *New England Journal of Medicine* 377.26, pp. 2545–2554.

Shah, Nirali N and Terry J Fry (2019). “Mechanisms of resistance to CAR T cell therapy”. In: *Nature Reviews Clinical Oncology* 16.6, pp. 372–385.

Shah, Nirav N, Fenlu Zhu, Carolyn Taylor, Dina Schneider, Winfried Krueger, Andrew Worden, Sharon Yim, Timothy S Fenske, Mehdi Hamadani, Bryon Johnson, et al. (2018). “A phase 1 study with point-of-care manufacturing of dual targeted, tandem anti-CD19, anti-CD20 chimeric antigen receptor modified T (CAR-T) cells for relapsed, refractory, non-Hodgkin lymphoma”. In: *Blood* 132.Supplement 1, pp. 4193–4193.

Shimada, Akira (2019). “Hematological malignancies and molecular targeting therapy”. In: *European journal of pharmacology*, p. 172641.

Singh, Harjeet, Matthew J Figliola, Margaret J Dawson, Simon Olivares, Ling Zhang, Ge Yang, Sourindra Maiti, Pallavi Manuri, Vladimir Senyukov, Bipulendu Jena, et al. (2013). “Manufacture of clinical-grade CD19-specific T cells stably expressing chimeric antigen receptor using Sleeping Beauty system and artificial antigen presenting cells”. In: *PloS one* 8.5.

Singh, Harjeet, JSE Moyes, MH Huls, and LJN Cooper (2015). “Manufacture of T cells using the Sleeping Beauty system to enforce expression of a CD19-specific chimeric antigen receptor”. In: *Cancer gene therapy* 22.2, pp. 95–100.

Singh, Nathan, Jessica Perazzelli, Stephan A Grupp, and David M Barrett (2016). "Early memory phenotypes drive T cell proliferation in patients with pediatric malignancies". In: *Science translational medicine* 8.320, 320ra3–320ra3.

Smith, Devyn M, Emily J Culme-Seymour, and Chris Mason (2018). "Evolving industry partnerships and investments in cell and gene therapies". In: *Cell stem cell* 22.5, pp. 623–626.

Somerville, Robert PT, Laura Devillier, Maria R Parkhurst, Steven A Rosenberg, and Mark E Dudley (2012). "Clinical scale rapid expansion of lymphocytes for adoptive cell transfer therapy in the WAVE® bioreactor". In: *Journal of translational medicine* 10.1, p. 69.

Somia, Nikunj and Inder M Verma (2000). "Gene therapy: trials and tribulations". In: *Nature Reviews Genetics* 1.2, pp. 91–99.

Sommermeyer, Daniel, Michael Hudecek, Paula L Kosasih, Tea Gogishvili, David G Maloney, Cameron J Turtle, and Stanley R Riddell (2016). "Chimeric antigen receptor-modified T cells derived from defined CD8+ and CD4+ subsets confer superior antitumor reactivity in vivo". In: *Leukemia* 30.2, p. 492.

Stadtmauer, Edward A., Joseph A. Fraietta, Megan M. Davis, Adam D. Cohen, Kristy L. Weber, Eric Lancaster, Patricia A. Mangan, Irina Kulikovskaya, Minnal Gupta, Fang Chen, Lifeng Tian, Vanessa E. Gonzalez, Jun Xu, In-young Jung, J. Joseph Melenhorst, Gabriela Plesa, Joanne Shea, Tina Matlawski, Amanda Cervini, Avery L.

Gaymon, Stephanie Desjardins, Anne Lamontagne, January Salas-Mckee, Andrew Fesnak, Donald L. Siegel, Bruce L. Levine, Julie K. Jadlowsky, Regina M. Young, Anne Chew, Wei-Ting Hwang, Elizabeth O. Hexner, Beatriz M. Carreno, Christopher L. Nobles, Frederic D. Bushman, Kevin R. Parker, Yanyan Qi, Ansuman T. Satpathy, Howard Y. Chang, Yangbing Zhao, Simon F. Lacey, and Carl H. June (2020). "CRISPR-engineered T cells in patients with refractory cancer". In: *Science*.

Stavrou, Maria, Brian Philip, Charlotte Traynor-White, Christopher G Davis, Shimobi Onuoha, Shaun Cordoba, Simon Thomas, and Martin Pule (2018). "A rapamycin-activated caspase 9-based suicide gene". In: *Molecular Therapy* 26.5, pp. 1266–1276.

Stroncek, David F, Jiaqiang Ren, Daniel W Lee, Minh Tran, Sue Ellen Frodigh, Marianna Sabatino, Hanh Khuu, Melinda S Merchant, and Crystal L Mackall (2016). "Myeloid cells in peripheral blood mononuclear cell concentrates inhibit the expansion of chimeric antigen receptor T cells". In: *Cytotherapy* 18.7, pp. 893–901.

Taylor, Lenise, Elizabeth S Rodriguez, Anne Reese, and Karen Anderson (2019). "Building a Program: Implications for infrastructure, nursing education, and training for CAR T-cell therapy." In: *Clinical journal of oncology nursing* 23.2.

Themeli, Maria, Isabelle Rivière, and Michel Sadelain (2015). "New cell sources for T cell engineering and adoptive immunotherapy". In: *Cell stem cell* 16.4, pp. 357–366.

Thommen, Daniela S and Ton N Schumacher (2018). “T cell dysfunction in cancer”. In: *Cancer cell* 33.4, pp. 547–562.

Till, Brian G, Michael C Jensen, Jinjuan Wang, Eric Y Chen, Brent L Wood, Harvey A Greisman, Xiaojun Qian, Scott E James, Andrew Raubitschek, Stephen J Forman, et al. (2008). “Adoptive immunotherapy for indolent non-Hodgkin lymphoma and mantle cell lymphoma using genetically modified autologous CD20-specific T cells”. In: *Blood, The Journal of the American Society of Hematology* 112.6, pp. 2261–2271.

Tipanee, Jaitip, Yoke Chin Chai, Thierry VandenDriessche, and Marinee K Chuah (2017). “Preclinical and clinical advances in transposon-based gene therapy”. In: *Bioscience reports* 37.6.

Torikai, Hiroki, Andreas Reik, Pei-Qi Liu, Yuanyue Zhou, Ling Zhang, Sourindra Maiti, Helen Huls, Jeffrey C Miller, Partow Kebriaei, Brian Rabinovitch, et al. (2012). “A foundation for universal T-cell based immunotherapy: T cells engineered to express a CD19-specific chimeric-antigen-receptor and eliminate expression of endogenous TCR”. In: *Blood, The Journal of the American Society of Hematology* 119.24, pp. 5697–5705.

Tumaini, Barbara, Daniel W Lee, Tasha Lin, Luciano Castiello, David F Stroncek, Crystal Mackall, Alan Wayne, and Marianna Sabatino (2013). “Simplified process

for the production of anti–CD19-CAR–engineered T cells". In: *Cytotherapy* 15.11, pp. 1406–1415.

Turtle, Cameron J, Carolina Berger, Daniel Sommermeyer, Laila-Aicha Hanafi, Barbara Pender, Emily M Robinson, Katherine Melville, Tanya M Budiarto, Natalia N Steevens, Colette Chaney, et al. (2015). *Anti-CD19 chimeric antigen receptor-modified T cell therapy for B cell non-Hodgkin lymphoma and chronic lymphocytic leukemia: fludarabine and cyclophosphamide lymphodepletion improves in vivo expansion and persistence of CAR-T cells and clinical outcomes*.

Turtle, Cameron J, Laila-Aicha Hanafi, Carolina Berger, Theodore A Gooley, Sindhu Cherian, Michael Hudecek, Daniel Sommermeyer, Katherine Melville, Barbara Pender, and Tanya M Budiarto (2016). "CD19 CAR–T cells of defined CD4+: CD8+ composition in adult B cell ALL patients". In: *The Journal of clinical investigation* 126.6, pp. 2123–2138.

Turtle, Cameron J, Kevin A Hay, Laila-Aicha Hanafi, Daniel Li, Sindhu Cherian, Xueyan Chen, Brent Wood, Arletta Lozanski, John C Byrd, Shelly Heimfeld, et al. (2017). "Durable molecular remissions in chronic lymphocytic leukemia treated with CD19-specific chimeric antigen receptor–modified T cells after failure of ibrutinib". In: *Journal of Clinical Oncology* 35.26, p. 3010.

Tyagarajan, Seshu, Tom Spencer, and Jonathan Smith (2019). “Optimizing CAR-T Cell Manufacturing Processes During Pivotal Clinical Trials”. In: *Molecular Therapy-Methods & Clinical Development*.

van den Bos, Christian, Robert Keefe, Carmen Schirmaier, and Michael McCaman (2014). “Therapeutic Human Cells: Manufacture for Cell Therapy/Regenerative Medicine”. In: *Disposable Bioreactors II*. Springer, pp. 61–67.

Vannucci, Laura, Michele Lai, Flavia Chiuppesi, Luca Ceccherini-Nelli, and Mauro Pistello (2013). “Viral vectors: a look back and ahead on gene transfer technology”. In: *New Microbiol* 36.1, pp. 1–22.

Verma, Inder M, L Naldini, T Kafri, H Miyoshi, M Takahashi, U Blömer, N Somia, L Wang, and FH Gage (2000). “Gene therapy: promises, problems and prospects”. In: *Genes and Resistance to Disease*. Springer, pp. 147–157.

Vormittag, Philipp, Rebecca Gunn, Sara Ghorashian, and Farlan S Veraitch (2018). “A guide to manufacturing CAR T cell therapies”. In: *Current opinion in biotechnology* 53, pp. 164–181.

Wahl, DR, B Petersen, R Warner, BC Richardson, GD Glick, and AW Opipari (2010). “Characterization of the metabolic phenotype of chronically activated lymphocytes”. In: *Lupus* 19.13, pp. 1492–1501.

Walker, Anthony and Robert Johnson (2016). “Commercialization of cellular immunotherapies for cancer”. In: *Biochemical Society Transactions* 44.2, pp. 329–332.

Walseng, Even, Hakan Köksal, Ibrahim M Sektioglu, Anne Fåne, Gjertrud Skorstad, Gunnar Kvalheim, Gustav Gaudernack, Else Marit Inderberg, and Sébastien Wälchli (2017). "A TCR-based chimeric antigen receptor". In: *Scientific reports* 7.1, pp. 1–10.

Wang, X, J Stefanski, O Borquez-Ojeda, J Qu, A Hack, Q He, et al. (2015). "Comparison of CTS Dynabeadsc CD3/CD28, Miltenyi TransAct CD3/28 and ExpAct beads for large-scale CAR T cell manufacturing". In: *European Society of Gene and Cell Therapy Collaborative Congress*.

Wang, Xiuyan and Isabelle Riviere (2016). "Clinical manufacturing of CAR T cells: foundation of a promising therapy". In: *Molecular Therapy Oncolytics* 3, p. 16015.

Warburg, Otto (1956). "On the origin of cancer cells". In: *Science* 123.3191, pp. 309–314.

Warr, Steve RC (2020). "ambr® 15 Microbioreactors for CHO Cell Cultivation". In: *Animal Cell Biotechnology*. Springer, pp. 43–67.

Wilson, Matthew H, Craig J Coates, and Alfred L George Jr (2007). "PiggyBac transposon-mediated gene transfer in human cells". In: *Molecular therapy* 15.1, pp. 139–145.

Windt, Gerritje JW van der and Erika L Pearce (2012). "Metabolic switching and fuel choice during T-cell differentiation and memory development". In: *Immunological reviews* 249.1, pp. 27–42.

Xing, Zizhuo, Brian M Kenty, Zheng Jian Li, and Steven S Lee (2009). “Scale-up analysis for a CHO cell culture process in large-scale bioreactors”. In: *Biotechnology and bioengineering* 103.4, pp. 733–746.

Xu, Ling, Yikai Zhang, Gengxin Luo, and Yangqiu Li (2015). “The roles of stem cell memory T cells in hematological malignancies”. In: *Journal of hematology & oncology* 8.1, p. 113.

Xu, Ping, Colleen Clark, Todd Ryder, Colleen Sparks, Jiping Zhou, Michelle Wang, Reb Russell, and Charo Scott (2017). “Characterization of TAP Ambr 250 disposable bioreactors, as a reliable scale-down model for biologics process development”. In: *Biotechnology progress* 33.2, pp. 478–489.

Yang, Yinmeng, Elad Jacoby, and Terry J Fry (2015). “Challenges and opportunities of allogeneic donor-derived CAR T cells”. In: *Current opinion in hematology* 22.6, p. 509.

Zaritskaya, Liubov, Michael R Shurin, Thomas J Sayers, and Anatoli M Malyguine (2010). “New flow cytometric assays for monitoring cell-mediated cytotoxicity”. In: *Expert review of vaccines* 9.6, pp. 601–616.

Zhang, Cheng, Jun Liu, Jiang F Zhong, and Xi Zhang (2017). “Engineering CAR-T cells”. In: *Biomarker research* 5.1, p. 22.

Zhang, Qi, Zimu Zhang, Meiyu Peng, Shuyu Fu, Zhenyi Xue, and Rongxin Zhang (2016). "CAR-T cell therapy in gastrointestinal tumors and hepatic carcinoma: from bench to bedside". In: *Oncoimmunology* 5.12, e1251539.

Zhang, Wei, Kimberly R Jordan, Brian Schulte, and Enkhtsetseg Purev (2018). "Characterization of clinical grade CD19 chimeric antigen receptor T cells produced using automated CliniMACS Prodigy system". In: *Drug design, development and therapy* 12, p. 3343.

Zhang, Zhang, Shunfang Qiu, Xiaopeng Zhang, and Wei Chen (2018). "Optimized DNA electroporation for primary human T cell engineering". In: *BMC biotechnology* 18.1, p. 4.

Zhu, Fenlu, Nirav Shah, Huiqing Xu, Dina Schneider, Rimas Orentas, Boro Dropulic, Parameswaran Hari, and Carolyn A Keever-Taylor (2018). "Closed-system manufacturing of CD19 and dual-targeted CD20/19 chimeric antigen receptor T cells using the CliniMACS Prodigy device at an academic medical center". In: *Cytotherapy* 20.3, pp. 394–406.

Zhu, Fenlu, Nirav N Shah, Huiqing Xu, Dina Schneider, Rimas Orentas, Boro Dropulic, Parameswaran Hari, and Carolyn A Keever-Taylor (2016). *CAR-T cell production using the Clinimacs® Prodigy system*.

Zwietering, Th N (1958). "Suspending of solid particles in liquid by agitators". In: *Chemical engineering science* 8.3-4, pp. 244–253.